Alignment of phosphor properties for improvement of phosphor-converted LED performance

Zur Erlangung des Grades eines Doktors der Naturwissenschaften (Dr. rer. nat.)
genehmigte Dissertation von Charlotte Bois aus Saint Maur des fossés
Februar 2014 — Darmstadt — D 17

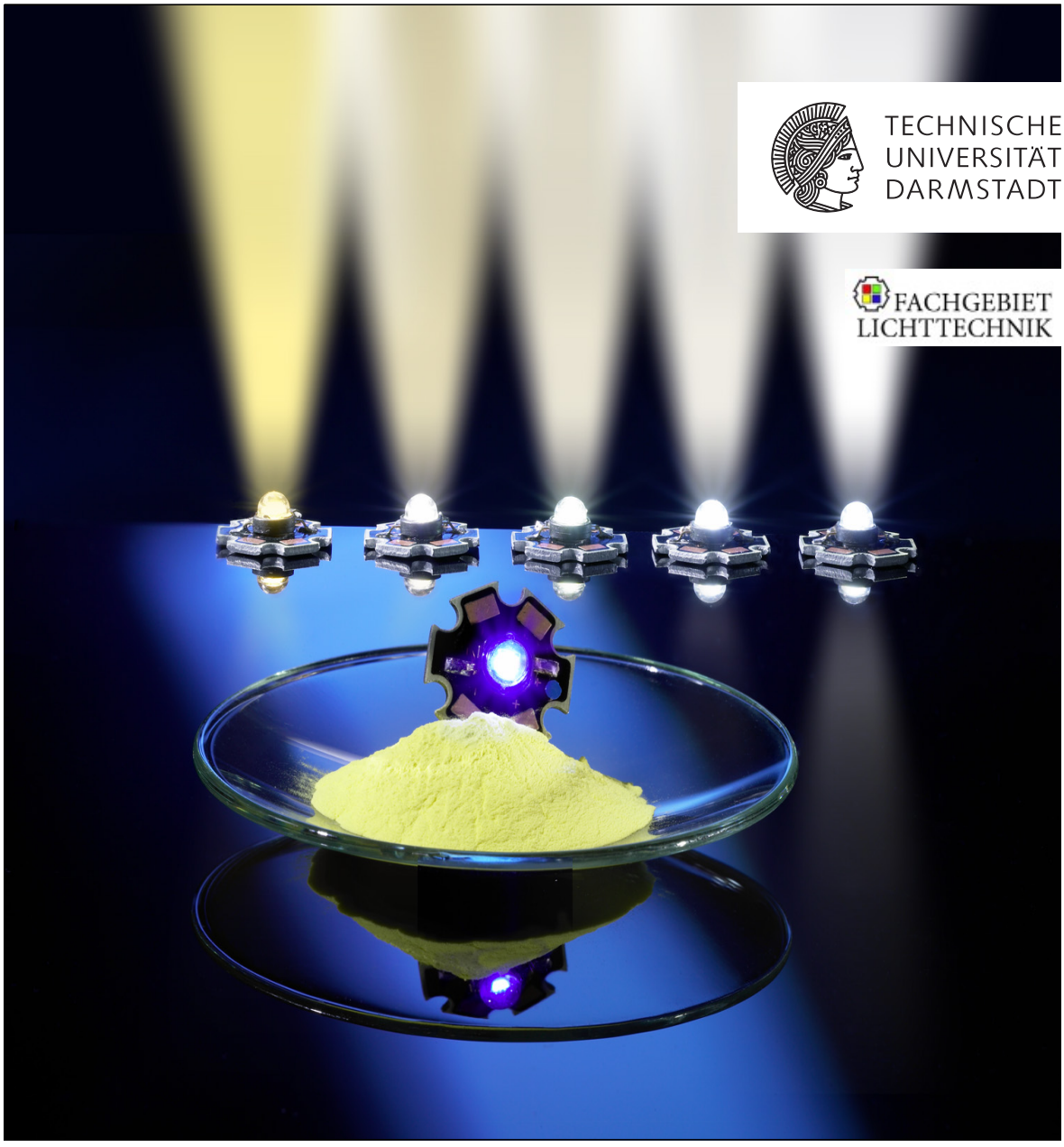

Alignment of phosphor properties for improvement of phosphor-converted LED performance

Genehmigte Dissertation von Charlotte Bois aus Saint Maur des fossés

1. Gutachten: Prof. Dr. Tran Quoc Khanh
2. Gutachten: Prof. Dr. Wolfgang Ensinger

Tag der Einreichung: 03.02.2014
Tag der Prüfung: 26.05.2014

Darmstadt — D 17

Erklärung zur Dissertation

Hiermit versichere ich, die vorliegende Dissertation ohne Hilfe Dritter nur mit den angegebenen Quellen und Hilfsmitteln angefertigt zu haben. Alle Stellen, die aus Quellen entnommen wurden, sind als solche kenntlich gemacht. Diese Arbeit hat in gleicher oder ähnlicher Form noch keiner Prüfungsbehörde vorgelegen.

Darmstadt, den 31.01.2014

(Charlotte Bois)

Alignment of phosphor properties for improvement of phosphor-converted LED performance

Dem Fachbereich Elektrotechnik und Informationstechnik
der Technischen Universität Darmstadt
zur Erlangung des akademischen Grades eines
Doktors der Naturwissenschaften (Dr. rer. nat.) genehmigte Dissertation

von

Dipl.-Ing. Charlotte Bois

geboren am 3. Dezember 1986 in Saint-Maur des fossés

Referent:	Prof. Dr. Tran Quoc Khanh
Korreferent:	Prof. Dr. Wolfgang Ensinger
Tag der Einreichung:	03.02.2014
Tag der Prüfung:	26.05.2014

D17

Darmstadt 2014

Preface

This PhD dissertation presents the results of my work completed in cooperation with the lighting department of the Technical University of Darmstadt and Merck KGaA.

I would like to thank Prof. Dr. Tran Quoc Khanh, director of the lighting department at TU Darmstadt for overseeing this work and to Dr. Peter Bodrogi for the pertinent scientific discussions. I am also grateful to Prof. Dr. Wolfgang Ensinger for assisting with the supervision of this dissertation as acting as my co-advisor.

Due to my participation with Merck KGaA, I learned more than just the facts reported in this dissertation. My Merck supervisor, Dr. Holger Winkler fostered my scientific achievements but also through his example, showed me how to develop inter-personal competencies.

During this PhD I had to physically overcome the some negative consequences from my serious bicycle accident. I had the chance to recognize the true value of the friends who surround me. They supported in overcoming many obstacles and encouraged me during times when my research results were confusing and also during the always challenging writing process. Special thanks to Joe who never stopped to believing in my abilities, to my lab colleagues Gorica, Martin and Mimoun who were always there for any kind of trouble and to Mike for always being proud of me. My thanks to Toni for simply being present in my everyday life and to all my friends, family and colleagues who participated psychologically or materially from near or far to help me complete this work! Through some very difficult times recently, I kept going, merci Nils. My successful emergence from this intense experience has contributed to integrate me in the local landscape as ``Deutsche Kartoffel ´´and also has participated in my finding my second home.

For all smiles and hope I received I would like to express my deepest appreciation.

Kurzfassung

Beispielsweise wird aktuell 12% des US-Strombedarfs für die Beleuchtung aufgebracht [1]. Die Entwicklung effizienter und umweltfreundlicher Lichtquellen ist also eine große Herausforderung. In den letzten Jahrzenten hat die Forschung im Bereich Solid State Lighting umfangreiche Fortschritte gemacht. Heutzutage sind LEDs durch ihren hohen Wirkungsgrad, ihre hohe Lebensdauer und ihren geringen Effizienzverlust über die Nutzungsdauer charakterisiert. Zudem haben Dimmbarkeit, geringe Farbverschiebung und hohe Farbqualität diese Technologie zu einer energiesparenden und nachhaltigen Lösung gemacht. In dieser Arbeit werden Leuchtstoff-konvertierte LEDs (PC-LEDs), welche auf diesem Gebiet als zukunftsweisend gelten, untersucht.

Eine Vielzahl an Parametern beeinflusst die Eigenschaften einer PC-LED. Diese Arbeit umfasst die Auswirkung von Leuchtstoffen auf PC-LEDs, von ihren Lumineszenz-Eigenschaften bis zur Endapplikation als fertiges Produkt. Eine interdisziplinäre Methode wurde hierfür entwickelt, welche chemische, physikalische, Fertigungs- und Prozess-Aspekte vereint.

Zunächst wurde der Einfluss der Leuchtstoff-Partikelgröße auf PC-LEDs untersucht. PC-LEDs wurden hierfür zu Beginn aus YAG aufgebaut und auf Lumineszenz-Eigenschaften gemessen. Die Resultate zeigen, dass je größer die Partikel sind, desto höher sind auch Anregungsgrad, Absorptionsgrad und Emission. Kleine Partikel weisen Strukturdefekte aufgrund eines frühen Wachstumsabbruchs während der Synthese auf, die dazu führen, dass das Licht eingefangen und die Lumineszenz herabgesetzt wird. Um gleiche Farbtemperaturen zu erhalten, benötigen YAG:Ce weißer LEDs eine steigende Leuchtstoff-Massenkonzentration mit zunehmender Partikelgröße. Die Konzentration zeigt eine lineare Abhängigkeit von der Partikelgröße. Auch der Lichtstrom erhöht sich mit zunehmender Partikelgröße. Große Partikel besitzen hohe Lumineszenz-Eigenschaften, und bei kleineren Partikeln haben optische Strahlungen zudem höhere Tendenzen zurückgestreut und von der LED absorbiert zu werden. Die bei weißen LEDs emittierten blauen und gelben Farbanteile sind im Verhältnis zueinander konstant, folgerichtig ändert sich der Farbwiedergabe-Index nicht. Ein gelber Ring-Effekt tritt bei winkelabhängiger Lichtverteilung von herkömmlichen LEDs mit homogen verteilter Silikon- und Phosphor-Schicht auf. Vergleichbare Ergebnisse in Bezug auf die Änderung der Korngröße konnten mit LuAG-Phosphor erzielt werden. Leuchtstoff, chemische Struktur und die Aktivator-Konzentration des Leuchtstoffes bestimmen die Lumineszenz-Merkmale. Die Partikelgröße ist darüber hinaus ein wichtiger Parameter bei der Bestimmung der nötigen Leuchtstoff-Konzentration, um bestimmte Farbtemperaturen zu erreichen sowie um die Leistung der LED zu erhöhen.

Die Farbwiedergabe wurde im Folgenden durch das Einfügen einer roten Farbkomponente verbessert. PC-LEDs wurden hierzu in unterschiedlichen Zusammensetzungen aus grünem (LuAG und Orthosilikat) und rotem (Oxynitrid und Oxyorthosilikat)-Phosphor aufgebaut. Die Wechselwirkung der Lumineszenz-Eigenschaften von Phosphor wirkt sich auf die benötigte Phosphorkonzentration aus. Lichtströme und Farbqualität sind stark abhängig von den Verteilungsspektren, welche miteinander verglichen werden, um bestmögliche Eigenschaften zu erzielen. Simulationen wurden durchgeführt, um die experimentellen Emissionsspektren der LEDs in Abhängigkeit der Partikelgröße sowie für grün-rot gemischte LEDs zu validieren. Die Ergebnisse in Bezug auf die erzielte Leistung sind zufriedenstellend. Die Farbtemperatur konnte aufgrund der Abweichung der spektralen Verteilung nur

mäßig simuliert werden. Diese Simulationen eignen sich jedoch dafür, eine Tendenz der PC-LED-Eigenschaften vorherzusagen, wodurch die Anzahl an experimentellen Versuchen reduziert wird. Diese Arbeit leistet somit einen aussagekräftigen Beitrag zur Forschung von Einflussfaktoren und Abhängigkeiten im Bereich der PC-LED Forschung in Anwendung auf YAG, LuAG und grün/roten Leuchtstoff-Mischungen.

Abstract

Lighting applications represent the consumption of 12% of the US electricity [1]. The development of efficient and environmentally friendly lighting sources constitutes an important challenge. In the last decades research in the area of solid state lighting succeeded to make considerable advances. LEDs are proving to be an innovative and promising technology designed to revolutionize the lighting market. Nowadays LEDs are characterized by their high luminous efficacy, long lifetime and slow depreciation of the luminous flux. Furthermore, the characteristics of dimmability, low color shift and high light quality establish this technology as an energy saving opportunity to significantly reduce the amount of energy consumed by lighting uses. The combination of powerful blue LEDs with broad emitting phosphors is the approach selected to be investigated in this work.

A great diversity of parameters plays a role in determining the properties of Phosphor-Converted LEDs (PC-LEDs). This dissertation outlines the specific impact of phosphors on PC-LEDs from their phosphor photoluminescence (PL) properties until their final application as a white LED product. The method elaborated in this study is interdisciplinary, associating technological, chemical, physical and processing aspects. The influence of phosphor particle size on PC-LEDs' properties is investigated. PC-LEDs based on YAG phosphor are built. PL properties of YAG phosphor powder are first measured. Results show that the larger the phosphor particles are, the higher their excitation, absorption and emission. Small particles exhibit structure defects due to early growth stoppage during the synthesis resulting in light trapping effects and thus deteriorating their PL. At constant Correlated Color Temperature (CCT) YAG white LEDs require increasing phosphor weight concentration for increasing particle size. Weight concentration shows a linear dependence on phosphor particle size. The luminous flux increases as well for larger particles. Besides enhanced PL properties of large phosphor particles, rays are more likely to be backscattered and absorbed by the LED chip in the case of small particles. White LEDs emit with constant blue and yellow proportions, the color rendering remains therefore unchanged. Angular distribution results in the yellow ring effect obtained on conventional coated PC-LEDs. The results obtained from analyses of the particle size on YAG PC-LEDs are confirmed with LuAG phosphor samples. Phosphor chemical structure and activator concentration determine the luminescent characteristics. Particle size corresponds to a parameter that contributes to the prediction of the phosphor concentration necessary to achieve PC-LEDs of target CCT and to improve the light efficiency.

The color rendering is improved by the introduction of a red component. Green (LuAG and orthosilicate) and red-orange (oxynitride and oxyorthosilicate) phosphors are mixed to create PC-LEDs. Interaction of phosphor PL properties significantly affects the phosphor concentration. Luminous fluxes and color quality depend greatly on the spectral distributions which are compared to define the best performance. Simulations attempting to reproduce PC-LED measured data are reported for YAG and LuAG sieved PC-LED fractions as well as green and red mixed PC-LEDs. Peer results are very encouraging, CCT results show a moderate match because of the spectral emission discrepancies. Simulations give a good qualitative trend thereby reducing the required number of PC-LED experimental tries.

The results of this work provide a pertinent contribution in the research field of PC-LEDs and their influencing factors when applied with YAG, LuAG and green/red phosphor mixtures.

Contents

List of Tables

List of Figures

List of Symbols and Abbreviations

Symbol / SI-Unity	Description
ΔE_i / -	color shift on the CIE diagram 1931 between test source and reference source
$\Delta u'v'$ / -	distance in the CIE u',v' chromaticity diagram between the source test and the reference illuminant of the corresponding CCT
(x, y)	chromaticity coordinates
Φ_e / W	radiant flux
Φ_V / lm	luminous flux
d_{50} / μm	median diameter of phosphor particle
d / -	distance in the CIE xy diagram between the blue LED and the source test
D / W	sum of the difference between simulated and measured radiant flux for each wavelength
E / lux	illuminance
I / cd	luminous intensity
n / -	refractive index
P / W	consumed power
Q_g	relative gamut area
$V(\lambda)$	luminosity function during the day
$V'(\lambda)$	luminosity function during the night
A	absorption coefficient
AlInGaP	Aluminum Indium Gallium Phosphide
CB	conduction band
CCD	charge coupled device
CCT / K	correlated color temperature
CFL	compact fluorescent lamp
CIE	commission internationale de l'éclairage

COB	chip on board
cps	count per second
CQS	color quality scale
CRI R_a / -	color rendering index
DR	diffuse reflection coefficient
ELiXIR	enhanced light extraction by internal reflection
G1	green 1
G2	green 2
InGaN	Indium Gallium Nitride
LED	Light Emitting Diode
LuAG:Ce	$Lu_3Al_5O_{12}:Ce^{3+}$
NIR	near infra red
PC-LED	phosphor-converted LED
PL	photoluminescent
PSD	particle size distribution
QE / %	quantum efficiency
R1	red 1
R2	red 2
RGB system	Red Green Blue color system
SEM	scanning electron microscopy
SMD	surface mounted device
SPE	scattered photon extraction
SSL	solid state lighting
UV	ultra violet
VB	valence band
WLED	white LED
YAG:Ce	$Y_3Al_5O_{12}:Ce^{3+}$

1 Introduction to efficient lighting system

Since 2012 incandescent lamps have been banned in Europe because 90 % of the energy they consume is released as heat. Energy saving and environmental considerations have oriented the efforts of lighting manufacturers towards alternative light sources. Improvement efforts have resulted in the development of halogen bulbs, gas discharge, fluorescent or compact fluorescent lamps. However none of these different approaches have achieved the targeted features associated with high efficiency, environment friendly components and the ability to illuminate objects with high color quality. Halogen bulbs suffer from poor efficiency due to the non-radiative majority of their emission and the subsequent heat production. Discharge lamps suffer from low color rendering. Compact fluorescent lamps show spikes in their emission spectrum and contain toxic mercury.

The potential for considerable improvement in lighting technology is recognized in light emitting diodes (LEDs) since their introduction from the solid state lighting field. Continuous LED development has demonstrated their expanding application to a wide variety of uses, where this technology is appropriate in terms of efficiency and energy saving. Since substantial benefits have already been proven, the LED market is increasing continuously during recent years. Compared to the conventional lighting LED solutions offer many exciting opportunities.

Besides their high efficiency specifically targeted in the visible range compared to other lighting systems (Table 1.1), LED technology presents many advantages. LEDs can be controlled and tuned in terms of color temperature with high color quality and absence of color shift by a change in temperature. LEDs can be tailored to suit the sensitivity of the human eye and their radiation closely match the sun spectrum. LEDs can be operated during at least 40,000 hours which is far longer than any other lighting system. Competing systems reach in the best cases a lifetime of 20,000 hours (fluorescent lamps). The light output also degrades gradually over the time. Burn out comparable to incandescent bulbs is not observed due to LED components' resistance to shock but also because LEDs are generally protected by optical features. These two factors lead to significant reductions in the cost of lamp replacement and maintenance. Energy and maintenance costs can also be reduced by an efficient dimming system. The lower power consumption and reduced carbon emission achieve important energy savings and position LEDs as environmentally friendly devices. Finally, the implementation of LEDs illustrates a suitable solution for lighting applications in directional lighting by reducing the need for reflectors and diffusers that can trap light and thereby reduce effectiveness. Well-designed LEDs deliver light efficiently to the intended location. In contrast, fluorescent and "bulb" shaped incandescent lamps emit light in all directions. This occasions therefore losses by light reabsorption or escape in a direction that is not useful. The considerable number of benefits offered by LED technologies virtually assures the future reliability and sustainability of LEDs for lighting applications.

LEDs are more and more integrated in our everyday life. They find many valuable applications in the domain of display technology, traffic lights or automotive interior, exterior and signal lamps. Their small designs allow them to be implemented as indicator lamps in a number of electronic devices and especially as warning devices. The resulting substantial savings in cost and significant reduction in the environmental impact on conventional power

Table 1.1.: Luminous efficacy of different lighting systems (*source: US DOE 2013*)

Product Type	**Luminous Efficacy / lm/W**
Warm White LED	94
Linear fluorescent system	108
Low pressure discharge system	104
Compact fluorescent lamp	73
Halogen incandescent lamp	20-25
Incandescent lamp	15

generation are very convincing arguments to move LEDs into general lighting applications for private homes or public buildings.

New generation LED based lighting sources consist of associating the performance of high power LED chips to broad spectrum emitting phosphors. This promising technology suitable for high quality general lighting is the object of our study. This PhD thesis highlights some aspects of the possible improvements to be realized in phosphor properties in order to optimize phosphor-converted LEDs (PC-LEDs). The structure of this work is outlined as follows. The next chapter concentrates on the historical and technological development of lighting systems. The latest advances on PC-LEDs will be described and analyzed. Chapter 3 defines the objectives and motivations of this work. The methodology of research is then more closely explained. Next, Chapter 4 describes the technical equipments utilized for the measurements and gives an estimation on the data error. The focus of Chapter 5 will be set on PC-LEDs properties made of YAG phosphor. Phosphor characteristics will be detailed followed by their influence on PC-LED properties and simulation of experimental results. Chapter 6 summarizes the results carried out on PC-LEDs based on LuAG phosphor. A similar approach is developed as for YAG phosphor, photoluminescent properties of LuAG phosphor are investigated for different particle sizes. Their influence on PC-LEDs is then studied with the help of measurement and simulation data. More complex PC-LEDs made of green and red phosphors are considered in Chapter 7. The improvement of light quality induced by these phosphor systems is determined. The final section recapitulates the conclusions reached as well as recommendations for future projects are presented.

2 From basics about lighting concepts to actual lighting technology

In the context of the development of innovative and efficient lighting sources, it is necessary to agree on the definition of the physical quantities characterizing light. Measures of light power are reviewed in the first section, which contribute to the evaluation of the efficiency of a light source from an energetic and qualitative point of view. The perception of light by the human eye is also of great interest. The parameters responsible for the impact of the light on humans are therefore also explained. A brief historical review of lighting systems is then presented, leading to the technologies that are nowadays the most efficient for the production of white light. These technologies are explored in the following section. The quality, efficiency and perception of the light created by this technology are decisive in determining its entry in our society, however acquisition costs have a great impact as well. A very important new trend could emerge in society if the concept is economically viable. Hence, the financial and environmental aspects are highly important. The recent scientific advances are summarized in a further section. These include the latest improvements concerning PC-LEDs, their properties and their key elements.

2.1 Definition of sizes characterizing the light

The light produced by a candle is very inefficient. Even in spite of this, candles are used in 7 out of 10 households [2]. The atmosphere created by the light source and its effect on humans must not be neglected. Several notions attempting to relate these perceptions of the light to the effect on humans have been researched and adapted to specific measurement dimensions. Color systems describing the light sources are developed in order to correlate spectral light distributions with light quality. These characteristics are detailed in this section.

2.1.1 Human perception of the light

Every color in the visible spectrum can be described in the optical field in terms of its wavelength. The correct perception of a color depends on the reflection properties of the object, but is only possible if the object is illuminated by a source possessing the correspondent wavelength. The observer is able to define an object by its lightness, hue and saturation. Lighting technology relies on the property of human eyes. The sensitivity of the eye therefore plays an important role in the perception of colors as it enables color around 555 nm (corresponding to green) to be appreciated brighter than in the red tones for example. The distribution of the luminosity's sensitivity for the human eye, $V(\lambda)$ is represented in Fig. 2.1 as a function of the wavelength. The luminosity function $V(\lambda)$, dimensionless, describes the photopic human eye's sensitivity (sight during the day), the curve $V'(\lambda)$ is valid for the scotopic domain (night vision) [3].

2.1.2 Quantification of the light

The light is characterized by an electromagnetic radiation wave which lightness can be determined. Radiometry is the science to measure the distribution of the radiation's power.

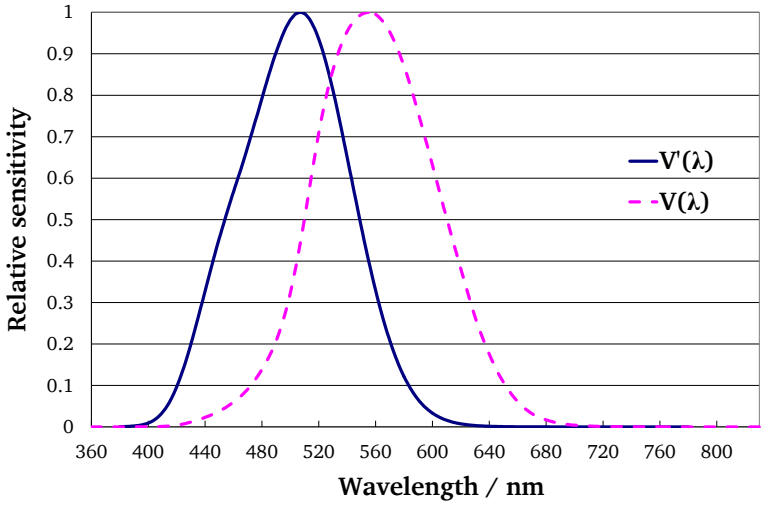

Figure 2.1.: Normalized spectral sensitivity curves for photopic vision (dashed line $V(\lambda)$, from 1924 CIE) and night vision (solid line $V'(\lambda)$)

The radiant flux Φ_e is the total power of electromagnetic radiation measured in Watts, eq. 2.1.

$$\Phi_e = \int_0^\infty S(\lambda) d\lambda \tag{2.1}$$

Where $S(\lambda)$ is the spectral power distribution.

Complementary to this, the photometry informs about the radiometric measurements related to the interaction with the human eye's perception. Photometric values are calculated from radiometric ones modified by the spectral sensitivity curve $V(\lambda)$. The photometric equivalent to the radiant flux (eq. 2.2), is the luminous flux Φ_V which is measured in lumen (lm).

$$\Phi_V = 683\text{lm/W} \times \int_{380}^{780} V(\lambda) S(\lambda) d\lambda \tag{2.2}$$

Other photometric quantities result by analogy from the radiometric parameters like the illuminance E expressed in eq. 2.3 in lux (lm/m^2) as the luminous flux (Φ_V in lm) per area unit (A in m^2).

$$E = \frac{d\Phi_V}{dA} \tag{2.3}$$

The luminous intensity I defined as the luminous flux per solid angle (Ω in steradian) in candela (cd = lm/sr) eq. 2.4.

$$I = \frac{d\Phi_V}{d\Omega} \tag{2.4}$$

The radiant flux of 1 watt at a wavelength of 555 nm produces a luminous flux of 683 lm following equation 2.5. K characterizes the luminous efficacy.

$$K = \frac{\Phi_v}{\Phi_e} = 683\text{lm/W} \times \frac{\int_{380}^{780} V(\lambda)S(\lambda)d\lambda}{\int_0^{\infty} S(\lambda)d\lambda} \tag{2.5}$$

The radiant efficiency or wall-plug efficiency η_e (dimensionless) denotes the ability of a light source to convert the consumed power P (watt) into radiant flux (watt), eq. 2.6.

$$\eta_e = \frac{\Phi_e}{P} \tag{2.6}$$

The luminous efficiency η_V in lm/W is the ability to convert the electrical power consumed (watt) into visible light (luminous flux), eq. 2.7.

$$\eta_V = \frac{\Phi_v}{P} = \eta_e \cdot K \tag{2.7}$$

2.1.3 Colorimetry and quality of the light

The sensation of color is complex to determine. A concept to describe this notion is based on the definition of chromaticity coordinates, color temperature and color rendering.

Chromaticity coordinates describe quantitatively the color of the emitted radiation. Any color with color coordinates situated on the line joining the two primary light source coordinates can be reproduced. Because of the properties of the human eye, the same chromaticity coordinates can be obtained for a combination of a few monochromatic sources, or for a source that irradiates a set of certain spectral lines. Sources of different spectra but with the same chromaticity are called metameric. That is why the perception of a white color for example can be realized by a sum of blue and yellow sources, or blue, green and red sources. However besides their spectral distributions, these two white colors can be distinguished by their luminous efficiency and by their color rendering index. It appeared experimentally that the colors could be the sum of three appropriate primary colors: red, green and blue ([R], [G] and [B]). However some colors, close to monochromatic colors fail to be a positive sum of these three components, but need negative amounts (subtractive colors). This negative effect has been removed creating imaginary stimuli [X], [Y] and [Z]. The tristimulus values X, Y and Z (i.e. the amounts of each stimuli in a color represented by a certain spectral power distribution) are obtained by integrating the spectrum with the standard color-matching functions $\overline{x}$, $\overline{y}$ and $\overline{z}$, which are characteristic for an standard observer (introduced by CIE (Commission Internationale de l'Eclairage) in 1931), shown in Fig. 2.2.

$$X = \int_0^{\infty} \overline{x}(\lambda)S(\lambda)d\lambda \tag{2.8}$$

$$Y = \int_0^{\infty} \overline{y}(\lambda)S(\lambda)d\lambda \tag{2.9}$$

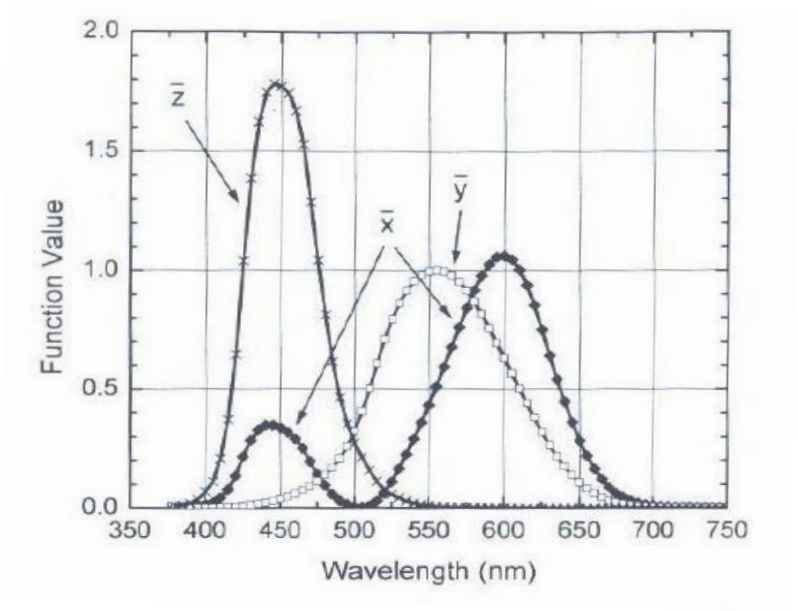

Figure 2.2.: 1931 CIE color-matching functions [3]

$$Z = \int_0^\infty \overline{z}(\lambda) S(\lambda) d\lambda \tag{2.10}$$

1931 CIE color-matching functions are tabulated at different wavelength intervals. The 1931 CIE green matching function $\overline{y}$ was matched completely with the 1924 CIE luminosity function $V(\lambda)$ for photopic vision. The functions $\overline{x}(\lambda)$, $\overline{y}(\lambda)$ and $\overline{z}(\lambda)$ are defined for a narrow matching field, to avoid any participation of the rod vision. An alternative set of color-matching functions $\overline{x}_{10}(\lambda)$, $\overline{y}_{10}(\lambda)$ and $\overline{z}_{10}(\lambda)$ is recommended for angles above 4° (CIE 1964). For convenience, the chromaticity coordinates (x, y) of a light source were introduced:

$$x = \frac{X}{X+Y+Z} \tag{2.11}$$

$$y = \frac{Y}{X+Y+Z} \tag{2.12}$$

The third coordinate z (eq. 2.13) contains no additional information. Though, an in-plane representation of the colors can be made by the chromaticity coordinates (x, y), see Fig. 2.3.

$$z = \frac{Z}{X+Y+Z} \equiv 1-x-y \tag{2.13}$$

The area enclosed under the contour of the horseshoe-shaped curve comprises all of the real colors. The 1931 CIE provides a simple color mixing means. A set of n primary sources with the chromaticity coordinates (x_i, y_i) and radiant fluxes Φ_{ei} will produce a color with the chromaticity coordinates calculated by eq. 2.14 and 2.15.

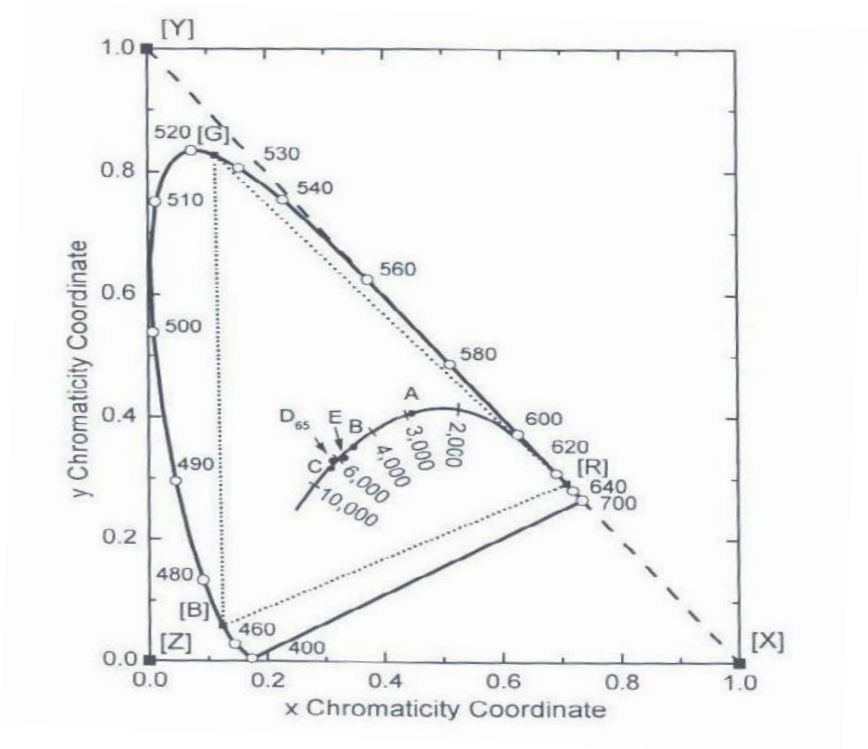

Figure 2.3.: 1931 CIE chromaticity diagram [3]

$$x = \frac{\sum_{i=1}^{n} x_i \Phi_{ei}}{\sum_{i=1}^{n} \Phi_{ei}} \tag{2.14}$$

$$y = \frac{\sum_{i=1}^{n} y_i \Phi_{ei}}{\sum_{i=1}^{n} \Phi_{ei}} \tag{2.15}$$

The correlated color temperature (CCT) of a light source is the temperature of an ideal blackbody radiator (determined by Planck's law) that radiates light of comparable hue to that light source. Color temperature communicates the color appearance of the light source. The solid line in Fig. 2.3 shows the color temperatures. LEDs are classified as warm-white (2700 K to 3500 K), neutral-white (3500 K to 4000 K) or cool-white LEDs with CCT higher than 4000 K (bluish in appearance). CIE data also includes four standard sources: A (Tungsten at 2856 K), B (direct sunlight approximatively 4870 K), C (overcast sunlight 6770 K) and D_{65} (daylight 6504 K). Point E marks equal energy (x=0.333; y=0.333), the colorless point. If the chromaticity of a source is not exactly equal to any of the chromaticities of the blackbody radiator, a CCT may be assigned to the source using chromaticity match with isotemperature lines.

The 1931 CIE diagram presents a non-uniformity towards the ability of the human eye to distinguish two close colors and is thought to be unsuitable. The eye is able to detect small variation of the color for the red. The density of hues is higher when moving from the white center to the red angle as when moving to the green. The Uniform Chromaticity Scaling (UCS) diagram (1960 CIE) was introduced to rationalize the colorimetric shifts. This diagram is obtained by mathematical conversion of 1931 CIE diagram, it is defined by

u, v and Y. Further color systems CIEUVW (CIE 1964 UCS) and CIELUV (CIE 1976 UCS) are developed from UCS 1960 and allows the comparison of color without considering the brightness of the light sources. CIE 1964 UCS is characterized by u, v and w and CIE 1976 by *u'*, *v'* and *L'*. *u'* is equal to *u* and *v'* is 1.5 times larger than *v*.

$\Delta u'v'$ is an additional metric that can help identify sources with excessively greenish or pinkish hues. This value features how far the chromaticity point of the test source is the locus of the daylight illuminants in the CIE *u'*,*v'* chromaticity diagram. It is calculated for the corresponding CCT by the following eq. 2.16.

$$\Delta u'v' = \sqrt{(u'_{test} - u'_{ref})^2 + (v'_{test} - v'_{ref})^2} \tag{2.16}$$

The general color rendering index (CRI R_a) indicates the quality of the light. CRI measures the ability of light sources to render colors, compared to a reference source. Two types of reference light sources are assumed, Planckian radiator and daylight. The reference light source has to have the exact value of CCT as the tested light source. If the CCT of the tested light source is higher than 5000 K then the spectral power of a phase of daylight is used as the reference source and in all the other cases the reference source is the Planckian radiator. The reflectivity spectra of 8 test color samples and 6 supplementary ones selected from the color palette introduced by MUNSELL are multiplied by the reference illuminant emission spectrum in order to obtain the reflected spectra for the 14 test color samples. The operation is repeated for the test source. The color shift ΔE_i to the reference source is graded (eq. 2.17) and gives the color rendering index R_i for each test color sample. For example R_9 value describes how closely the test source renders a saturated red color. R_a value is determined from the arithmetical average of the values R_1 to R_8 [5]. Color shifts and color rendering indexes are dimensionless

$$R_i = 100 - 4.6 \cdot \Delta E_i \tag{2.17}$$

However critics have been addressed to this approach to determine the CRI R_a. Critics are directed to poor correlation with the visual color rendering of many spiked or narrow band sources, the obsolete color space considered or the small number of reflectance samples. A proposition was made by SMET et al. to introduce CRI2012 values that is based on a model with highly uniform color space and that considers a set of 210 real reflectance samples [6].

The color quality is also suggested to be evaluated by another metric Color Quality Scale (CQS). CQS is a proposal of a new metric, which aspires to replace the current CRI with which it shares the computation principle. Nevertheless CQS uses a larger set of reflective samples, all of high chroma. Additionally, the CQS penalizes sources with smaller rendered color gamut (Q_g) areas. The scale of the CQS is converted to span 0–100, and the uniform object color space and chromatic adaptation used in the calculations are updated [7].

2.2 History of lighting technologies

The fire firstly used some 500,000 years ago is the first artificial portable light source, developed in the form of a torch. The discovery of the wick, a capillary cord that draws fuel up to the flame was the key component in the oil lamp, developed some 10,000 years ago [3]. The candle is based on the same principle: a wick leading from the fuel to the flame, which is in that case beeswax or paraffin wax, melting in the heat of the flame. Candles emit approximately 13 lumens which corresponds to about 0.16 lm/W [2]. The visible emission is caused by pyroluminescence, which is due to radiative transitions in excited atoms and ions, recombination of ions to form molecules, and incandescence of solid particles in the flame. Combustion results in high levels of excitation of atoms and molecules. Candles release an energy of 80 watts. The majority of the energy is converted into heat, which does not make this source suitable for an efficient lighting application. All the light is indeed produced by electronic transitions from higher to lower energy states. Excitation to higher states may be achieved by several techniques. Up until the beginning of the nineteenth century, flame produced by combustion still remained the only source of artificial light.

The incandescent lamp was patented in 1879 by Thomas Edison. The incandescent filament lamp consists of a filament made of carbon through which an electrical current is passed. The lamp is filled with an inert gas such as argon in order to reduce the evaporation of the filament. The light is radiated from the incandescence of the filament. During the following 150 years their luminous efficacy was enhanced from 1.5 lm/W to 16 lm/W [3]. The major amount of energy is transformed into heat, which limits the efficiency of the device. The filament was then improved to be made of tungsten. The condensation of the evaporated tungsten filament darkens the inner surface of the bulb. A breakthrough in the incandescent lighting device was to enrich the inert gas with halogen gas owing to a decrease of the tungsten deposition on the inner bulb surface. At moderate temperatures the halogen reacts with the evaporating tungsten, the halide formed being moved around in the inert gas filling. At some time it will reach higher temperature regions, where it dissociates, releasing tungsten and freeing the halogen to repeat the process.

Gas-discharge lamps were the next step in the development of artificial lighting sources. An electrical discharge between an anode and a cathode ionizes the filled gas (noble gas), the electrons released are accelerated by the electrical field and bring the additional filled gases like sodium, mercury or metal halide to an excited state. When the electrons fall back to their original state, they emit a photon. The electro fluorescence in the ultra violet domain can be, in the case of the fluorescent lamp, converted to visible light by contact with the fluorescent coated bulb. Hewitt patented in 1900 the mercury vapor lamp [8].

Fluorescent lamps were invented in 1938 with a luminous efficacy increasing from 50 to 100 lm/W over the next 60 years. Then the sodium vapor lamp was invented in 1965. Over the following 40 years the luminous efficacy was raised from 106 to 146 lm/W [9]. Thus the typical improvement rate of luminous efficacy is in traditional lamps only 1.1-1.2 times per decade. The light sources previously listed have kept a relatively constant value for the past 30 years.

„Electroluminescence“ was first introduced by Henry Joseph Round in 1906, while he was experimenting with SiC (carborundum) and effectively created the first LED. The next 50 years were followed by little progress until research on semiconductors started. In the 1950s, academic and industrial researchers carried out many experiments to generate light emission on the p-n junction of diodes using a number of materials. The results were disappointing

as light emission was low in intensity, the LEDs were expensive and only a few colours were available [10]. During the early 1960s, Texas Instruments Company sold LEDs emitting at 870 nm for US $130, and General Electric launched red LEDs for around US $260. Hence these early LEDs were expensive and sold only in very low volumes. In 1964, IBM used GaAsP LEDs on circuit boards in an early mainframe computer as on-off indicator lights: this was perceived as a significant breakthrough as it provided lighting in a new role to both manufacturer and end-user. The specificity of this innovation was that the LED could be mounted directly onto the circuit board, it used little power, and had a long lifetime thereby eliminating maintenance. These attributes are the ones used today to drive the replacement of other light sources with LEDs as todays LEDs have become more efficient, cheaper and brighter.

Thus, although infra-red and red LEDs have been around for over 40 years, it was only the arrival of bright blue LEDs that heralded the genesis of the present solid state lighting revolution. Research that led to the development of the blue LEDs followed from reports on III-V nitrides that allowed the production of high-quality crystals of GaN, AlGaN, GaInN. In the early 1990s, Nakamura and co-workers followed up this work to develop low resistive p-type GaN and AlGaN. The bright blue InGaN LEDs were prepared, along with blue-green LEDs. This was followed with the fabrication of bluish-purple laser diodes. The semiconductor technology ensures a wide range of color emission due to the different energy transitions. The InGaN LED was patented by Nakamura in 1994 and the InGaN/YAG:Ce was patented by Nichia in 1997 [8]. This innovation led to advances in the InGaN technology, which were to initiate the wide-scale commercialization of blue and green solid state sources as well as the development of white LEDs. A full range of colored LEDs was then available and this facilitated their use in many colored lighting applications displacing more traditional lighting methods [9].

The first white LED had a lumen efficacy of 5 lm/W, being much lower than that of an incandescent lamp (13 lm/W). However, the efficacy of white LEDs was rapidly enhanced due to improvements in the blue LEDs light output (Fig. 2.4). Nowadays current commercial white LEDs reach 150 lm/W. The lumen efficacy was drastically improved, compared with that of traditional lamps, by about 30 times per decade and LED improvements have not yet slowed their pace [11].

2.3 Development of white lighting systems from solid state

During the last 50 years, considerable progress has been made in solid-state light-emitting devices. The efficacy of solid state lighting (SSL) based on InGaN LEDs has increased by over ten times during the past decade. Cool white LEDs exhibit efficiencies higher than linear fluorescent lamps (LFLs) already emitting more than 100 lm/W. Warm white 1 W LEDs now surpass compact fluorescent lamps (CFLs) showing efficacies of 60-70 lm/W [12]. At the present time, technical advances in solid-state light sources are continuing with sources continuously becoming more powerful, brighter and more efficient [13]. White light production is based on this technology. Several techniques enable the creation of white light from LEDs. Fig. 2.5 summarizes the different alternatives.

- A mix of red, green and blue colored LEDs is a possible method (RGB system).
- The combination of an exciting LED and a single phosphor is offered.
- A pumping LED can be associated with several phosphors.

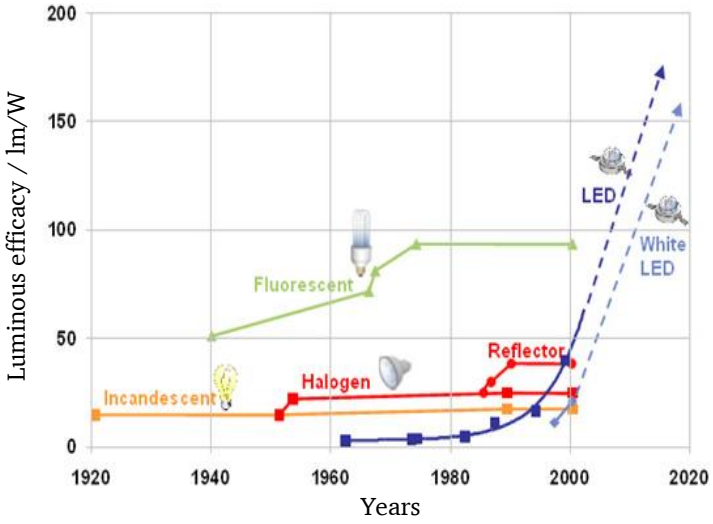

Figure 2.4.: Luminous efficacies of different lighting systems over the years. *Source* : United States Department of Energy (DOE) Solid State Lighting report 2013

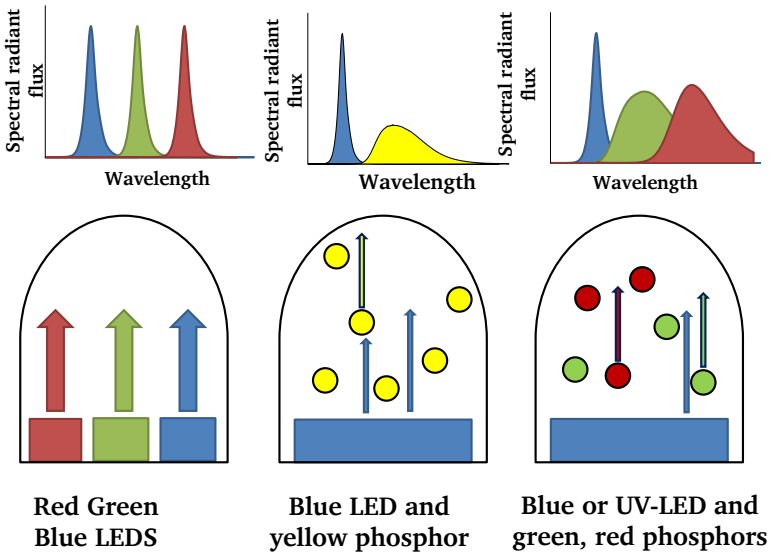

Figure 2.5.: White light production systems

RGB System

RGB system is based on the principle of mixing the three primary colors, red, green, and blue with suitable intensities to generate white light. With currently available LEDs, the generation of white light can have luminous efficacies of approximately 45 lm/W. Note that because the human eye's reduced response to the red color, the emission intensity of the red color LED must be higher to generate white light with acceptable color rendering index. In addition, the efficiency for the green LEDs is lower than for the other colors (see Fig. 2.6). Control of the wavelengths, the relative power levels and also the spectral width of emission is required. The narrower the emission peak of the LED, the closer its color is to the saturated colors on the periphery of the CIE diagram. This enables us to increase the range of color gamut possible to illuminate. But the color rendering index that can be achieved from three narrow band-emitting LEDs is poor. This three-color approach is potentially very efficient for

display backlighting, but the cost is expected to be high as it involves InGaN and AlInGaP technologies with each LED of different drives. With four-LED chips better color rendering index can be reached, making their application suitable for general lighting. However this would increase the cost of such LEDs.

Mixing blue, green and red LEDs presents further problems. The perceived color may change with viewing angle due to the discrete wavelengths of the light used. Multiple-LED chip requirements make this approach relatively expensive. Obtaining a light source of homogeneous chromaticity represents a challenge because of the different driving currents of the diodes, different behavior towards temperature, and the color degradation because of moisture [14].

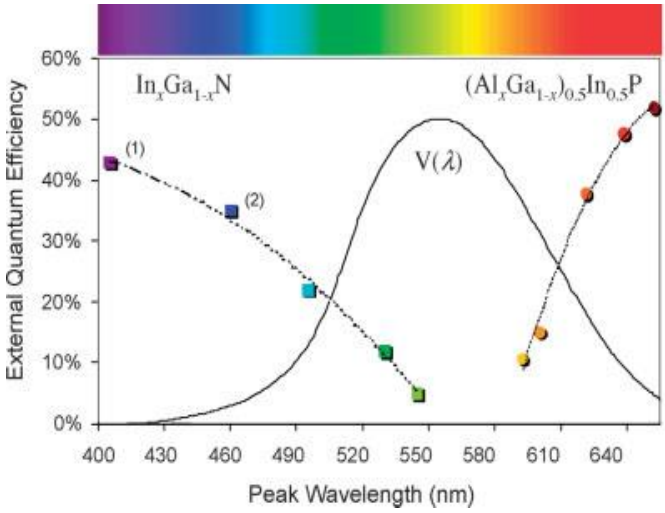

Figure 2.6.: LED Efficiency of LEDs based on InGaN- and AlInGaP-LED over the visible range of wavelength, *V(λ)* is the luminosity function (After Krames et al. 2007)

UV-LED combined to phosphor

The introduction of phosphor presents the advantage of broadening the emission band. An LED emitting UV radiation is used as the excitation source for blue, green and red phosphors. These phosphors which are excitable in the UV are already known from the cold cathode lamps based on the same principle. The LED has a high energy level because of the short wavelength. Owing to the emission in the UV not increasing the luminous flux, the optical power is therefore lower than the emitted power. The UV emission corresponds to the exciting light source but does not contribute to the visible light output.

Blue LED and yellow phosphor

For this technique a blue LED of high emission power is combined with a yellow phosphor of broad emission, typically a YAG:Ce phosphor. Yttrium atoms can be substituted by Gadolinium for example in order to shift the down conversion and tune the cold white light produced. White light of daylight color temperature (CCT $>$ 4000 K) and moderate color rendering (CRI 70) can be reached. These PC-LEDs find many applications where color quality is not a key requirement, including backlights for portable displays, indicators and street lights. This technology only requires one LED chip emitting in the visible. In addition, the phosphor efficiency is high. This gives this approach a good efficiency. Recent

results reported that a one-chip high-power white LED was significantly enhanced, to 203 lm at 350 mA with a luminous efficacy of 183 lm/W [9]. Because the only two constituting elements of PC-LEDs are easy to adapt to each other, they are cheaper than RGB systems. However about 40 % of the electrical power is transformed into optical power.

Blue LED and phosphor mixture

The issue of color rendering can be solved by increasing the number of phosphors mixed. A single LED chip peaking in the blue excites the phosphor mixture (usually green and red) emitting at longer wavelengths. The aim is to complete the PC-LED emission spectrum with phosphors in order to approach the blackbody radiation for the target CCT. Adding a red component fulfills the emission deficiency around 600-650 nm ascribed to the sole presence of YAG. This enables the increase in color quality values in red tones (R_9) and the production of warm white illumination. Nevertheless as we will explain later, the interaction between phosphors is an important factor that must be taken into consideration.

Solid state sources present the major benefit to generate light with high efficiency, resulting in important energy savings. Also potentially huge environmental advantages are emerging from the efficiency and durability of solid-state emitters. Furthermore solid-state emitters allow one to control the emission properties with much higher precision. This approach permits to custom-tailor the emission properties for specific applications [13]. The lifetime of these light sources is high and the decrease in efficiency is only moderate but monotone. LEDs can theoretically work tenth thousand hours under perfect conditions. However, the LED chip is very sensitive to many kinds of damage such as electrostatic discharge, moisture, high temperature, chemical oxidation, and shock [15]. Therefore packaging is a determinant consideration and key factor in order to realize the low-cost industrial commercialization of these lab achievements. LED housing protects the chips from these damages. Packaging also enhances light extraction so that it enables high luminous flux to be reached and dissipates generated heat from the chip to increase reliability and lifetime [16]. The U.S. DOE has set a 2015 efficacy target of 138 lm/W for warm white packages, a significant technical advance that would lead to SSL market penetration in many more lighting product segments [12].

2.4 Economic impact of lighting systems

Today, 18% of the total electric energy consumption is consumed by lighting applications [3]. This field therefore presents enormous potential to reduce electricity consumption and save energy by using more efficient light sources. LED technology exhibits the required quality to impose itself as leader for general lighting [17]. The purchasing price remains high however. Improvements have to be realized to educate consumers as well as the lighting community about the apprehension to invest more for LED lighting but with higher energy saving potentials and longer lifetimes. This would definitely increase the acceptance of LEDs on the lighting markets.

The cost of LED lighting products varies greatly. High quality products and sophisticated design are provided at premium cost. Though, the cost of the production for LED devices has decreased dramatically using scaling effect in recent years, mainly due to the introduction of LED technology for the production of high-definition televisions [18].

In order to understand the economic viability of LED lighting, it is important to consider the two main cost drivers, i.e. the total energy consumption and the cost of purchasing LED devices over time.

Considering these factors enables the user to analyze the total costs and compare LEDs to the traditional compact fluorescent or halogen lamps, and shows the advantages of the alternative LED technology. White LEDs can reach lifetimes of 100,000 hours [19]. This corresponds to 11.4 years of continuous operation, or 22.8 years at 50 % usage. These long life LED lamps thus possess 20 times the life span of an average halogen lamp with about 5,000 hours.

A sample calculation for total cost over the life span including lamp characteristics, energy consumption and operating costs is listed in Table 2.1, comparing LED, fluorescent and halogen lamps. Based on the usage on 100,000 hours, the data reveals the true cost of a light source, which corresponds to the energy consumption but also the cost and time of replacement.

Savings are significant, especially when a large number of lamps is installed. When it comes to office buildings and skyscrapers, maintenance and replacement of incandescent and fluorescent bulbs can be enormous.

Table 2.1.: Characteristics for evaluating costs of LED, compact fluorescent lamps (CFL) and halogen tungsten light source. Based on [19] with extended calculations.

	LED	**CFL**	**Halogen**
Lifespan / hours	100,000	10,000	5,000
Number of bulbs needed for 100 k hrs use	1	10	20
replacement cycle (at 50 % usage) / years	22.8	2.3	1.1
Cost per bulb / $	53	9	4
Cost for bulbs equivalent to 100k hrs use / $	53	90	75
Cost of replacement per bulb (5 min labor @ 3.75 $) / $	-	34	71
Watts per bulb (equivalent to 50 W lumination)	10	16	50
kWh used per year at 50 % usage	44	70	219
kWh used over 100k hrs	1,000	1,600	5,000
Cost of electricity per year (@ $0.21/kWh) / $	9	15	46
Cost of electricity over 100k hrs (@ $0.21/kWh) / $	210	336	1,050
Total cost per light for 100k hrs use / $	**263**	**460**	**1,196**

For the prior calculated total cost per light source, the operational lifetime was assumed to be exactly 100,000 hours or 22.8 years at 50 %usage. To calculate the break-even point in cost for the LED lamp with fluorescent and halogen lamp respectively, the duration is now considered to be variable, i.e. the cost is drawn as a function of the duration in Fig. 2.7. The calculation is based on the data of Table 2.1 for one light bulb and 50 % usage respectively.

The graph clearly shows the all-time high cost of halogen and the sharp decrease of cost for LED after its initial high upfront cost for one LED unit. Over time, fluorescent and halogen lamps both account for higher energy consumption and thus higher running cost as well as replacement costs. The break-even point of LED and halogen lamp is calculated to 1.1 years, i.e. when operating only 1.1 years or less, the halogen lamp costs less than the LED including

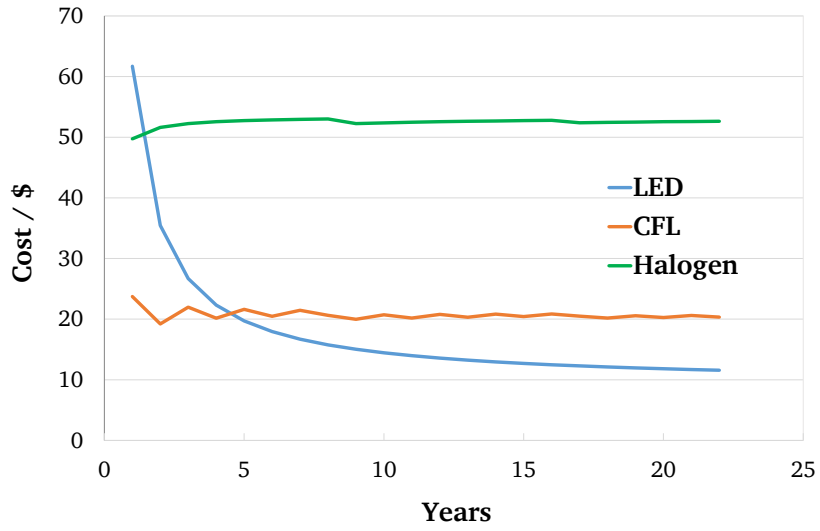

Figure 2.7.: Average total cost per years operated for LED, CFL and halogen lamp. Plotted using data of Table 2.1

initial investment and operating costs. Similarly the fluorescent lamp is less expensive for an operation duration of 4.6 years or below and costs more than LED lights beyond 4.6 years.

LED lighting is therefore appropriate to not only reduce power consumption but also to save money over the life of the source, even at higher cost per bulb at the initial stage. Furthermore, the ability to dim and instantly control the light level and color temperature using LED technology combined with an intelligent lighting system offers even greater levels of energy saving potential, far beyond that of any conventional technology [19].

2.5 Actual research situation on phosphor-converted LEDs

A preliminary study of the status of advances for the main topics of this study, namely in the field of PC-LED is presented in this section. The latest techniques and research done in the area of PC-LEDs and their composing elements (blue LED chip, phosphors and binder) are summarized. Research gaps could be identified concerning some interaction aspects between LEDs and phosphors or the influence of phosphor physical properties on LEDs, which justify the choice of the investigated topics in this PhD dissertation. Recent literature is detailed concerning the phosphor, its impact on a PC-LED, the role of the binder and the simulation of PC-LED systems.

2.5.1 Role of the phosphor in the LED

This section describes the principal characteristics of phosphors: their synthesis, chemical composition resulting in specific electronic transitions and how to influence their emission. The major phosphor groups are presented and the phosphors used in this study are pointed out.

Phosphor synthesis

The synthesis method of phosphors plays a significant role in determining the microstructure, luminescence properties, and quantum efficiency of phosphors. Solid-state reaction corresponds to the conventional process using powdered raw materials as the starting materials (see Fig. 2.8). Due to their relatively rough grains, these phosphors require a quite high sintering temperature to obtain phosphors with designed compositions and desired performance [20]. The particle size distribution is not controlled and the synthesis must take place under specific atmospheric conditions. At high temperature, e.g. at 1500°C, the solid-state reaction and combustion methods are preferred for high luminescence intensity though large irregular particles are obtained [21].

To reduce the sintering temperature, it is necessary to use powders of phosphor compounds with a very small grain size and a narrow size distribution. For this purpose, phosphor raw materials are prepared by various wet-chemistry methods, including among others hydrothermal synthesis, chemical co-precipitation, sol–gel process [22] or combustion synthesis [23], resulting in premixed phase precursor before firing (Fig. 2.8). The phosphors used for this study are synthesized by co-precipitation, wet chemical method.

The firing temperature often is a little below the melting temperature of the host material. If that is impractical because of excessively high-melting temperatures of the host material, the crystallization is facilitated at lower temperatures by addition of a “flux” (frequently a halide) to the premixed phase before firing [24]. The flux plays an important role in improving crystallinity and enhancing grain growth. It contributes to control the morphology and size of phosphors. The addition of a flux improves the luminescence intensity and reduces the reaction temperature of fluorescent materials. The stability of the moisture content and the emission intensity is increased as well [25].

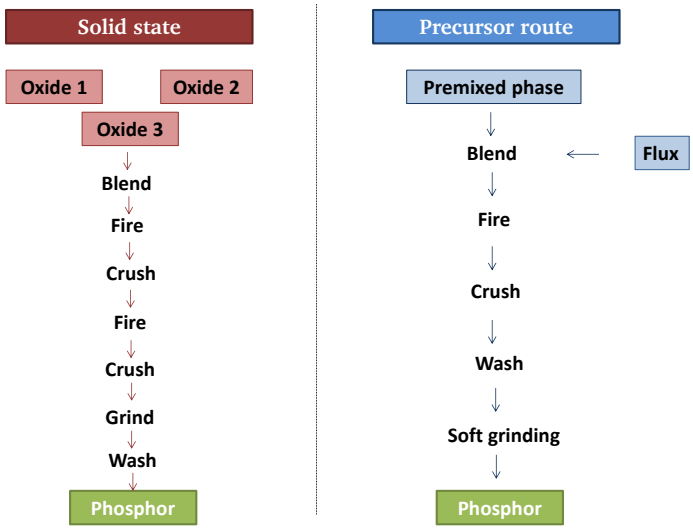

Figure 2.8.: Phosphor synthesis route: Solid state reaction and wet chemical with precursors

Although significant progress has been achieved, phosphor synthesis methods are affected by procedure constraints to respect. It may become necessary to conduct the experiment in dry boxes or clean rooms because of moisture sensitivity. Increasing the sintering temperature could promote the luminescence intensity because it improves the crystallization of YAG particles and favors the doping of activator ions into the host lattice. Red shifting happens

in the activator emission from the products derived from the combustion method and solid-state reaction compared with those from sol–gel and co-precipitation methods because the smaller particles obtained by sol–gel and co-precipitation methods have a higher surface tension than those of the bulk derived by the combustion method and solid-state reaction [21].

Phosphor composition

Phosphors consist of a transparent crystalline host lattice in which ions are substituted by luminescent centers named activators. The presence of a co-activator may be necessary to generate the luminescence of the activator. Both activators and possible co-activators are inserted into the host crystal during the sintering process of the synthesis at elevated temperatures, the firing [24]. The luminescence processes of a phosphor can be divided into two parts, one related to the host and the other occurring around and within the activator. Hence these two elements are essential for the choice of the phosphors chemical composition [26]. The host lattice must be optically transparent not to absorb the activator excitation and emission.

The activator cation must be appropriately chosen for the design of high efficiency phosphors. This latter must be optically active and have a large energy gap between emitting and ground state in its crystalline environment in order to generate photons. The activator must be able to absorb energy to produce a radiative transition without dissipating it. The host lattice must match with the activator's concerning energy level conditions. The valence state of the introduced activator must be easily established and stable at the risk of losing its luminescent properties [27].

The activators perturb the band structure by inserting local quantum states located between the band gap. The major radiative mechanism in extrinsic luminescence occurs by electron-hole recombination. This is possible by transitions from conduction band to acceptor state, donor state to valance band or donor state to acceptor state. It may happen that the transition is localized on the activator atom center. In any case, two selection rules have to be met:

- Parity selection rule: for an allowed optical transition, the electric dipole moment has to change during the transition. If not, the transition is parity forbidden. (Allowed: $\Delta l = \pm 1$).
- Spin selection rule: for an allowed optical transition there is no 'flip' of the electron spin. If there is, the transition is spin-forbidden. (Allowed: $\Delta S = 0$).

Selection rules can be 'by-passed' by mixing of states to make 'forbidden' transitions slightly allowed. Forbidden transitions still may take place, however much more slower, resulting in photon release times of milliseconds to seconds rather than nanoseconds for allowed transitions. It is important to notice that practical phosphors having atomic luminescent centers often release photons via 'forbidden' transitions. The surrounding atoms in a crystal may lift the restrictions of ideal selection rules because they lower the symmetry of atomic states [11].

The example of Ce^{3+} energy levels in a $Y_{3-x}Al_5O_{12}{:}Ce_x^{3+}$ (YAG) structure, used in this study is represented in Fig. 2.9. Ce^{3+} has only one electron in the 4f state. An energy of 50,000 cm^{-1} (6.2 eV) is necessary for Ce^{3+} as free ion to pass from the $4f^1$ state to the $4f^0\ 5d^1$ excited state. Inserted in a host lattice, some electrons of the host lattice move into the orbitals

of the central ion and reduce the cationic valency. Due to the expansion of the electron cloud, the distance between electrons increases, reducing the interaction between them. This effect called the nephelauxetic effect reduces the excited energy level of Ce^{3+} in YAG. The electromagnetic interaction between Ce^{3+} and its environment (crystal field) decreases once again the excitation energy. The ground state of Ce^{3+} is split into $^2F_{7/2}$ and $^2F_{5/2}$ with an energy difference of about 2200 cm^{-1} [28], see Fig. 2.9. 4f-5d transitions are parity and spin allowed. The 5d state is split by crystal field and, hence, there are three Ce^{3+} absorption bands in the excitation spectrum located in the UV and visible at 340 and 460 nm [29]. Both the asymmetry and the position of this band vary, depending on the Ce^{3+} concentration, though the center of the peak is usually around 550 nm [30]. The broad emission band centered at 532 nm arises after Stokes shift (difference between the energy of absorption (higher) and emission (lower, thus longer wavelength)) from the combination of the lowest energy of 5d bands and the 4f states (580 nm and 520 nm) [31].

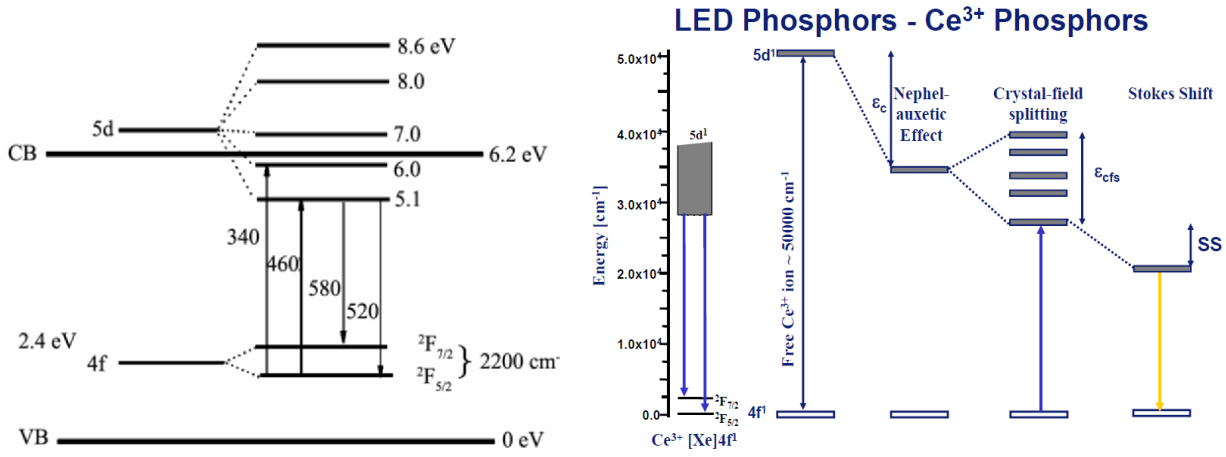

Figure 2.9.: Energy level scheme of Ce^{3+} and in $Y_3Al_5O_{12}$ (YAG) host lattice on the left after [31], on the right after [32]

Phosphor color emission tuning

Depending on the host lattice into which they are inserted, activator's energy levels and transitions are changed. Luminescent centers show emission and excitation spectra shifted over wavelengths. The emission color can therefore be tuned. The coupling to the lattice has to be taken into consideration for many transition metal ions: for the s^2 ions and for rare-earth ions showing d-f emission [33]. The covalency, crystal field and symmetry of the host lattice are determinant factors.

Increasing the covalence of the activator ligand bond reduces the interaction between the electrons since they spread out over wider orbitals. The electronic transitions between energy levels shift to lower energy with increasing covalency (nephelauxetic effect). High covalency also induces a reduction of the electronegativity difference between the constituting ions [34]. Hence the charge transfer transitions between these ions shift to lower energy.

The influence of the surroundings is also of great importance. Activator ions occupying a small sized site induce a strong crystal field and strong transitions at high energy. The different symmetry of the crystallographic sites occupied by the activators contributes to

inhomogeneity broadening. Optical transitions can therefore occur at a slightly different energy at the surface in comparison to in the bulk.

Photoluminescent (PL) characteristics can be tuned by varying the chemical composition of the activator. The structure of the host lattice has an influence on the luminescence and also determines the stability of the phosphor. The dopant, its nature, concentration and combination with other dopants play a very important role as well. Empirical observations in garnet structures [11],[20] indicate that increasing the size of the dodecahedron ion (Y^{3+}) or decreasing the size of the octahedron ion (Al^{3+}) increases the splitting of the crystal field and shifts the Ce^{3+} emission towards longer wavelengths [35]. This empirical rule is validated by Wu et al. [36]. They report that reducing the substitution of Ga in $Y_3(Al,Ga)_5O_{12}$:Ce [20] which decreases the lattice constant, corresponds to an increase of the ratio d_{88}/d_{81} (distance of two oxygen-oxygen bonds in the dodecahedra structure). This implies a compression of the cubic polyhedron [36] and shifts the emission and excitation to longer wavelengths.

Type of phosphors

A wide array of phosphor materials has been developed over the years. Depending on their application and more specifically the excitation source (UV or visible), phosphors must meet different requirements concerning their excitation spectra. Their emission can be optimized by their chemical composition. Phosphors can also be distinguished by their type of host lattice. Garnet structures, silicates or orthosilicates mainly emitting in the green or yellow [20], exhibit high luminescence but low color rendering and low thermal stability [25]. Sulfides can emit from deep blue to red [20]. However they present the important drawback of being very sensitive to water which leads to the production of H_2S. This volatile and reactive product diffuses to other LED components, for example to the Ag mirror, where it converts Ag into black Ag_2S. A dense particle coating would prevent the diffusion of water towards the phosphor surface. Although this measure is sufficient to obtain usable LED phosphors with the composition $(Sr_{1-x}Ca_x)S$:Eu, the thiogallates such as $SrGa_2S_4$:Eu are still not applied in LEDs, since they exhibit pronounced thermal quenching. The luminescence of the green-emitting thiogallate is strongly quenched with increasing temperature, i.e. its quantum efficiency (ratio of the emitted and absorbed photons) is reduced by 50 % at 170°C [33]. Great efforts have been made to develop blue, yellow, green and red silicon based nitride phosphors. Covalent ternary, quaternary or more covalent nitride compounds allow activator sites and are suitable for white LED (WLED) applications. 5d excited states of rare earth dopants decrease in silicon nitride lattices because of large crystal field splitting and a strong nephelauxetic effect. The emission color of rare-earth ions (Eu^{2+}, Ce^{3+}, Yb^{2+}) depends strongly on the surrounding environment including symmetry, coordination, covalence, bond length, site size and the crystal field strength in which they reside. Emission wavelength is then able to be tuned over a wide range. Nitride phosphors have high thermal stability but low efficiency [25]. However, restrictive synthesis conditions have to be respected. The synthesis can be realized by solid state reaction, gas reduction or nitridation. This must in any case occur under nitrogen atmosphere [37].

The most important phosphors for LED application are gathered in table 2.2, classified by emitting color and type of host lattice. The activator determines the color of the emission depending on, as already demonstrated, the activator surrounding [38].

Phosphors used for the PC-LED investigations of this study are $Y_3Al_5O_{12}:Ce^{3+}$ (YAG:Ce), $Lu_3Al_5O_{12}:Ce^{3+}$, $(Ba,Sr)_2SiO_4$:Eu and nitrides. The two former phosphors emit in the yellow

Table 2.2.: Phosphor used with blue exciting LED

Phosphor Color	Chemical Composition	Host lattice type
green phosphors	$(Y,Lu)_3(Al,Ga)_5O_{12}:Ce^{3+}$	garnet
	$SrGa_2S_4:Eu^{2+}$	thiogallate
	$(Ba,Sr)_2SiO_4:Eu^{2+}$	orthosilicate
	β-SiAlON:Eu^{2+}	silicon nitride
	$(Sr,Ba)Si_2O_2N_2:Eu^{2+}$	silicon oxynitride
yellow phosphor	$(Y,Gd)_3Al_5O_{12}:Ce^{3+}$	garnet
	$Tb_3Al_5O_{12}:Ce^{3+}$	garnet
	$(Sr,Ca,Ba)_2SiO_4:Eu^{2+}$	orthosilicate
red phosphor	$(Sr,Ca)S:Eu^{2+}$	sulfide
	$(Ca,Sr)_2Si_5N_8:Eu^{2+}$	silicon nitride
	$(Sr,Ba)_3SiO_5:Eu^{2+}$	silicon oxynitride

and green and have cubical garnet structures. The example of YAG is represented in Fig. 2.10. The refractive indices of YAG:Ce and LuAG:Ce are 1.8 and a density of 5.65 g/cm^3 and 6.2 g/cm^3 respectively. The orthosilicate is a green emitter material with a refractive index of 1.7 and density of 5.17 g/cm^3 in an orthorhombic crystal system. The red phosphors are research material which composition remains confidential.

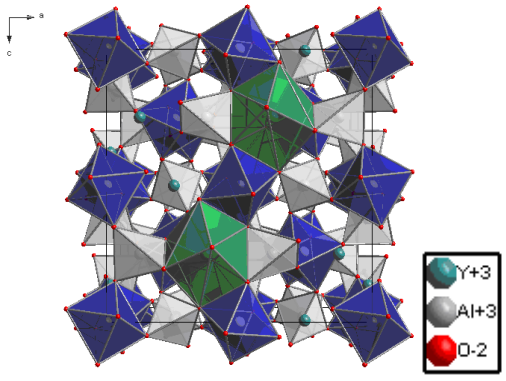

Figure 2.10.: Crystalline structure of garnet phosphor $Y_3Al_5O_{12}$ after [39]

2.5.2 Influence of the encapsulant on the LED

Phosphor particles are mixed with an encapsulant before being dispensed on the LED chip. The encapsulant plays several roles. It enhances the light extraction with a better refractive index and creates an index gradient between the LED chip and the air. Patent [40] has been published claiming higher efficiency for encapsulant of high refractive index ($n = 1.7$). Indeed Snellius' law predicts the angle direction change at the interface between two media (eq. 2.18).

$$n_1 sin(i_1) = n_2 sin(i_2) \tag{2.18}$$

with n_1, n_2 refractive indices and i_1, i_2 incident and refraction angles of the rays in the encapsulant and air, respectively.

Due to the difference in refractive index between the chip and the air, the total reflection is a limiting factor influencing the best light extraction. Rays emitted from the chip are plotted in Fig. 2.11. Light can be extracted from the semiconductor's chip having a refractive index of 3.5 and the air (n=1) only for angles between 0° and 17° before total reflection. When a layer of binder with a refractive index of 1.5 is implemented on the top of the LED chip, the maximal outcoming angle possible to be transmitted at the first interface is increased to 25° and from the binder to the air the angle can be up to 42° until the total reflection is active. The encapsulant medium also prevents from moisture which causes the corrosion of the chip, any shock, contaminant or hostile environment [41].

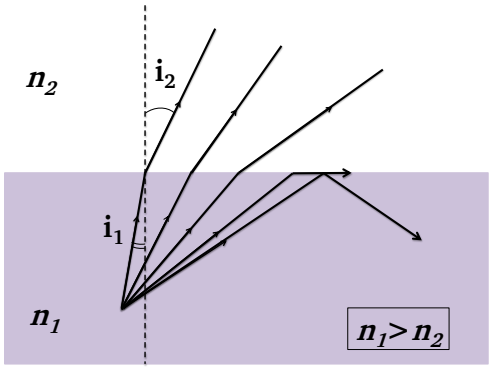

Figure 2.11.: Scheme of the total reflection process due to a change in refractive index at an interface

However several challenges are associated with the choice of the encapsulant. The encapsulant may degrade under thermal conditions and absorb the emitted radiation which deteriorates the light output [42]. Stirring the phosphor and silicone binder mixture introduces bubbles despite removing the air by vacuum treatment. The high viscosity of the silicone binder makes it extremely difficult to completely remove all bubbles. During the curing process these bubbles expand and flow to the top of the silicone layer. Moisture can penetrate into the bubbles and reduce the light efficiency. Constrained by the adhesion strength and affected by any impurities, an initial crack will emerge when the concentrated stress cannot be relieved. During use of the LEDs, the initial crack will grow and expand and delamination can occur when heat or force is loaded [15]. Current and temperature stresses induce yellowing and cracking of the encapsulant [43]. These harmful effects reduce the light extraction as well.

Improved silicone binders have been developed to attenuate these issues. High technical encapsulant can reach a refractive index of 1.64 with 88 % transparency in the visible and long lasting thermal stability [44]. This corresponds to a 14 % better light efficiency extraction than conventional epoxy. Good encapsulants should have

- high thermal stability,
- low moisture absorption,
- high transparency,
- and high refractive index.

This medium should also exhibit a coefficient of thermal expansion that matches the substrate at the risk of shrinkage or internal stress. One suitable material is silicone binder formulated as a "molecular hybrid" between glass and organic linear polymers. Hence this type of silicone binder, polysiloxane, combines the hard and brittle properties of silica and the softness and flexibility of silicone polymers. Its properties can be adjusted by changing the crosslink density and the ratio of linear to branched silicon species. The functional groups can be adapted to also reach a high viscosity, which is useful for slowing down the sedimentation process of the phosphor particles. This settling challenge can also be solved by the use of a jetting dispensing process [45]. Silicones can be cured by platinum catalysed addition [42]. The binder is prepared in two parts, Part A usually contains the platinum catalyst and Part B the hybrid functionalized siloxane.

2.5.3 Status of actual phosphor-converted LED advances

Better light output can be achieved by improving the blue LED chip. LED's technologies have been developed to enhance light extraction. These developments have taken place in the material composition related to the refractive index [46], and the choice of dopant or surface treatment. The latter can involve the roughening of the top surface of the LED [15] or metalization of the LED backside. These processes transform the LED surfaces in order to raise the extracting cone of the light. The total internal reflection can be optimized to occur at higher angles. Stefanov et al. reported a light extraction increase of 11 % and 24 % by metalizing the backside of a rough and of a polished LED backside respectively [47]. Improving the design the LED sidewalls also increases the light extraction [3]. The influence of surface roughening, first introduced by Bergh and Saul contributes to the light extraction efficiency [48].

The introduction of the phosphor layer on the top of the blue LED plays a considerable role for the optical properties. The reflection on the phosphor particles induces an additional source of light extraction loss. A simulation was performed on a YAG film illuminated by a blue LED positioned in one case on the same side as the detector, to measure the reflection, and in another case the detector is placed behind the phosphor film to estimate the transmission. Results showed a reflection 1.5 times higher than the transmission [49]. A study carried out on measurements with a double integrating sphere [50] showed that the blue emission is transmitted to 85 % by the phosphor film and reflected to 15 %. In contrast, yellow light projected on the phosphor layer is transmitted to 75 % and reflected to 25 %.

These results show the importance of considering the optical properties of the phosphor in order to understand and influence the mechanisms of a PC-LED. Phosphor concentration is a relevant parameter influencing the color of the PC-LEDs but also having repercussions on their efficiencies. The impact of the phosphor concentration (quantity of phosphor particles in the volume of binder) on the LEDs has been studied by simulation. The quantity of YAG necessary to reach cool white LEDs is found to result in high luminous efficacy for low phosphor concentration so that light trapping remains low but on a thick layer in order to still reach the phosphor particle number necessary to achieve the target CCT [51]. A simulation on two phosphor layers of different concentrations revealed a reduction of the LED power by increasing the phosphor concentration in the layer closest to the LED chip because of the probable backscattering and absorption of the light by the chip. Higher power can be obtained at constant CCT by increasing the phosphor concentration in the phosphor layer more distant from the chip [52]. Liu et al. demonstrated that the luminous efficiency

increases with the phosphor concentration until a certain value because of the increase of the phosphor emission close to the standard luminosity function $V(\lambda)$ [50]. The efficiency then drops because of the phosphor re-absorption [53]. Phosphor concentration has been investigated as well on YAG ceramic PC-LEDs. It was also found that phosphor ceramic thickness increases the yellow emission and reduces the blue one by absorption. Highly concentrated PC-LEDs reach phosphor emission saturation. These conclusions confirm the results obtained for PC-LEDs made of phosphor in powder state [54].

Phosphor dispensing techniques

After measuring the phosphor reflection and transmission properties, it is obvious that the distribution of phosphor particles in the silicone binder layer plays an important role in enhancing LED efficiency. It is possible to take profit of the optical properties in order to better control the PC-LED efficiency. Four phosphor configurations are developed:

- conformal, Fig. 2.12a
- remote phosphor, Fig. 2.12b
- enhanced light extraction by internal reflection (ELiXIR), Fig. 2.12c
- conventional or in cup, Fig. 2.12d.

A thin phosphor layer is deposited on the LED chip recovered by the silicone binder corresponds to the conformal coating technique. Remote phosphor configuration consists in moving away the phosphor layer from the chip, leaving a transparent medium between the die and the phosphor [55]. Enhanced light extraction by internal reflection (ELiXIR) PC-LED utilizes a semitransparent rather than diffuse phosphor layer that is separated from the chip by an air gap. The phosphor coating is called conventional or in cup when phosphor particles are spread out homogeneously in the binder layer directly in contact with the LED chip.

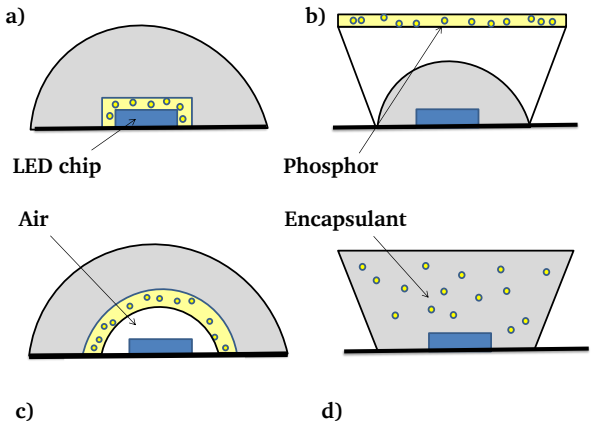

Figure 2.12.: Scheme of all possible coating configurations a) conformal coating, b) remote phosphor, c) enhanced light extraction by internal reflection (ELiXIR), d) conventional coating

The work of Narendran has shown by simulation that conventional coating causes 12 % of the light to be reflected back to the die with more than 25 % lost between phosphor, reflector cup and the die. An experimental set-up made of two integrating spheres [56] measured

53 % of light reflected to the die and 47 % transmitted. ZHU et al. concluded that though placed at a remote location, still 60 % of the light is directed back to the die. This remote technology was patented [57], [58] and developed by Chen in 1999, Duggal in 2001, Reeh in 2003 and Duclos in 2003. The concept of Scattered Photon Extraction (SPE) optimizes the light extraction by surrounding the LED die by a lens reshaped to extract a significant portion of the back-transferred light before it is absorbed and lost within the package (Fig. 2.12 b) [59], [60]. Improvement of 60 % in light output and efficient extraction of back transferred light could be reached compared to commercial conventional coated WLED.

The influence of a cap, convex or hemispherical cup made of encapsulant n=1.6 on the top of a remote phosphor or conformal coating was investigated. The LED performance is described in combination with the use of a diffuse or specular cup. Simulation results identify the remote phosphor arrangement with a hemispherical cap in a diffuse reflector as the highest extraction efficiency light source. A hemispherical cap and diffuse reflector contribute to increase the total internal reflection angle. A remote phosphor reduces the absorption of the light output by the LED chip [61]. The improvement of the light output with the help of a cap on the top of the PC-LED is confirmed by LIN et al. [41].

Remote phosphor presents the advantage of increasing the light extraction. The angular homogeneity though shows a yellow ring effect due to the longer path to the outer perimeter of the package and thus more phosphor conversion. Patterned remote phosphor [62] consists in a regular remote phosphor configuration from which the phosphor has been coated by pulsed spray [63] with a circular shaped mask. Patterned remote phosphor decreases slightly the luminous efficiency, but improves considerably the angular color homogeneity. LIU et al. validate as well the highest quality concerning efficiency and color quality of remote phosphor systems, particularly hemispherical remote phosphor towards conformal coating [64].

ALLEN and STECKL suggest that the ELiXIR luminaire also remedies the yellow ring effect. It consists of a blue LED located at the center of a hemispherical polymethyl methacrylate (PMMA) shell with an interior phosphor coating composed of a fluorescent dye dispersed in a modified PMMA matrix. This technology nearly eliminates phosphor emission and LED reflection back into the LED chip by separating the chip and phosphor and reduces the number of mirror reflections by use of internal reflection at the air/phosphor layer interface [65].

Impact of the phosphor particle size on the phosphor-converted LED

The influence of phosphor particle sizes on the PC-LED properties has been studied. It has been reported that increasing the YAG:Ce phosphor particle size implies an increasing phosphor concentration to reach the target CCT [66], without specifying the orgin of this phenomenon. Luminous flux increases as well with the phosphor particle sizes imputed according to HUANG et al. to the better crystallinity of large particles and defects on the surface of small phosphor particles [67]. This investigation has been carried out on three phosphors of different manufacturer and efficiency [68], and on four samples having broad particle size distribution (PSD) and not optimized synthesis resulting in non-spherical morphology [67]. Simulations computed that 2 μm diameter phosphors present the lowest luminous flux and particles larger than 10 μm generate high luminous flux. Complementary HU et al. suggested high luminous flux for particle size from 6 to 8 μm [69].

A comparison between YAG and TAG-based PC-LED simply affirmed a 15-20 % enhancement of the LED efficiency by use of narrow PSD [70].

A combination simulation study about phosphor coating configuration and phosphor particle size is presented. TRAN and SHI reported that the best lumen output is reached for 4000 K and for particles 20 μm diameter in case of in cup LEDs. LEDs efficiencies based on phosphor particles from 50 nm to 50 μm exhibit low trapping efficiency for nanoparticles or particles of size around the wavelength of light. Remote phosphor LEDs show highest luminous flux for 20 μm particle size. The latter have higher luminous flux values than in cup LEDs and are less dependent on the particle size than the in cup configuration.

With increasing phosphor particles, rays are more scattered in the horizontal direction and less in the backward direction. This study also demonstrated that an increase in phosphor particle size implies a higher phosphor concentration [71]. SHUAI et al. considered the simulation of phosphor particle size on luminous efficacy for three phosphor configurations: remote phosphor, conformal coating and conventional dispensing. Independent of the phosphor particle size, a remote phosphor configuration is better than in cup, which is better than conformal coating. The trend concerning the particle size and the LED light output is once again validated. Lowest luminous flux is found for phosphor particles of 0.8 μm and highest luminous flux for phosphor of 20 μm [72].

Simulations were also conducted for different silicone refractive indexes in combination with the influence on the phosphor particle sizes (3, 7.8 and 12 μm). For the same color coordinates, it is confirmed that particles of increasing size require higher phosphor concentration. Besides the phosphor concentration is also dependent on the binder refractive index. Radiant flux is the highest for larger particles. However the refractive index match plays a role between phosphor and binder. If the refractive index of phosphor and binder coincide this leads to a radiant flux maximum independent of the phosphor particle size. Nevertheless simulated differences of radiant fluxes would not be able to be demonstrated experimentally because of the small deviations computed compared to usual variability measurements [73].

The control of the phosphor particle size is a serious issue. It has an impact on the phosphor concentration and exhibits improvement potentials on the LED radiant flux. However practical considerations in the silicone binder slurry must not be neglected. Sedimentation of phosphor particles are simply caused by gravity. Due to heavier TAG:Ce phosphor particles, the phosphor concentration profile in the PC-LED changes, particles homogeneously in suspension in the slurry settle on the LED chip and reduce the efficiency expected from the promising photoluminescent (PL) results [74]. A contradictory study confirmed this sedimentation phenomenon but unfortunately did not mention any information about the phosphor particle size. A simulation related to this effect did not refer to changes in the light extraction efficiency, CCT or angular color uniformity [69]. An alternative method to coat the LED is by pulsed spray [63]. This method enhances the luminous efficacy by 8 % and enhances the angular color uniformity.

Angular homogeneity of phosphor-converted LEDs

The major work conducted on color angular homogeneity has been researched by SOMMER et al. by simulation using the software ASAP. The variation of chromaticity over the angles

is either phosphor layer height or concentration dependent [75]. By increasing the phosphor layer height or the phosphor concentration, the angular chromaticity first exhibits high variation between the center of the LED and the periphery. An LED emission showing the chromaticity distribution is represented in Fig. 2.13.

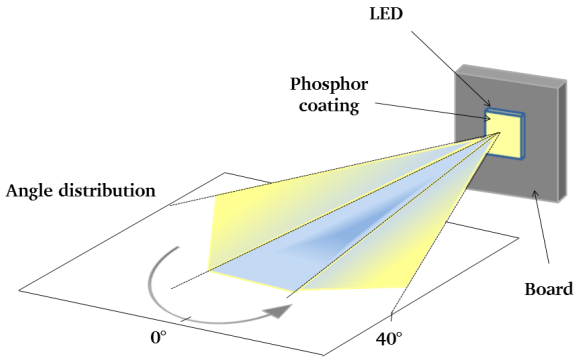

Figure 2.13.: Chromaticity distribution of a PC-LED

The chromaticity distribution is at wide angle yellowish because of the presence of more phosphor particles situated on the way path of the blue rays emitted at 40° for example than in the 0° direction. When the phosphor layer height increases at constant phosphor concentration, the number of phosphor particles on the path way of the blue ray at wide angle decreases, thus the chromaticity has a more constant behavior over the angles. A further study presents results highlighting the impact of phosphor particle size on the color coordinates spatial distribution of PC-LEDs [76]. Simulations demonstrate that constant color coordinates over the angles are obtained for increasing phosphor particle size by increasing the height of phosphor layer at constant concentration or by increasing the phosphor concentration. These conclusions agree with the results of the previous section 2.5.3 and complete these results which unfortunately did not consider the angular homogeneity of the colors. However the color coordinates treated in [76], reached for the phosphor samples differing by their particle size are varying from x=0.30 to x=0.33. It can be argued that the chosen particle sizes are not realistic to any practical experiment. No particle size distribution can be that mono disperse, meaning diameters can be so closely distinguished (10, 6, 5 and 3 μm).

High extinction coefficients show distortion of the angular color uniformity, blue on the edges, yellow in the middle: absorption takes place in close proximity to the die [77]. Based on extinction and scattering coefficients simulations demonstrated that 2 μm phosphors present the best angular color uniformity. Angular color uniformity deteriorates for particles larger than 10 μm. Moderate angular uniformity is suggested for particle sizes from 6 to 8 μm [78].

Phosphor-converted LEDs based on different phosphors

Single phosphor-converted LEDs are usually realized with YAG:Ce because it offers the possibility to reach cool WLED with high luminous efficiency. However these PC-LEDs suffer from poor color rendering due to the lack of red components. A simple approach developed to overcome this shortcoming is to mix a yellow or green phosphor with a red component.

This can be, for example, realized by an all nitride PC-LED in combination with a blue LED. 2-PC nitride LEDs contribute to enhance the color quality [37]. LEDs based on 3 or 4 nitride phosphors are able to reach color rendering up to 95 [79]. PC-LEDs based on a mixture of four oxynitrides and nitrides successfully achieve color rendering up to 98 on a broad range of CCT with a luminous efficacy of 30 lm/W [80].

Due to the absorption of green or yellow emission by red phosphors, specific phosphor arrangements in the PC-LED must be established to minimize this emission loss. Some combinations of green and red phosphors are presented in Fig. 2.14 a) conventional coating with homogeneous mixture b) remote phosphor with red and green phosphor layers c) and d) conventional coated PC-LED with green and red phosphor layers. The importance of the phosphor particle size even for a mixture of phosphors is demonstrated [66]. Settling of green phosphor induces a green layer on the top of the LED chip whose emission will participate in the excitation of the red phosphor and will be absorbed. The luminous efficiency is hence reduced.

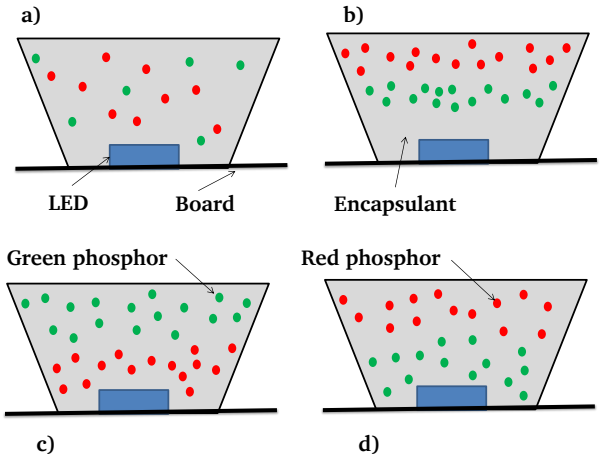

Figure 2.14.: PC-LEDs of different green and red phosphor configurations for white PC-LED. a) conventional coating with homogeneous mixture b) remote phosphor with red and green phosphor layers c) and d) conventional coated PC-LED with green and red phosphor layers

Efficiency of homogeneously mixed yellow and red PC-LED can be increased by a multi layered phosphor configuration. This technique gives the opportunity to increase the luminous flux by 18 % owing to a difference among refractive indices [81] and to reduce the junction temperature due to reduced back reflection [82]. The arrangement of the red and green phosphor layer is of great interest to improve the interactions between phosphors. Several parameters (phosphor quantum efficiency, phosphor coating configuration) must be considered in order to determine the optimal phosphor layer configuration. Simulations on SPE and conventional coating PC-LED revealed better luminous efficiency with a red layer on the top for SPE and the opposite phosphor layer configuration for conventional coating ([56], [81]).

2.5.4 Phosphor-converted LEDs simulation in the literature

LEDs can be simulated by Monte Carlo simulations. They are based on probabilistic methods that involve random events. A statistical approach is applied to create the photons escaping

the light source. Light propagation is described with respect to the optical properties. Incident rays are following the diffuse reflection and transmission laws defined in eq. 2.19, [83].

$$T + R = 1 \tag{2.19}$$

With T the transmission and R reflection coefficients.

Scattering theories enable the description of the photon trajectories. When particle size is smaller or comparable to the wavelength of the light source, Rayleigh or Mie theories respectively predict the behavior of the light [84]. In the case of phosphor particles, optical properties established by Mie should be considered [85]. Rayleigh scattering relationships (eq. 2.20) are generally preferred due to the complexity of the Mie scattering (eq. 2.21). It is then assumed that the particle is sufficiently small so that the particle encounters a uniform electric field at any moment. Within the Rayleigh regime the angular dependence is negligible, in contrary to the Mie regime where forward scattering dominates (Fig. 2.15).

$$I_{scat} = I_0 \left(\frac{1 + cos^2\theta}{2R^2} \right) \left(\frac{2\pi}{\lambda} \right)^4 \left(\frac{n^2 - 1}{n^2 + 2} \right) \left(\frac{d}{2} \right)^6 \tag{2.20}$$

With I_0 incident ray energy, θ scattering angle, R distance from scatterer, n refractive index, d diameter of particle.

The scattering cross section according to Mie theorie is defined as follow:

$$\sigma_{scat} = \frac{\lambda^2}{2\pi} \sum_{n=0}^{\infty} (2n+1)(|a_n|^2 + |b_n|^2) \tag{2.21}$$

With a_n and b_n parameters depending on Ricatti-Bessel function.

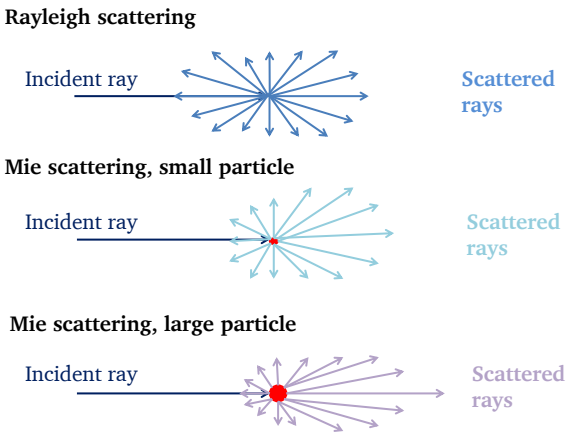

Figure 2.15.: Schematic distributions of rays scattered in Rayleigh regime and Mie regime with small and large particles

The association of light propagation principles and random events deliver a powerful tool to virtually reproduce PC-LEDs. Literature reports about parameters of simulations applied to

phosphor systems. Simulated ratio of blue and yellow power in a silicate PC-LED was demonstrated to fit the measurements [86]. A model based on energy balances also predicts the ratio between blue and yellow emissions ([87], [88]). It was found that measured angular scattering properties correlate with the simulation [89]. However this study presents results of power measurements compared to simulations performed on PC-LED systems made of differing phosphors. Another study pretends to validate the simulations without giving real information about power or chromaticity comparison between measurements and simulations ([90], [91]).

3 Objectives and motivations of the thesis

This chapter demonstrates first the plurality of the vast PC-LED field to explore, before specifying the focus of our study. The topics investigated in this PhD dissertation complete the latest research advances outlined in the previous chapter. The scientific approach in 3.2 details which issues will be treated in this work. The last section of this chapter underlines the singularity of the interdisciplinary methodology developed within this thesis.

3.1 Phosphor-converted influencing factors

LEDs are taking their place as leading lighting source thanks to their numerous advantages. They feature high energy efficiency, long lifetime, energy saving possibilities, environmentally friendly components and easy adaptive design. However they are still a wide domain to be explored. A broad field of investigation which will lead to many further improvements remains to be researched. Therefore all the parameters influencing PC-LEDs are first described. The scheme in Fig. 3.1 gives a first impression of some of the factors for potential new developments.

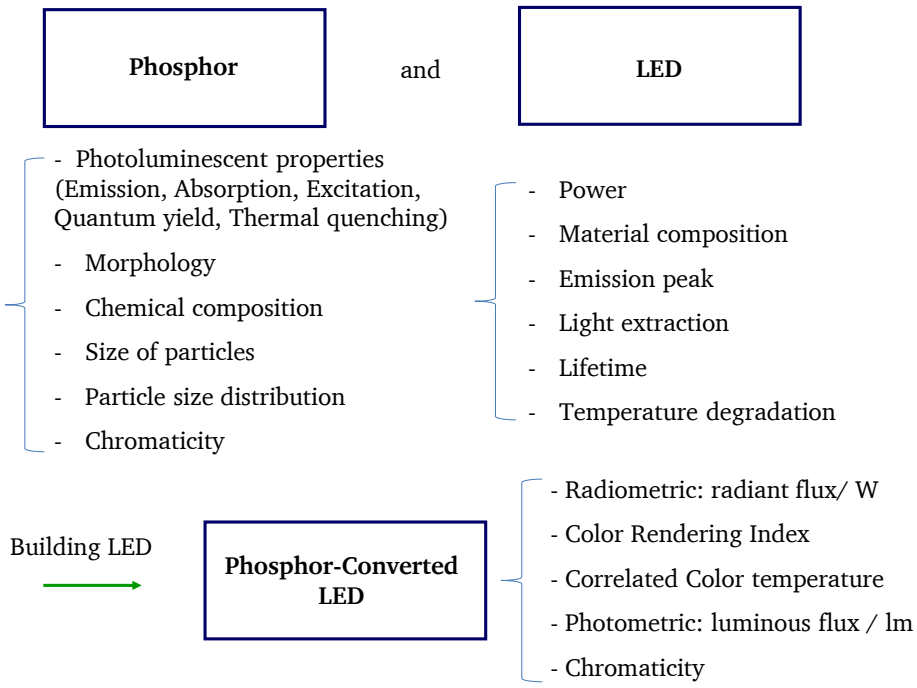

Figure 3.1.: Influencing factors of a phosphor converting system

The excitation source is the fundamental element of an LED. The LED properties can be modulated by the dimension of the die and therefore the power of the LED. This latter itself is governed by the material composition and the light extraction. The choice of the semiconductor determines the emission wavelength. The method used to grow or spread the semiconductor on the board is also a decisive parameter. The surface treatment is another topic of research to enhance the light extraction. The lifetime of the LED and its temperature

degradation are important characteristics of the LEDs also depending on the structure of external optics. All these parameters significantly influence the LED performance.

Phosphor is then dispensed on the top of the LED. The phosphor chemical composition has an impact on its PL properties, its emission wavelength, excitation domain and spectral absorption. The chromaticity and thermal quenching are dependent on the defects present in the phosphor structure. The synthesis route for the phosphor is also of great importance, it particularly gives indications of the physical aspects of the phosphor, namely the morphology of the particles, their size and size distribution.

The technique used to deposit the phosphor on the LED can be diverse, either as powder embedded in a silicone binder, close or decentered from the LED chip or as a ceramic die. The refractive index and absorption coefficients of supplementary components also play a role in the light extraction.

These elements are key aspects of the PC-LEDs characterized by the efficiency and lighting quality. PC-LEDs are defined by their radiometric or photometric values, as well as their color appearance (chromaticity) or CCT and by their color rendering to determine the quality of the emitted light.

PC-LEDs are composed of many different parts able to be modified by a great number of factors. The result is a very complex system. This study is restricted and limited to the influence of the phosphor on the PC-LED properties. The focus of this study is the investigation of the dependence of the physical phosphor particles on the PC-LED properties for the first time in a single phosphor-system PC-LED. A 2-phosphor-system is considered in a second case. The aim of this study is to establish a correlation from experiments between all these parameters in order to possibly predict the PC-LEDs performance characteristics.

3.2 Description of the scientific approach

YAG:Ce is the first phosphor involved in PC-LEDs in order to emit white light since research of Nakamura in 1995. Its synthesis has been developed and can be realized following several routes: mix and fire, wet chemical, and precipitation. It is now well understood and fine synthesis improvements allow the focus to be placed on the morphology of the particles. YAG:Ce phosphor is also a well-known and robust material. For these reasons, this study rests first upon PC-LEDs made of YAG:Ce. The emphasis is placed on the understanding of PC-LEDs' mechanisms and the interaction between all components. One fundamental phosphor parameter influencing the PC-LED properties and efficiency is the phosphor particle size. Previous studies considered this factor. However investigations have been conducted by simulation only and with no direct validation. Studies have also been performed on YAG phosphors with varying particle sizes but from different manufacturers. The efficiencies of the YAGs compared in the publications are not equivalent and the particle size exhibits broad distribution. The influence of the phosphor concentration on the PC-LEDs and their brightness has already been reported [67]. However no investigation has been published characterising the PL properties of the phosphor in the powder state as well as the PC-LEDs properties for phosphor fractions extracted from the same batch with narrow PSD. These are the results presented in this work. The effect of the blue exciting wavelength on the phosphor concentration associated to the influence of the refractive index of the silicone on the LEDs is experimentally investigated.

The stable garnet structure is investigated in the following chapter when Lutetium is introduced in the lattice, implying a shift in the energy levels. Lutetium aluminium oxide activated by Cerium LuAG:Ce, applied as phosphor, emits in green tones. The chemical composition of LuAG:Ce is considered, namely the Cerium activator concentration. This new research consists of studying the influence of the particle size and the Cerium concentration simultaneously. Once again a detailed description of the different phosphor PL properties is provided. The study is based on phosphor application in PC-LEDs and the measurement of their properties. This technique offers the possibility for the first time to compare the phosphor particle sizes for two garnet materials.

Phosphor particle size significantly affects LED emission patterns. In the literature angular distribution investigations are performed only by simulation. Computed results are exploited without comparison to experimental data. Any reference to concrete analyses is missing. Reported results are sometimes not realistic for practical reasons. Phosphor physical parameters as regards sedimentation could not be estimated and are neglected in the simulation. Furthermore very little color variations are mentioned and practically not possible to obtain. PC-LEDs exhibit color deviations owing to uncontrollable experimental impurities and inhomogeneity. The phenomena observed in the previous works show values in the range of experimental deviations. In contrast, this dissertation takes into consideration real PC-LED angular measurements to understand the effect of the particle size on the PC-LED chromaticity.

The focus of this work is not particularly set on the efficacy of LEDs themselves, but on the potential improvements brought by the phosphors. This study is incorporated in the framework of the company Merck KGaA and focuses on economic and industry profitable phosphor research developed for LED applications. The performance of the phosphor itself is most important. The chemical composition is decisive for the phosphor efficiency but their physical properties also influence their performance. Phosphor final application is in the LEDs, that is why it is so critical to test and understand the mechanisms in the LEDs.

PC-LEDs represent a very complex system. Many possible influencing parameters to tune the LED properties exist. Each LED must be experimentally tested. Maintaining every experimental parameter exactly identical is impossible. This leads to variations of the results and induces deviations in the LED properties. A great number of experiments is required in order to demonstrate the influence of one factor. The establishment of a model describing PC-LEDs would enable the prediction of PC-LED behavior. This would also save time and raw materials. Mathematical models fail because comprehension of the physical and optical principles is essential. The simulation software Lighttools considering determinant properties of each component is tested. Studies often assume that simulations are equivalent to real experiments' definitive proof. Few reports tell about the capacity of the software to reproduce measured spectra. This dissertation delivers a new perspective on a full description of measured and simulated spectra in terms of light output, its quality and preference. The simulations are carried out for increasing phosphor particle sizes of LuAG and YAG. The comparison with experimental data indicates if the software is suitable.

PC-LEDs find their major applications in the area of general lighting systems. Several phosphors have to be mixed in PC-LEDs in order to approach the suns radiation spectra and to raise the lighting color quality. A red emitting phosphor needs to be added to complete the spectrum. Efficiencies of high quality PC-LEDs are widely published. However they concentrate on one point of research, light output. Unfortunately no correlation is made between

phosphor concentrations, light output and light quality. This fundamental information is revealed within this dissertation. CCT are reached from 2700 K to 6500 K for PC-LEDs based on a matrix of two green and two red phosphors. A method to reach the target CCT is developed. The origin of the interaction between these phosphors is also explained. Finally the comparison of simulated and measured spectra, which has not been published previously, is presented to predict PC-LED spectra and save many experimental attempts.

3.3 Methodology of work

A multi-disciplinary approach was used to achieve the results reported in this dissertation. The principles of chemistry, physics and mathematics were applied in order to better understand the processed that determine the properties and behavior of PC-LEDs.

This was also true for the work done to better understand the importance of particle size. The investigation of the particle size is realized on phosphor particles that are extracted from the same batch of material (YAG and LuAG) having the same chemical properties. The technology of wet sieving classifies rigorously the phosphor particles by size into fractions of narrow PSD. PL properties of all phosphors are systematically measured. Scanning electron microscopy illustrates the 3D morphology of the particles and validates the particle size measurements.

PC-LEDs are fabricated following the same dispensing process: conventional coating. The selection of the LEDs to be filled up with phosphor is made so that the chosen LEDs have the most similar characteristics, in order that the possible variations noted on the white LED properties can be attributed only to the parameter being studied, for instance the particle size of the considered phosphor in Chapter 5 or 6. Conventional coated PC-LEDs are then built. Optical parameters of these PC-LEDs are measured. The number of PC-LED built validating the chromaticity requirements is optimized. A balance must be found between the statistical reproduction of the measured data and the economical and material investment necessary to reach PC-LEDs with target CCT. Every LED measurement is carried out on 8 LEDs to demonstrate reproducibility. Their standard deviations and averages are given. LED measurement uncertainties represented on the graphs are two standard deviations calculated from the same series of produced LEDs. One parameter, the phosphor concentration, is modified at the same time to reach white LEDs for each sample. It permits the reduction in degrees of freedom of the possible LED property. This allows us to conclude specifically about the influence of the varied parameter e.g. the phosphor matrix in Chapter 7.

Simulations are performed on the same LED design model for the corresponding LED type. Exact optical properties of the LED package are indicated in the simulation model. Measured PL properties empirically modified are implemented. The more simulated rays that are traced the more accurate the PC-LED spectra that are displayed. Simulations are run with 100,000,000 rays. This decision corresponds to a compromise between time and power of computation. The simulation parameters chosen lead to results of good resolution. The majority of the input parameters are kept constant. Power spectral distributions of simulated and measured PC-LED are compared. The comparison of their optical power as well as quality of the light or phosphor concentration contributes to the validation of the simulation tool. This investigation method remains simple with varying as few PC-LED parameters as possible in order to reach the best conclusions on the validation of the simulation. With convincing results, a possible optimization of these parameters is conceivable which would considerably reduce the number of experiments required.

4 Technical equipment

Several process and measurement methods are necessary to investigate phosphor particles, their size, morphology, luminescence properties and their influence on PC-LEDs. The equipment related to the LED technology is detailed as well. Measured characteristics, principle of measurement and set-ups of the devices used for this study are described in this chapter. Experimental or technical limits have to be recognized and defined, thus an estimation of the uncertainty range is also given. The technical equipment facilities are provided by Merck KGaA, all measured and simulated measurements result from a personal execution.

4.1 Microscopic imaging of the phosphor

Scanning Electron Microscopy (SEM) gives an indication on the morphology of the phosphor particles. The structure of the phosphor and its crystal growth can be observed. Micrographs are obtained by means of a scanning electron microscope Zeiss Leo 1530. SEM is a technology based on the detection of secondary electrons, back scattered electrons and characteristic X-Rays. Electrons with an energy ranging from 0.2 keV to 40 keV interact with the sample. The reflection of high-energy electrons by elastic scattering and emission of secondary electrons by inelastic scattering result in the identification of the sample topography. Thereby particles from 1 to 100 μm can be identified, an example can be seen in 4.2.3.

4.2 Phosphor particle size measurement

The phosphor is a powder composed of discrete particles, and each particle may be a single crystal or contain grain boundaries. The study of influence of the phosphor particle size requires the measurement of their diameter and distribution.

4.2.1 Measures characterizing particle size measurements

Size and distribution of phosphor particles are fundamental data influencing optical properties such as reflection or emission of light. The size of a homogeneously spherical particle is defined uniquely by its diameter. Every particle has its own shape, it can be elongated because of agglomerates, or cubic for example. Depending on the particle morphology, more than one dimension might be required to specify its size. Hence particles have to be assimilated to an equivalent spherical volume even if they do not exactly correspond to a sphere [92] of which the average diameter is measured. Phosphor samples usually exhibit particles of varying average diameters. The representation of the phosphor particle's proportion over the equivalent diameter is defined as the particle size distribution (PSD). The PSD can be set as a function of the absolute number of particles or as a function of their volume. Using the volume function gives more importance to the large particles and tends to shift the curve to higher particle diameters. A very important amount of small particles has to be present in the sample to be represented in a volume distribution, and only a few large particles can provide a peak on the volume distribution (Fig. 4.1). The volume distribution may mislead the

understanding of the PSD in the sample. That is why particular importance will be given to the number distribution and all measured PSD plots in this study show numbered weighted distributions. Conversion of number distribution to mass (volume) distribution can result in important errors unless the width of the distribution is narrow. For example, if the range is 10:1 the omission of a single 10 unit particle (volume=1000) is equivalent to the omission of 1000 one unit particles. In order to obtain accurate volume distribution data it may therefore be necessary to size millions of small particles in order to get a statistically acceptable count of the coarse end of the distribution.

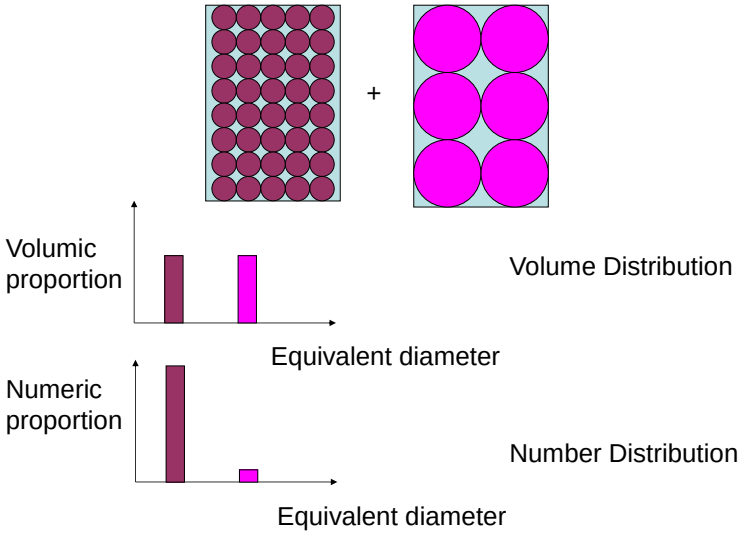

Figure 4.1.: Number and volume particle size distribution diagram influenced by different particle sizes

Characteristic values are defined to describe a number weighted PSD diagram such as the percentile values of the PSD d_{10}, d_{50} and d_{90}. A d_{10}= 5 μm value means that 10 % of the sample has an average diameter smaller than 5 μm, d_{50} gives the median average diameter of the sample, and the d_{90} value describes the average diameter at the 90 % percentile of the sample. The ratio d_{90}/d_{10} gives information on the width of the PSD. A ratio close to 1 means a narrow PSD.

4.2.2 Phosphor particle size measurement set-up

Technical equipment at our disposal to measure phosphor samples PSD are

- AccuSizer
- Coulter counter
- laser diffractometry.

Both former equipments offer the possibility to directly measure the particle number distribution. Laser difffractometry measurements deliver only volume weighted particle size distributions and proceed by computing the number distribution from the volume distribution, which enhances the risk of potential errors.

Coulter counter principle consists in two electrodes immersed in an electrolyte solution. An electrical current flows between the electrodes through an orifice. Phosphor particles passing through the orifice cause changes in resistivity. The impedance variation are proportional to the particle volume. The main drawbacks of this technique is the measurement range. Too large particles may obstruct the aperture.

Therefore the apparatus chosen to measure the particle size distribution is an optical method. PSD measurements are realized on AccuSizer 780/SIS, PSS Nicomp. The sample is introduced, the concentration is adapted in the autodilution chamber in order to eliminate particle coincidences in the sensing photozone. Excessive dilution results in too low account rate and poor statistical accuracy of the PSD, while overly concentrated suspensions produce distortions in the distribution. The sample passes through the single particle optical sensing (SPOS) sensor (Fig. 4.2). Light exctinction detector determines particles larger than 1 μm by measuring the light decreasing intensity coming from the laser caused when particles traverse the sensing photozone. An additional detector receives the light scattered by particles from 0.45 to 1 μm. The resulting size is displayed in real time as absolute counts versus equivalent diameter for each diameter channel logarithmicly displayed over the total size range covered by the sensors [93], [94].

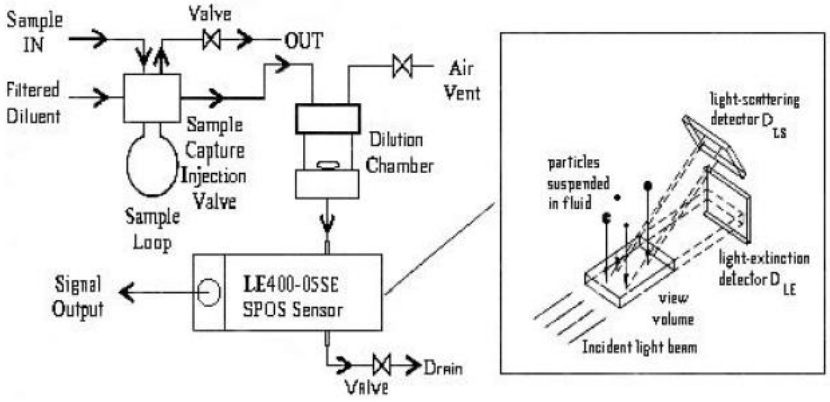

Figure 4.2.: Schematic diagram of the AccuSizer apparatus, from Particle Sizing Systems

4.2.3 Measurement data restrictions

Caution should be taken, that the wavelength of the laser is not situated in the excitation domain of the phosphor. In the case of AccuSizer, photoluminescence of the phosphor can be excluded due to the use of a red laser.

By particle size measuring equipment, the assumption is made that particles are spherical. Nevertheless SEM pictures exhibit some particles having a cubic structure on the surface of the particles. It should also be noted that they grow together and are agglomerated. This leads to an erroneous equivalent diameter. An ultrasound bath treatment is performed before the measurements to prevent possible agglomerates.

All the measurements collected by this method show a grey area on the graph for particles smaller than 1 μm. This domain exhibits a great number of particles. An example is plotted in Fig. 4.3.

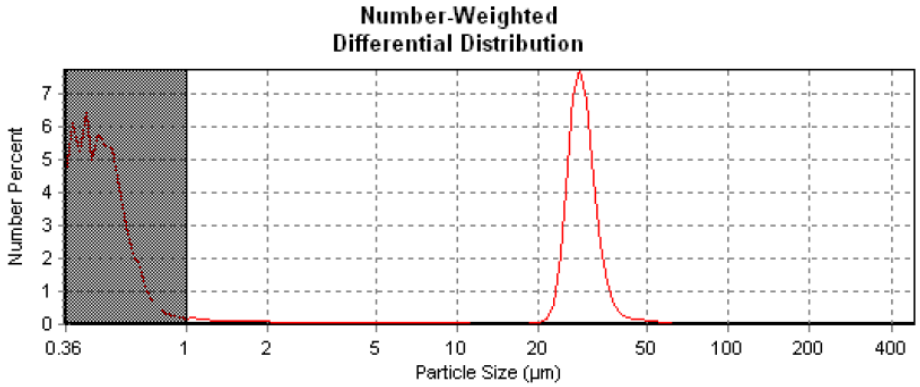

Figure 4.3.: Particle size distribution from AccuSizer measurement

The relevance of the presence of these small particles could not be proven. Uncertainty about the measurement technique in this domain (smaller than 1 μm) was omitted because of the possible shadow generated by the particles on the optical detector. This domain of particle size was particularly investigated. The samples were filtered on a 0.45 μm filter in order to remove the small particles. The filtrate is analysed with the help of the Dynamic Light Scattering technique (Zeta Sizer) able to detect only small particles (smaller than 1 μm). Neither the Zeta Sizer measurements nor the SEM pictures revealed the presence of such small particles. From the scanning electron microscopy picture of the smallest phosphor particles (Fig. 4.4) the trace of matter which would be measured by the AccuSizer or the Zeta Sizer corresponds to the structure phosphor particles. Until now it has not been shown how strong the fine structure is hooked on the surface and whether or not it could move freely when in a suspension. A more probable explanation is that large particles generate several signals on the light scattering detector. Despite high clean experimental conditions, some impurities could also originate in small particle detection.

For all these reasons, particle size distributions used for the rest of the study will neglect the possible presence of phosphor particles smaller than 1 μm.

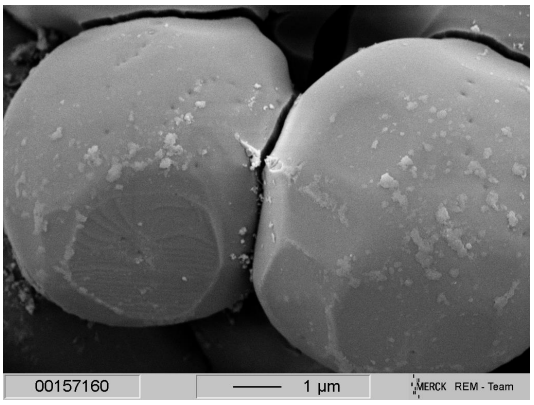

Figure 4.4.: Micrography showing the fine structure of two YAG particles

4.3 Separation of phosphor particles

The phosphor produced in a wet chemical way forms a powder consisting of different grain sizes. The investigation of the phosphor particle size effect on PC-LEDs follows after isolating phosphor fractions of narrow PSD from bulk material. The particles have to be separated and classified into fractions of increasing average diameters. The separation by size of the particles is realized by sieving process. This procedure is described below.

4.3.1 Wet sieving principle

The sieving process allows the particles to be separated depending on their size over the time. It consists in depositing the amount of phosphor powder sample to be sieved on the top of one or more sieves with decreasing mesh size (Fig. 4.5). The PSD of the bulk material can be established as explained in the previous section and enables to identify how many and how broad the sieving class should be selected. The sieve tower is composed of stacked sieves, commercially available of 100, 50, 36, 30, 28, 25, 20, 15, 11 and 5 μm meshes. Particles of small size fall through the mesh until they are stopped by a sieve of smaller mesh, where they are collected. The activation of the motion of the particles through the sieves can be achieved by hand, or automatically with a vibrating apparatus. The success of the sieving is indicated by an adequate time and sample load of the sieves.

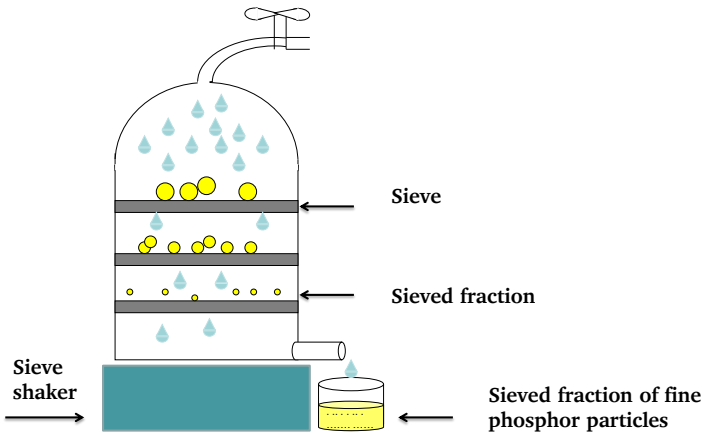

Figure 4.5.: Wet sieving equipment

The stability of the garnet material is so high that by mechanical contact with the sieve, YAG:Ce would form a metal complex because of the abrasion when using a metal sieve. Specific conditions have to be respected regarding the material used for the equipment. Nylon sieves from Retsch are employed to perform the separation.

The advantage of dry sieving is the autonomy of the system. The sieves can be vibrated for hours without paying great attention to the process. The sieving is said to be finished when the masses of the different step sieves remain constant. However this technique leads to a low yield and does not have the ability to separate particles smaller than 11 μm, or with sizes differing by only a few micrometers.

This is the reason why water flow is introduced into the system. The dry sieving process is transformed to wet sieving. Particle size separation is helped by the carrying force of a fluid to pass through the mesh of the sieves. The fluid passed through the tower of sieves can be collected and filtered to gather the fine fraction of the powder. The particles, of course, must not be soluble in the fluid. For garnet phosphor, water is used as the fluid. Also, a tensioactive solution is added to the water in order to enhance the particle sliding through the meshes. This method offers the advantage to be more efficient than the dry sieving process because of the better separation of possible agglomerates in the powder. Furthermore, fractions of particles with sizes close to each other can be isolated. Nevertheless this equipment needs more attention because of the risk that the mesh suddenly obstructs while the fluid is still flowing.

This separation technique enables the achievement of narrow particle size distributions for fractions of equivalent diameter down to 5 μm.

4.3.2 Limits of wet sieving

Wet sieving experiments have been repeated on several charges (see section 5.1.1) and show similar results. The sieved fractions exhibit the same particle size distributions. The wet sieving process is reproducible. Though the particle size distribution obtained seems to not correspond perfectly to the mesh of the sieves. The sieve is made of nylon fibres which divide the surface into squares having a length given from the manufacturer. Even when the size distribution is defined in the manufacturer's certificates, the mesh also shows an opening size distribution. It means that some meshes are broader than expected. Moreover, the length announced corresponds to the side length of the square mesh. Some particles are able to pass through the diagonal of the square mesh. For example, a sieve having 36 μm mesh allows particles that are not perfectly spherical with a size up to 50 μm to cross the sieve. This explains the not perfectly monodispersive distribution of the sieved fractions.

4.4 Characterization of phosphor luminescence

Fluorescence properties of the phosphor is required in order to identify its essential role in the PC-LED. The description of the technical equipment and its sensitivity is presented.

4.4.1 Description of the apparatus

The photoluminescence properties of the phosphor are measured with an Edinburgh Instruments Spectrometer FS920. The light source is a Xenon Arc Lamp: Xe900 which is a 450 W ozone free xenon arc lamp that emits continuous radiation from 230 nm to 2600 nm. The light escapes the lamp and propagates through several optics: mirror, grating and lens as shown in Fig. 4.6.

The wavelength is determined by passing through a monochromator before entering in contact with the sample in the middle of the integrating sphere. Phosphor powder is poured into a Teflon vessel placed on a holder in the integrating sphere. The phosphor sample is flattened in order to create a smooth surface. As shown in Fig. 4.7 the exciting light interacts with the upper surface of the phosphor sample, which corresponds to a reflection measurement

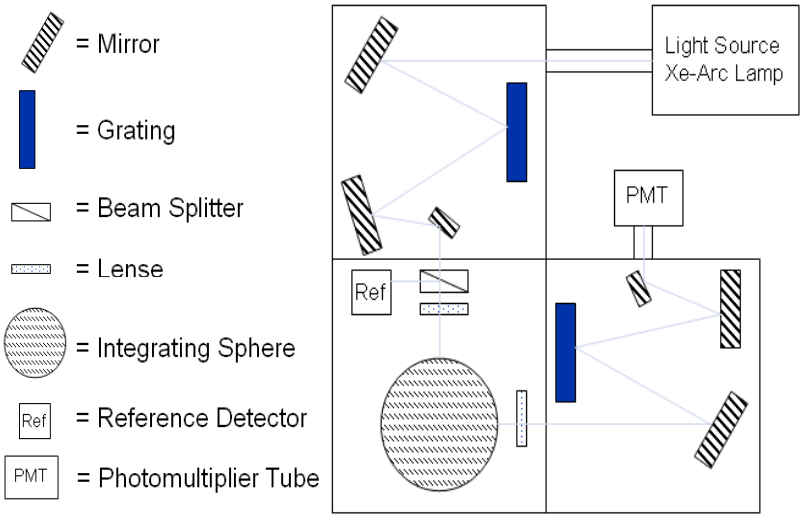

Figure 4.6.: Scheme of Spectrometer FS920

mode in opposition to a transmission measurement mode not available on this equipment. Another monochromator and optic part follow the way of the beam after the sample before the beam is finally collected by a photomultiplier detector.

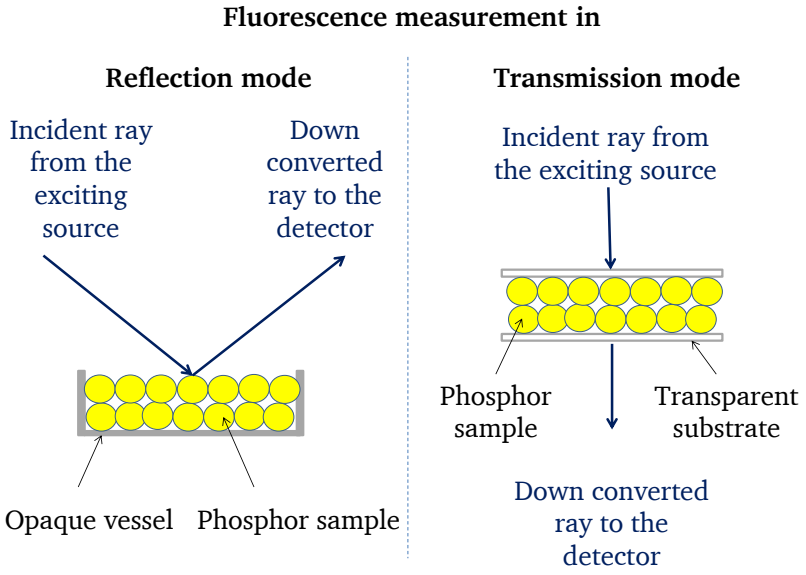

Figure 4.7.: Reflection and transmission fluorescence measurement modes

The spectrofluorometer measures steady state luminescent spectra with single photon counting sensitivity. The measurements possible to be achieved are phosphor emission, reflection and excitation. Spectral correction is necessary to obtain the true excitation and emission spectra of the sample, free from any instrumental effects. Uncorrected excitation spectra are affected by the spectral output of the light source and the throughput of the monochromator. The correction file is obtained by using the built-in calibrated reference detector that monitors a fraction of the excitation light. Similarly, raw emission spectra are affected by the monochromator efficiency and the spectral response of the detector.

The emission spectrum is recorded by imposing a wavelength chosen as a function of the system in which the phosphor will be applied. With the help of the monochromator, the width of the wavelength interval can be determined very precisely and set down to 1 nm. The light excites the phosphor powder sample filled in a recipient and the down converted light emitted by the phosphor is collected on the detector in the wavelength domain set by the second monochromator and corresponding to the phosphor emission (an example of YAG:Ce emission is plotted in Fig. 4.8).

Scanning the light source every nanometer from 250 to 500 nm and measuring its emission at a constant wavelength situated where the phosphor maximal emission happens, enables the recording of the excitation spectrum (a typical YAG:Ce excitation spectrum is displayed in Fig. 4.9).

Screening synchronously both excitation and emission monochromators for every wavelength in the visible region while measuring the light emission of the sample describes the reflection spectrum of the phosphor powder. The reflection of the light source has to be subtracted from the photon amounts collected at the detector.

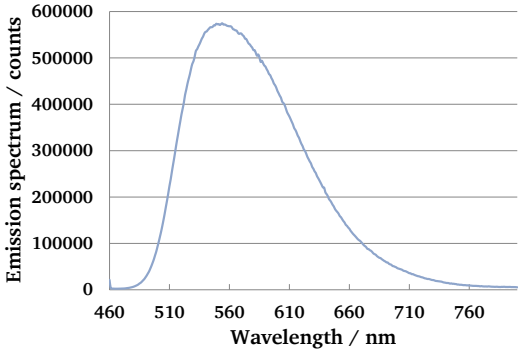

Figure 4.8.: Typical emission spectrum of a YAG:Ce phosphor

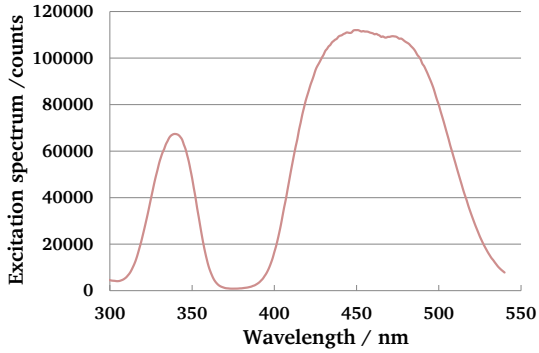

Figure 4.9.: Typical excitation spectrum of a YAG:Ce phosphor

4.4.2 Spectrometer sensitivity

The spectrometer uses monochromators with high quality diffraction gratings for high dispersion and excellent imaging quality. Spectral details as close as 0.1 nm can be resolved over the spectral range from UV to NIR .

Single photon counting is an unparalleled method for the measurement of low level optical radiation. A peak count rate of $>$ 750,000 count per second (cps) and a signal to noise ratio of $>$ 6000:1 for a measurement of a water Raman spectrum under standard measurement conditions are guaranteed. Single photon counting is the most sensitive measurement technique in the field of fluorescence spectroscopy. It is fast and has a high dynamic range. Photons are counted in a time window, which sweeps across the full time range following each excitation pulse, creating a histogram of counts versus time. Measurements are repeated three times and added to improve the signal to noise ratio. PL data shown in this study are averaged on four repeated measurements.

4.5 Phosphor-converted LED technical data

LEDs are made from the mixture of a transparent silicone binder (OE 6550) from Dow Corning with refractive index of 1.54 and phosphor. The effects of YAG:Ce^{3+}, LuAG:Ce^{3+}, orthosilicate, oxyorthosilicate and nitride phosphors in PC-LEDs are examined. Phosphor and silicone binder are weighed by means of a Satorius ME 36S balance. The weight of the samples is determined with an accuracy of 0.001 mg. The Speedmixer DAC 150 SP from Hauschild assures a sample homogeneous mix. This is realized by spinning at high speed at the end of a holding arm and by rotation around the sample axis. The two components are mixed in appropriate proportions. The slurry is poured into the LED chip in order to create a conventional coating. LEDs are finally cured at 150°C in order to polymerize the silicone and to form networks, capturing the phosphor in the suspension.

4.5.1 LED packages

Experiments are carried out with two different LED types, Chip on Board (COB) LEDs and Surface Mounted Device (SMD) LEDs with four different emitting wavelengths. The InGaN LED characteristics are summarized in Table 4.1. COB LEDs present a more compact technology, with gold bond wiring, adhering the chip directly onto the substrate. This adaptive technique enables the realization of appropriate and targeted designs. SMD LEDs are typically used in the industry and are therefore important to be involved in the study. The low driving current and the ease of industrial scale-up, due to the placement and soldering from the same side, contributed to making SMD LEDs widespread. Blue LED emission stimulates the phosphor. Consequently the LED must be specific to the phosphor. The LED wavelength emitting interval has to correspond to the exciting domain of the phosphor. For the experiments of this study the LED should emit from 425 nm to 475 nm to be the most suitable and efficient.

Table 4.1.: Maximum emitting wavelength, luminous flux, current and volume of the LED cavity for different blue LED types

LED Type	Maximum peak wavelength / nm	Luminous Flux / lm	Current used / mA	Volume to fill up above the chip / mm
COB - LED type 1	441 ± 1	5.5 ± 0.3	350 ± 0.1	39.7
SMD - LED type 2	454 ± 1	0.52 ± 0.01	20 ± 0.1	7.4
SMD - LED type 3	445 ± 1	0.36 ± 0.01	20 ± 0.1	7.4
SMD - LED type 4	450 ± 1	0.46 ± 0.01	20 ± 0.1	7.4

The LED type 1 (Fig. 4.11) is a COB LED emitting at a peak wavelength of 441 ± 1 nm. A typical emission spectrum of LED type 1 is shown in Fig. 4.10. The die inserted in the high power LED has an area of 880 x 880 μm^2 and delivers 212 ± 4 mW optical power when operated at 350 mA. The design of the LED is composed of the COB surrounded by a 2.5 mm high steel ring glued on the board on which the phosphor liquid mixture will be introduced to partially convert the blue emission.

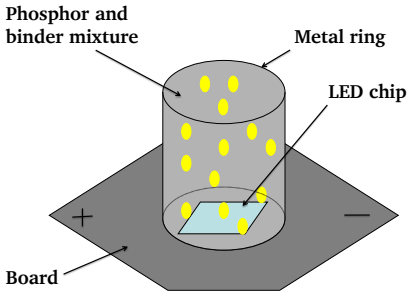

Figure 4.10.: COB LED, LED type 1

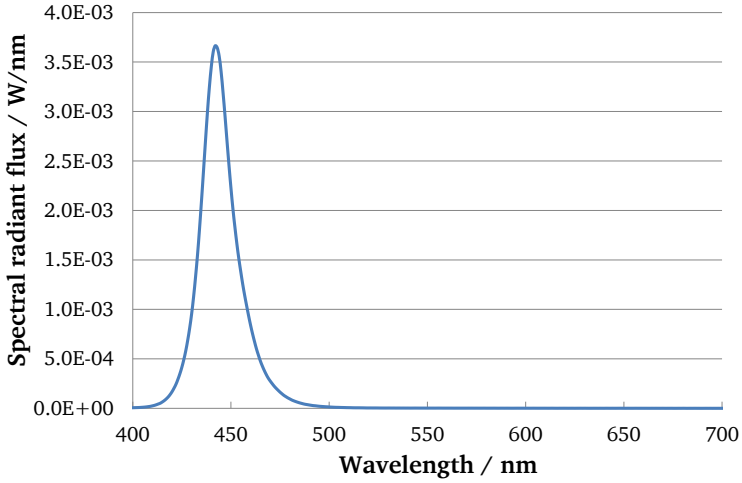

Figure 4.11.: Emission spectrum of LED type 1 (COB) operated at 350 mA at 25°C

The LED types 2, 3 and 4 are composed of a chip inserted in an empty device (see Fig. 4.12). These three types of SMD are low power LEDs. They all have dimensions of 35 mm x 28 mm and are operated at 20 mA. The LED cavities each have the same phosphor slurry volume to fill. The difference between these LED types comes from the emitting wavelength peak: LED type 2 at 454 nm, LED type 3 at 445 nm and LED type 4 at 450 nm.

Figure 4.12.: LED type 2, 3 and 4

The selected binning domain specified Table 4.1 is narrow so that conclusions on PC-LED results cannot be inferred to any blue LED variation.

4.5.2 Phosphor dispensing system

On an industrial scale a considerable number of white LEDs are produced every day. Manufacturers have the possibility to coat a phosphor and silicone binder on a blue LED chip. The phosphor and silicone mix is a viscous slurry, which complicates the accuracy by spreading a constant phosphor amount. Dispensing systems as CDS 6200 from Essemtec enable the jetting of fluids over a wide range of viscosity at high speed. A series of LEDs are automatically filled following the program entered in the controlling software. The valve ensures the reproducibility of the LED chip coating. The mass of injected phosphor mixture is controlled for every PC-LED. Even if the viscosity of the phosphor and silicone binder is high, the issue of sedimentation has to be considered. Phosphor particles settle with the time in the cartridge before jetting. Particular attention has to be paid to the homogeneity of the slurry. This would lead to the manufacturing of LEDs having different CCT because of varying phosphor amount in the coated layer.

4.6 LED measurements

Spectral power distributions are measured with PC-LEDs with an integrating sphere for the standard measurement. PC-LED properties depending on the observation angle are recorded on an optical bench.

4.6.1 Integrating sphere equipment

PC-LED optical properties are measured with a spectrometer CAS 140 CT from Instrument Systems. The spectrograph (Fig. 4.13) is housed in a mechanically robust block. The incident radiation is first collimated by a concave mirror and guided on to the diffraction grating, where it is spatially split into its different spectral components. A second concave mirror focuses the various spectral components of the light onto different columns of the CCD detector, thus capturing the light's spectrum in a single acquisition.

For standard photometric and radiometric measurements the spectrometer is equipped with a 250 mm integrating sphere (Fig. 4.14). COB LEDs are externally cooled in order to be constantly measured at 25 °C. LED absolute spectral radiant flux is recorded from 370 nm to 780 nm. Luminous and radiant fluxes, CCT, CRI and color coordinates are computed by the software.

10-times measurement on a white LED certified by PTB (Physikalisch- Technische Bundesanstalt, physical and technical federal institute) results in chromaticity deviations $\Delta x = 6.5{\cdot}10^{-5}$ and $\Delta y = 1.7{\cdot}10^{-5}$. The deviation on the luminous flux is 4 % and on the wavelength of 0.5 nm.

4.6.2 Goniometric measurement

The LEDGON goniophotometer from Instrument Systems determines the spatial radiation distribution of LEDs. Measurement is made over all the forward hemisphere of an emitting LED. A high angle resolution of 0.1° provides measurements even for narrow emission angle

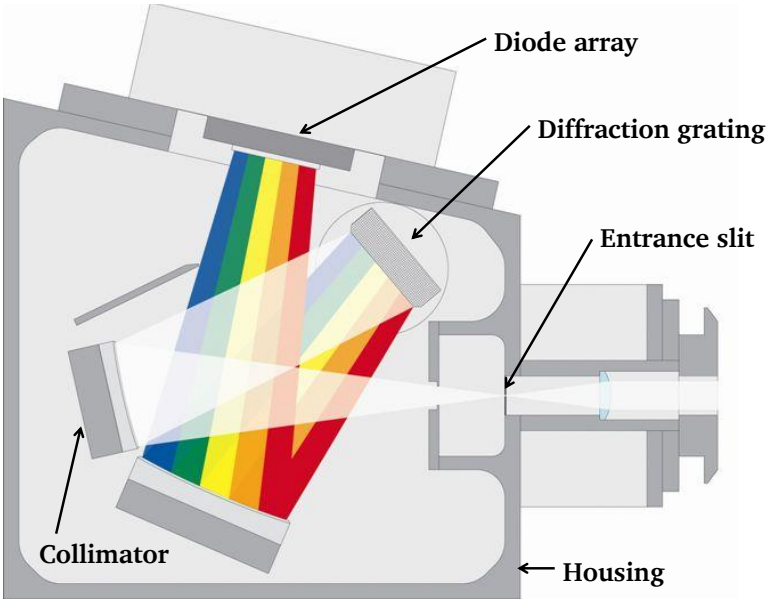

Figure 4.13.: Optical scheme of LED spectrometer

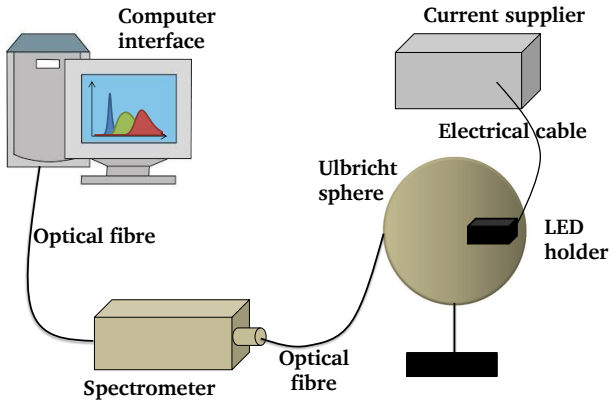

Figure 4.14.: Scheme of LED spectrometer

LEDs. In combination with the CAS 140CT spectroradiometer, additional spectral parameters, such as the angle dependence of color coordinates or CCT, can also be measured. The set-up consists of an optical rail with a mounted rotation stage rotating the LED from -90° to +90° in a horizontal plane (Fig. 4.15). LED spectra are measured every 3°. The optical probe is located at the opposing end of the optical rail, and can be positioned at a distance of 70 cm with respect to the LED. The whole set-up is contained in a lightproof housing with a hinged cover.

4.7 Lighttools simulation software

The system chosen to be the most appropriate to describe PC-LED emission spectra is a ray tracing commercial software. Experimental results are simulated. The validation of the measurements by simulation offers the possibility to optimize experimental parameters from simulation results.

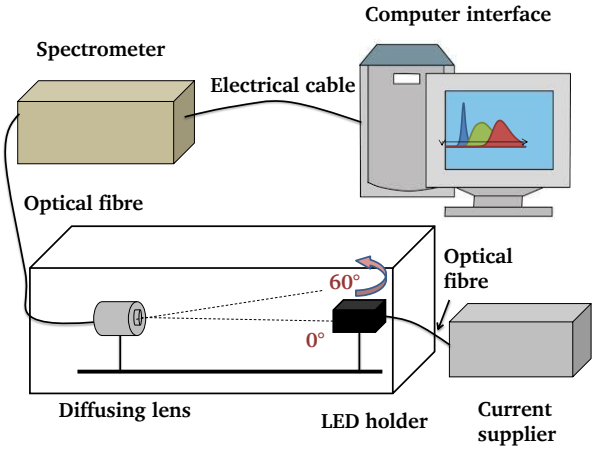

Figure 4.15.: Scheme of LED optical bench

The behavior and propagation of light are described by the Maxwell's equations, nevertheless their resolution requires tremendous calculation effort in finite, heterogeneous structures, and therefore cannot be used in trying to calculate light propagation in complex geometries such as those used for LEDs. The laws of geometrical optics constitute a very good approximation in the limit of dimensions larger than those of the wavelength used. Ray tracing is a Monte Carlo based method that uses the laws of geometrical optics to statistically simulate the behavior of light in a given system. It requires a good knowledge of the geometry and of the optical properties of all the different materials present in the system. Rays of light are shot randomly from the different light emitting sources and follow the rules of geometrical optics until they are either absorbed or exit the system. Since the ray tracing method relies on the rules of geometrical optics, it is unable to describe and calculate phenomena such as interference or diffraction, which can only be described by optical wave theory. However in our study, these effects are either taken into account differently, or they are negligible. Our study uses the commercial ray tracing software Lighttools, version 7.3.0.

Lighttools is a MS-Windows based ray tracing software developed by Optical Research Associates. It enables the user to create systems, define their optical properties and simulate the behavior of light propagation by Monte Carlo based ray tracing. Lighttools' basic ray trace is a non-sequential ray trace. This means that in general there is no field point associated with the ray, only a starting point and a direction, and no predetermined order of surfaces to traverse. The starting point of a ray can be anywhere in space (even inside an element) and the ray direction can be any direction in space. Once started, the ray continues in space, hitting whatever elements it encounters in the order determined by the laws of optics until it encounters a stop condition.

There are many possible variations of the ray tracing algorithm that have different convergence speeds and computation time. For example, as a ray hits an interface, some algorithms will split this ray at this interface and give a different weight to the transmitted and the reflected wave according to the Fresnel coefficients, while other algorithms will randomly pick either reflected or transmitted, with the probabilities depending on the Fresnel coefficients. While the first will require fewer rays to get a good approximation of the behavior of light, it will also require more computational power because each ray is doubled into two rays at every interface. Fig. 4.16 presents the simplified algorithm applied by Lighttools that does not split rays. Once the geometry is well defined, and the optical properties of all the different materials are known, it is possible to randomly generate rays of light. For each

ray, the origin and the direction are randomly chosen in the emitting regions, and the ray of light can be propagated until it hits an interface. Once the ray has hit an interface, the algorithm first computes the probability that the ray is absorbed during its propagation, using the absorption coefficient of the given material. It will then randomly pick, according to that probability whether or not the ray is absorbed. If it is, then the program will take it into account and shoot a new ray. If not, the program will probabilistically decide if the ray is reflected or transmitted, according to the material and interface properties. The ray can then continue its propagation in the new direction it has been given, until it either hits a new interface, where the same process will take place, or escapes the defined geometry. By counting all the rays that have been absorbed versus all the rays that have escaped, one can, for example, calculate the extraction efficiency for an LED geometry design.

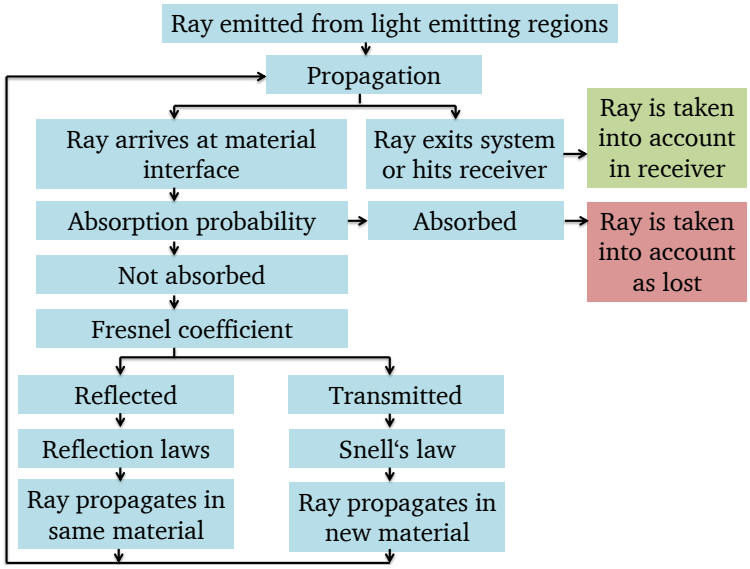

Figure 4.16.: Flow diagram of a simplified raytracing algorithm

Geometry and design of the lighting system are implemented in Lighttools (Fig. 4.17). The software offers the opportunity to create modules devoted to:

- light sources defined by their radiant or luminous flux, their geometrical design and their spectral radiant distribution
- constituting elements described by their shape in three dimensions, their material including the correspondant optical properties (refractive index, transmission) and structure of the surface
- detectors which can be planar, spherical, absorbing or not, collecting information about the spectral distribution, chromaticity, luminous and radiant fluxes.

A specific module is developed for the investigation of phosphor. In this module phosphor materials can be added to an already existing material (silicone binder in this study). Phosphor materials must be defined by:

- their refractive index,
- their photoluminescent properties,
- the radius of the particles and their distribution,

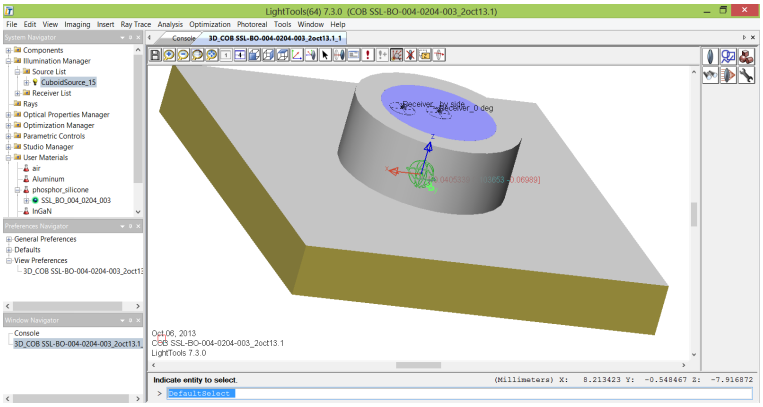

Figure 4.17.: Design of COB LED on Ligttools

- their concentration.

The photoluminescent characteristics take into consideration

- the emission spectrum which is entered as relative intensity and can be given for different excitation wavelength,
- the absorption spectrum which is defined as the probability that incident light will be absorbed in the phosphor material, and
- the quantum yield which is the relative conversion efficiency reported as the number of absorbed photons over the number of luminescent photons. The efficiency is expressed as a function of excitation wavelength.

For scatterers the radiant flux is calculated as a function of the angles at the boundary of a spherical particle according to Mie relations. Only spherical particles are considered in the Lighttools model. The computations for Mie scattering can be intensive, so many of them are performed in Lighttools prior to ray tracing to improve ray tracing speed. For instance, the angular radiant flux distribution for a Mie scatterer is precomputed and stored in memory. These computations are performed whenever a Mie scatterer is first defined, or whenever a new spectral region is defined for a system with a Mie scatterer. If the particle size is much smaller than the wavelength of incident light, then the Rayleigh equations are used instead of the Mie equations. In Lighttools, the Rayleigh equations are used if the radius of the particle is 0.1 times the size of the wavelength or smaller.

These determinant input parameters describing the phosphor behavior correspond to physical measures presuming a promising understanding of the phosphor down conversion phenomenon. Moreover the optical theory used to compute the radiation distribution is based on the Mie or Rayleigh calculation methods to predict the light distribution of scatterers.

It is possible to extract lots of information from a Lighttools simulation. For example in LED chip simulations, the “ray report” generated by the program enables us to know how much light was extracted by each component of the LED. For phosphor simulations, it is possible to determine the output spectrum of the whole device, along with the directionality of the emitted light and the efficiency of the system. Radiant spectral distributions, photometric information as well as CCT and CRI R_a are computed.

The model used as a pattern in this study contains the same information about the LED size, power and spectral distribution of the blue LED and PL characteristics of the phosphor as the experimental data. The exact size characteristic of the LED package was implemented. The phosphor samples have differing particle size distributions given as input parameters. Data required by the software and implemented are obtained from experimental measurements as explained in the previous sections. The phosphor concentration required to fit the simulation to the practical measurement is the optimized parameter. Two detectors are placed in the model side by side to the emitting surface. One detector is situated at the top of the phosphor layer, at the center of the device. The other detector is located off center from the middle of the chip. This enables one to compare the simulated spectra with the goniometer measurements.

It is important to understand that many of the optical properties of each material are quite hard to access, as for example the absorption coefficient. Also the different LED chip geometries that are simulated also are ideal models, while real chips might have defects that will affect the way the light propagates in the chip. Thus an exact quantitative result should not be expected from the ray tracing simulations. Rather than that, what should be expected of the simulations is the study of the effect of a particular parameter, the general behavior of light in the structure or the relative efficiency of different chip geometries.

The PL measurements implemented as parameter in the software originate from the set-up described in 5.1.2 which records the emission, absorption and excitation spectra in reflection mode on phosphor powder samples. Lighttools recommends to implement PL measurements performed on single crystal phosphors. Besides the PL measurements are realized in reflection mode which might also lead to diverging results.

Lighttools assumes that phosphor particles are spherical because the software computes scattering properties based on the perfect case of Mie theory. The assumption for the experimental phosphor samples is partially verified as can be seen on the SEM pictures in section 5.1.1, even if efforts were made to synthesize phosphor particle with a smooth and spherical morphology.

5 Studies and research on the YAG:Ce phosphor

$Y_{3-x}Al_5O_{12}:Ce_x^{3+}$ (YAG:Ce) was the first phosphor developed to produce white light emitting diodes (WLEDs). Its synthesis is nowadays controlled and improvements have been realized on its efficiency and morphology. Though the color rendering of WLEDs fabricated with this phosphor are still low due to the lack of longer wavelengths, the knowledge acquired over the years about its characteristics is well developed. This allows us in this chapter to discuss the experiments of high quality YAG:Ce with a perfect morphology and to be able to reveal the YAG:Ce based phosphor-converted LED mechanisms. The effect of phosphor particle size on LED optical outputs, angular homogeneity and phosphor requirements are detailed. This chapter includes the investigation of the YAG:Ce phosphor, its impact on the application as white LED and the validation of the experimental results by simulation using optical software.

5.1 Phosphor powder investigations

First a complete description of YAG:Ce phosphor characteristics will be detailed. This comprises the determination of particle sizes and their distribution, the macroscopic structure of the surface and the fluorescence properties of YAG:Ce phosphor. This enables us to explain the role of YAG:Ce phosphor when it is used in white LEDs.

5.1.1 Particle size distribution

Two batches of YAG:Ce luminescent material were prepared following the synthesis reported in Chapter 2. Bulk materials YAG 1 and YAG 2 were produced. Particle size distributions (PSD) of YAG 1 plotted in Fig. 5.1 exhibit a large particle size distribution extended from 6 μm to 17 μm. The YAG:Ce phosphor particles were separated by a wet sieving process in order to classify phosphor particles into size fractions of increasing particle size and with narrow PSD. The wet sieving procedure was repeated on the two batches. Tables 5.1 and A.1 in Appendix A report the median particle diameter (d_{50}), the particle size interval d_{10} to d_{90} and the ratio d_{90}/d_{10} of the sieved fractions. Several sieved fractions with narrow distribution were extracted from this starting luminescent material. The similar results obtained on YAG 1 and 2 validate the efficiency and reproducibility of the wet sieving method. Obtaining phosphor diameters so close together and small median particle sizes demonstrate the value of wet sieving.

Nevertheless, the particle size distributions obtained do not correspond perfectly to the mesh of the sieves (Table 5.1). As mentioned in section 4.3.2 nylon sieves show an opening size distribution which is accentuated by high sample load or vibration during the sieving process. The length of the diagonal of the mesh size is also to consider.

5.1.2 Scanning electron microscopic pictures

The morphology of the YAG phosphor particles from different sieved fractions is recorded by a Scanning Electron Microscope (SEM), see Fig. 5.6.

Table 5.1.: Average particle diameter d_{50}, particle size width $d_{10} - d_{90}$ and ratio d_{90}/d_{10} of YAG 1 and its sieved fractions

Sample	Treatment	d_{50}/ μm	d_{10}-d_{90} μm	d_{90}/d_{10}
YAG 1	bulk material not sieved	11	6.5-21.4	3.3
YAG 1 #0	sieved under 5 μm	9	6-10	1.6
YAG 1 #1	sieved between 11 and 5 μm	9	9-13	1.5
YAG 1 #2	sieved between 15 and 11 μm	15	11-19	1.6
YAG 1 #2b	sieved between 20 and 15 μm	21	16-26	1.6
YAG 1 #3	sieved between 25 and 20 μm	28	24-33	1.4
YAG 1 #4	sieved between 28 and 25 μm	31	28-40	1.4
YAG 1 #5	sieved between 30 and 28 μm	33	30-42	1.5
YAG 1 #6	sieved between 36 and 30 μm	37	32-47	1.5

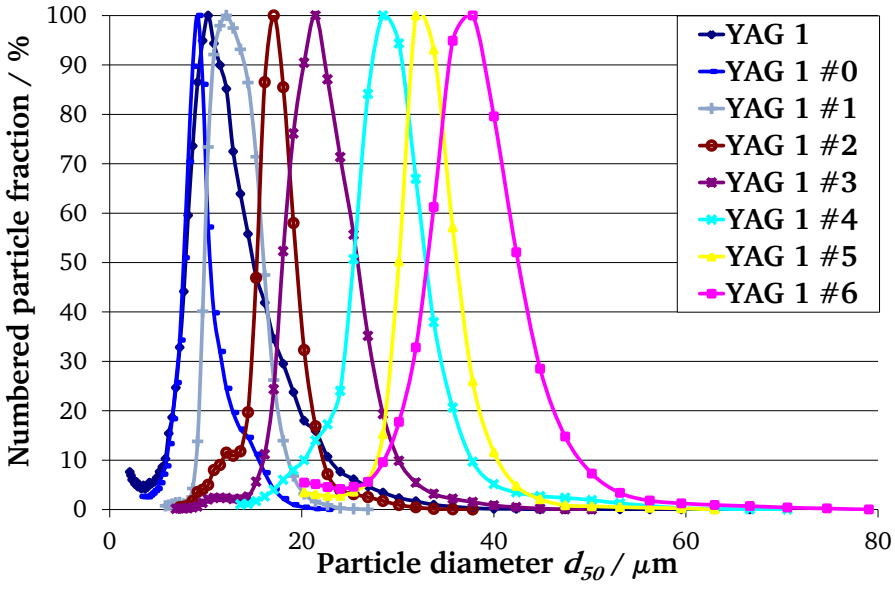

Figure 5.1.: Particle Size Measurements with AccuSizer of YAG 1 and sieved fractions

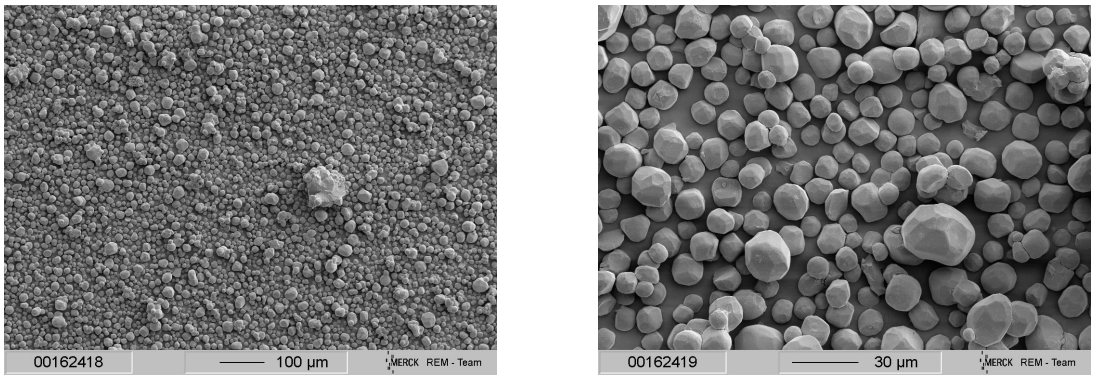

Figure 5.2.: YAG 1 (d_{50}=11 μm)

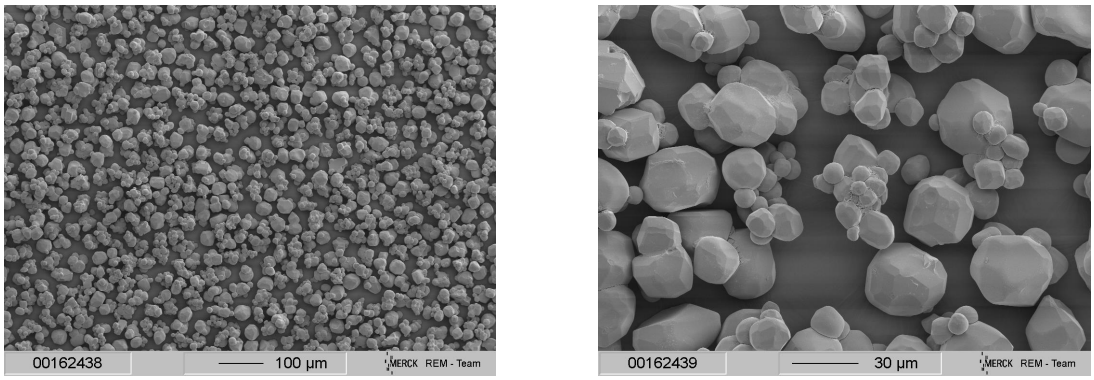

Figure 5.3.: YAG1 #6 (d_{50}=37 μm)

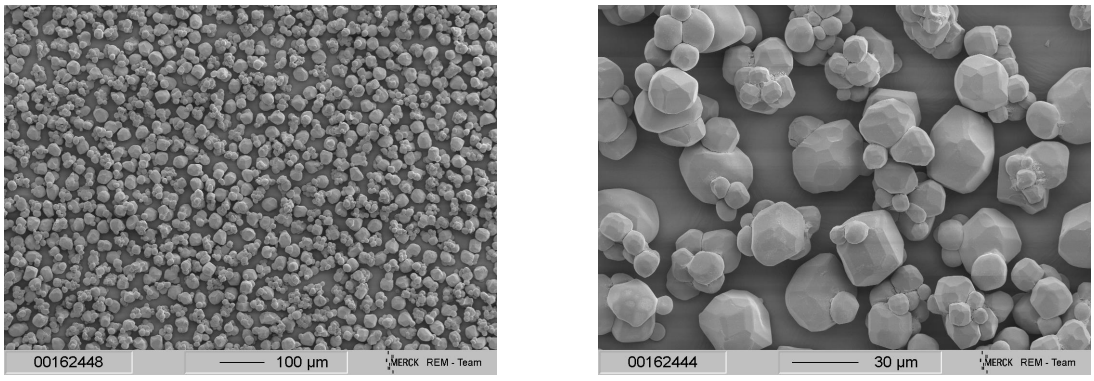

Figure 5.4.: YAG1 #5 (d_{50}=33 μm)

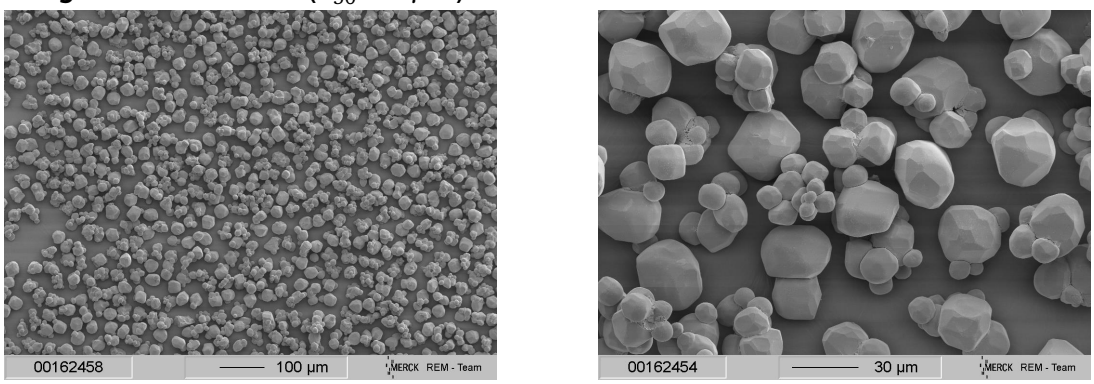

Figure 5.5.: YAG1 #4 (d_{50}=31 μm)

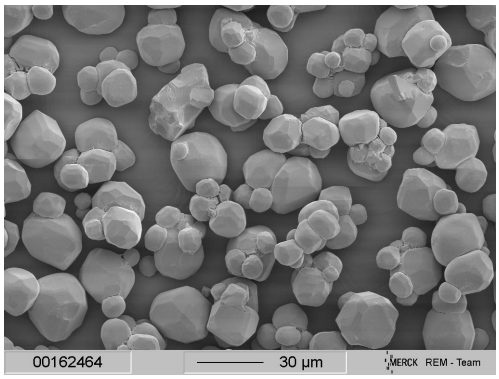

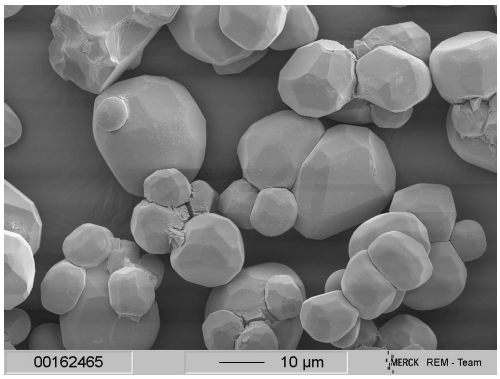

Figure 5.6.: YAG1 #3 (d_{50}=28 μm)

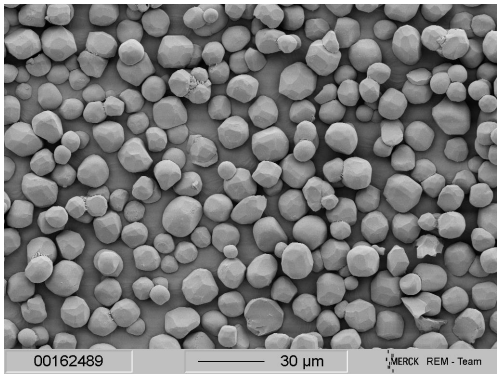

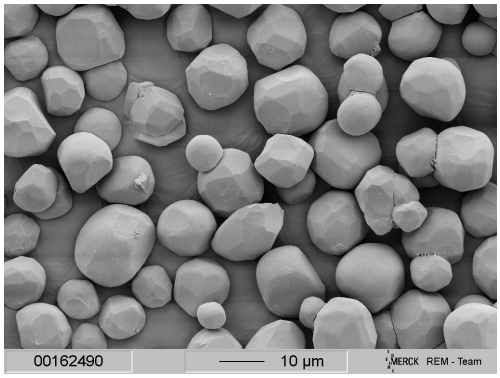

Figure 5.7.: YAG1 #2 (d_{50}=15 μm)

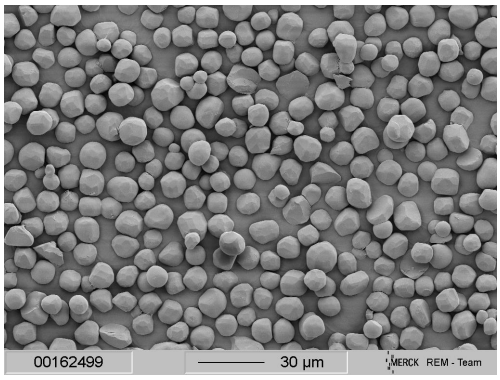

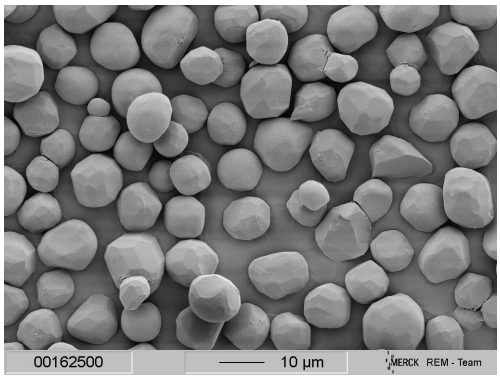

Figure 5.8.: YAG1 #1 (d_{50}=11 μm)

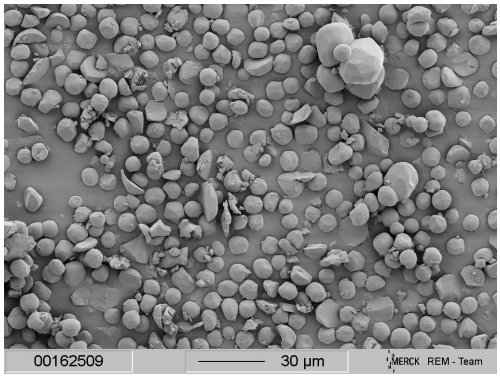

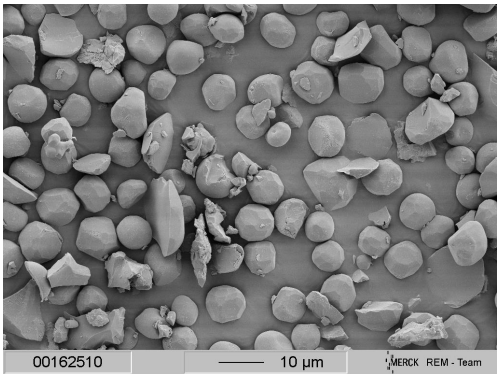

Figure 5.9.: YAG1 #0 (d_{50}=9 μm)

Figure 5.10.: SEM pictures from the sieved fraction of YAG 1

The images depict spherical particles with a homogeneous smooth surface where crystal faces can be seen. The scale confirms the particle sizes of the sieved fractions already measured by the counting method from section 4.2.2. The SEM pictures of YAG 2 and sieved fractions represented in Fig. A.1 of the Appendix A also validate the reproducibility of the efficiency of the wet sieving process.

5.1.3 Photoluminescence properties

Photoluminescence (PL) was measured on each of the different particle sizes of the sieved samples. The excitation spectrum is first presented. The excitation of YAG:Ce shows a broad spectral band in the visible wavelength range from 430 nm to 480 nm and also in the UV at about 338 nm but with a weaker effectivity (see Fig. 5.11). Free Ce^{3+} with $4f^1$ electronic configuration has two ground states (see 2.5.1). Electrons go to $5d^0$ excited states split into several energy levels by spin orbit coupling. The transitions to the two lowest states correspond to the excitation band at 340 and 450 nm. The excitation maximum at 450 nm is plotted as a function of the particle size d_{50} in Fig. 5.12. Particles with a diameter between 15 μm and 37 μm in the range of our study are very likely to be excited at 450 nm. Their excitation level remains equal. However a light tendency can be observed from the smallest particles size until 21 μm: the larger the phosphor particles the higher the excitation level they have.

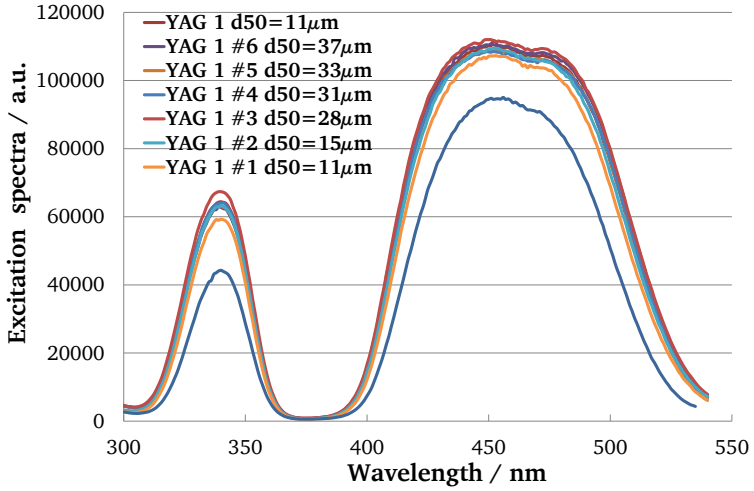

Figure 5.11.: Excitation spectra of particles of YAG 1 and sieved fractions

Next, absorption characteristics are considered. Samples exhibit moderate absorption level from 375 nm up to 425 nm which becomes low from 500 nm and above. The material absorbs up to 500 nm and especially at 450 nm in the visible. This explains the yellow color of the YAG:Ce phosphor powder. The high absorption and excitation levels around 450 nm make YAG:Ce suitable for phosphor applications combined with pumping blue LEDs. Figure 5.13 shows the absorption maximum at 456 nm for increasing phosphor particle sizes. The excitation wavelength can be better absorbed by particles of increasing size (from 9 μm to 37 μm in the context of the study). These observations on the absorption confirm the previous excitation results. Absorption intensity is also significantly lower for the 9 nm particle size sample.

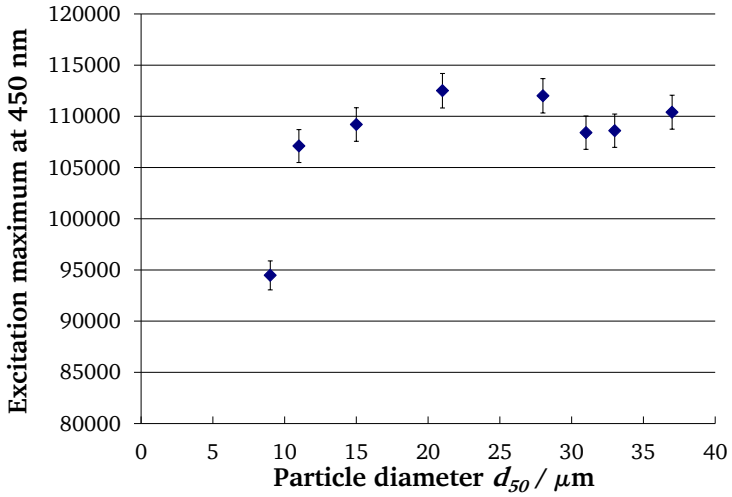

Figure 5.12.: Excitation maximum at 450 nm as a function of the particle size diameter d_{50}(YAG 1)

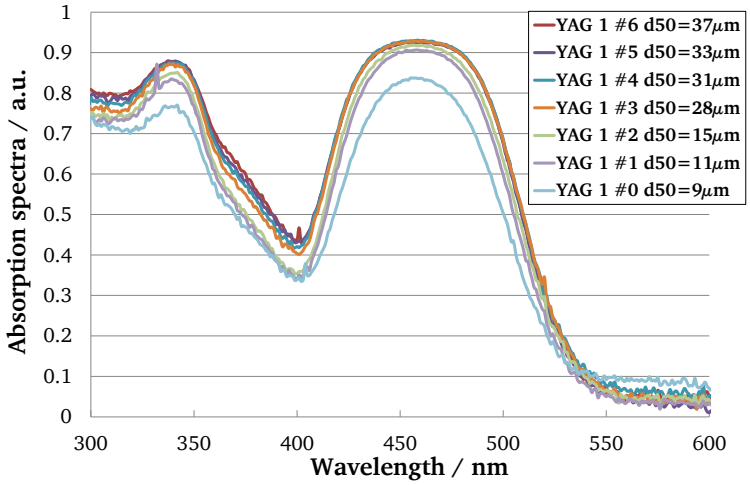

Figure 5.13.: Absorption spectra of particles of YAG 1 and sieved fractions

Finally, fluorescent spectra are measured and displayed in Fig. 5.15 for YAG 1 and its sieved fractions under excitation at the wavelength of highest excitation, in that case at 450 nm. YAG:Ce phosphor emission spectrum extends on a broad spectral band from 500 nm to approximately 625 nm with a maximum at 554 nm. This generates an emission of yellow radiation. Figure 5.16 reports the emission maxima at 554 nm as a function of the particle size. This plot shows that all sieved fractions attain the maximum with comparable emission except for the smallest particle size (9 μm). The emission degree remains high and almost constant for particles from 12 μm to 37 μm.

In summary, phosphor particles with decreasing sizes lead to a decrease of absorption level, resulting in a decrease of excitation and emission properties. In the range of the particle sizes studied, the luminescent values stabilize for particles above 28 μm.

Phosphor surface increases by reducing the phosphor particle diameter. Small particles exhibit larger specific surface. The crystal structure stops per definition at the surface of the

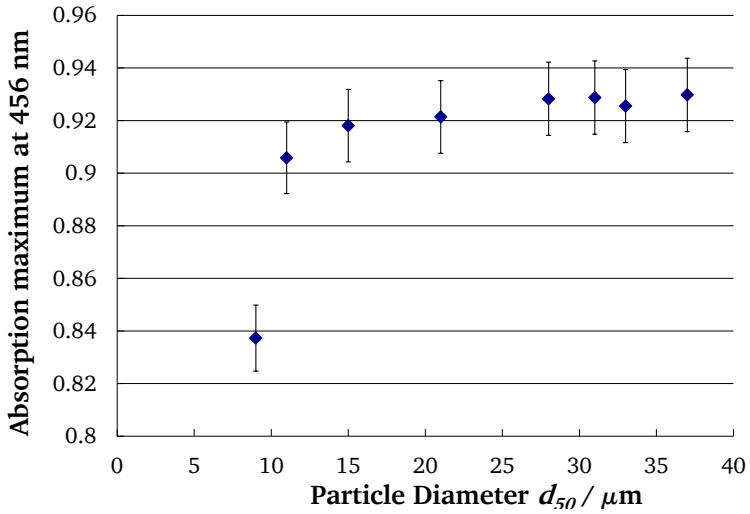

Figure 5.14.: Absorption degree at 456 nm as a function of the particle size diameter d_{50} (YAG 1)

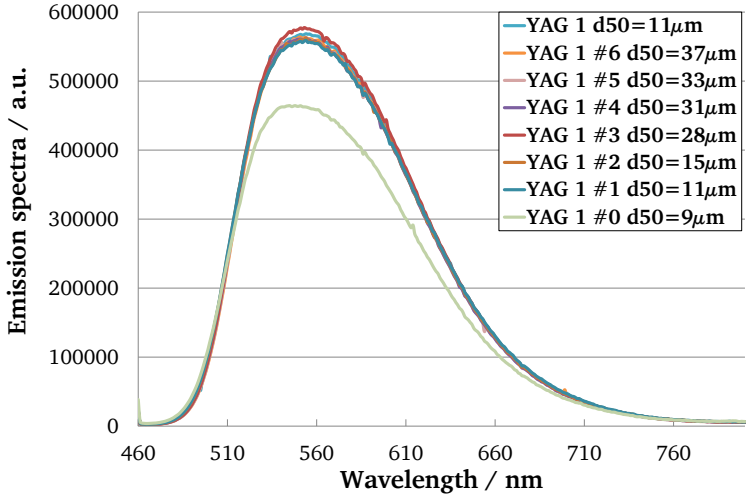

Figure 5.15.: Emission spectra of YAG 1 and sieved fractions for particles with increasing particle diameters d_{50}

particle which induces defects. These defects transform the incident radiation into phonons which therefore deteriorate the luminescent properties of small phosphor particles.

5.2 YAG:Ce Phosphor-converted white LEDs

The focus will now be on PC-LEDs based on the YAG:Ce phosphor previously described in the previous section 5.1. The impact of particle size, morphology or PL properties of the YAG:Ce phosphor will be investigated on LED output. The influence on phosphor concentration, angular homogeneity and optical efficiency of the phosphor-converted LEDs will be explored.

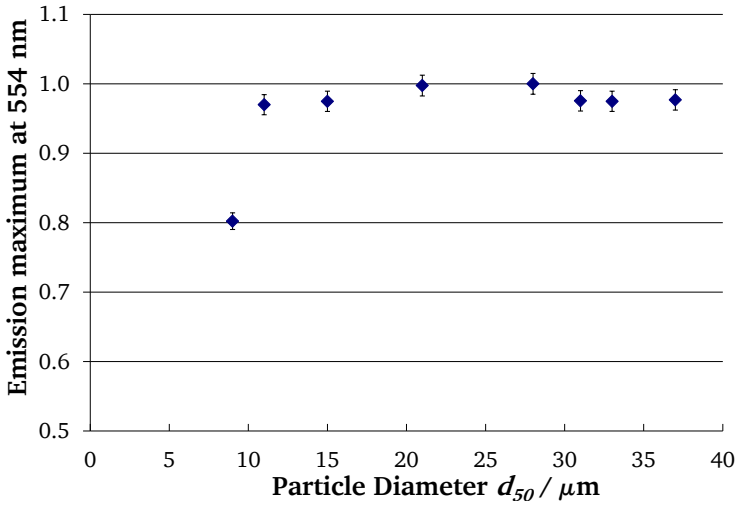

Figure 5.16.: Relative intensity of emission as a function of particle size diameter (YAG 1)

5.2.1 White LEDs characteristics

In this section, the approach to achieve a PC-LED with specific chromaticity will be reported. The properties of white LEDs based on several phosphor particle sizes will then be compared: required phosphor concentration, lightness and angular homogeneity. The impact on WLEDs of the blue emitting diode and silicone binder is also treated.

Obtaining White LEDs

Producing a PC-LED is an easy process. The challenging step comes from the adjustment of the parameters in order to meet the photometric and radiometric requirements. The LED must have defined characteristics in terms of luminosity, CCT, spectral distribution, color rendering and angular distribution, and should be reproducible.

By fixing the LED package and YAG phosphor material characteristics, only the phosphor concentration can influence the LED outputs. The phosphor concentration represents the factor which is the easiest to vary in practical experience and plays an important role in a PC-LED. Increasing the phosphor concentration enables the creation of LEDs evolving from blue tones up to yellow ones. Chromaticity coordinates can be defined from the emission spectrum of each light source and can be positioned on the CIE diagram. The location on the CIE diagram of a series of concentrations moves along a straight line (see Fig. 5.17). The LED, which does not contain any phosphor, is situated in the blue domain as it corresponds to a blue LED.

As long as the phosphor material remains the same (YAG:Ce phosphor synthesized in the same way), the possible color coordinates reached are the same, even if the particle size is different. Increasing the phosphor concentration not only influences the corresponding color of the LED but also the luminous flux. Even if a higher phosphor concentration would produce a high LED efficiency, the color rendering is also a determinant criterion and may favor good spectral quality versus light intensity (see section 5.3.1).

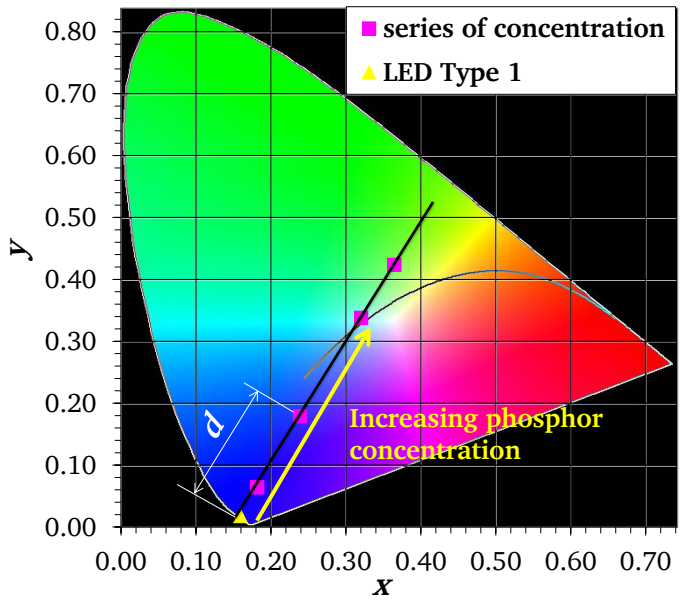

Figure 5.17.: Phosphor concentration variation in a PC-LED (LED type 1 and phosphor: YAG 1 concentration growing from 1; 3; 5 and 7 weight percent) on a CIE (1931) diagram

The evaluation of the required phosphor quantity in order to be situated on a specific location on the CIE diagram is the next topic. To solve this issue, the method described below (Fig. 5.18) is established. It is based on computing the distance d, separating the PC-LED color coordinate and the blue LED position on the CIE diagram following the eq. 5.1.

$$d = \sqrt{(x_{PC-LED} - x_{blueLED})^2 + (y_{PC-LED} - y_{blueLED})^2} \tag{5.1}$$

In the present situation, the target is to produce white LEDs. Based on the same blue LED and the different sieved fractions, WLEDs of the same color coordinates should be achieved. YAG phosphor enables only to reach cold WLEDs, a red component is missing for warmer WLEDs. The blue LED determines one position on the CIE diagram. The color of the phosphor sets another point. The chromaticity of LEDs made up of this phosphor is positioned on the line joining the coordinates of the blue LED and the phosphor. The WLED is defined at the intersection of this straight line with the Planckian locus. $\Delta u'v'$ defines the distance between color coordinates of the LED and the Planckian locus or to the phase of daylight for color temperatures equal to or smaller than 6500 K on the 1976 CIE diagram. An LED is declared as white when the condition $\Delta u'v' < 0.002$ is verified.

Characteristics of the white LEDs

White LEDs are fabricated following the process mentioned above based on different sieved samples of phosphor. The influence of the YAG:Ce particle size on the white PC-LED is investigated. The methodology is to fix the color temperature identically for the PC-LED based on different phosphor particle sizes. This enables one to compare the measurements performed on the LEDs and to determine the effect of the phosphor particle size.

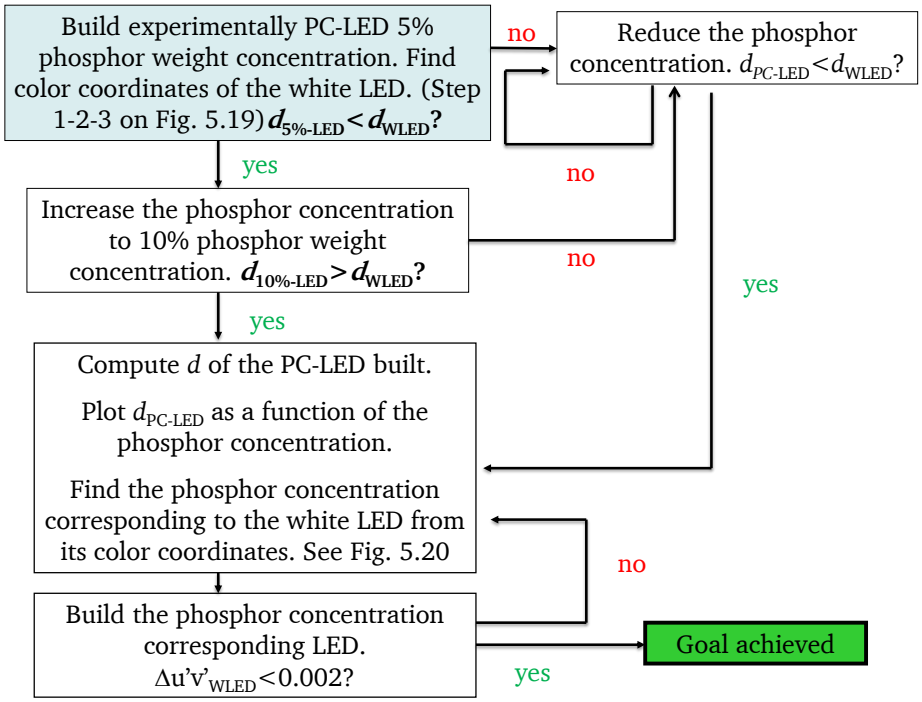

Figure 5.18.: Method to fabricate a white PC-LED

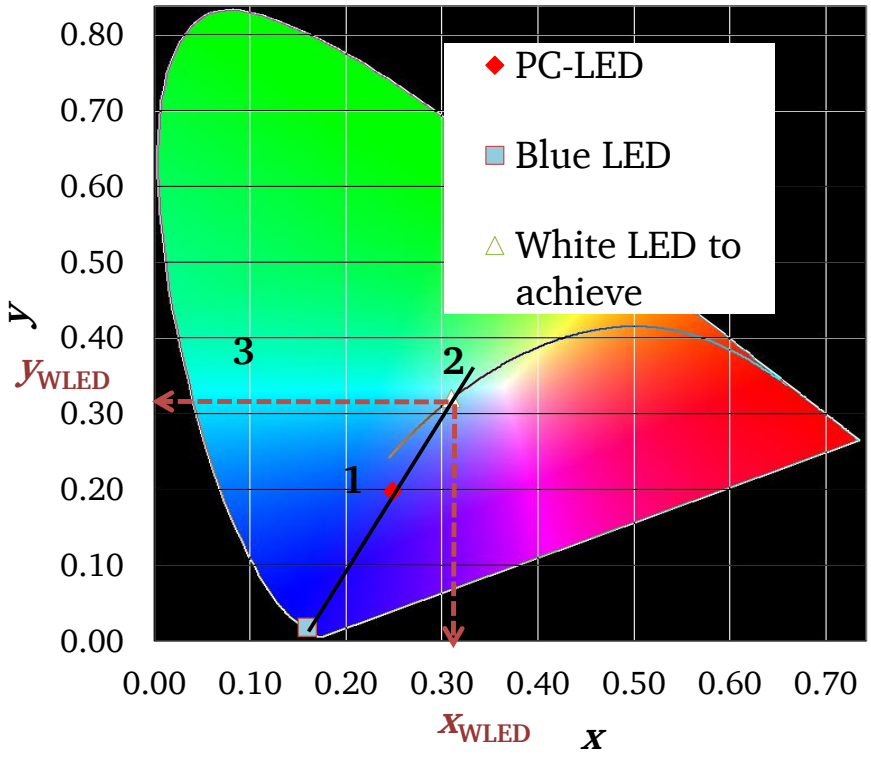

Figure 5.19.: Graphical determination of the white LED color coordinates. Legend: 1) Generate PC-LED 2) Join the blue LED and the PC-LED to cut the Planckian locus 3) Find the color coordinates of the white LED

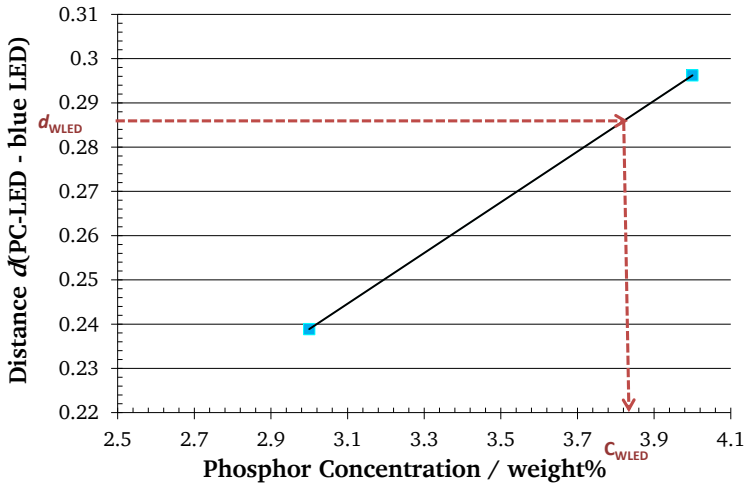

Figure 5.20.: Graphical determination of the WLED phosphor concentration

WLEDs have a similar CCT of 7000 K (Fig. 5.21 and 5.22) for LEDs type 1 (COB). The WLED is achieved by crossing the locus of the daylight illuminants on the CIE diagram 1976: $\Delta\ u'v' < 0.002$ (see Fig. 5.22), like already stated. The average and standard deviations of color characteristics measured for 8 WLED type 1 (COB) YAG 1 of each sieved fraction are shown in Table 5.2. The produced WLEDs correspond to the specifications of the ANSI C78.377-2008 standard for a cold white LED with a CCT of 6500 K (see Fig. 5.21).

Table 5.2.: Color coordinates with their standard deviations within 8 samples, correlated color temperature (CCT) with standard deviations and distance to Planckian locus ($\Delta u'v'$) for white LEDs type 1 (COB) YAG 1 and sieved fractions

	x	y	Δx	Δy	CCT / K	ΔCCT / K	$\Delta u'v'$
YAG 1	0.3076	0.3130	0.0047	0.0098	7010	430	$3.6{\cdot}10^{-3}$
YAG 1 #6	0.3079	0.3143	0.0048	0.0095	6969	406	$2.9{\cdot}10^{-3}$
YAG 1 #5	0.3079	0.3149	0.0073	0.0148	7013	626	$2.2{\cdot}10^{-3}$
YAG 1 #4	0.3068	0.3137	0.0066	0.0129	7088	635	$2.2{\cdot}10^{-3}$
YAG 1 #3	0.3092	0.3171	0.0056	0.0112	6870	494	$1.6{\cdot}10^{-3}$
YAG 1 #2	0.3087	0.3143	0.0128	0.0246	7148	1184	$4.2{\cdot}10^{-3}$
YAG 1 #1	0.3091	0.3146	0.0101	0.0198	6982	808	$3.3{\cdot}10^{-3}$

The chromaticity values of the WLEDs provided from an average of 8 LEDs for each fraction show an important CCT variation. This represents a very challenging issue for the industry. Chromaticity variations are difficult to control. Small inhomogeneity in the phosphor slurry, any impurity or absorption defect of the board can induce visible differences on the LED emitting color. Meticulous precautions were taken to work under same conditions, still LEDs from the same experimental batch exhibit differing color values. The 8 selected LEDs are collected after several experimental tries and are thus the result of hard perseverant labor.

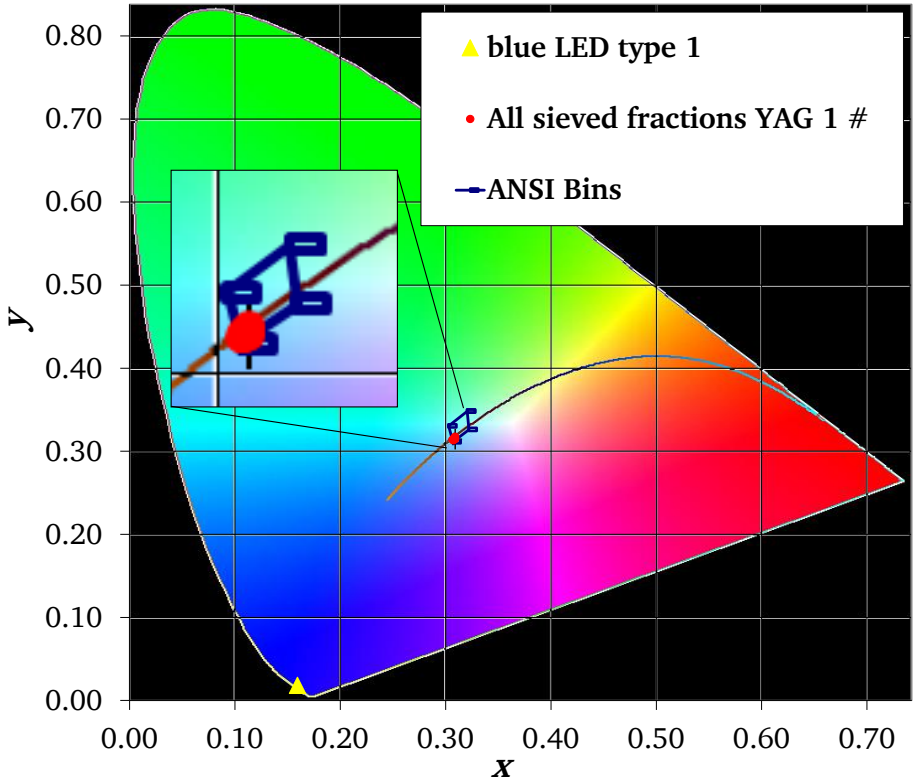

Figure 5.21.: *x,y* coordinates of YAG 1 PC-LEDs and sieved fractions on the CIE diagram 1931 with deviations and zoom on Planck's curve

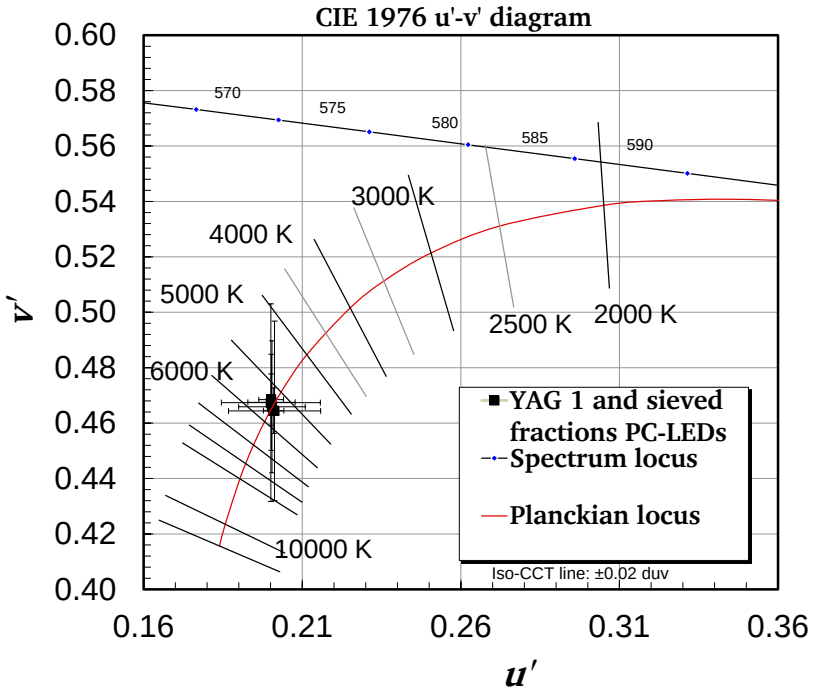

Figure 5.22.: *u',v'* coordinates of YAG 1 PC-LEDs and sieved fractions on the CIE 1976 diagram with deviations

5.2.2 Phosphor concentration

The concentration of phosphor required to reach WLEDs from phosphor having different sizes is investigated. The results can be seen in Fig. 5.23 (for LED type 1 (COB) and types 2,3,4 (SMD)). Influences on several parameters should be noted concerning the phosphor concentration required for WLEDs:

- Regarding particle size

  It can be concluded that PC-LEDs based on increasing phosphor particle size must have increasing phosphor weight concentration to reach the same color coordinates.

- Regarding volume of the LED

  The higher the volume of phosphor mixture contained in the LED cavity, the lower the corresponding phosphor concentration (see later in 5.2.3).

- Regarding LED package

  Neither the size of the die nor the emission wavelength of the LED plays a role on the relationship between phosphor concentration and phosphor grain size in the range of this study.

- Regarding wavelength of the chip

  The longer the distance from the blue LED to the white PC-LED on the CIE diagram (d_{WLED}), the more phosphor must be mixed in the PC-LED to achieve the same CCT. This phenomenon is particularly illustrated on LED types 2, 3 and 4, because these SMD PC-LEDs differ only by their blue LED emission. The corresponding explanations will be given in 5.2.3.

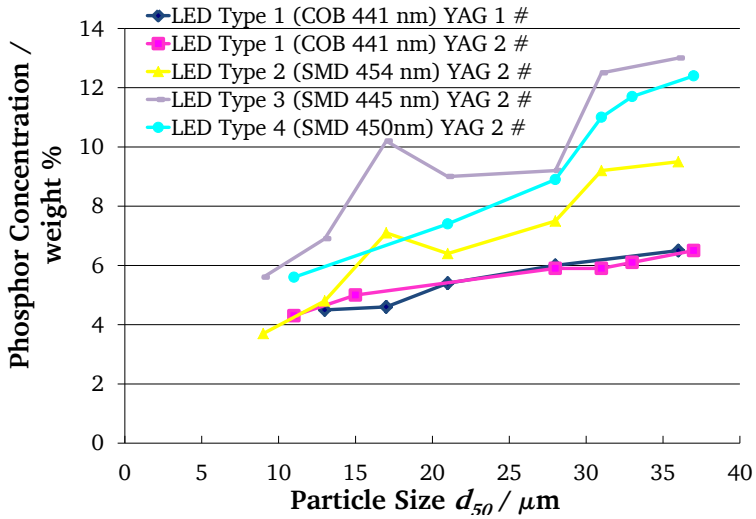

Figure 5.23.: Phosphor concentration as a function of the phosphor grain size for LED type 1 (COB) (YAG 1 and 2), and LED Type 2, 3, 4 (SMD) (YAG 2)

Even if YAG 1 # and YAG 2# show identical PSD and PL properties, the concentration required to reach PC-LEDs of similar white color chromaticity differ slightly (Fig. 5.23 for YAG

1 and 2 LED type 1). Experiments generate little variations in color chromaticity or volume of phosphor slurry filled which have consequences on the phosphor concentration required.

Considering the phosphor PL properties, it was found that phosphors with large particle sizes exhibit the best absorption properties and this type of phosphor is more efficiently excited by the LED emission spectrum. These phosphor particles emit as a consequence yellow radiation of higher energy while still in the powder state. As the density of the phosphor does not depend on phosphor particle size, WLEDs should be achieved by phosphors having large particles and lower concentrations. This contradicts the effect observed (see Fig. 5.23).

Images of the phosphor layer in LED type 1 (COB) are shown in Fig. 5.24. For the WLEDs with phosphor particle sizes from 31 μm to 37 μm the outlines of the chip are clearly seen. The clarity of the pictures are obtained by focusing on the chip surface which is easily seen due to the phosphor particles settled to the bottom. The WLEDs with smaller particles are well distributed in the phophor layer and diffuse the light. Thus the plane of the LED chip cannot be focused because of the phosphor particles in the planes above, as it can be seen in Fig. 5.29, 5.28, 5.27, 5.26. Large particles (down to 31 μm in our study) are more likely to settle on the bottom of the LED because they are heavier. During the curing process of the LED, the viscosity of the silicone decreases and these particles are able to settle, whereas smaller particles need a longer time than the curing time to settle (see section 5.2.6). It is therefore difficult to estimate the proportion of settled particles, but this could explain that the phosphor concentration needed is higher for large particles. The phosphor particles participating in the down-conversion mechanism are situated above the chip, the effective phosphor concentration is for larger particles lower. Decreasing the particle size enables the luminescent material to stay in suspension and contributes to the phosphor conversion process.

There are two linear zones for particle size versus concentration for WLEDs (see Fig. 5.23). The separation between the two zones occurs at particle size of 27 μm. The change in the slope of the straight lines may be attributed to particle settling. However, the relationship remains linear in the two zones.

The consideration of the number of phosphor particles present in the WLEDs is a further hypothesis for the phosphor concentration's reduction when the phosphor particle size decreases. The number of phosphor particles can be computed by eq. 5.2 and 5.3, according to phosphor density, its weight contained in the WLEDs, its size and volume. The representation of the number of phosphor particles to achieve a WLED as a function of the particle size is displayed in Fig. 5.31. The smaller the particles are the more particles need to be present in the LEDs to emit a similar white light because of their decreasing PL properties.

$$N = \sum_i f_i n_i \tag{5.2}$$

$$N = \frac{m_{phosphorinWLED}}{V_{part} d} \tag{5.3}$$

N = total number of phosphor particles

i = class number of particle size

f = frequency of the class

Figure 5.24.: YAG1 #6 (d_{50}=37 μm)

Figure 5.25.: YAG1 #5 (d_{50}=33 μm)

Figure 5.26.: YAG1 #4 (d_{50}=31 μm)

Figure 5.27.: YAG1 #3 (d_{50}=28 μm)

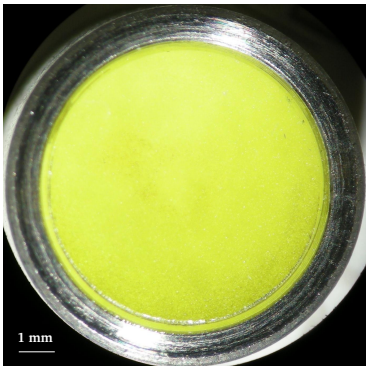

Figure 5.28.: YAG1 #2 (d_{50}=15 μm)

Figure 5.29.: YAG1 #1 (d_{50}=11 μm)

Figure 5.30.: Phosphor layer within the metal ring after curing under microscopy

n = number of particles per class

$m_{phosphorWLED}$ = mass of phosphor in the white LED / g

V_{part} = volume of the phosphor particle / cm^3

d = density of the phosphor / g/cm^3

The plot of the phosphor surface area as a function of the phosphor particle diameter (see Fig. 5.32), demonstrates that a higher area is necessary in the case of small particles to attain a WLED in order to compensate for inferior PL properties than in the case of larger particles (see section 5.1.3). Small phosphor particles show enhanced scattering and are

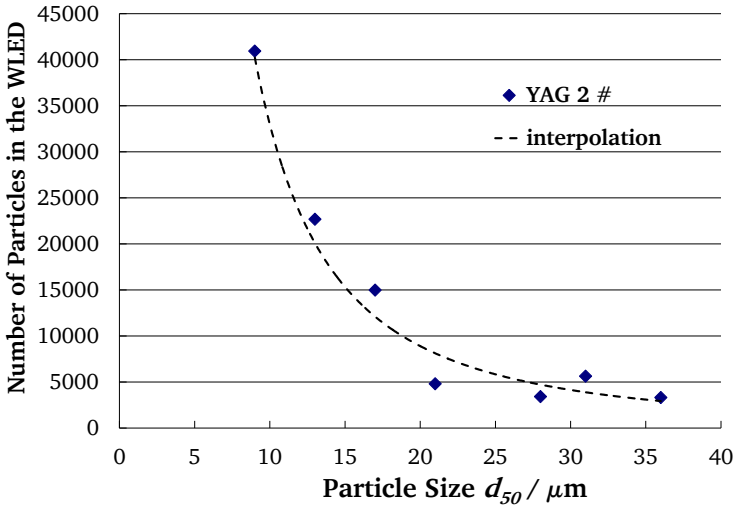

Figure 5.31.: Number of particles in the white LED as a function of the phosphor size d_{50} (LED type 2 (SMD))

characterized by their low absorption and emission. A high number of phosphor particles has to balance the PL properties which corresponds to large emitting area but still low phosphor concentration.

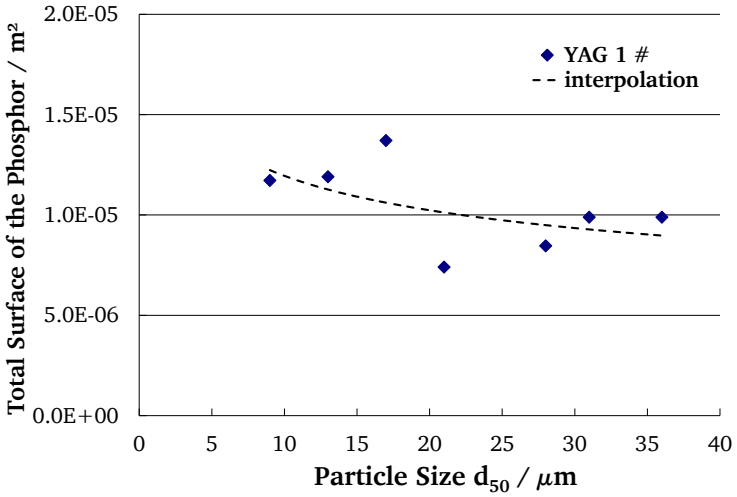

Figure 5.32.: Area of phosphor particles in the WLED as a function of the particle diameter d_{50} (LED type 2)

5.2.3 Influence of the blue emitting chip

Creating PC-LEDs made of phosphor powder and silicone binder deposited on a blue emitting chip can be interpreted in terms of their chromaticity color coordinates on a CIE x, y chromaticity diagram. Blue LED and phosphor are characterized by their chromaticity coordinates on the CIE diagram. The WLED is defined at the intersection of the straight line binding blue LED and phosphor with the Planckian locus. Depending on the wavelength of the blue chip and consequently a different position on the CIE diagram, the WLED based on

the same phosphor will automatically intersect the Planckian locus at a different place, and thus the WLED will have other color coordinates.

The effect of chip wavelength can be easily illustrated by the comparison between LED type 2, 3 and 4 in Fig. 5.33. Indeed, for the same phosphor these white PC-LEDs only differ in their emission wavelengths and therefore their color coordinates. The distance d_{WLED} separating the blue LED from the white LED on the CIE diagram indicates the amount of phosphor required to reach this WLED. The distance $d_{LED445nm}$ (type 3) is longer than $d_{LED454nm}$ (type 2). This implies that the phosphor concentration is higher for LED type 3 (445 nm) than type 2 (454 nm) (see Fig. 5.33 and Table 5.3).

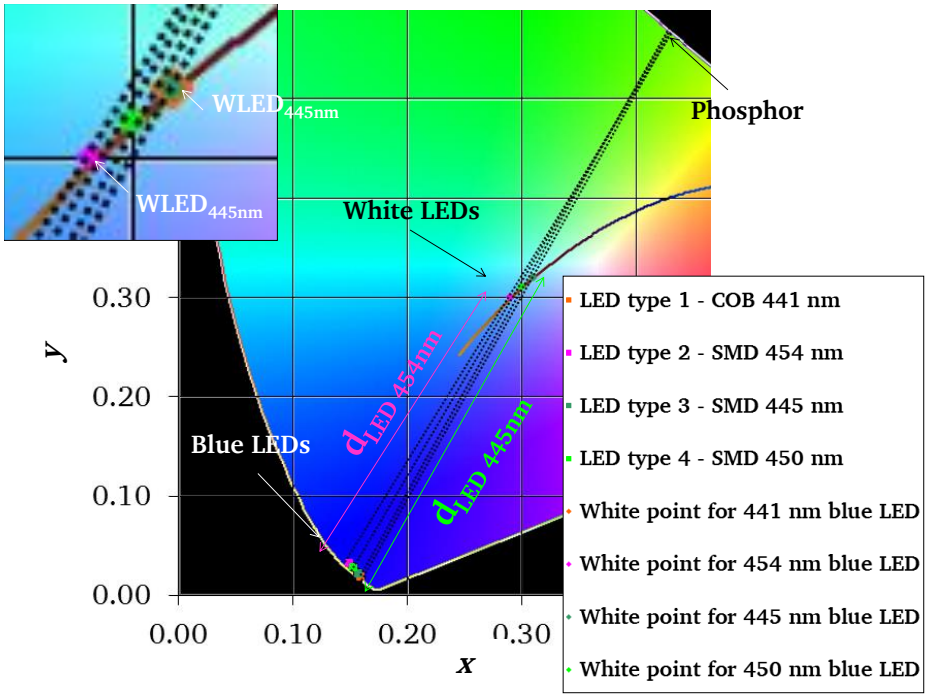

Figure 5.33.: CIE Diagram 1931 with the color coordinates of the blue LEDs, phosphor and corresponding WLEDs. Zoom on WLED domain is shown

The LED type 1 (COB) contains a higher volume of phosphor and silicone (39 mm^3 versus 7 mm^3 for the LED type 2, 3 or 4, SMD LEDs). The weight concentration of the phosphor in the LED is lower in the case of the COB LED type 1 because more phosphor particles are available in a more extended volume. Table 5.3 shows the phosphor concentration as a function of the particle size for WLEDs. Higher concentrations are required in LEDs with smaller volume independently of particle size.

5.2.4 Output of the white LEDs

The influence of particle size on luminous efficacy is shown in Fig. 5.34. The luminous flux decreases slightly for particles from 36 to 28 μm and steeply for smaller particles. As we already published in [95], the luminescence properties reveal the same phenomenon as the PL in regard to the particle size. With increasing particle sizes the exciting beam of the blue LED is better absorbed, the phosphor is better excited and emits at a higher intensity. Moreover the phosphor weight concentration increases with the particle size which enhances the mechanism. Scattering properties must also be considered. Mie theory can be applied

Table 5.3.: Phosphor concentrations of White LED for LED type 1 and 4 in the case of several sieved fractions

	particle size d_{50}/ μm	phosphor concentration / weight%	
		in LED type 1 (COB)	in LED type 4 (SMD)
YAG 1 #6	37	6.5	12.4
YAG 1 #5	33	6.1	11.7
YAG 1 #4	31	5.9	11
YAG 1 #3	28	5.9	8.9
YAG 1 #1	11	4.3	5.6

for small particles. These latter emit namely in every directions in contrary to larger particles which show an emission more directed to the front of the LED. In case of small particles, the phosphor-converted light is sent back to the chip or board or other phosphor particles and is consequently absorbed. Backscattering participates in the LED emission reduction observed for particles of decreasing size.

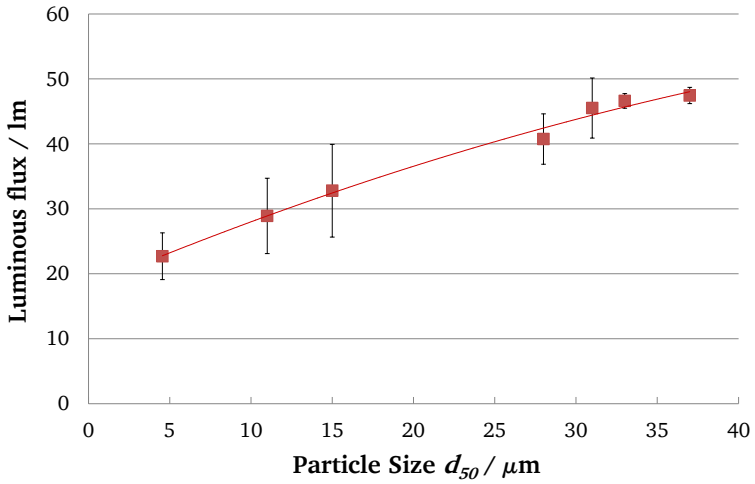

Figure 5.34.: Luminous flux depending on the particle sizes $d_{50}$of WLED made of YAG 1# and LED type 1 (COB)

The WLED radiant flux distribution over the wavelength shown in Fig. 5.35 describes a typical cold white LED, having a low color rendering index of 65. The curves prove that the LEDs have the same color coordinates, since the ratio between the blue portion from the LED and the yellow portion from the fluorescence remains equal independent of the phosphor size. The global intensity decreases by reducing the phosphor particle size, leading to a reduction of the luminous flux. The quality of the light characterized by the color rendering is, for the same reasons as the constant color coordinates, not affected by the phosphor particle size (see Table A.2).

Regarding radiometric output, radiant flux integrates the spectral power of an LED spectrum over the wavelength (Fig. 5.35). Luminous flux corresponds to the radiometric spectral distribution of an LED transformed by the curve of the human eye's sensibility $V(\lambda)$. Since all PC-LEDs emit for each wavelength with the same proportions, the standard luminosity function acts as a coefficient and radiant flux show the same trend as the luminous flux. Both radiant and luminous fluxes decrease when the phosphor particle size decreases (see in Fig. A.10 of Appendix A).

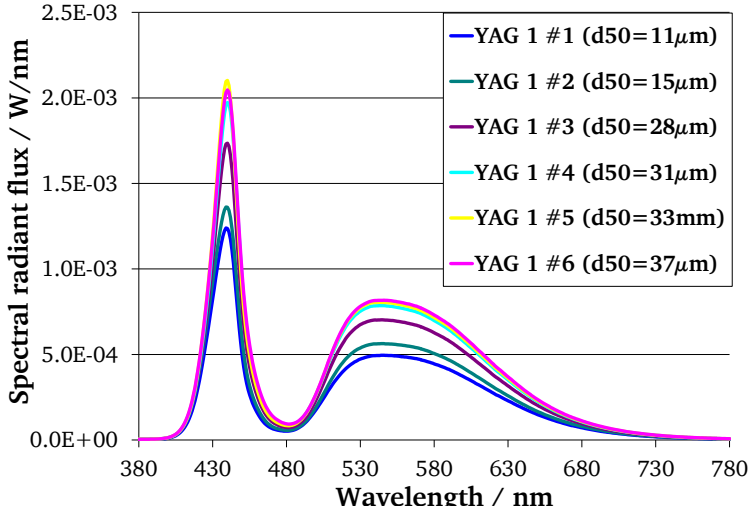

Figure 5.35.: White LED emission spectra for different particle sizes (YAG 1 # LED type 1 (COB))

5.2.5 Angular homogeneity

The question of equal distribution of the white LEDs radiation over the emission angles is discussed below. The angular properties were measured on an optical bench rotating the LED on a goniometer as described in section 4.6.2. The angular distribution of the blue LED illuminance (E), without the presence of phosphor is represented in Fig. 5.36. Because of the LED package (type 1, COB) and especially its ring, the light is strongly restricted and cannot propagate beyond 45°. 33° is the theoretical emitted angle calculated from the geometry of the ring above which rays are not directly exiting the LED without being reflected by the ring. These rays can then be anew reflected or absorbed by the device.

The presence of the phosphor enables the light to be extracted from the package up to 60°, as can be seen in Fig. 5.37. The angular light intensity distribution is not affected by the change of the phosphor size for WLEDs. The spatial distribution of the white LEDs' illuminance shows the same trend as of the blue LEDs'. White LEDs containing particles with small diameters emit at a lower intensity. This result identified by integrating sphere measurements is confirmed by this analysis and extended to every emission angle.

The CCT was analyzed also as a function of angle (Fig. 5.38). A bluish white light is emitted at 0° and tends to be more yellow at wider angles (decreasing of the CCT). This trend does not depend on particle size. However, the decrease of the CCT variation increases in importance when the particles become smaller. The CCT difference between 0° and 60°

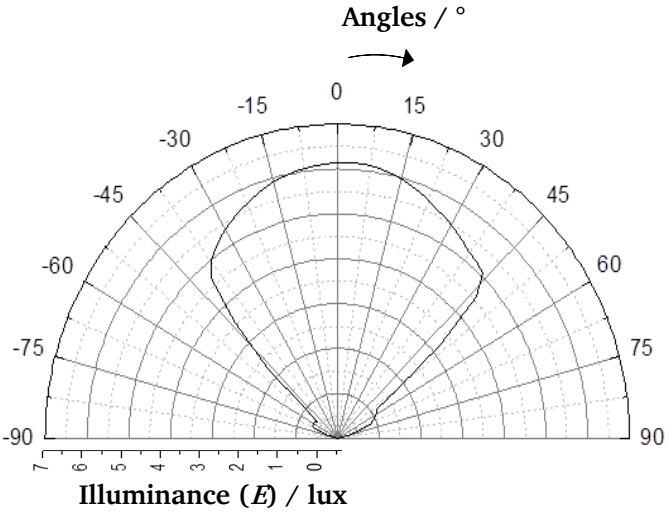

Figure 5.36.: Angular illuminance of a blue LED

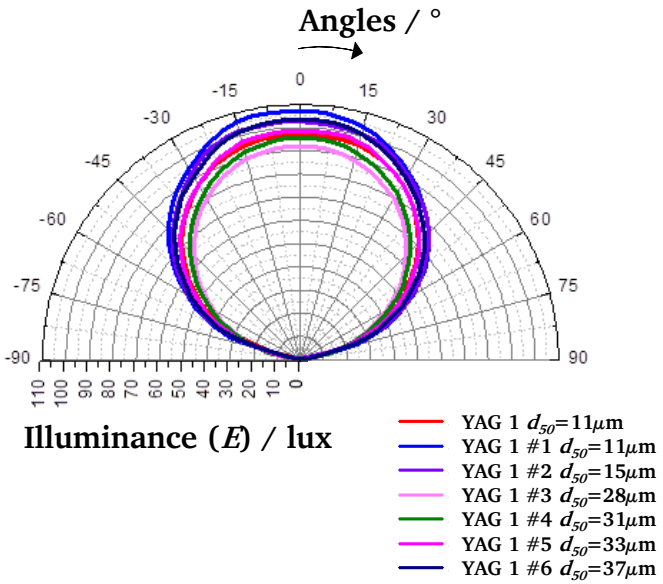

Figure 5.37.: Angular distribution of the illuminance for different phosphor sizes

changes from 15 % for phosphor particle sizes of 36 μm to 6 % for particle sizes of 17 μm particles. CCT difference increases slightly to 8 % for 5 μm diameter particles.

The CCT variation for large particles can be explained by the decreasing number of phosphor particles and enforced phosphor settling process. In contrary phosphor particles of about 20 μm are homogeneously distributed in the phosphor layer and their concentration is still moderate. Besides decreasing phosphor particles show enhanced scattering properties which favors an emission in every direction and contributes to a homogeneous light distribution. Hence the color of the light emitted does not vary much over the angles. Within the studied range, LEDs based on phosphor particles of 17 μm exhibit the best color homogeneity over the angles.

The reason why the emitted light is much more yellow on the side with small particles relies on geometrical considerations. The number of particles present in the phosphor layer of WLEDs has already been reported in 5.2.2. The number of particles increases when the phosphor particle size decreases, even if the phosphor weight concentration is lower. The direction of the beam directed to the side is longer than at 0°. The probability of the blue light to contact a phosphor particle and to be converted into a yellow light increases for small particles because there are more particles (Fig. 5.39). This phenomenon is named yellow ring effect.

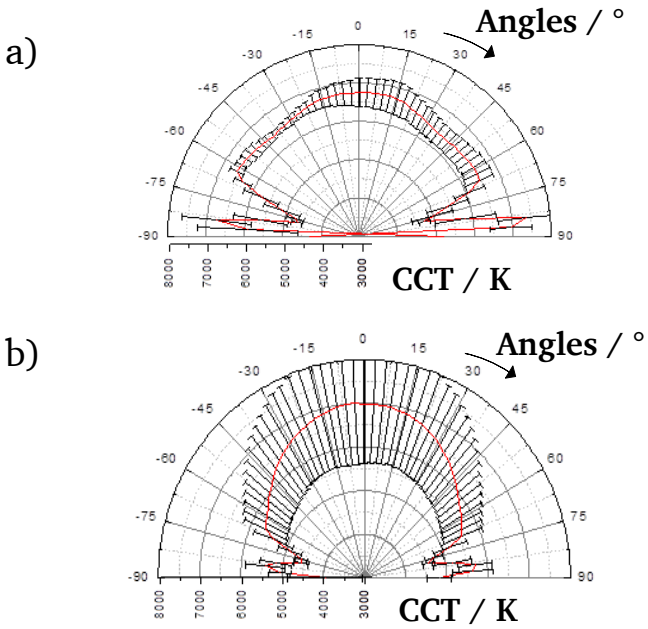

Figure 5.38.: Angular measurement of the correlated colour temperature for different phosphor particles (LED Type 1 a) YAG 2 #2 d_{50} = 17 μm b) YAG 2 #1 d_{50} = 13 μm)

The angular distribution of the LED type 1 YAG 1 # and type 4 is displayed in Fig. A.11 of the Appendix A.

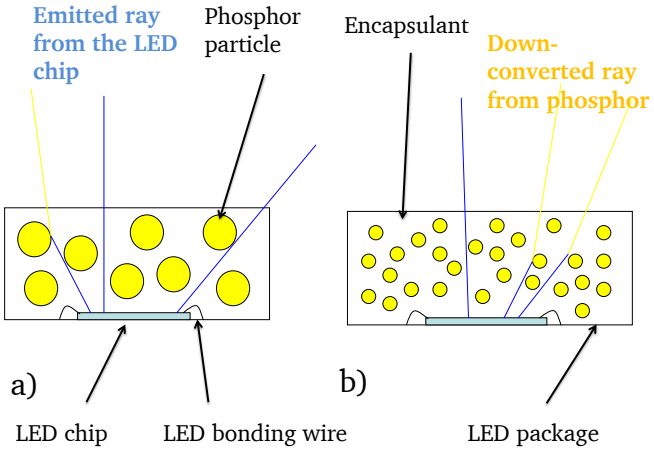

Figure 5.39.: Ray tracing of the light in the white LED in case of a) large particles (high weight concentration but still low number of particles) and b) small particles (low weight concentration but high number of particles)

A typical behavior for the spectral radiant flux over the measurement angle is shown in Fig. 5.40. The proportion of yellow radiation at 60° is about a half of the blue emission while it is about a third at 0°. This confirms the conclusion from Fig. 5.38 that the proportion of phosphor emission is higher and thus the CCT lower at wider angles of the LEDs than in the normal direction.

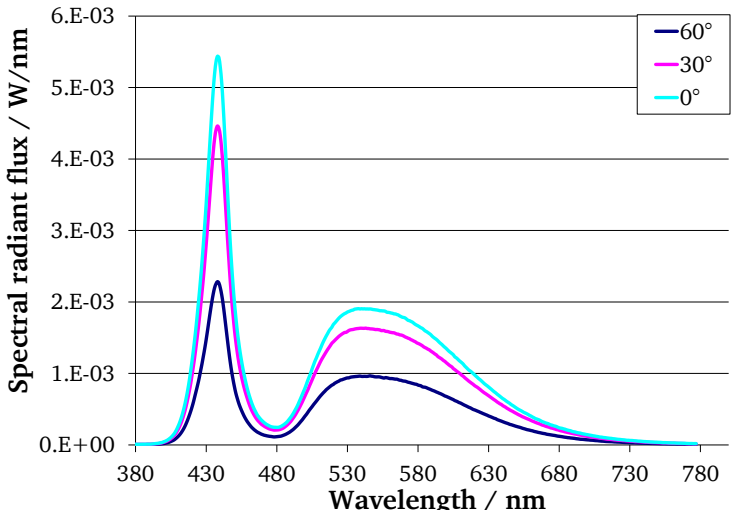

Figure 5.40.: White LED spectral radiant flux depending on the LED measurement angle

5.2.6 Influence of the binder

A PC-LED consists of the LED chip, a phosphor or a mix of phosphors spread into a binder, in our case silicone. The role of the binder is also important. Besides the transparency in the visible, two characteristics are particularly decisive in the choice of a binder: the refractive index and the viscosity.

The influence of refractive index (OE 6550 Dow Corning n=1.54) on light emission and chromaticity is presented in Fig. 5.41. The results obtained with a high refractive index silicone show the best light extraction because of the increase of the total reflection angle, as explained in section 2.5.2. The luminous flux is enhanced by using a high refractive index silicone binder. Compared to a lower refractive index silicone (OE 6350HF Dow Corning n=1.4), the high refractive medium leads to an LED color shift into the red tones. The silicone absorption is not constant over the wavelength.

The transmission of the high refractive index silicone is measured through a 0.52 mm thick layer sample. On an linear optical bench, the sample is positioned between the light source and the detector. Light emitted by the reference lamp with sample (silicone layer) is compared to the measurement without sample. Measured data are obtained by subtraction of these two data sets. Experimental results are plotted in Fig. 5.42. Even if the transmission is over 99 % in the visible, an absorption increase of 99 % transmission at 380 nm to 99.5 % transmission at 780 nm can be identified. This difference in transmission repeated several times by rays being reflected inside the silicone layer leads to large transmission losses which are wavelength dependent. This effect explains the shift of color coordinates a little to more reddish colors.

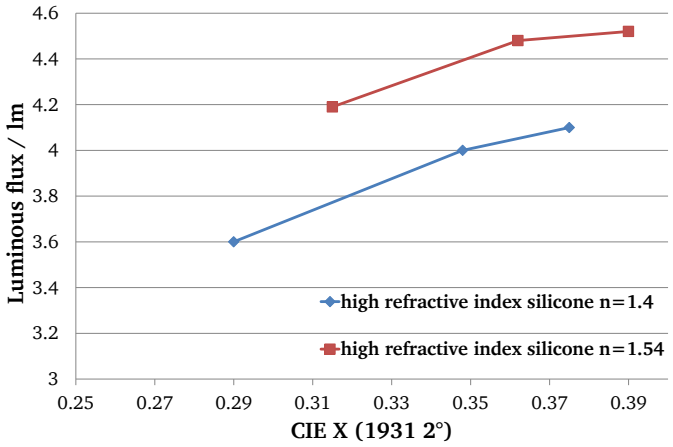

Figure 5.41.: Color coordinates and luminous flux for LED 3, 4.5 and 6 weight% phosphor concentration (from left to right) in the case of a low and high refractive index silicone

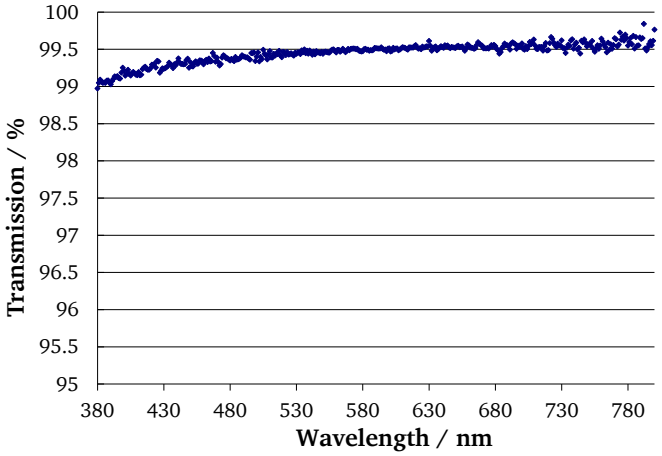

Figure 5.42.: Spectral transmission of 1.54 refractive index silicone through 0.52 mm thick layer

The viscosity is now considered. The time dependence of phosphor particle sedimentation is shown in Fig. 5.43. The computation is based on Stokes' law (eq. 5.4) applied with the experimental parameters of the studied materials.

$$V = \frac{2r^2 g \Delta\rho}{2\eta} \tag{5.4}$$

V : settling speed / m/s

r : radius of the sphere / m

g : acceleration / m/s^2

$\Delta\rho$: volumic mass difference between the particle and the fluid / kg/m^3

η : viscosity of the fluid / Pa·s

At the beginning of the curing process silicone viscosity decreases because of the temperature increase which facilitates the deposition of particles on the chip surface. This validates the previous observations of the LED images in Fig. 5.24. However, silicone viscosity rises again when the silicone starts to polymerize. The particles are then captured in the polymerization matrix in order to build a solid phosphor layer.

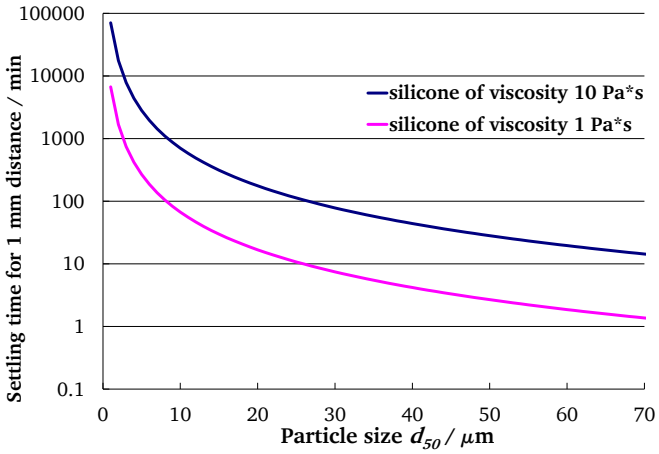

Figure 5.43.: Computed settling time of phosphor particle on logarithmic scale depending on their particle size d_{50} for two binder viscosities

Independently of the silicone viscosity, the tendency is that the larger the phosphor particles are, the faster the particles settle. The overall curing time is of one hour, though the polymerization starts before. The low viscosity silicone presented in Fig. 5.43 corresponds to the catalyst of the silicone used in this study. Particles exceeding approximately 25 μm should therefore not be used with this silicone binder. Else the phosphor layer would not be homogeneous. A mixture of this silicone binder to ensure the polymerization and a higher viscosity silicone is chosen for this study. This improves the settling time of 25 μm particles from 10 minutes to 100 minutes for 1 mm sedimentation. Following criteria have to be considered for use of silicone binder for LED application:

- high refractive index to improve the light extraction
- short time polymerization in order to limit the phosphor settling
- high viscosity in order to slow down the settling process during the beginning of the curing process while the rise in temperature decreases the viscosity.

5.3 Predicting LED emission spectra

LED components are influenced by a vast number of factors. Their interactions have to be experimentally tested and investigated in order to understand the mechanisms and obtain LEDs with target color coordinates or luminous flux. Being able to predict the LED properties from the LED package characteristics and phosphor PL measurements without building the PC-LEDs practically would be very useful to reduce the development time.

In this section, the emphasis will be on the understanding of the composition of a PC-LED spectrum with an analytical method, identifying the limits and with the help of an optical simulation, attempting to reproduce the results collected from the experiments.

5.3.1 Understanding phosphor-converted LED spectra

A spectrum of a PC-LED is composed of the blue exciting LED chip and the phosphor down-converted component. At first sight it seems that the simple addition of the blue LED and the fluorescent emission spectrum (eq. 5.5) communicates the same information as revealed by a phosphor-converted LED spectrum. However, Fig. 5.44 contradicts this hypothesis. Discrepancies can be found in three wavelength regions: 410-445 nm, around 490 nm and 500-530 nm.

$$S(\lambda) = \alpha S(_{blue}) + \beta S(_{phosphor}) \tag{5.5}$$

With α and β coefficients depending on the LED and the phosphor characteristics respectively.

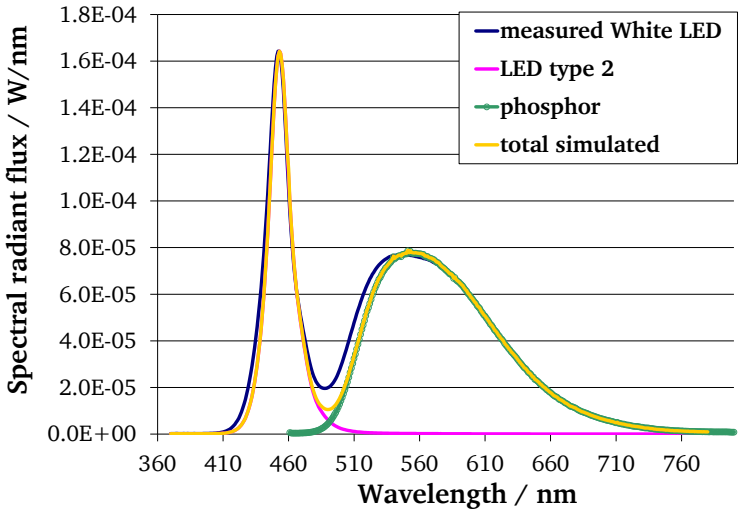

Figure 5.44.: Mathematical addition of the blue LED and the emission spectra of phosphor in comparison to a measured phosphor-converted LED

The PL proprieties obtained from the emission, reflection and excitation of the phosphor are related to the measurement equipment. This measuring set-up remains an informative source based on the interaction between the first layers of phosphor particles. The vessel containing the phosphor powder implies that the beam does not enter deeply into the sample. The beam may come again in contact with the sample surface and alter the information due to probable multiple reflections. As already mentioned in 4.4.1 phosphor PL properties are measured in reflection mode. When the phosphor is excited in the LED, the rays are transmitted through the phosphor layer which corresponds thus to a transmission mode. The transmission properties have to be taken into consideration. In addition, the basic combination of phosphor and LED spectra neglects the reflection or excitation spectrum characterizing each phosphor. These criteria are essential in order to generate an LED spectrum as close to reality as possible. PL measurement data should therefore be exploited cautiously.

Transmission properties

Recording the transmission properties of a phosphor layer as a function of wavelength can be a hint to describe the physical mechanisms taking place in the LED. This analysis was

carried out by measuring the radiation emitted through the phosphor positioned in front of the integrating sphere. Figure 5.45 shows the difference between emission spectra provided by the usual equipment measuring by reflection on the sample surface (reflection mode) and another set-up measuring in transmission mode.

A part of the emission spectrum obtained under transmission conditions disappeared compared to the reflection mode emission. The phosphor layer used for the transmission experiment is dense, thus a portion of the emission spectrum is absorbed by the phosphor layer itself. It is known from the reflection characteristics that between 500 and 525 nm, the absorption decreases from its maximum value (Fig. 5.13). The emission is truncated because of self-absorption where the difference between emission curves measured in reflection or transmission mode in Fig. 5.45 reaches a maximum at 525 nm.

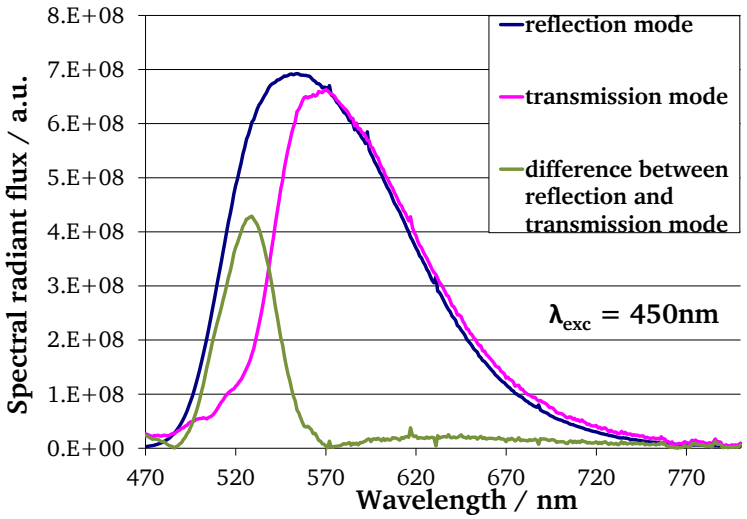

Figure 5.45.: Photoluminescence measured on the surface of YAG 2 (reflection set-up) and through the powder (transmission set-up) at 450 nm excitation

The transmission occurring in the LED amplifies the reflection phenomenon which is enhanced when the phosphor is concentrated.

Over-concentrated PC-LEDs

PC-LEDs were realized with an increasing phosphor concentration in the mixture of silicone and phosphor. The concentration was tuned from 1 % to 80 % with YAG 2 of broad PSD and median particle size, d_{50} of 12 μm. The same experiment was performed with a sieved phosphor YAG 2 #1, having a narrow PSD and a d_{50} value of 13 μm. The color coordinates of these PC-LEDs are displayed in Fig. 5.46. The blue LEDs used during the experiments are LED type 2 (SMD LED). A series from 1% to 40% phosphor concentration was also carried out on YAG 1 LED type 1 (COB LED), so that the influence of the thickness of the phosphor layer, the blue emitting LED and the phosphor particle size and distribution on the PC-LED properties can be investigated as well.

It should be noted that for any phosphor or exciting blue LED (LED type 1 or 2) the color coordinates are located on a line passing through the blue LED. This conclusion is in harmony with results from section 5.2.1. The line is oriented in the same direction and cuts the Planck's curve on the same point for the same LED type independent of the particle size

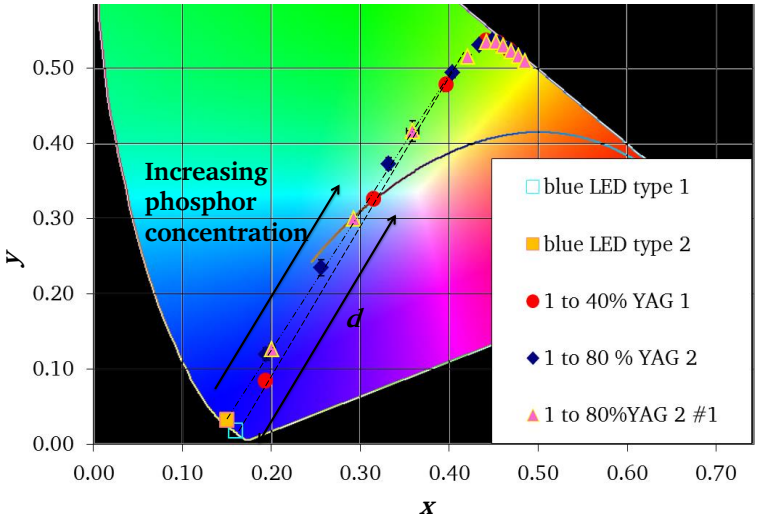

Figure 5.46.: Color coordinates on the CIE Diagram 1931 of a PC-LED with rising phosphor concentration 1, 5, 10, 20, 30 and to 40 % YAG 1 d_{50}= 11 μm LED type 1 (COB LED); 1, 5, 10 % and every 10 % until 80 % YAG 2 d_{50}= 12 μm LED type 2 (SMD LED); 1, 5, 10 % and every 10 % until 80 % phosphor YAG 2 #1 d_{50}= 13 μm, LED type 2 (SMD LED)

distribution of the phosphor and its size. When using another type of LED, having a different peak wavelength and thus different color coordinates, the WLED is reached at another locus of the Planck's curve. This validates the results obtained in section 5.2.1. The concentration series begin to deviate from the straight line when the concentration rises above 20 %. The length of the segment d on the CIE diagram connecting the blue LED to an LED of certain phosphor concentration was computed (according to eq. 5.1) and is plotted in Fig. 5.47. For small until moderate concentrations up to 15 %, the tendency is linear, as assumed in section 5.2.1. In over-concentrated LEDs (with phosphor concentrations above 30 %) the distance remains constant. When the concentration increases over that limit, the LED spectrum changes because of self-absorption which shifts the LED chromaticity.

Figure 5.48 depicts the emission spectra of highly concentrated PC-LEDs. The blue emission peak is completely absorbed by the phosphor particles and does not appear on the spectrum anymore from the phosphor concentration of 40 %. The blue emission participates entirely in the excitation of the great amount of phosphor. At high concentration the phosphor is forming a layer so compact that the blue rays from the LED could not even be extracted from the device before exciting a phosphor and being absorbed. This phenomenon is known as total conversion. The maximum of the phosphor peak seems to be shifted to longer wavelengths. This impression is given because the phosphor emission is trapped in the phosphor layer. A portion of the spectrum up to 540 nm is absorbed owing to self-absorption.

The measurements obtained in transmission mode (see section 5.3.1) were performed without silicone binder in contrary to the ones from Fig. 5.48. Even if the silicone binder plays a important role on the light extraction and wavelength dependent absorption, both experiments confirm phosphor self-absorption.

The PC-LED luminous efficacy was also investigated as a function of the phosphor concentration (Fig. 5.49). A maximum is reached at a concentration higher than the one necessary to emit white light. The increasing presence of phosphor particles allows more phosphor con-

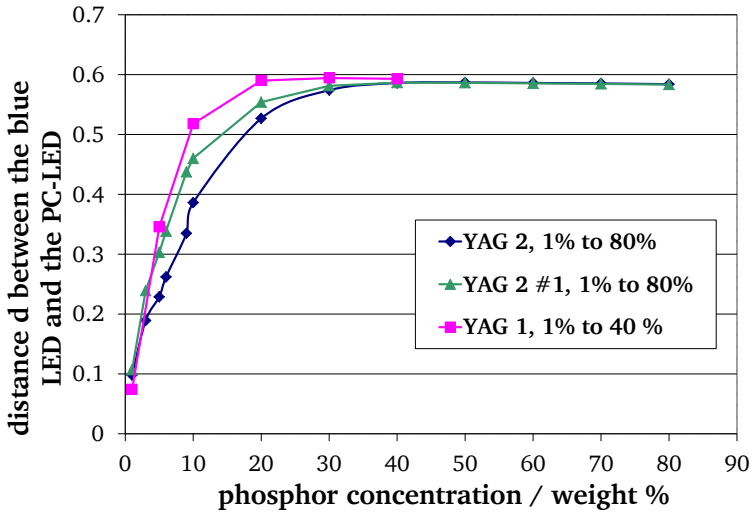

Figure 5.47.: Distance d on the CIE diagram 1931 between the blue LED and the PC-LED for 1% to 40% YAG 1 d_{50}= 11μm LED type 1 (COB LED); 1% to 80% YAG 2 d_{50}= 12μm LED type 2 (SMD LED); (1% to 80%) phosphor YAG 2 #1 d_{50}= 13μm, LED type 2 (SMD LED)

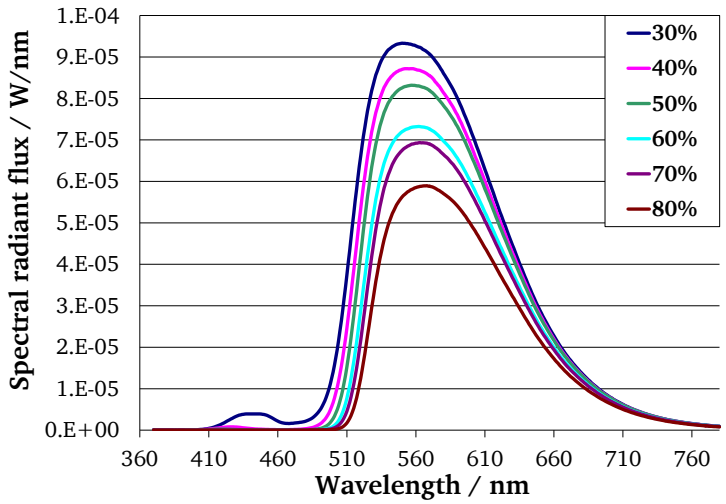

Figure 5.48.: PC-LED emission spectra with YAG 2 d_{50}= 12 μm LED type 2 (SMD LED) concentrated from 30 % to 80 %

version. Luminous flux is weighted by the standard luminosity function peaking at 555 nm. Increasing the phosphor conversion of large emission band at about 560 nm favors the luminous flux output and so the luminous efficacy. Nevertheless, too many phosphor particles reduce the intensity because of self-absorption. The blue light is then completely converted, the peak of the blue LED slowly disappears and the down converted rays are reflected on the phosphor particles themselves. The higher the concentration the more light is trapped inside the phosphor layer. Phosphor self-absorption generates a loss in intensity and this is why the luminous efficacy then declines.

The analytical investigations gave the evidence that PL properties provide an explanation for the fluorescent mechanisms involved in a PC-LED. Still, limits have to be admitted, about

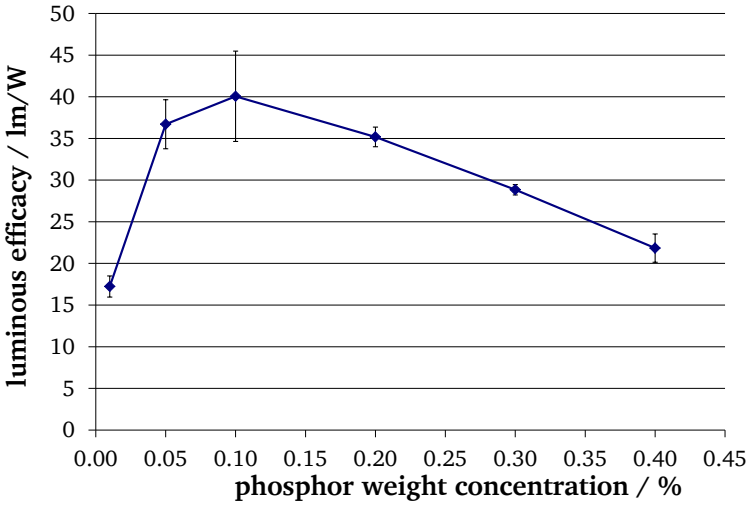

Figure 5.49.: Luminous efficacy of PC-LED type 1 (COB LED) with increasing phosphor concentration (YAG 1)

the possible restrictions related to the measurement, reproducibility between devices and difficulty to estimate the energy loss. Perfect measurement of properties is not possible, for example reflection cannot be measured without multiple reflections. Moreover transmission impact ascribed by the binder should also be taken into consideration in a model describing PC-LEDs.

5.3.2 Predicting phosphor-converted LED spectra by simulation

The experimental part conducted so far permitted us to understand the mechanisms taking place when PC-LED emission spectrum is produced. These processes can be summed up in Fig. 5.50.

- The blue exciting light (I_0) can pass through the phosphor particle layer without any conversion and escape the silicone layer. Though the power is then reduced from the absorption coefficient of the binder medium (I).
- The light from the LED (emitted around 450 nm) may be reflected on a phosphor particle at the same wavelength, losing the power corresponding to the absorption coefficient (A) of the phosphor at this wavelength.
- The exciting beam can be down converted and emit with a shifted wavelength (Stokes Shift, SS) with an efficiency depending on the quantum efficiency (QE) of the phosphor.
- Finally this down converted light can be reflected and lose a portion of intensity by re-absorption. The more phosphor particles are present, the higher the probability, that the down converted beam meets another particle. The intensity will decrease each time more owing to the absorption.

Nowadays software exists to take into consideration the properties of each separate entity present in the system and predict the result of each components' combination. One of the software programs intending to meet all these specifications is Lighttools.

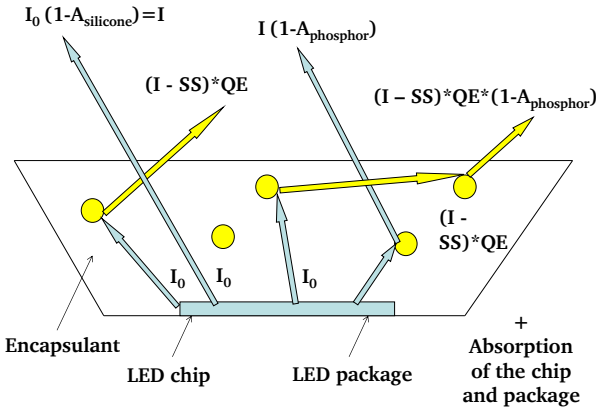

Figure 5.50.: Mechanisms inside the LED

Comparison of spectra between simulation and measurements

A model representing respectively the type of LED 1 and 4 was optimized with Lighttools. These two LED packages are investigated. Emission spectra of PC-LEDs of the sieved fraction previously studied are simulated for both packages. Photometric values, light quality and light preferences of the simulation are compared with measurements from the laboratory of 8 measured LEDs. As explained in section 4.7, Lighttools bases the computation of PC-LED emission spectra on input parameters essential for a promising description of the physical mechanisms.

The models are corresponding to the geometry of the two packages (LED type 1 and 4). The refractive index of the silicone and phosphor are set to 1.54 and 1.8 respectively. The transmission of the silicone is 89 % for 1 mm. The phosphor and silicone layer is coated by a conventional dispensing method. The following phosphor characteristics are based on the luminescent measurements:

- Down converted radiations are measured for the phosphors. The phosphor emission spectrum is empirically adjusted so that multiple absorption is considered. The same normalized spectra represented in Fig. 5.51 are implemented for every sample.
- Measured excitation spectrum implemented as parameter is plotted in Fig. 5.51.
- Fig. 5.51 depicts also the absorption properties that are derived from the reflection measurement.

The walls of the cup containing the luminescent material are assumed to have a reflectivity equal to 1. The experimental PSD is implemented for each phosphor sieved fraction. Optimizing the phosphor concentration for each phosphor sample leads to an increasing correlation between the simulation and the experiment.

The results of the simulation spectra of different particle sizes are presented in Fig. 5.52 for LED type 4 and in Fig. A.12 for LED type 1 in Appendix A. The simulated and measured emission spectra are plotted as well as their spectral differences.

The difference between the simulated (dashed lines) and measured emission spectra (full lines) represented by the dotted line in Fig. A.12 and 5.52 enables one to identify at which wavelength discrepancies of simulation occur. Simulated and measured phosphor down conversion as well as the emission around 480 nm at the junction point in the spectrum

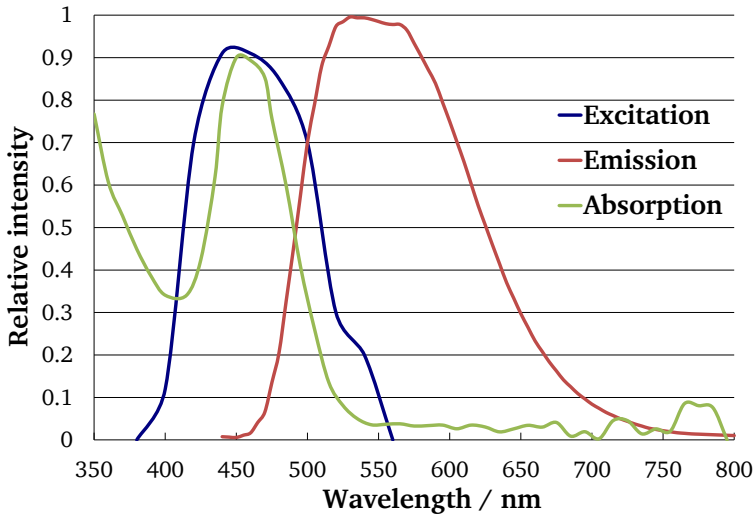

Figure 5.51.: Relative emission, absorption and excitation spectra used as parameter in Lighttools

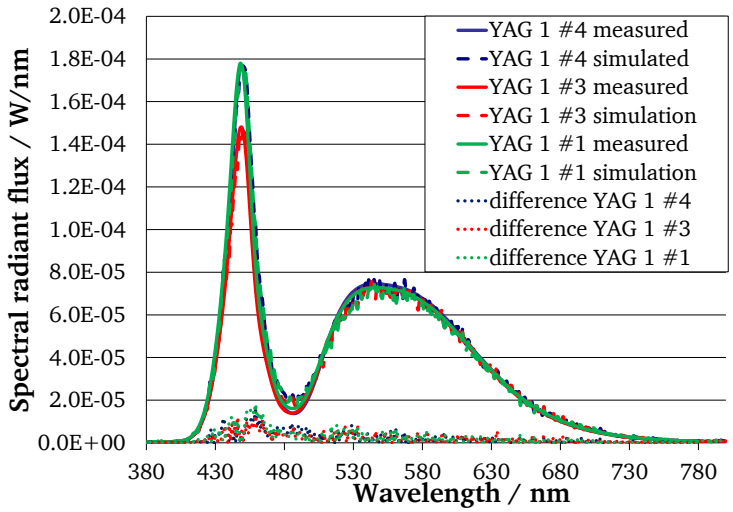

Figure 5.52.: Comparison simulation and measurement of the LED type 4 (SMD LED)

between blue emission and phosphor exhibit a good fit: simulated and experimental curves overlap and the difference is small. The simulation differs from the measurements around the position of the blue peak. The spectral position of the blue peak wavelength itself is well predicted by the simulation. Differences arise concerning the shape of the blue emission peak. Simulations of the blue LED chip without phosphor perfectly reproduced the blue emission peak but simulations did not match any more when the phosphor was introduced into the program. The mismatch can be ascribed to the phosphor itself. The measured absorption data of the phosphor we implemented in the simulation as an input parameter may not have been appropriate: they might have been too high in the wavelength interval of the blue emission. PL input data are obtained by measurement in reflection mode whereas LED work on transmission mode.

The photometric, chromaticity and color quality values are summarized in Table 5.4 for LED type 4 and Table A.2 in Appendix A for LED type 1. There are different ways to evaluate the difference between simulated and measured LED emission spectra. The extent of the error

can be evaluated by the emission intensity difference for each wavelength (see Fig. A.12 and 5.52). Another way to evaluate this error is the computing of a standard measure widely used in lighting engineering which characterizes the perceived quality of white tones i.e. whether the white tone of the PC-LED can be considered as an acceptable or preferred white tone (e.g. without any disturbing greenish shade) when it is assessed visually by the human user. This measure is the white tone chromaticity difference $\Delta u'v'$ between the chromaticity point of the PC-LED and its so-called reference light source in the CIE u',v' chromaticity diagram. The reference light source is a phase of daylight above 5000 K CCT or a blackbody radiator below 5000 K. The reference light source has the same CCT as the PC-LED. These chromaticity differences are also listed in Table 5.4 for LED type 4 (SMD LED) and Table A.2 in Appendix A for LED type 1 (COB LED).

Table 5.4.: Simulated and measured characteristics of LEDs type 4 (SMD LED)

	YAG #1		YAG #2		YAG #4		YAG #6	
	sim.	meas.	sim.	meas.	sim.	meas.	sim.	meas.
CCT / K	7925	7439	6588	6489	7641	7100	7742	7402
CRI R_a	75	74	73	71	74	72	75	73
R_9	-4	-12	-23	-31	-11	-20	-10	-16
luminous flux / lm	4.2	4.3	4.2	4.3	4.3	4.4	4.5	4.4
$\Delta u'v'$	0.007	0.005	0.001	0.002	0.006	0.004	0.006	0.005
Q_9	86	86	89	89	87	86	87	85
Q_g	91	91	90	89	90	90	90	90
Q_a	71	71	72	71	70	70	71	69

Because of the not complete matching of the simulated and measured spectral power distributions, the two CCT values do not match. Such differences (ΔCCT=200 K - 500 K) are visually well noticeable. The general color rendering property of the PC-LEDs represented by the value of the CIE color rendering index (CIE CRI R_a) exhibits quite similar values for simulation and measurement. All these values (in the range R_a =71-76) represent only a moderate color rendering property which are, in general, not suitable for general indoor lighting. R_9 values of measurement and simulation are also similar in the sense that all of them (R_9 = -3 to 26) represent visually unacceptable (bad) color rendering for red object colors. The reason of the R_9 differences is that the simulation does not agree exactly with the measurement in the spectral range between 500 nm and 560 nm. The calculated measure of the visual quality of the white tone represented by the value $\Delta u'v'$ is very similar for both cases (measured and simulated). Although white tone differences in the range $\Delta u'v'$ =0.001 - 0.003 is visually noticeable, this accuracy of the simulation is still very usable to be able to design a phosphor mixture of an intended white tone. Luminous flux differences are considerable, up to 15 %. But as the tendency of the influence of phosphor particle size is well reproduced by simulation, the simulation method presented here is able to show the right way for a comprehensive PC-LED light source design. The values of the CQS metric represent either the combined color rendering and color preference property of the light source (Q_a is a general index and Q_9 characterizes the visually important red colors) or a measure of color gamut, Q_g, the so-called relative gamut area. The concept of color gamut means the extent

of the set of all possible object colors that appear under the current light source (some light sources tend to suppress saturated object colors while other light sources are able to accentuate saturated object colors). For all CQS measures, there was a good agreement between measurement and simulation.

The simulated LED power chip from the model describing the LED type 1 and 4 was first attempted to be kept equal to the experimentally measured 1.2 W and 64 mW respectively. This configuration could not deliver simulations comparable to LED measurement due to losses in the practical experiment, due to the heat, electrical contacts or other imperfections that could not be estimated. In order to consider only rays emitted directly from the chip, the detector was brought closer to the LED. The detector area covers therefore only a portion of the LED emission. The simulated LED output is then lower than for the laboratory analyses and thus the LED power has to be increased. LED power were adjusted in the simulation to 4.6 W and 1.2 W respectively.

Phosphor concentration is the parameter to optimize in order to adjust the real and simulated outputs. By increasing the phosphor concentration the phosphor conversion increases. This results from the augmentation of the yellow broad band. The radiant flux of the blue exciting peak declines because it excites and is absorbed by increasing number of phosphor particles. These observations concur not only with the experimental results but also with the optical properties computed by the software.

The required phosphor concentrations that fit best the experiments are collected in Table 5.5. The necessary weight concentration for the experimental WLED was converted into the number of particles. The trend of phosphor concentrations involved in this simulation matches with the experimental results, phosphors of increasing particle sizes see their number increase in the WLED. The order of magnitude of the particle number varies because of the model adaptation in terms of LED power already mentioned. The change in phosphor concentration as a function of the particle size has a comparable variation between the simulation and experiments for both LED types as shown by their ratios. Concentration ratios between experiments and simulations for particle sizes d_{50} from 37 μm to 28 μm remain almost constant. They can be assimilated to a calibrating factor to correlate simulated and measured number of particles. However the concentration require in the simulation for smaller particles differ from the measurements. Small particle size corresponds to the domain where Lighttools change the scattering properties calculation from Mie to Rayleigh theory. This may be the reason of the increasing variations.

Angle screening simulations

The goniometer measurement showed that the light produced at an angle of 0° seemed bluish (cold white) and the light considered at a greater angle was turning yellow (warm white). The CCT computed by the simulation are reported in Table 5.6 (LED type 2 (SMD)) and A.3 (LED type 1 (COB)) in Appendix A. This conducts to a verification of the experimental conclusions. However, the CCT variation between the LED emission in the normal direction and at 60° of the LED computed by the software is independent of the particle size. Goniometer measurements identify a varying color difference with the particle size. In the range of the particle size studied, the software does not reproduce the angular effect on the particle size. Lighttools does not compute angular scattering as a function of the particle size, but simulates according to a lambertien or gaussien model to be selected.

Table 5.5.: Phosphor concentrations in white LEDs for simulated and experimental values for the LED type 1 and 2.

	Number of particle/mm³ in LED Type 1			in LED Type 4		
	sim.	exp.	ratio	sim.	exp.	ratio
YAG 1 #6 d_{50} =37 μm	225	$4.33 \cdot 10^4$	193	255	$8.26 \cdot 10^4$	324
YAG 1 #5 d_{50} =33 μm	245	$5.73 \cdot 10^4$	234	300	$1.10 \cdot 10^5$	366
YAG 1 #4 d_{50} =31 μm	250	$6.69 \cdot 10^4$	267	325	$1.25 \cdot 10^5$	384
YAG 1 #3 d_{50} =28 μm	375	$8.92 \cdot 10^4$	238	480	$1.37 \cdot 10^5$	285
YAG 1 #2 d_{50} =15 μm	1400	$5.00 \cdot 10^5$	357	950	$7.40 \cdot 10^5$	779
YAG 1 #1 d_{50} =11 μm	2300	$1.09 \cdot 10^6$	474	2900	$1.42 \cdot 10^6$	490

Table 5.6.: Simulated CCT and variation from detector at 0° and at 60° for the LED type 2

	CCT / K		Variation / K
	0°	60°	
YAG 1	7307	6753	554
YAG 1 #6	8243	7521	722
YAG 1 #5	9228	8318	910
YAG 1 #4	8001	7359	642
YAG 1 #3	7730	7150	580
YAG 1 #2	6617	6226	391
YAG 1 #1	8525	7648	877

Influence of the silicone

The impact of the refractive index of the silicone binder on the LED efficiency was investigated. The relationship between the LED colors and the refractive index of the medium embedding the phosphor particles coincides with the measurements. As already seen in section 5.2.6, a higher refractive index binder shifts the LED color to higher color coordinates. Figure 5.53 proves that the total power is increased in accordance with Descartes' refractive law. The deviation of the color coordinates towards warmer colors is shown in the simulation by the enhancement of the phosphor emission when using a high refractive index medium. The peak responsible for the blue portion remains constant.

5.4 Conclusion on YAG:Ce phosphor

This chapter investigated YAG:Ce phosphor properties depending on their particle sizes. The influence of the phosphor particle size on the phosphor-converted LED outputs was studied.

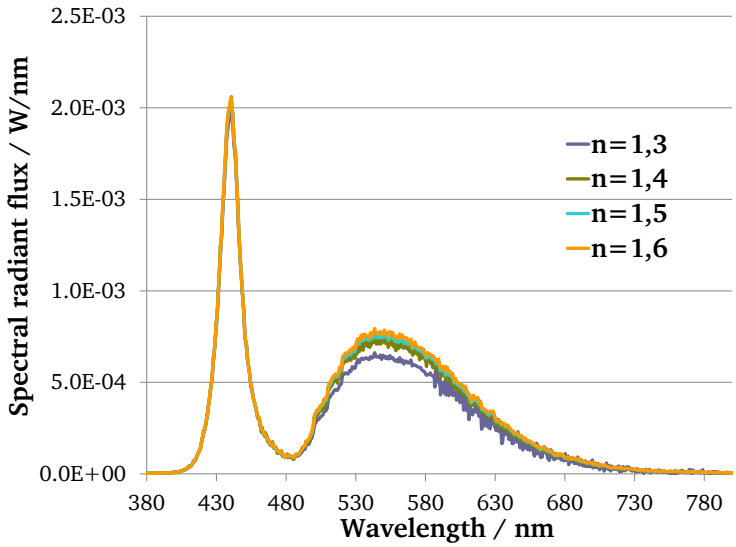

Figure 5.53.: LED spectra with different refractive index binder (LED Type 1 based on YAG 1)

The separation of these luminescent spherical particles was performed by a wet sieving process resulting in narrow particle size distributions (see 5.1.1) and reproducible results. The photoluminescence (PL) of YAG:Ce phosphor shows better absorption, excitation and fluorescent emission properties for particles from 15 μm to 35 μm compared to particles having a diameter between 5 μm and 15 μm (see 5.1.3). Small particles are more susceptible to have crystalline defect at their surface which induces a reduction of the PL properties.

White LEDs of similar CCT based on different phosphor particle sizes were fabricated. The phosphor weight concentration required to reach white LEDs increases with growing phosphor particle diameter (section 5.2.2). However the phosphor settles when the particles are large because of their mass.

Investigations carried out in this study have shown that the light output of white PC-LEDs depends on:

- the chip characteristics: its excitation wavelength corresponding to a good excitation's domain of the phosphor and the efficiency of the chip itself,
- the phosphor: its PL properties, morphology and the particle size,
- the LED package and its capacity to extract the light
- and the encapsulant with its refractive index and viscosity.

Considering the particle size parameter, it can be concluded that the emission intensity increases with increasing phosphor particles. Backscattering in the case of small particles is absorbed by the chip or package and reduces the light output. The study is limited to phosphor particle sizes from 5 μm to 37 μm (see 5.2.4).

Phosphor-converted LEDs with different phosphor particle sizes noted discrepancies in the angular homogeneity of the emitted light. The yellow ring phenomenon is illustrated. The LED becomes yellow when measuring at viewing angles far from the normal direction. Moreover, the color variation over the angles increases from 6 % to 15 % by using increasing phosphor particle sizes (see 5.2.5). Small particle scattering properties homogenize the chromaticity.

The phosphor particle size influences the PC-LED properties. Large phosphor particles enable white LEDs to emit with higher radiant flux and show a homogeneous chromatic angular distribution. The phosphor amount is also important. PC-LEDs based on small phosphor particles show reduced spectral radiant distributions compared to the large phosphor sizes. The yellow ring effect is pronounced in the case of large particles. Moreover, the phosphor quantity required to reach white LEDs is low. A compromise has to be reached between high efficacy, phosphor quantity and chromatic angular distribution. Higher luminous fluxes could even be attained for PC-LEDs with greater phosphor amount, however the LED would be yellowish.

The positions on the CIE diagram of the LED chip (its wavelength) and the phosphor determine the amount of phosphor necessary to develop white PC-LEDs. Finding a model describing the impact of the phosphor remains a challenging issue. Analytical results enable partially to take into consideration all the parameters playing a role in the LED. Approximations are still required to predict losses in the phosphor converting process considering the transmission or multiple reflection effects (see 5.3.1).

An optical simulation software was tested in order to predict PC-LED performance and possibly reduce the number of experiments, (see 5.3.2). Spectral radiant fluxes showed a good fit in the domain of phosphor wavelength but differing radiant distributions on the blue peak emission due to the complexity to obtain absorption data without multiple reflections and in transmission mode. The trend measured for the emission depending on the phosphor particle size of WLED could be verified by simulation. Simulated and measured spectral emissions differ on the short wavelength domain and a precise simulation of the color values and luminous flux is thus not possible. Color rendering values and color preferences could be well simulated.

The phosphor concentration required by the software for the series of sieved fractions shows the same trend as for the experiments, however with a varying coefficient. The simulation is not able to replace the experiments concerning the phosphor concentration fine tuning. Experimental variation of 0.5 weight % show drastic chromaticity changes. The simulation software permits the prediction of a qualitative trend of a new PC-LED system, with different chip, phosphors, silicone binders or LED designs. Detailed description of the luminous flux or required phosphor concentration is difficult.

6 Studies and research on the LuAG:Ce phosphor

Phosphor-converted LEDs (PC-LEDs) based on YAG:Ce phosphor results in cool white LEDs. The quality of the light is improved when the spectrum of the light source tends to the one of the blackbody (sun). LuAG phosphor offers the possibility to complete the PC-LED emission in the green color domain. The combination of LuAG:Ce and YAG:Ce in PC-LEDs fulfills the emission spectrum of the PC-LEDs and extends the color gamut. This chapter presents the study of PC-LEDs obtained with only LuAG:Ce. The influence of the phosphor particle size is investigated simultaneously to the activator chemical composition of LuAG:Ce. The characteristics of LuAG:Ce as phosphor powder are first studied: its morphology, particle size and photoluminescence (PL). The focus is then set on the influence of the phosphor particle size on the LED properties.

6.1 Phosphor powder characteristics

The physical and luminescent properties of $Lu_{3-x}Al_5O_{12}:Ce^{3+}_x$ (LuAG) Lutetium Aluminium Garnet doped with Cerium is investigated for two Cerium concentrations. Lutetium is replaced in LuAG 1 at 2.70 % by cerium and for LuAG 2 at 0.63 %. In order to study the influence of the phosphor particle size in the PC-LEDs, bulk samples LuAG 1 and LuAG 2 require a preliminary treatment. The samples are sieved by the wet chemical according to the method described in section 4.3.1. LuAG 1 and LuAG 2 phosphor particles are separated into sieved fractions of LuAG 1 #1 to LuAG 1 #8 with increasing particle sizes and LuAG 2 #1 to LuAG 2 #9. LuAGs are synthesized following the same procedure and thus have constant chemical properties. Their classification by particle size is required to lead this study. The particle size is the only varying parameter for each LuAG.

6.1.1 Particle size distribution

LuAG 1 and 2 have a wide particle size distribution (PSD) as shown in Table 6.1 and Table B.1 in Appendix B reporting the median phosphor diameter d_{50}, the particle size width d_{90} to d_{10} and the ratio d_{90}/d_{10}. The wet sieving process separated the particles as a function of their size. Nevertheless as already seen for YAG:Ce, this technique is experimental and because of the sieve mesh opening distribution, it is not possible to collect particles having exactly the same diameter in one fraction. PSD of the sieved fractions extracted from the bulk materials LuAG 1 and 2 (see PSD in Fig. 6.1 for LuAG 2) are still very narrow.

6.1.2 Scanning electron microscopy

SEM pictures of LuAG 2 are shown in Fig. 6.10. They depict isomorphic spherical phosphor particles. This very regular morphology illustrates the well dominated synthesis. The particle sizes (Table 6.1) measured by optical set-up described in section 4.2.2 are confirmed on these micrographs. The sieved fractions have phosphor particles of decreasing diameter. Similar observations can be inferred to the SEM pictures of LuAG 1 and the sieved fractions in Fig. B.1 of the Appendix B.

Table 6.1.: Median particle diameter d_{50}, particle size width $d_{10} - d_{90}$ and ratio d_{90}/d_{10} of LuAG 2 and its sieved fractions

Sample	Treatment	d_{50}/ µm	d_{10}-d_{90}/µm	d_{90}/d_{10}
LuAG 2	bulk material not sieved	35	5-70	14
LuAG 2 #1	sieved under 5 µm	4.4	1.4-6	4.3
LuAG 2 #2	sieved between 11 and 5 µm	8.5	3-13	4.3
LuAG 2 #3	sieved between 15 and 11 µm	17.6	12-22	1.8
LuAG 2 #4	sieved between 20 and 15 µm	22	19-27	1.4
LuAG 2 #5	sieved between 25 and 20 µm	26.9	19-33	1.7
LuAG 2 #6	sieved between 28 and 25 µm	31.5	22-37	1.6
LuAG 2 #7	sieved between 36 and 30 µm	37	32-46	1.4
LuAG 2 #8	sieved between 50 and 36 µm	47	38-63	1.6
LuAG 2 #9	sieved between 100 and 50 µm	70	54-89	1.6

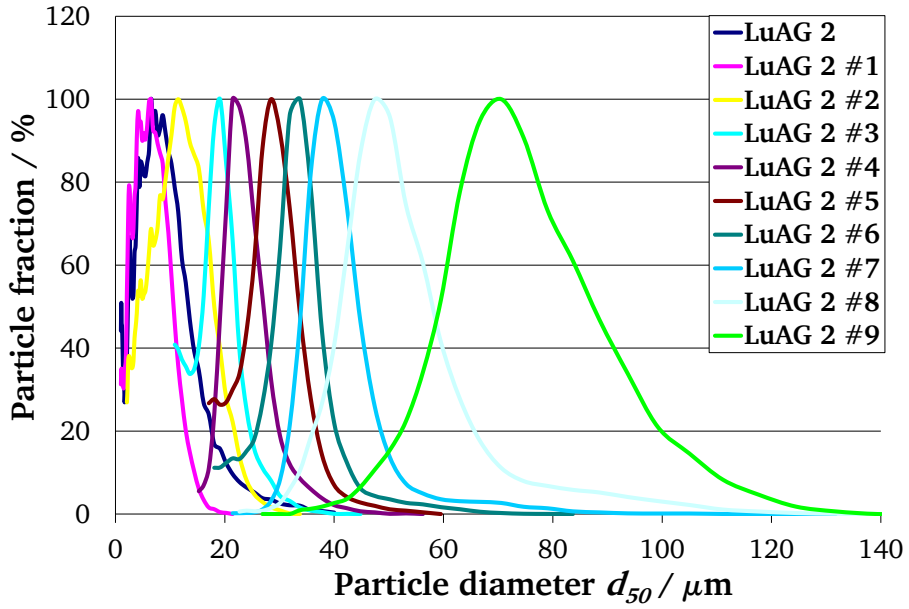

Figure 6.1.: Number weighted particle size distribution of LuAG 2 and its sieved fractions

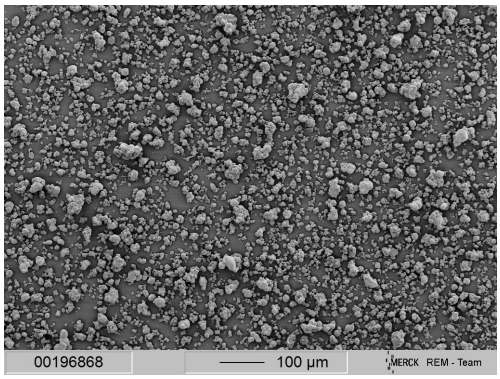

Figure 6.2.: LuAG 2 (d_{50}=35 μm)

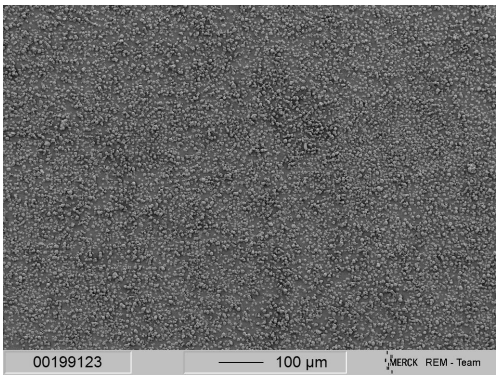

Figure 6.3.: LuAG 2 #1 (d_{50}=4.4 μm)

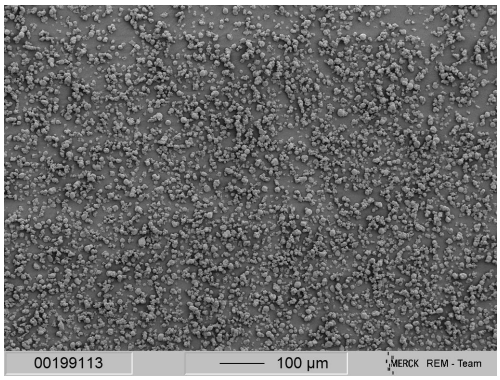

Figure 6.4.: LuAG 2 #2 (d_{50}=8.5 μm)

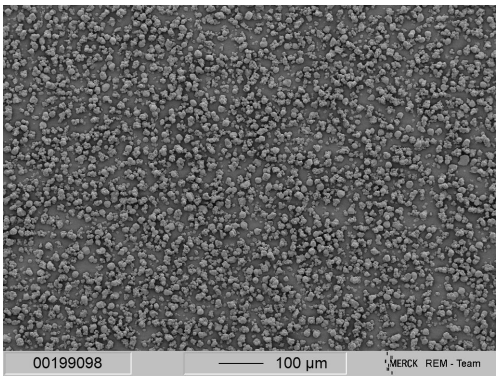

Figure 6.5.: LuAG 2 #3 (d_{50}=17.6 μm)

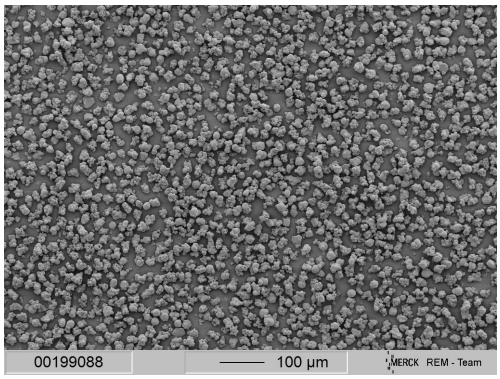

Figure 6.6.: LuAG 2 #4 (d_{50}=22 μm)

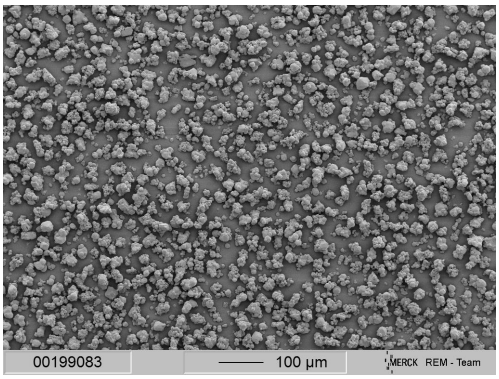

Figure 6.7.: LuAG 2 #5 (d_{50}=27 μm)

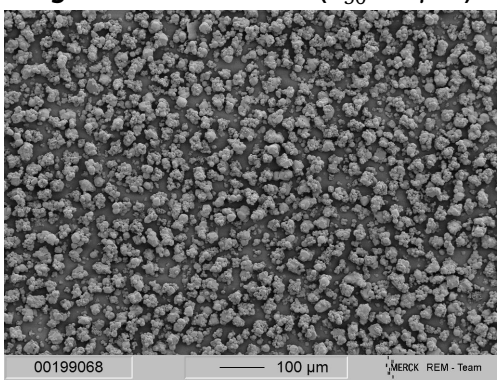

Figure 6.8.: LuAG 2 #6 (d_{50}=31 μm)

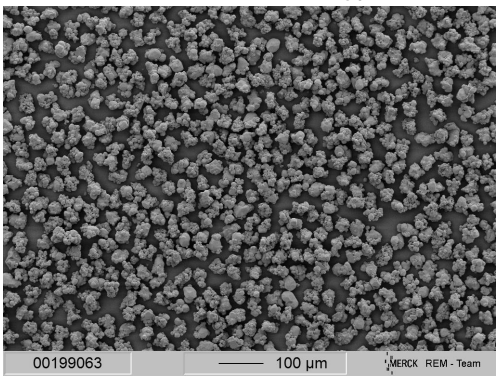

Figure 6.9.: LuAG 2 #7 (d_{50}=37 μm)

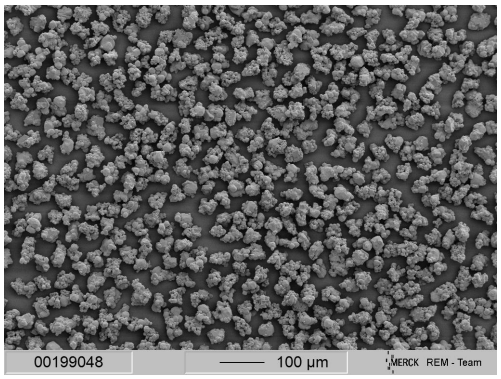

Figure 6.10.: LuAG 2 #8 (d_{50}=47 μm)

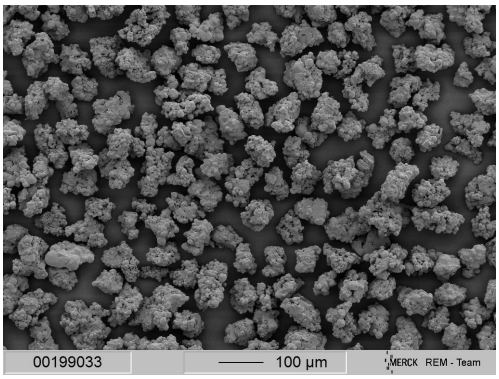

Figure 6.11.: LuAG 2 #9 (d_{50}=70 μm)

Figure 6.12.: SEM pictures from the sieved fraction of LuAG 2

6.1.3 Photoluminescence properties

PL properties are measured for LuAG 1, LuAG 2 and their corresponding sieved fractions. Excitation spectra of the two bulk materials are plotted in Fig. 6.13. It is first to be noted that the dopant concentration extends the peak wavelength. The structure of the lattice and the chemical elements remain the same, the number of Lutetium ions substituted changes. Cerium III in the LuAG lattice host shows several electron transitions from 5d to 4f and split the excited 5d state into several states because of the spin orbit coupling (see section 2.5.1). Electrons can be excited from the $4f^1$ ground state to the lowest 5d energy states, which produces the large excitation peak in the visible at about 443 nm. Further energy states can be reached in the UV for higher energies. In our study LuAG with high Cerium concentration (LuAG 1) exhibits a broader excitation band than LuAG 2. The crystal field splits more by the increasing activator surrounding [96]. The excitation peak is thus extended for LuAG 1.

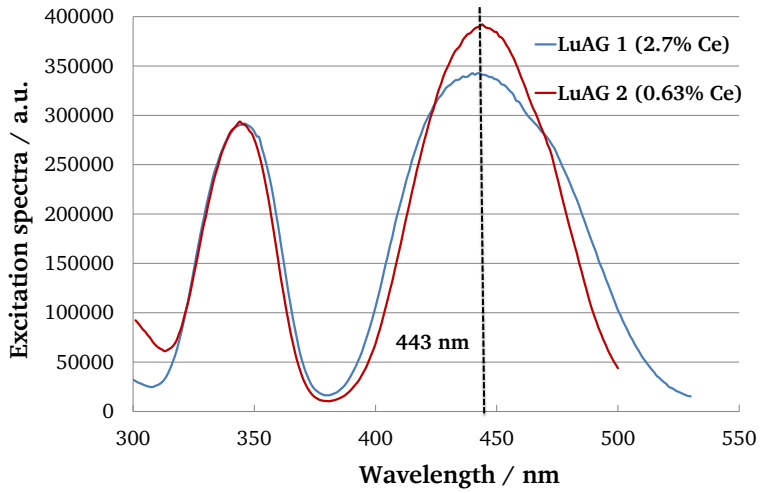

Figure 6.13.: Excitation spectra of LuAG1 and 2

The excitation maximum is reported as a function of the median phosphor particle size d_{50} for LuAG 1 and 2 in Fig. 6.14. For both dopant concentrations phosphors with increasing particle size reach higher excitation intensities.

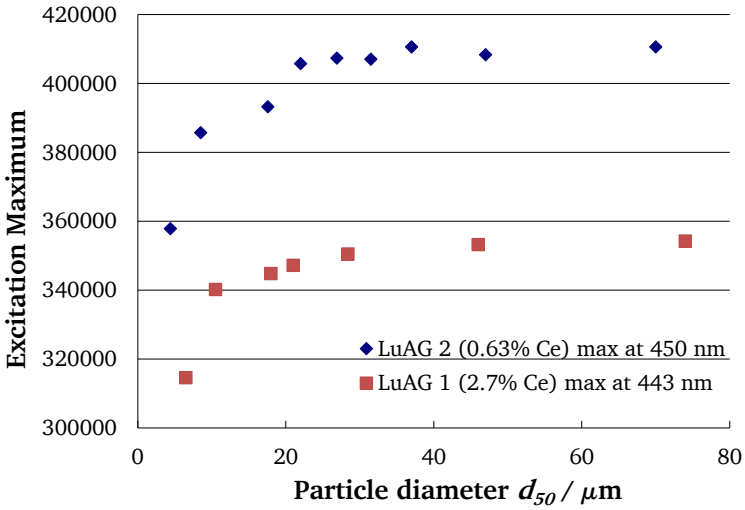

Figure 6.14.: Excitation maxima depending on phosphor particle size d_{50} for LuAG1 and 2

Absorption properties have been recorded for LuAG 1 and 2 as shown in Fig. 6.15. Absorbance spectral distribution does not depend on the dopant concentration. The characteristic absorption maximum at about 450 nm is a perfect match for an application with blue exciting LEDs. Different Cerium concentrations do not lead to a wavelength shift. Absorption has higher intensity for LuAG 1, i.e. with higher Cerium concentration. This implies that absorption increases with the activator concentration. The more activator sites, the higher the probability to absorb the exciting radiation.

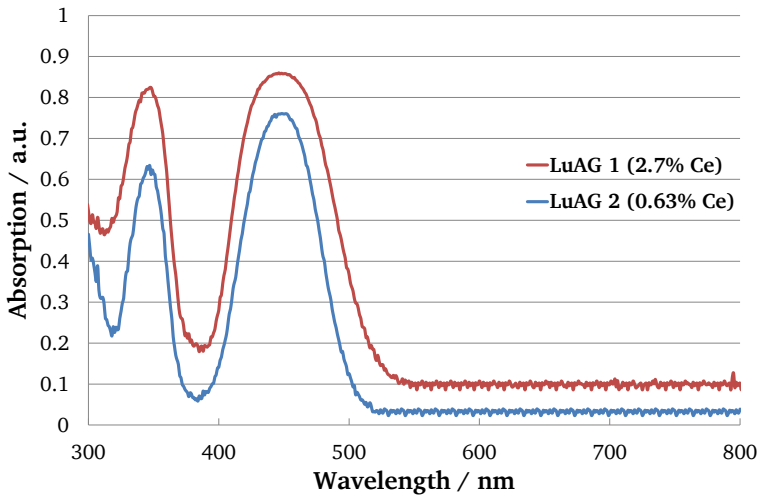

Figure 6.15.: Absorption spectra of LuAG 1 and 2

Absorption maxima are plotted for LuAG 1 and 2 as a function of the phosphor particle sizes d_{50} in Fig. 6.16. A similar trend is observed for the excitation. Phosphor particles of increasing diameter reach higher absorption.

As in YAG:Ce, Cerium has two possible electron transitions when relaxing from the lowest excited state to the degenerated 4f ground states. The combination of these photon emissions generates the greenish broad emission band of LuAG. These two emission peaks can be easily distinguished for LuAG even at room temperature. Fig. 6.17 shows the emission of

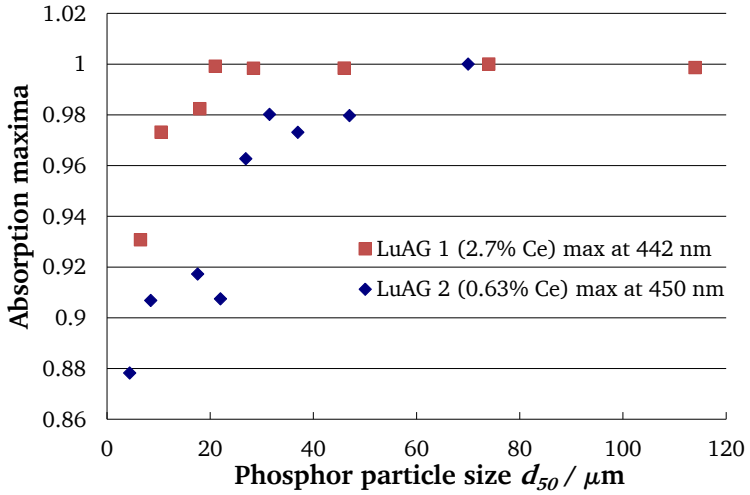

Figure 6.16.: Absorption maxima as a function of the phosphor particle size d_{50} of sieved fractions LuAG 1 and 2

LuAG 1 and 2. 5d-4f emission of Ce^{3+} depends strongly on the strength of the crystal field and its surroundings. Hence, doping LuAG structure with Cerium implies the replacement of Lutetium atoms by Cerium atoms in dodecahedral sites and leads to an increase of the crystal field because of the increasing atom diameter in the host crystal. The emission on the lowest 4f ground state is favored, the second emission peak moves towards the red region. Moreover increasing the activator concentration results in the apparition of Cerium sites whose 5d energy level is lower than the energy of intrinsic Cerium ions [96]. The emission peak at 542 nm becomes predominant.

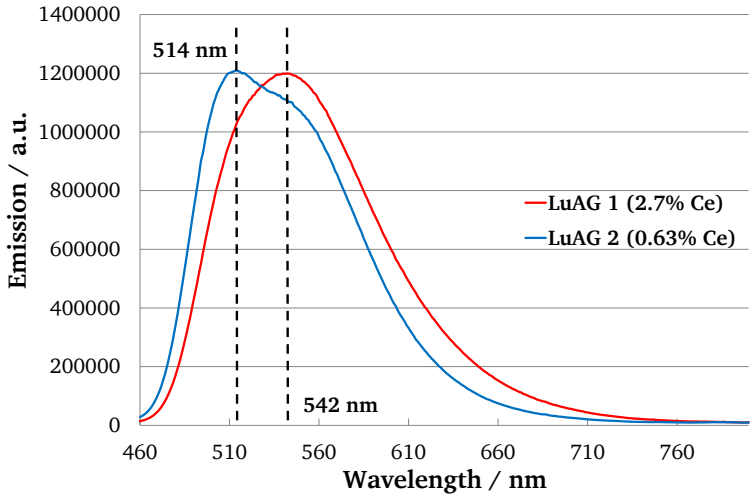

Figure 6.17.: LuAG 1 and 2 emission spectra

The influence of the phosphor particle size on the LuAG emission is represented in Fig. 6.18. The emission maxima at 543 nm for LuAG 1 and at 514 nm for LuAG 2 are dependent on the phosphor particle size. The trend to recognize is high emission intensity with increasing phosphor particle size for both LuAG dopant concentrations. The intensity for particles over 46 µm starts to decline. It is to be mentioned, that for large diameters, particles are not

considered to be single particles anymore but aggregates as can be verified on the SEM pictures in Fig. 6.10.

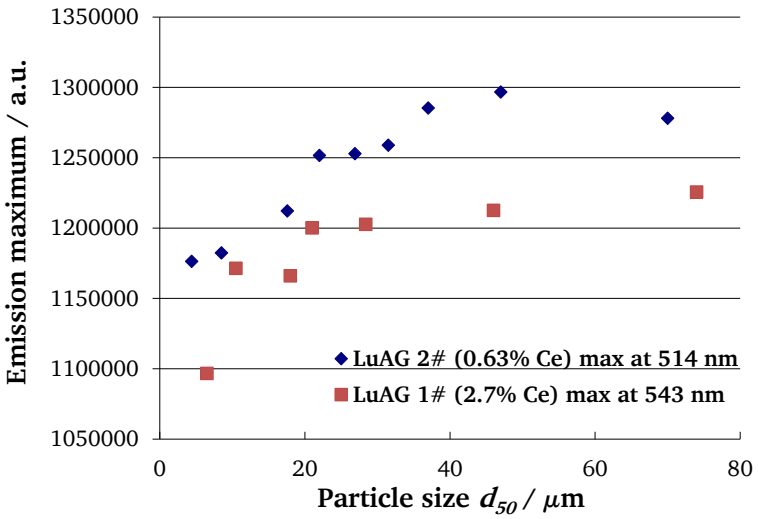

Figure 6.18.: Emission maxima of the sieved fractions from LuAG 1 and 2

Photoluminescence results reveal the tendency of higher absorption, excitation and emission intensities for increasing particle sizes. Phosphor structure causes these results. Small particle surfaces are affected by material defects in the microstructure attributed to a stop in the crystal formation in an early stage of synthesis. This correlates to increased reflectance in the case of small particles and therefore to an emission decrease. Moreover, Mie theory is applicable for this range of particle sizes and plays an important role. The predicted scattering properties show that light scattering is enhanced for decreasing phosphor particle sizes. Variation of phosphor particle size influences the scattering properties and leads to deteriorating PL for small particles.

6.2 Phosphor-converted LEDs based on LuAG:Ce phosphor

PC-LEDs have been made with the phosphor of the sieved fractions of LuAG 1 and 2. PC-LEDs, all of LED type 1 (COB LED) have been produced following the same process (described in 4.5) in order to be comparable. The required phosphor concentration, radiometric and photometric properties as well as chromaticity as a function of the angle distribution of these PC-LEDs are investigated.

6.2.1 Chromaticity of the phosphor-converted LEDs

PC-LEDs studied in this chapter consist of LEDs type 1 (COB) with conventional coating, covered homogeneously by a silicone and phosphor mixture as described in section 2.5.3. LEDs containing the fractions LuAG 1 #1 to LuAG 1 #7 and LuAG 2 #1 to LuAG 2 #9 of narrow particle size distributions are fabricated.

In order to draw specific conclusions about the phosphor particle size effect in PC-LEDs, PC-LEDs meeting strict requirements are selected. Phosphor must only differ from its d_{50} and PC-LEDs must have very similar chromaticities. LEDs' color coordinates specified in Table 6.2

and B.2 in Appendix B are reached. The chromaticity deviations ($\Delta u'$, $\Delta v'$) calculated from the standard deviations of the PC-LEDs' color values, are also summarized. The experimental difficulty to realize several LEDs meeting the chromaticity conditions implies that the number of studied LEDs is low and varies through the phosphor fractions, see last column of Table 6.2. The industry is confronted with this important issue to produce PC-LEDs of specific color characteristics. Reproducing LEDs having color coordinates with such small deviations represents a challenge for the LED producer. This is the reason why commercial LEDs are classified by colors varying over several digits on the CIE diagram to be realizable on a supply chain (binning procedure).

These LuAG LEDs correspond to light green colored LEDs. PC-LEDs based only on LuAG cannot produce any white light. The combination with a red, red-orange phosphor component makes this possible. PC-LED is in itself a complex system; this is why in this chapter only one phosphor will be studied before introducing other phosphor contributions in the next chapter. The determination of the LuAG PC-LED color values was achieved by evaluating the proportion of blue and green component needed to reach cool white LEDs of a usable color rendering level in the next chapter, in combination with a red-orange phosphor. Such colored LEDs are not suitable for general lighting, but they can have certain unusual accent lighting applications. Thus the criteria describing the color quality of white light (color rendering, color gamut, visual white tone quality, color preference) are not described in this section.

Table 6.2.: PC-LEDs (LuAG 2) color characteristics (x,y) (u',v') and chromaticity deviations calculated from the color variation obtained for the repeated samples ($\Delta u'$, $\Delta v'$) and number of PC-LED fabricated for each sieved fraction

	x	y	u'	v'	$\Delta u'$	$\Delta v'$	number of LEDs
LuAG 2	0.2457	0.3099	0.1578	0.4479	0.0019	0.0124	8
LuAG 2 #1	0.2454	0.3113	0.1572	0.4486	0.0012	0.0032	8
LuAG 2 #2	0.2453	0.3140	0.1563	0.4502	0.0009	0.0062	8
LuAG 2 #3	0.2451	0.3150	0.1559	0.4507	0.0008	0.0029	5
LuAG 2 #4	0.2458	0.3188	0.1552	0.4530	0.0015	0.0097	8
LuAG 2 #5	0.2456	0.3167	0.1557	0.4518	0.0012	0.0119	8
LuAG 2 #6	0.2444	0.3123	0.1562	0.4491	0.0017	0.0063	8
LuAG 2 #7	0.2446	0.3151	0.1555	0.4507	0.0014	0.0051	5
LuAG 2 #8	0.2445	0.3130	0.1560	0.4495	0.0005	0.0036	6
LuAG 2 #9	0.2456	0.3171	0.1556	0.4520	0.0005	0.0041	6

Average chromaticity point specifications for the different PC-LEDs sieved fractions and their deviations are listed in Table 6.3.

6.2.2 Phosphor concentration in the phosphor-converted LEDs

PC-LEDs consist in associating phosphor powder, LuAG phosphor in our study with a blue emitting diode. The conception of this physical principle can be understood concretely on

Table 6.3.: Average chromaticity of LuAG PC-LEDs from sieved fractions and corresponding deviations

target	u'	v'	$\Delta u'$	$\Delta v'$
LuAG 1 and sieved fractions	0.1722	0.443	0.0008	0.0011
LuAG 2 and sieved fractions	0.1562	0.4503	0.0008	0.0016

the CIE diagram. Fig. 6.19 depicts the two basic components of a PC-LED: the blue emitting COB LED and the phosphor represented by its color values. The straight line joining these two points describes all the PC-LEDs possible to be built from this configuration. Phosphor powder is embedded in silicone binder slurry. Increasing the phosphor amount and thus the phosphor concentration shifts the PC-LED chromaticity from the pure blue LED chromaticity point (0 % phosphor concentration) to the other end of the segment for very high phosphor concentration. In order to attain PC-LEDs with the required PC-LED color points, the appropriate phosphor concentration is determined experimentally, following the scheme in Fig. 5.18 as explained in YAG Chapter. The chemical and structural composition of phosphor fractions extracted from LuAG 1 remains constant, that is why the segment on the CIE diagram has the same position. There is no influence of the phosphor particle size on the chromaticity of the LEDs which are possible to build. Nevertheless some chromatic discrepancies are noticed in the experimental work. Practically, a great number of PC-LEDs is realized in the same run repeated several times. Even if the phosphor concentration stays constant, measured by the most precise balance using blue LEDs of a narrow binning, chromaticity deviances are observed from the expected same color values supposed to be obtained. This is possibly due to some inhomogeneity in the slurry, impurities on the exciting LEDs, even if all the influencing parameters are kept as constant as possible.

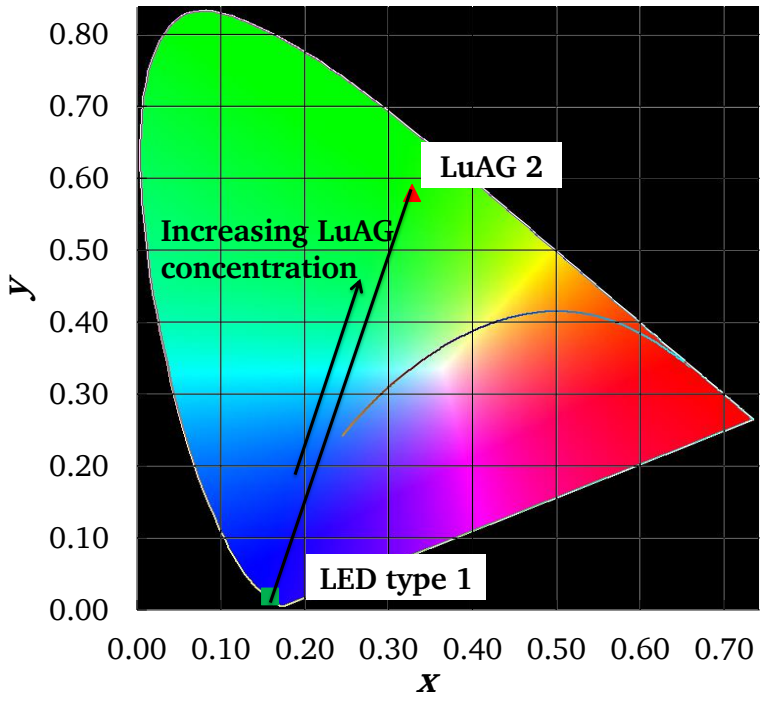

Figure 6.19.: CIE 1931 diagram of blue LED and phosphor color characteristics

Experiments with several phosphor concentrations are realized for each LuAG # fraction until PC-LEDs of the same color values are obtained. For the same matching color coordinate the phosphor concentration in the PC-LED is plotted against phosphor grain size (Fig. 6.20). The dependence of the concentration on the phosphor particle size should be noted. Indeed the relationship shows a linear dependence.

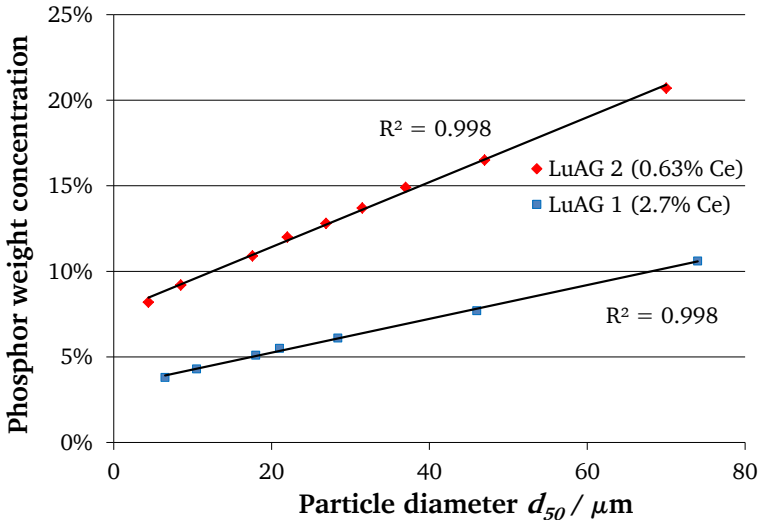

Figure 6.20.: Dependence of the phosphor concentration as a function of its particle size

The phosphor concentration is directly proportional to the phosphor size. The fitting parameter R^2 is close to one. The results are validated for both dopant concentrations. Only the equation factors change from LuAG 1 to LuAG 2 because of their different chemical composition. As already seen in 6.1.3 LuAG fractions differ from their PL properties. These changes influence the phosphor concentration necessary to reach a PC-LED of specific color coordinates. The larger the phosphor particles, the higher the needed phosphor concentration. Two explanations can be inferred from this behavior. Even if PL have increasing intensity with increasing particle size, because of their higher weight, large phosphor particles settle on the chip while curing due to the viscosity drop with the temperature. The particles are not homogeneously spread throughout the whole phosphor layer anymore. Only the phosphor particles deposited on the surface of the chip are excited by the blue LED light and participate in the PC-LED emission. A higher phosphor concentration is then required for increasing phosphor particles. Besides, the number of particles has been computed from the density and the phosphor distribution according to eq. 5.3. The results are plotted in Fig. 6.21. This confirms that even if the weight phosphor concentration is higher for increasing particle sizes, fewer particles are necessary to emit light of the same chromaticity.

Achieving PC-LEDs with precise chromaticity is an important challenge and denotes significant potential for savings. Knowing the behavior of a phosphor depending on its particle size provides the capacity to predict phosphor concentration required to reach a specific color point. Many experimental attempts trying to match the requirement could be saved.

6.2.3 Phosphor-converted LED efficiency

Radiometric and photometric properties of LEDs fulfilling the chromaticity restrictions detailed in the previous section are investigated. PC-LED spectral power is measured for the

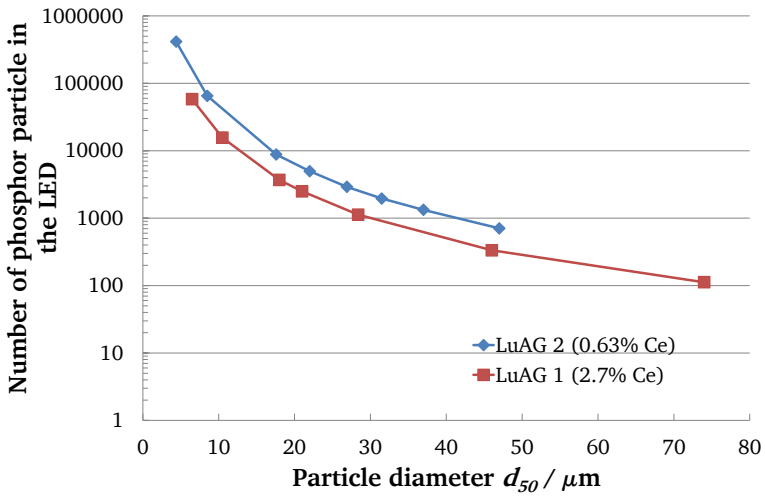

Figure 6.21.: Number of phosphor particles comprised in the LED as a function of the phosphor diameter for LuAG 1 # and 2 # on logarithmic scale

complete set of sieved fractions. The spectral distributions of the sieved fractions extracted from LuAG 1 are shown in Fig. 6.22. COB LEDs type 1 operated at 350 mA are used as blue exciting emission.

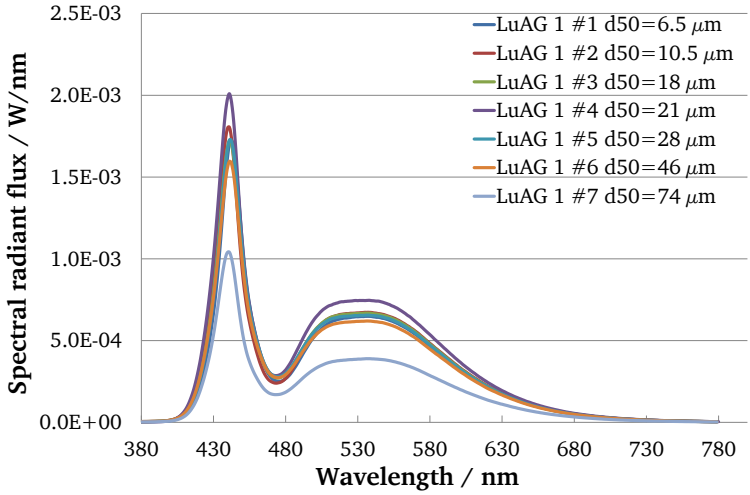

Figure 6.22.: Emission spectra of PC-LEDs made of all LuAG 1 sieved fractions

The proportion between blue peak and phosphor emission stays constant. This equilibrated combination guarantees the same chromaticity within all the PC-LEDs. The LED spectra only differ in their emission. The radiant flux is reported as a function of the phosphor particle size in Fig. 6.23 for LuAG 1 # and LuAG 2 #. LuAG 1 # and 2 # show comparable radiant fluxes for large particles. From 10 µm to 30 µm LuAG 1 # feature higher values than LuAG 2 #. This originates from the emission properties of the phosphor. LuAG 1 has a higher Cerium concentration. As already seen in 6.1.3, LuAG 1 emission peak is red shifted with a maximum at 543 nm (in contrary to 514 nm for LuAG 2) and dominating the spectrum. In that particle size domain, the area of the LuAG 1 phosphor emission is larger which results in higher radiant fluxes.

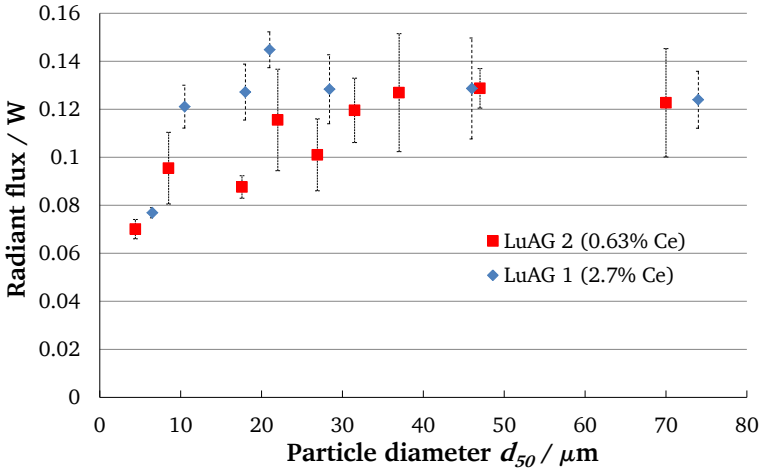

Figure 6.23.: Dependence of the radiant flux on phosphor particle size for LuAG 1# and 2#

Radiant flux tends to rise with the phosphor particle size. However a maximum seems to be reached for phosphor particle sizes of about 20 μm. This trend is independent of the dopant concentration. Results on LuAG 2 # confirm the observed phenomenon. PL increasing intensity with increasing phosphor particle size induces again the same effect on the emission properties. In addition scattering properties play an important role. Mie theory reveals scattering directed to the front direction for increasing particles sizes. On the other hand it leads to an omnidirectional scattering in case of decreasing phosphor particles. It therefore generates higher backscattering absorbed by the LED chip. Light output for decreasing particle sizes is consequently lower.

6.2.4 Angular distribution of the phosphor-converted LED chromaticity

In addition to the LED chromaticity, overall light output and phosphor concentration, phosphor particle size also plays a role on the LED color homogeneity as a function of the angle. The angular dependence of the LED chromaticity is evaluated by the measurement of the CCT. Thus CCT is measured every 3° for the complete sieved fraction set from LuAG 1 and 2. Fig. 6.24 describes a series of CCT measurements realized on all PC-LEDs available meeting the chromaticity requirements.

The color of the LED varies for each sample depending on the detecting angle. All samples show similar trends. LEDs emit with high CCT value at 0°, which means in the normal direction. At wider angles lower CCT values are measured. This reveals a lower contribution from the blue peak. The spectra thus exhibit a higher proportion of phosphor emission. This can be understood by the geometry of the PC-LED. The path of the blue light is longer from the chip (to escape the phosphor layer) at wide angles than in the normal direction. Blue rays directed to the side have more chances to excite a phosphor particle and provoke its emission. The phenomenon described is known as the yellow ring effect (yellow as analogy to YAG phosphor). The particle size has a great impact on the angular distribution of the colors. In order to determine how strong this influence is, the CCT difference between 0° and 60° is calculated for each fraction and plotted in Fig. 6.25.

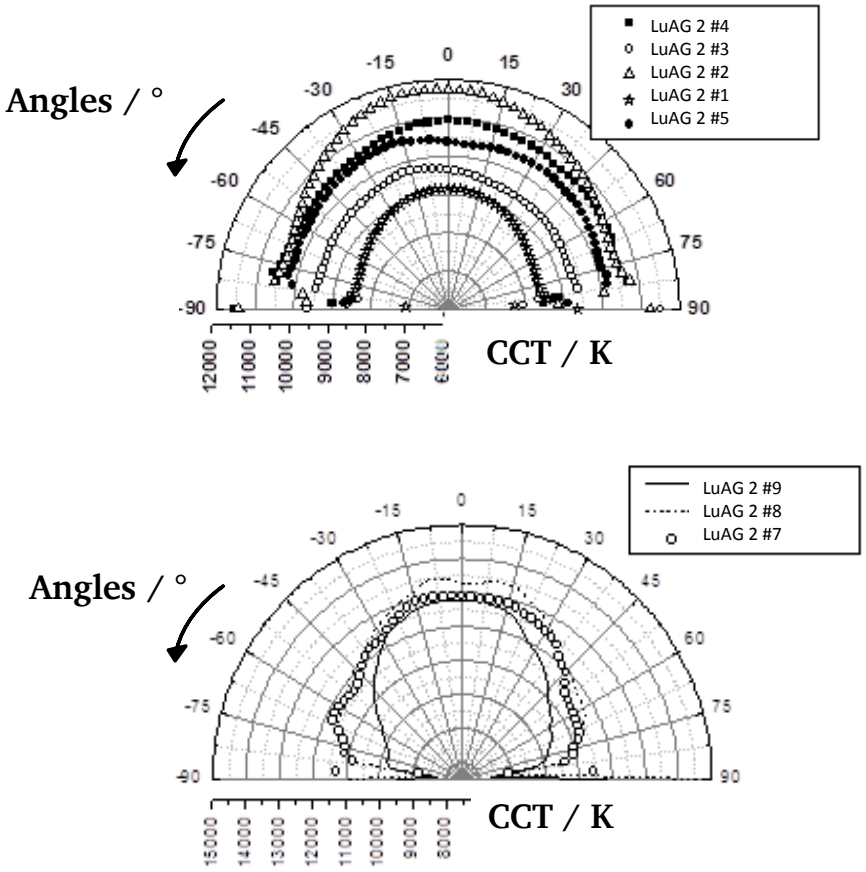

Figure 6.24.: CCT angular distribution for LuAG 2 #1 of $d_{50} = 4.4\,\mu m$, LuAG 2 #2 of $d_{50} = 8.5\,\mu m$, LuAG 2 #3 of $d_{50} = 17.6\,\mu m$, LuAG 2 #4 of $d_{50} = 22\,\mu m$, LuAG 2 #5 of $d_{50} = 27\,\mu m$, LuAG 2 #7 of $d_{50} = 37\,\mu m$, LuAG 2 #8 of $d_{50} = 47\,\mu m$, LuAG 2 #9 of $d_{50} = 70\,\mu m$

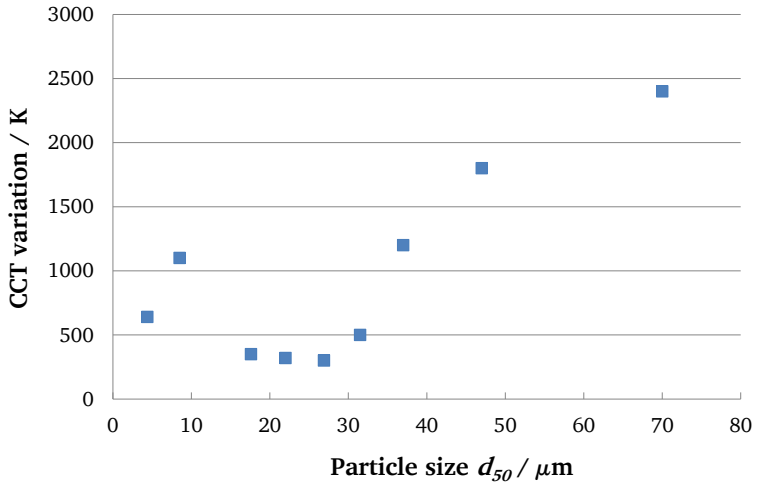

Figure 6.25.: CCT variation between 0° and 60° as a function of the particle size

The CCT variation is clearly dependent on the phosphor particle size. It is noticeable that the variation decreases until it reaches a minimum for particles of about 25 μm. Then the variation increases again. Three domains can be distinguished:

- the small particle domain until 15 μm
- the intermediate domain for particles about 20 μm
- and the large particle domain above 25 μm.

Small particles are homogeneously spread in the silicone binder layer. As seen in Fig. 6.21 the number of small phosphor particles is high. It is known from the Mie theory that small particles scatter the light in all directions. This leads on one hand to backlighting which decreases the overall light output but also to a slightly higher phosphor emission on the side which balances the yellow ring effect. CCT measured on LEDs from phosphor particles about 20μm have the lowest variation. These LEDs show the most homogeneous angular distribution in chromaticity. The phosphor particles are still well spread in the phosphor layer. There are fewer phosphor particles than for LEDs containing small particles. As a result blue light has more chances to escape the LED without being converted. In contrast, larger phosphor particles settle on the surface of the chip because they are heavier. Homogeneous color distribution over the angles is very difficult to reach because it is strongly dependent on the amount of particles deposited on the LED chip. It deteriorates the reproducibility rate to obtain LEDs of the same CCT. As seen in Table 6.2 fewer LEDs could be produced from large phosphor particles. At wide angles, the probability of the blue light to escape the LED is low because of the thick and dense phosphor layer settled directly on the chip. At 0° some blue rays succeed to escape the PC-LED and participate in the mix of LuAG emission and blue component to create the PC-LED. At wider angles the path through phosphor particles is even longer and blue light contributes mostly to excite the phosphor. In addition, large particles favor scattering in the normal direction. Phosphor emission is then clearly predominant at wide angles.

The control of the particle size has once again important consequences on the LED properties. The angular homogeneity in chromaticity of the light can be optimized and improved by correctly choosing the appropriate phosphor particle size.

6.3 Prediction of phosphor-converted LEDs

Considerable efforts must be invested to realize and optimize PC-LEDs in the laboratory. Developing methods to reduce the experimental part saves time and simplifies the research. PC-LED is a complex system in which a lot of parameters interact. A simple model based on a basic relation of linear functions does not exist. The emission of the blue LED and the phosphor emission following eq. 5.5 is too approximate and does not reflect the measured results. Parameters like the absorption, excitation spectra, and influence of the silicone binder must be taken into consideration in order to properly simulate a PC-LED. PC-LEDs experimentally built based on LuAG 1 # and 2 # are computed with Lighttools. The attempt is made to obtain comparable light output from the simulation and experiments.

6.3.1 Lighttools simulation parameters

Lighttools generates geometrical objects assigned by their optical properties. A COB PC-LED constructed on its basic elements is created. Phosphor material requires input parameters describing the PL properties as emission, excitation and absorption spectra but also phosphor concentration, refractive index and PSD. All the parameters implemented in the software are crucial physical characteristics for the Mie calculation. They are determinant to achieve good simulation results. The first PL entered parameters are strictly the ones measured by the experimental set-up. It appears that matching problems between simulation and measurement are encountered from 470 nm until 700 nm. Lighttools simulates on the basis of single crystal data. The experimental equipment measures phosphor not in transmission like in the LED but reflecting on a flat surface of a phosphor sample which generates multiple reflections. The re-absorption effect influences the emission spectra. As already seen in section 5.3.1 re-absorption can be clearly revealed for high concentration LEDs. Another experimental set-up performing on single crystal phosphors would allow providing the appropriate PL information. PL inputs shown in Fig. 6.26 have been empirically adapted in order to obtain the best simulation fit. Most changes have been applied to emission spectra that have been extended to shorter wavelengths in order to compensate for the emission part at about 500 nm absorbed by the multiple reflections. Other parameters like power also had to be re-scaled because of the different position of the detector between experiment and simulation. In the experiments the detector collects all the rays by means of an integrating sphere, the detector is positioned in the simulation in the center of the LED surface.

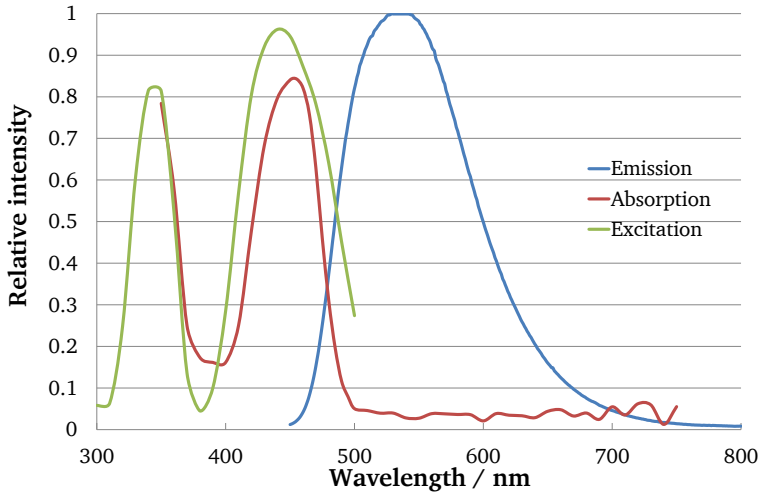

Figure 6.26.: Emission, Absorption and Excitation spectra implemented as parameters in Lighttools for LuAG 1

6.3.2 Simulation results

On the same approach as in the experimental part the phosphor concentration is optimized to fit the PC-LED emission spectra with respect to the chromaticity requirements for the set of sieved fractions. The comparison of simulated graphs and the measured spectra is displayed in Fig. 6.27 and 6.28 for LuAG 1 #1, LuAG 1 #2 and LuAG 1 #5. Fig. B.10 and B.11

in Appendix B show spectral distributions of LuAG 2 #3 and LuAG 2 #5. The differences between simulated and measured radiant fluxes are plotted in the same graphs.

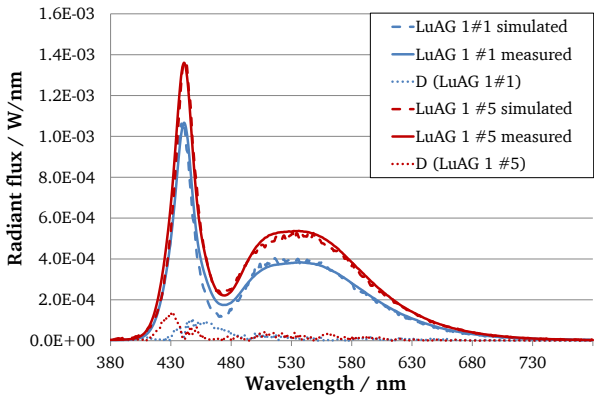

Figure 6.27.: Simulation and measurement of PC-LEDs increasing particle sizes for LuAG 1#1 $d_{50} = 6.5\,\mu$m, LuAG 1#5 $d_{50} = 28\,\mu$m

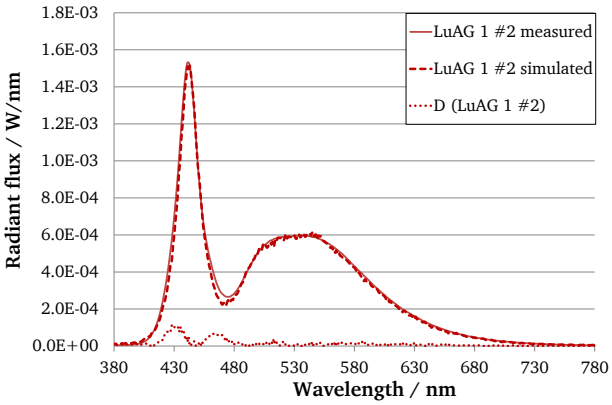

Figure 6.28.: Simulation and measurement of PC-LEDs increasing particle sizes for LuAG 1#2 $d_{50} = 10.5\,\mu$m

Lighttools simulates using logical physically based principals. Simulated PC-LED emission spectra show the same trends as the experimental results. The higher the phosphor concentration, the more blue light is absorbed and the higher the phosphor-converted emission.

The dotted line shows the difference between the simulated and the measured PC-LED emission spectra. Simulated and measured PC-LED spectra exhibit a good match from 520 nm on i.e. in the main spectral range of the phosphor part of the PC-LED's emission curve. It should be noted that the phosphor's photoluminescence data given as an input parameter in the software are of great influence and may enable a consistent simulation of down conversion emission. It should be emphasized that the success or failure of simulation depends especially how carefully the input data are prepared. The software itself is a good tool but it is up to the user to provide a good input for the software. Matching problems of the spectral radiant flux distributions are situated at about 430 nm and also at the transition point between the blue pump LED and the green phosphor at 470 nm. At this spectral transition point, the simulated emission is too low. This is probably caused by the measurement mode in reflection of the samples. The discrepancies originate from the input absorption data of the phosphor. Indeed a single blue LED can perfectly be simulated by the software. The phosphor has therefore an influence on the representation at 430 nm of the blue peak. Despite empirically scaled PL inputs simulations do not match perfectly the measurements at 470 nm. PL properties should be performed in transmission on single crystals in order to eliminate any possible error source. Computing emission spectra considering adapted absorption properties considerably enhances the transition area between LED and phosphor. The multiple reflections occurring during the measurement is countered by the absorption spectra empirically adjusted.

Radiant flux and chromaticity differences between measurement and simulation can be seen in Table 6.4. As already mentioned, these LuAG PC-LEDs are colored LEDs without any white point and with no corresponding reference light source. Therefore, the chromaticity difference $\Delta u'v'$ is computed here in a different sense from in section 5.2.1. Here, it is computed between the simulated and measured chromaticity points of the LuAG emission spectra. $\Delta u'v'_{ms}$ is calculated according to eq. 6.1.

$$\Delta u' v'_{ms} = \sqrt{(u'_{sim} - u'_{meas})^2 + (v'_{sim} - v'_{meas})^2} \tag{6.1}$$

There is a different way to estimate the difference between simulated and measured LED emission, D which has no physiological meaning but considers the radiant flux variation. The spectral difference measure designated by D was defined here as the sum of the spectral radiant flux differences between simulation and measurement at each wavelength.

Table 6.4.: Radiant flux and chromaticity differences between measurement and simulation. The quantity D is defined as the sum of the spectral radiant flux differences between simulation and measurement at each wavelength

	Radiant flux / W			$\Delta u'v'_{ms}$	D / W
	simulated	measured	deviation/%		
LuAG 1 #1	$7.42{\cdot}10^{-2}$	$7.64{\cdot}10^{-2}$	3	0.0036	0.005
LuAG 1 #2	$1.08{\cdot}10^{-1}$	$1.16{\cdot}10^{-1}$	3	0.0047	0.005
LuAG 1 #3	$1.06{\cdot}10^{-1}$	$1.22{\cdot}10^{-1}$	13	0.0006	0.017
LuAG 1 #4	$1.08{\cdot}10^{-1}$	$1.37{\cdot}10^{-1}$	7	0.0015	0.011
LuAG 1 #5	$9.98{\cdot}10^{-2}$	$1.32{\cdot}10^{-1}$	3	0.0016	0.033
LuAG 1 #6	$1.02{\cdot}10^{-1}$	$1.06{\cdot}10^{-1}$	3	0.0013	0.006
LuAG 1 #7	$1.08{\cdot}10^{-1}$	$1.16{\cdot}10^{-1}$	6	0.0032	0.010

As can be seen from Table 6.4, measured radiant flux and simulated radiant flux agree up to about 13%. The difference in the shape of the spectral emission curves implies discrepancies in the chromaticity point of the LuAG PC-LEDs up to $\Delta u'v'_{ms} = 0.0047$ which is a visually well noticeable difference. The computed D values demonstrate that the agreement between the simulated and the measured emission spectra varies among the different PC-LEDs (#1-#7) considerably. As seen above, despite these differences, the simulation provided usable results concerning radiant flux. Accurate chromaticity simulation, however, remains an important challenge as the chromaticity point depends on the relative shape of the emission spectrum (measured or simulated) strongly. A spectral mismatch in the 440 nm - 470 nm range is decisive for the chromaticity match between simulation and measurement. As for the YAG simulations, the emission of the blue LED could not be simulated in a satisfying way. Phosphor absorption properties are suspected to cause this difference in the simulation of the blue part of the PC-LED's emission spectrum. The tendency of the influence of phosphor particle size could be well simulated. It should be mentioned that the Lighttools software is based on the theoretical assumption of spherical particles and this does not correspond to reality. Two other factors, the heat lost at the chip and the reflectance of the metal ring which contains the phosphor, are approximated only roughly. These approximations might also have caused the spectral deviations shown above.

6.3.3 Simulated and experimental phosphor concentration

The comparison of the required phosphor concentration is an important factor influencing the quality of the simulation. The results are summarized in Table 6.5.

The simulated number of phosphor particles required to match the emission spectra does not correspond at first sight to the experiments. However their ratio remains almost stable for

Table 6.5.: Simulated and measured number of phosphor particles in PC-LEDs for LuAG 2

	d_{50} / μm	number of particles in simulation	experimental number of particles required	yield
LuAG 2 #1	4.4	11500	415129	36.1
LuAG 2 #2	8.5	3500	65109	18.6
LuAG 2 #3	17.6	1100	8791	8
LuAG 2 #4	22	600	4973	8.3
LuAG 2 #5	26.9	400	2914	7.3
LuAG 2 #6	31.5	300	1953	6.5
LuAG 2 #7	37	200	1329	6.6
LuAG 2 #8	47	100	704	7

particle sizes from 17.6 μm to 47 μm. This scaling factor only changes for particles smaller than 10 μm. The PC-LED system from the lab was reproduced as identical as possible into a geometrical system in Lighttools. The different position of the detector measuring the light output implied to re-scale the power of the LED but stayed constant for all the simulations. In the same way, the phosphor concentration needed to be adjusted. The influence of the phosphor particle size could be well simulated considering this one scaling factor for the phosphor concentration. The phosphor concentration can be predicted from the simulation.

It is suspected that the software encounters difficulties to simulate phosphor with particle size too small (LuAG 1 #1 and LuAG 1 #2). The Mie theory model used in the algorithm arrives at its computational limits. The developed model implemented in Lighttools results though for the rest of the sieved fractions in satisfying simulation results able to reproduce the trend of the phosphor particle size influence.

6.4 Conclusion on LuAG:Ce phosphor

LuAG photoluminescence has been investigated. The study has been conducted for two Cerium activator concentrations. The activator concentration has an impact on the broadening of the phosphor emission. LuAG:Ce shows due to its energy level two emission bands at 514 nm and 543 nm. LuAG 1 with high Cerium concentration of 2.7 % exhibits a peak at 543 nm dominating the large emission band, LuAG 2 with 0.67 % Ce reveals a higher contribution of the peak at 514 nm. Both LuAG are suitable for use as phosphor in PC-LED. The green hue denotes the capacity to extend the color gamut and fulfills the gap in combination with YAG for example. YAG exhibits a maximum peak at 554 nm and LuAG at 514 nm or 543 nm depending on the dopant concentration. The excitation wavelength corresponds perfectly to blue LED emission peak. The influence of the phosphor particle size on the PL properties confirmed the results obtained in Chapter 5 with YAG. LuAG and YAG both have a garnet structure. The same conclusions are observed, namely increasing phosphor particle sizes leads to higher excitation, absorption and emission.

PC-LEDs were fabricated with the LuAG sieved fractions. Chromaticity points are kept constant for PC-LED realized with all the samples, only letting the required phosphor concentration vary. Phosphor concentration shows a linear relationship to the particle size, inde-

pendent on the dopant concentration. PC-LED reaches a maximum efficiency for particles of about 20 μm. Too large phosphor particles settle on the chip of the LED and in the range of our study slightly lowers the PC-LED efficiency. This conclusion verifies the YAG results and is validated for both Cerium concentrations.

The angular distribution shows a ring effect. The light escaping at wide angles exhibits lower CCT. This means that more phosphor emission is emitted at wide angles, or complementary that less blue light has the chance to exit the phosphor layer. This phenomenon is dependent on the phosphor particle size. The concentration of the phosphor particles plays an important role. High number of small particles is present in the PC-LEDs. The path of blue rays is longer when directed to the side of the LED. The probability of the blue light to excite a phosphor particle and be converted is high. By increasing the phosphor particle size and so reducing the number of particle, blue light has more chance to escape the LED. For large phosphor particles sedimentation has to be taken into consideration. Phosphor particles form a layer on the LED chip which increases the angular inhomogeneity of the PC-LED color. The best chromatic uniformity is then reached for phosphor particles about 10 μm. Scattering in every direction of small phosphor particles provides also color uniformity.

A model was researched to predict the experimental results. Many parameters have an impact on the PC-LED results. The Lighttools software is appropriate for qualitative PC-LED prediction and able to compute from Mie theory considering all significant parameters. Experiments require a high time investment, the simulation offers the potential of an important time saving by reproducing the PC-LED results. Phosphor PL properties have to be considered, as well as optical properties of the LED package or the silicone binder. Empirical adaption was performed on the PL spectral properties to be closer to the theoretical model employed by the software. Because of a different position of the detector, the LED power has also been adjusted. The trend found for particle size investigation is able to be verified by simulation. Simulated and measured radiant fluxes show up to 17 % deviations. Their spectral distributions match in the wavelength domain of the phosphor emission. The blue exciting peak at 430 nm could not be well simulated because of the too high absorption of the implemented phosphor data. The junction between blue LED and phosphor emission at 470 nm shows also differing spectral distributions. Spectral discrepancies in the transition wavelength area between the LED and phosphor emission originate from the experimental set-up used in reflection mode to measure the PL properties. Emission spectra divergences result in PC-LEDs of non concordant chromaticity points. Lighttools considers a perfect model and experimental factors cannot be exactly controlled. The phosphor concentration is able to be adapted from the simulation to the experiment with the help of a factor which remains constant for the same phosphor system and for particles down to 10 μm. However precise prediction of the phosphor concentration is not possible for experimental tries. Small particles seem critical to be simulated because of the particle size limit of the scattering theories used in the software. Large particles also do not validate the assumption the spherical particles, because they are made of agglomerated particles.

7 Phosphor-converted LED systems with green and red phosphors

The aim of the general lighting project is to develop an effective, environmentally friendly illumination system. The combination of several phosphors improves the color rendering of the LEDs. LEDs made from different phosphor associations will be compared for warm white LEDs of CCT from 2700 K to cool white LEDs with CCT of 5000 K. LEDs will be built experimentally first. Then the experimental set-up will be reproduced using optical simulation software. Simulations will be performed in order to validate the computation results for a model based on two phosphors.

7.1 Phosphor system

It is felt that combining several phosphors in a PC-LED is a promising idea. Light radiated becomes close to the sun emission or to the halogen tungsten light spectra, for better color rendering and is able to illuminate and make distinguishable different colors by the human eye. Increasing the complexity of the system by introducing one more phosphor represents a challenge in understanding the resulting interaction. Phosphor components provided for the experiments are:

- LuAG:Ce, green 1 (G1)
- orthosilicate, green 2 (G2)
- oxyorthosilicate, red 1 (R1)
- and oxynitride, red 2 (R2) .

With one phosphor, the possibility to reproduce every color situated on the line joining the blue LED and the phosphor on the CIE diagram has been demonstrated. Mixing several phosphors offers the advantage of a wider emission spectrum of colors.

7.1.1 Photoluminescent characteristics

Phosphor powder spectroscopic characteristics determine PC-LED radiation. In this chapter several phosphors are mixed together. It is of great importance to measure the emission, reflection and excitation of the phosphor separately and in the powder state. Indeed the samples interact significantly with each other and their relationship enables the developers to identify the mechanisms occurring in the PC-LEDs. PL properties have been measured for the set of phosphors using the equipment presented in section 4.4.1.

Emission

The emission is first presented in Fig. 7.1 for G1, G2, R1 and R2. Phosphors were excited at 440 nm, which corresponds to the wavelength peak of LED type 1 emission used during the experiments. G1 corresponds to the green LuAG 2 from the previous chapter and exhibits the typical broad emission characterizing LuAG made of two peaks as described in Chapter 6. The emission maximum peaks at 514 nm and due the broad emission band, the

dominant wavelength is shifted at 549 nm. G2 shows a narrower green emission known for orthosilicates with a maximum peak situated at 524 nm. The emission shapes of both red-orange phosphors are similar. They differ by their emission peak located at 615 nm for R1 and 600 nm for R2. The combination of these phosphors provides the possibility to fulfill the visible emission spectrum.

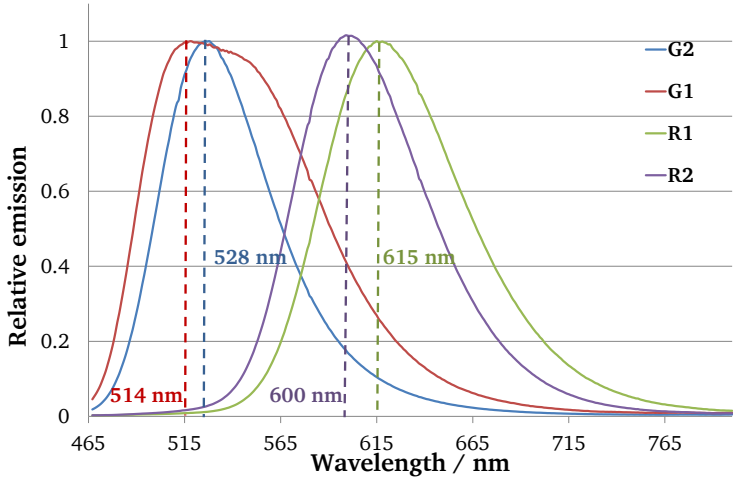

Figure 7.1.: Measured emission spectra of G1, G2, R1 and R2, excitation at 440 nm

Excitation

Excitation spectra were recorded every nm and are shown in Fig. 7.2. Garnet phosphor G1 differs in the UV by its lower excitation values in comparison to the green orthosilicate (G2), oxyorthosilicate (R1) and oxynitride (R2). LuAG (G1) only has one excitation peak in the UV at 345 nm whereas the other phosphors exhibit high excitation potentials in the UV range. G1 shows an excitation peak in the blue domain at 445 nm. Excitation intensity decreases for G1 after its maximum at 445 nm and for G2 after its maximum at 415 nm in the visible range. In contrast, oxyorthosilicate and oxynitride show high excitation potential in the visible range and reach their maximum excitation at approximately 420 nm. Emission of green phosphors is situated in the range of excitation of the red-orange phosphors.

Reflection

Absorption properties are deduced from the diffuse reflection measured as detailed in section 4.4.1 following eq. 7.1. Results of absorption measurements for the green and red-orange phosphors are shown in Fig. 7.3.

$$A = 1 - DR \tag{7.1}$$

with A the absorption coefficient and DR the diffuse reflection coefficient.

G1 absorption spectrum is characterized by two maxima, in the UV at 345 nm and in the visible range with a maximum peak at 445 nm. G1 continues to absorb between 385 and 510 nm, however with lower intensity. The absorption drastically decreases after the second absorption peak. G2 has a high absorption intensity up to 435 nm which then decreases until 510 nm to reach constant low absorption values. Green phosphors in our study are

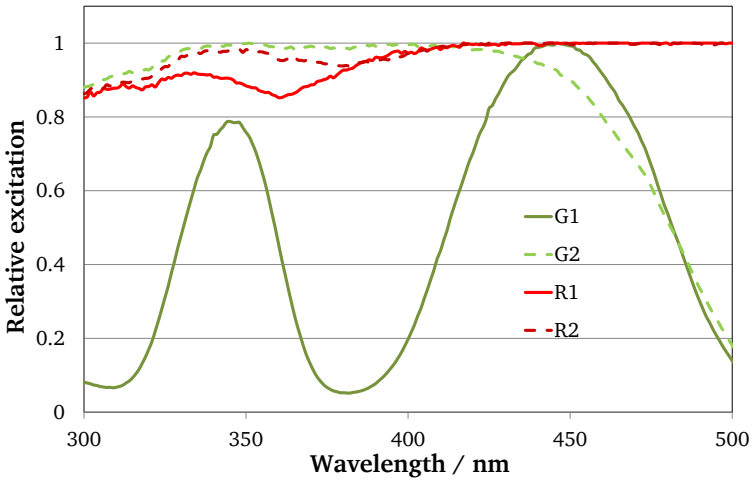

Figure 7.2.: Measured excitation spectra of G1, G2, R1 and R2

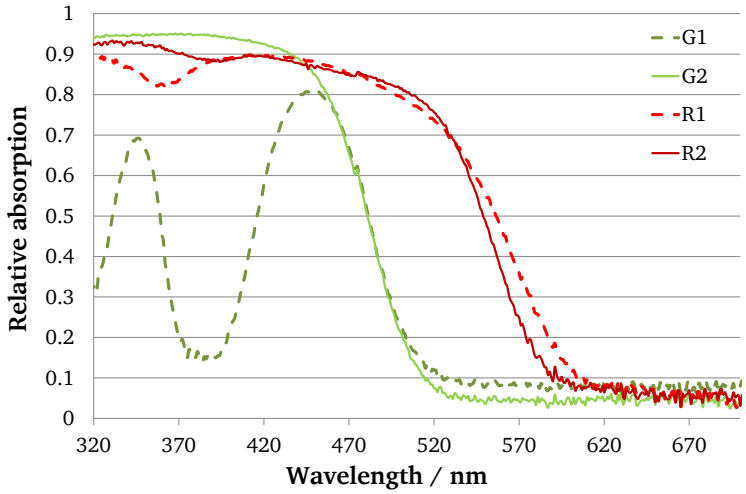

Figure 7.3.: Measured absorption spectra of G1, G2, R1 and R2

suitable for use with blue LEDs. Red phosphors absorb in the UV continuously until 500 nm in the visible range. The absorption then drops to its minimum value at 590 nm and 610 nm for R2 and R1 respectively. They are not only absorbing the blue emission of the LED but also the emission of the green phosphors. As a conclusion, on the PL properties of the presented system of phosphors, G1, G2, R1 and R2 are appropriate for application with the blue LED. They are excitable in the emission domain of the blue LED and also able to absorb its radiation. The combination with red phosphors implies the loss of a part of the green phosphor emission which will excite and be absorbed by the red components. Green phosphors differ in the broadness of their emission peaks. R1 exhibits an emission spectrum similar in shape to R2 with the maximum shifted from 600 nm to 615 nm.

7.1.2 Color coordinates

Four phosphor mixtures can be obtained from the phosphors at our disposal. The color points of each phosphor are represented in Fig. 7.4 on the CIE diagram. Triangles binding green

and red phosphors in addition to the blue LED, corresponds to the color gamut illustrating the combination of phosphors. The larger the surface of the triangle, the more colors are possible to be created from this light source.

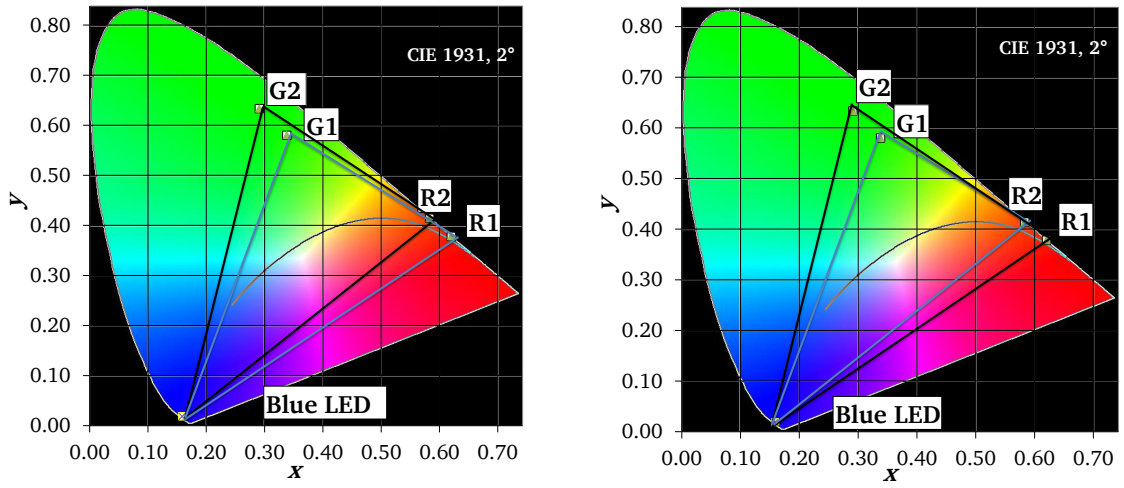

Figure 7.4.: CIE Diagram 1931 of the measured color gamut obtained from G1/R1/Blue and G2/R2/Blue (on the left), G1/R2/Blue and G2/R1/Blue (on the right)

Color tones of objects can be distinguished by the human eye when the light source illuminates the same tone as the object reflects. The triangle formed by the green, red and blue components defines the colors possible to be emitted by the light source. The larger the triangle area is, the more nuances are possible to be seen on diverse objects. The size of the triangle gives a first indication on the possible quality of the light produced by these phosphor compositions. At first sight the combination G2 and R1 let speculate on the best color quality.

7.1.3 Particle size distribution

Particle size distributions of the phosphors are measured and the results are presented in Table 7.1.

Table 7.1.: Particle size of G1, G2, R1 and R2

	G1	G2	R1	R2
d_{50} /μm	22	18	20	14

Particle size measurement reveals a d_{50} comprised between 14 μm and 22 μm for the four phosphor samples. These values correspond to particle sizes suitable for PC-LED applications because of the lack of heavy particles, and thus no risk for large particles to sedimentate on the LED chip and the lack of too small particles which reduces the emission intensity due to the probable defect formation in the structure. Fractions of phosphor differing from their diameter as close as for YAG and LuAG are not possible to obtain. Sieving would not be successful on these samples due to their non-spherical shape. Nitrides belong to lately discovered phosphor materials, their synthesis is elaborated and sintering parameters can

still be optimized to improve their morphology. Still PSD of the phosphor depict narrow distributions.

7.2 Phosphor-converted LEDs

PC-LEDs based on these four phosphor combinations were built. The phosphors are first poured and stirred homogeneously together with the help of a planetary centrifuged mixer. The appropriate silicone binder quantity is then introduced. The slurry is stirred and spread in the ring on the top of the LED chip type 1 (COB). The method used is conventional coating. After one hour curing time, photometric and radiometric LED properties are measured.

7.2.1 Correlated color temperature reached

Table 7.2 summarizes the matrix of phosphor used to build the PC-LEDs and the corresponding CCT values. Following conditions are imposed concerning the color points of these LEDs. A deviation of 100 K to the target CCT is accepted and a distance $\Delta u'v'$ equal to or smaller than 0.001 to the Planckian locus is tolerated. For CCT exceeding 4500 K, $\Delta u'v'$ is calculated to a phase of daylight D_{65}. These tight restrictions considerably reduce the number of LEDs matching the requirements. The number of LED built is also indicated in parenthesis in Table 7.2.

Table 7.2.: CCT and number of corresponding PC-LEDs in parenthesis of green G1, G2 and red R1, R2 phosphors

	G1	**G2**
R2	2700 K (3)	2700 K (3)
	3000 K (5)	3000 K (2)
	3500 K (1)	3500 K (1)
	4000 K (1)	4000 K (4)
	5000 K (1)	5000 K (2)
	5500 K (1)	5800 K (1)
	6500 K (1)	6500 K (2)
	7900 K (1)	7500 K (1)
R1	2700 K (2)	2700 K (2)
	3000 K (3)	3000 K (3)
	4000 K (2)	3500 K (1)
	4500 K (2)	4000 K (4)
	5000 K (1)	4500 K (3)
	5500 K (1)	5000 K (1)
	6000 K (2)	6000 K (1)
	6500 K (1)	8000 K (2)
	9000 K (3)	

7.2.2 Phosphor concentration in phosphor-converted LEDs

Phosphor concentration must be determined to achieve a specific CCT. The phosphor concentration combines three components related by two parameters: a certain ratio of green/red phosphor and the adapted silicone binder quantity. These determining factors for the experiments depend on the target CCT. The ratio of green and red phosphor and their dilution in the silicone binder have to be taken into consideration and be determined experimentally in two steps. The method developed to reach the desired CCT is explained in Fig. 7.5.

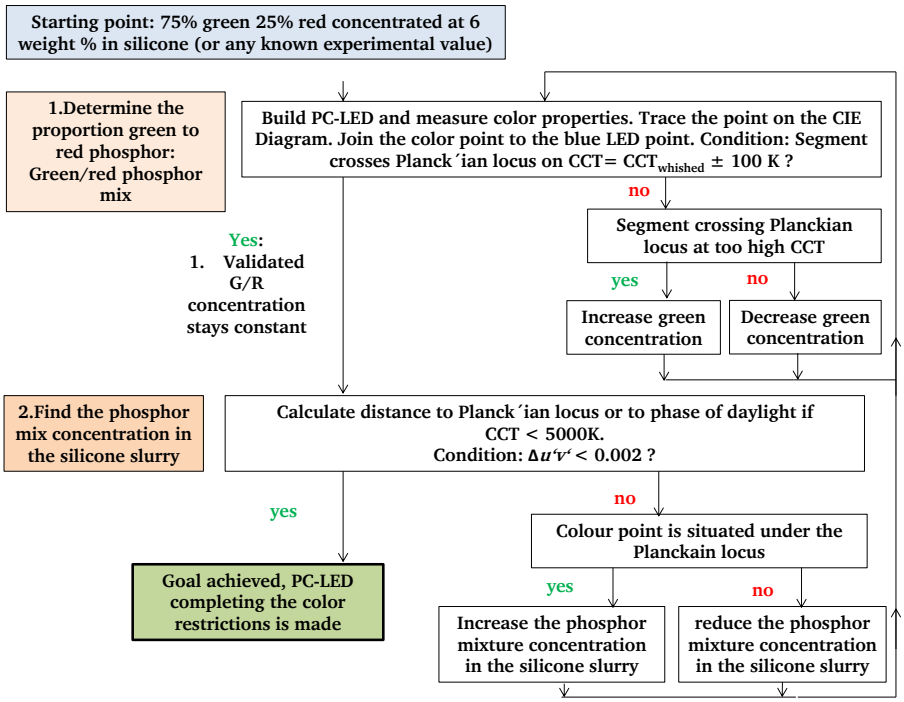

Figure 7.5.: Flow diagram describing how to find the appropriate phosphor concentration

A starting green/red concentration based on similar experiments previously conducted or a standard 75% green/25% red concentration has to be mixed. The proportion in which the phosphor mix has to be diluted must be estimated as well. A phosphor concentration of 6 weight % can be taken as a starting point. The first step consists of finding the appropriate green and red proportion to match the CCT. The segment joining blue LED and PC-LED chromaticity points on the CIE diagram is plotted (step 1 in Fig. 7.5). Depending on the position where this segment crosses the Planckian locus, the phosphor ratio has to be adjusted following the conditions on the scheme. When the segment passes on the target CCT represented on the Planckian's curve, the correct ratio is reached. In a second step the phosphor mixture concentration in the silicone has to be determined. On the same principle as for PC-LED with one phosphor, the PC-LED color point migrates along the segment between blue LED and phosphor mixture (segment [Blue LED-A] in Fig. 7.6). The phosphor mixture is considered as a unique "new" phosphor having a color point situated between the green and red phosphor taken separately (segment [G1R1] in Fig. 7.6). Decreasing the phosphor mixture concentration in the slurry (with silicone) shifts the PC-LED color point along the segment towards the blue LED. All parameters are set when Δu'v' is smaller or equal to 0.002. Fig. 7.6 shows the graphic representation of the green and red ratios and their concentrations in the silicone slurry required for the PC-LEDs based on G1 and R1 on the CIE diagram.

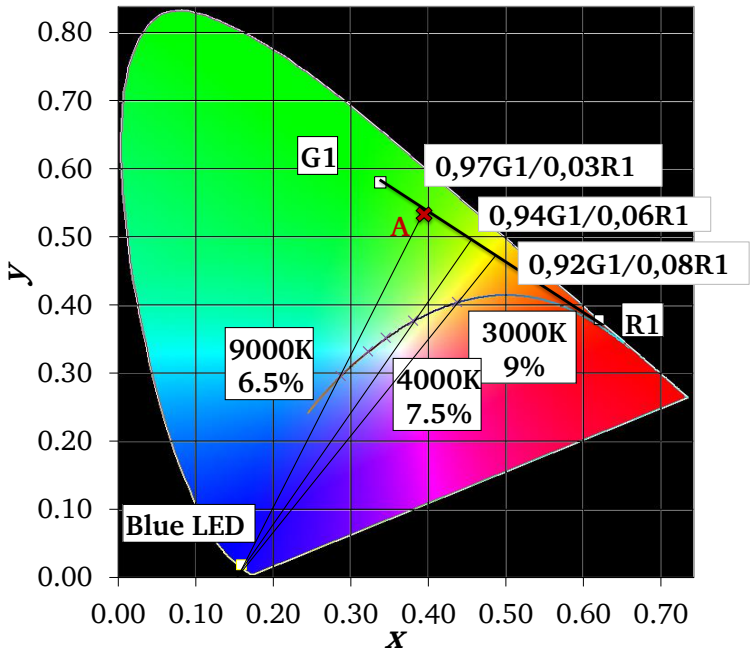

Figure 7.6.: CIE diagram of the required G1/R1 phosphor weight contributions in the PC-LEDs for 3000 K, 4000 K and 9000 K and the weight percentage of green and red phosphor mixture in the silicone layer

The phosphor concentration depends on the target CCT, the higher the CCT, the more shifted to small x and y is the white point. Consequently the corresponding green-red phosphor mixture has an increasing green ratio. For the example in Fig. 7.3, the ratio raises from 3000 K to 9000 K from a weight fraction of 0.92 G1 and 0.08 R1 to 0.97 G1 and 0.03 R1. The proportion in which the green and red phosphor is mixed to silicone binder determines the position of the PC-LED chromaticity point on the segment linking the color points of the specific phosphor mixture (point A on Fig. 7.6)and the blue LED. The closer the white point is to the blue LED, the less phosphor mixture is required. 6.5 weight % is necessary to achieve 9000 K in contrast to 9 weight % for 3000 K. The dependence of the green phosphor concentration as a function of the CCT is plotted in Fig. 7.7.

G1, G2, R1 and R2 concentrations necessary in the silicone slurry for the PC-LEDs of specific CCT are detailed in Table 7.3.

Green phosphor proportion increases with the CCT for every phosphor system. Indeed, the warmer the light, the more red component is required and therefore the lower the green concentration in the ratio in Fig. 7.7. A clear predominance of the green proportion in the ratio green/red can be noted, down to 50% for the lowest CCT (or warmest white PC-LEDs). This is due to the PL properties. Green emission is absorbed by the red phosphor.

Fig. 7.7 shows that G1 concentrations are higher than G2 concentrations required to reach every target CCT. Comparing red phosphor concentrations, the contribution of R2 in PC-LEDs is higher than the contribution of R1. These results are validated by the green and red phosphor ratios also in the silicone slurry (Table 7.3).

A specific CCT is reached by approaching the emission spectrum of the test source to the black body radiation characterized by a continuous spectrum over the whole range of wavelengths

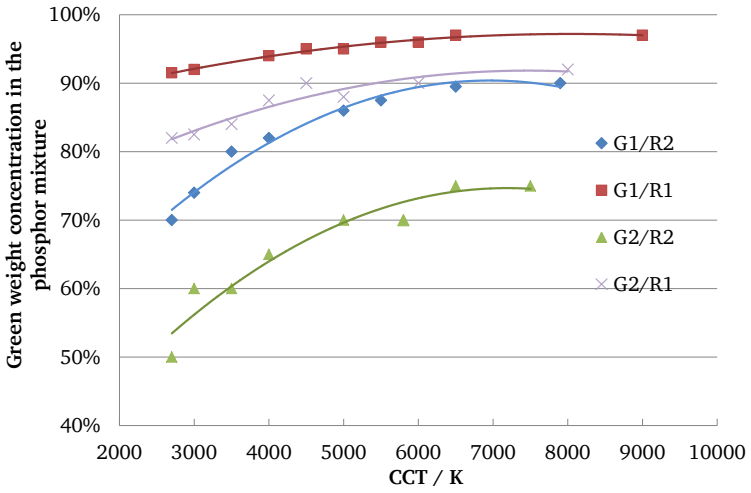

Figure 7.7.: Green proportions in the phosphor mix depending on the CCT

Table 7.3.: Green and red phosphor ratios in PC-LEDs weighted by the silicone proportions

	G1			G2		
	CCT / K	Green	Red	CCT / K	Green	Red
R2	2700	0.065	0.028	2700	0.038	0.038
	3000	0.068	0.024	3000	0.042	0.028
	3500	0.065	0.016	3500	0.042	0.028
	4000	0.066	0.015	4000	0.039	0.021
	5000	0.065	0.011	5000	0.041	0.017
	5500	0.061	0.009	5800	0.042	0.018
	6500	0.060	0.007	6500	0.038	0.013
	7900	0.060	0.007	7500	0.037	0.012
R1	2700	0.082	0.008	2700	0.049	0.011
	3000	0.083	0.007	3000	0.050	0.011
	4000	0.081	0.005	3500	0.046	0.009
	4500	0.076	0.004	4000	0.044	0.006
	5000	0.075	0.004	4500	0.044	0.005
	5500	0.072	0.003	5000	0.045	0.006
	6000	0.072	0.003	6000	0.042	0.005
	6500	0.068	0.002	8000	0.037	0.003
	9000	0.063	0.002			

in the visible. R2 emits at shorter wavelengths than R1. PC-LEDs with R1 will emit a more extended spectrum than R2. A smaller red phosphor amount is then required to reach the target CCT with R1 phosphor. This is validated by the ratios green/red from Fig 7.8 but also considering the varying silicone quantity required in Table 7.3.

The quantity of G1 necessary in the PC-LED is higher than in the case of G2. G1 exhibits a broader emission. This green emission participates to the excitation of the red phosphor and is consequently absorbed. Both red phosphors are better excited in combination with the G1 phosphor. The necessary quantity of G1 is used on one hand for the excitation of the

red phosphors, and therefore absorbed, and on the other hand as green emitter. In addition, the activator concentration is higher for G2 and its density is lower than G1 too. This means that at same weight, G2 phosphor will contain more atoms and even more activator will be inserted in the host lattice. G1 necessary quantity is as a result higher than G2. These arguments are proved in Table 7.3 by the overall amount of red phosphor (mixed with silicone) complementary to G1 and G2, compared at constant red phosphor.

The distance between the green phosphor color point and the prolongation of the blue and PC-LED color point (point A on Fig. 7.6) is not proportional to the green concentration in the phosphor mixture because of the PL phosphor interaction already mentioned. There is also no linear relationship between green concentration and CCT. CCT on the Planckian locus are not equidistant.

Concentration of phosphor mixture in the silicone binder is represented in Fig. 7.8. The higher the CCT, the more saturated are the colors of the PC-LEDs. The distance between blue LED and CCT on Planckian locus increases with decreasing CCT. An increasing phosphor concentration is then required for warmer light sources. Still because CCT are not distributed equidistantly on the Planckian locus, the phosphor mixture concentration in the silicone is not linearly dependent on the CCT.

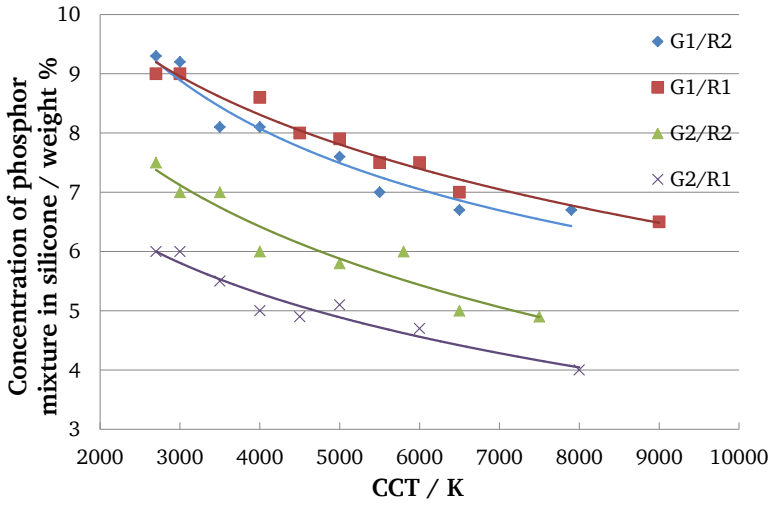

Figure 7.8.: Experimental phosphor mixture concentration in the silicone slurry as a function of the CCT

7.2.3 Phosphor-converted LEDs lighting properties

The efficiency and suitability of the phosphor powders and their mixtures is finally tested once the LEDs are built. Efforts were taken that PC-LEDs only differ from the nature of the phosphors. PC-LEDs are built with the same blue LED design, same driving currents and have similar CCT in order to better compare the matrix of phosphor systems. Emission spectra are recorded for the set of PC-LEDs based on the phosphor system studied. Spectral distributions of the PC-LEDs are illustrated in Fig. 7.9, 7.10 for G1/R1, G1/R2 and in Appendix C for G2/R1 and G2/R2 in Fig. C.1, C.2 for several CCTs.

Warm white LEDs are reached by increasing the amount of red phosphor. This leads to predominantly red peaks on the power spectral distribution. As red phosphors are excited

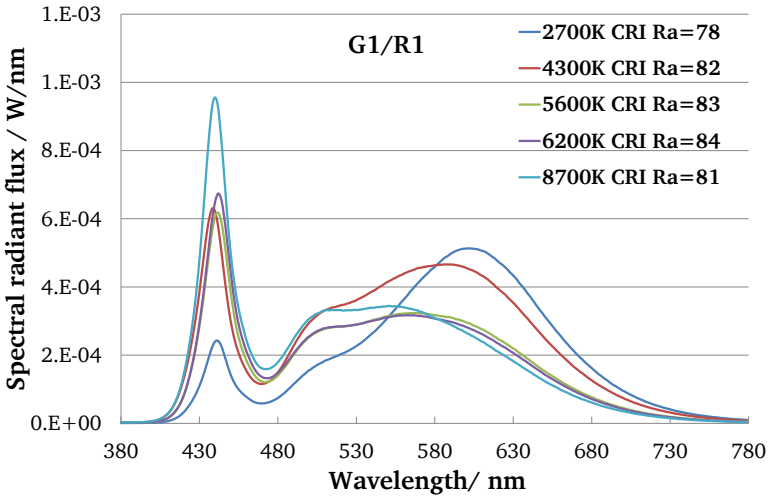

Figure 7.9.: Measured spectral radiant fluxes of PC-LEDs made of G1/R1 system for several CCT

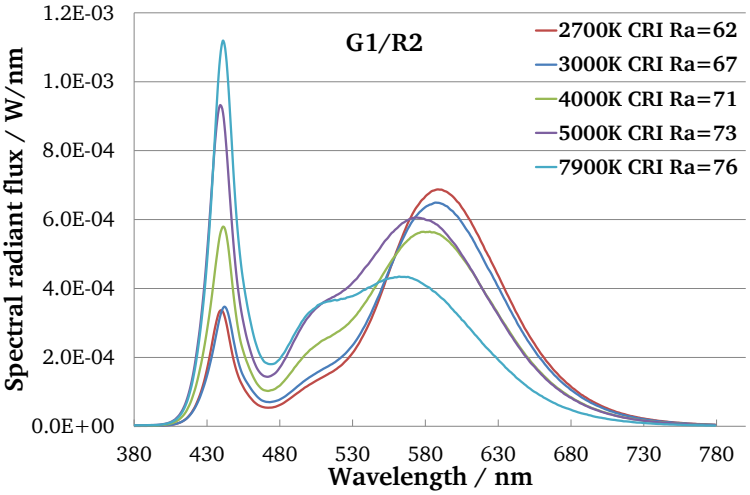

Figure 7.10.: Measured spectral radiant fluxes of PC-LEDs made of G1/R2 system for several CCT

and absorb the green phosphor radiation, the amount of green phosphor still has to be high in order to achieve the right color temperature. Both phosphors require the excitation from the blue LED and absorb its emission. This results in a very low blue emission. When white LEDs are becoming colder, less red phosphor is necessary. The green emission increases in importance and the blue emission even more so. Cold white LEDs are characterized by a reduction of the red part and thus equilibrated blue, green and red emissions. The amount of green phosphor needs also to be reduced because not absorbed by the red phosphor anymore for cold white LEDs, the emission presents then a strong blue peak, a moderated green one and a slight red influence. The behavior of the spectral distribution is, in general, independent of the phosphor system. Differences can be established for the exploitation of these curves ascribed by the luminous efficacy, the quality of the light or a measure of the color gamut Q_g. Q_g is the so-called relative gamut area. The concept of color gamut means the extent of the set of all possible object colors that appear under the current light source (some light sources tend to suppress saturated object colors while other light sources

are able to accentuate saturated object colors). Radiometric, photometric and light color characteristics are therefore measured and listed in Tables 7.4 to 7.7.

Table 7.4.: Measured luminous efficacy, distance to Planckian locus and quality of the light for G1/R1

CCT / K	2700	3000	4000	4500	5000	5500	6000	6500	9000
luminous efficacy / lm/W	20.5	20.6	16.1	19.7	14.2	17.5	16.5	24.5	16.7
$\Delta u'v'$ / $\cdot 10^{-3}$	0.49	0.37	0.36	0.26	3.97	3.43	4.84	3.55	2.76
CRI R_a	78	79	83	82	83	83	83	81	81
R_9	-4	-2	13	14	14	18	21	3	16
$G_{lightsource}$	91	91	95	95	96	96	97	93	95
luminous flux / lm	25.1	25.3	19.5	24.2	20.0	21.0	20.3	29.5	21.2
radiant flux / W	0.078	0.078	0.061	0.077	0.065	0.069	0.069	0.097	0.076

Table 7.5.: Measured luminous efficacy, distance to Planckian locus and quality of the light for G1/R2

CCT / K	2700	3000	3500	4000	5000	5500	6500	7900
luminous efficacy / lm/W	26.0	26.1	25.4	23.0	28.8	27.8	25.8	20.0
$\Delta u'v'$/ $\cdot 10^{-3}$	1.16	0.92	1.71	0.88	0.09	5.21	3.22	2.34
CRI R_a	61	65	70	71	73	75	76	76
R_9	-67	-58	-47	-44	-36	-29	-25	-21
$G_{lightsource}$	83	85	88	88	89	91	91	90
luminous flux / lm	31.5	23.5	31.0	29.7	34.3	33.4	33.4	26.4
radiant flux / W	0.087	0.065	0.089	0.086	0.104	0.104	0.108	0.089

White PC-LEDs chromaticity points are located from $0.09 \cdot 10^{-3}$ to $5 \cdot 10^{-3}$ to the Planckian locus. Within the same phosphor system, the proportion of blue, green and red emissions varies over the CCT but balanced, so that the sum of radiant flux over the wavelength shows no specific behavior. Radiometric values correspond to the spectral radiant flux weighted by the luminosity function which peak is situated at 555 nm. From warm white LEDs to cold white LEDs the spectral radiant flux remains relatively constant about this wavelength,

Table 7.6.: Luminous efficacy, distance to Planckian locus and quality of the light for G2/R1

CCT / K	2700	3000	3500	4000	4500	5000	6000	8000
luminous efficacy / lm/W	18.7	15.4	15.2	23.3	18.2	16.0	17.3	23.6
$\Delta u'v'/ \cdot 10^{-3}$	1.37	1.02	1.22	0.47	0.66	4.98	3.41	2.71
CRI R_a	82	84	84	85	85	85	82	81
R_9	14	23	32	38	43	48	48	49
$G_{lightsource}$	94	98	100	99	100	101	102	100
luminous flux / lm	23.9	19.5	18.9	28.1	23.3	20.0	21.3	31.0
radiant flux / W	0.075	0.061	0.060	0.089	0.075	0.066	0.072	0.109

Table 7.7.: Luminous efficacy, distance to Planckian locus and quality of the light for G2/R2

CCT / K	2700	3000	3500	4000	5000	5800	6500	7500
luminous efficacy / lm/W	25.3	26.6	24.9	19.8	22.7	18.9	23.8	25.3
$\Delta u'v'/ \cdot 10^{-3}$	1.72	1.00	1.56	1.07	0.63	2.02	2.02	3.72
CRI R_a	63	67	70	72	74	75	75	76
R_9	-58	-28	-39	-31	-20	-16	-11	-4
$G_{lightsource}$	85	91	89	91	91	93	93	93
luminous flux / lm	32.4	33.6	32.1	25.7	28.0	24.2	30.8	32.2
radiant flux / W	0.090	0.093	0.090	0.074	0.084	0.075	0.097	0.106

there is thus no specific tendency to recognize for the luminous flux over the CCT for each phosphor system and consequently for the luminous efficacy.

Still R2 globally has higher luminous efficacies than R1. R2 peaks at 600 nm, close to 555 nm, highest sensitivity $V(\lambda)$ for the human eyes. WLEDs with R2 exhibit then higher luminous efficiencies than with R1. In addition G1 emission depicts also a high intensity at 555 nm. Thus with the same red phosphor, light output is favored for PC-LEDs made of G1. The phosphor system with G1 and R2 is energetically the most efficient.

If the optical power perceived by the human eye does not substantially change over the CCT, the color quality represented by CRI R_a values or the color gamut, shows a clear dependence. Best color quality lights are obtained by approaching the emission spectrum to the reference illuminant emission. Reference illuminant spectra have different shapes depending on the CCT. The difference between test source and reference illuminant spectra (Fig. 7.11) is cumulated over the wavelengths and listed in the Table 7.8. R1 in combination with G1 or G2 shows increasing values in CRI R_a, R_9 or the relative gamut area for warm white LEDs until a maximum at about 5000 K, and decreases then slightly when reaching very cold white LEDs. For 5000 K LEDs emission in all spectral regions is well represented and close to the reference illuminant emission, leading to the best color quality results. Warm white or cold white LEDs exhibit emission favored in red or blue region respectively, which weights the emission spectrum and affects the CRI by reducing it. The difference between test source and reference illuminant shown in Table 7.8 illustrates the following trend. For one system the lower the difference is, the higher the CRI. CRI values depend on the resemblance of the test source to the reference illuminant. R2 mixed with G1 or G2 exhibits color quality increasing monotone from warm white to cold white LEDs. Warm white LED power distribution has a major peak in the red domain and very low green emission intensity because of its absorption by red. This induces a low color rendering. Cool white LEDs have lower contribution of the red phosphor which enhances the green peak. The CRI values are improved but the blue emission still remains low. Spectra showing equivalent proportions of blue, green or red, in that case cold white LEDs (6500 K) possess therefore the best CRI values.

Only phosphor combinations G1/R1 at 5000 K and 6000 K and G2/R1 at 3100 K, 4000 K, 4300 K and 5200 K exhibit good general color rendering ≥ 84. This is due to the fact that the two red-orange phosphors (R1, R2) do not emit enough in the red – deep red spectral range (610 nm – 660 nm) hence they do not provide enough red spectral content to illuminate important reddish objects.

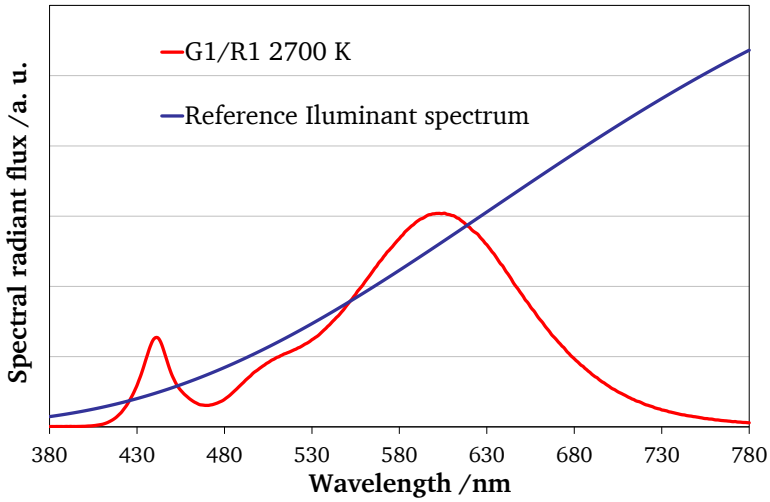

Figure 7.11.: Emission spectrum at 2700 K and its corresponding reference illuminant (a.u. arbitrary unity)

The influence of the red phosphor has a significant impact on the quality of the white light. R1 exhibits higher values for CRI R_a, R_9 (critical parameter indicating how accurate the red tones can be illuminated) and Q_g than R2. Shifting the red emission from 600 nm to 620 nm improves substantially the quality of the light source. Hence the white LED emission covers

Table 7.8.: Differences between reference illuminant and test source compared to the CRI R_a of G1, G2, R1 and R2 phosphor system.

	G1			G2		
	CCT / K	Diff.	CRI R_a	CCT / K	Diff.	CRI R_a
R2	2700	323	61	2700	314	63
	3000	277	65	3000	270	67
	3500	222	70	3500	233	70
	4000	202	71	4000	203	72
	5000	190	73	5000	190	74
	5500	174	75	5800	174	75
	6500	156	76	6500	159	75
	7900	177	76	7500	181	76
R1	2700	282	78	2700	276	82
	3000	254	79	3000	224	84
	4000	161	83	3500	193	84
	4500	157	82	4000	160	85
	5000	152	83	4500	167	85
	5500	149	83	5000	149	85
	6000	139	83	6000	140	82
	6500	152	81	8000	165	81
	9000	167	81			

a wider spectrum. Green phosphors also play a role in the quality of the light. G2 has higher CRI R_a, R_9 and Q_g than G1. Though G1 emits at a wavelength starting at 510 nm, which closes the gap between the blue and the phosphor emission and is expected to enhance the color quality, color quality and relative gamut area are lower than for G2. The color coordinates on the CIE diagram shown in 7.4 predicted better color quality with G2. This is validated here by the experimental results. The relative color gamut area (Q_g) validates the improved light quality of PC-LEDs made from R1 rather than R2 and G2 rather than G1. The combination of G2 and R1, an orthosilicate that peaks at 524 nm and a oxynitride that peaks at 620 nm, gives the best color quality results taking into account the color rendering, the perception of red tones and the relative color gamut area.

7.3 Simulation of experimental data

The attempt to reproduce experimental results using a simulation is performed once again with the software Lighttools. Experimental PL data are implemented for the computation. The aim of the simulation is to be able to reproduce emission spectra from routine experimental analyses. Simulations are compared to experiments in order to evaluate if the software is capable of predicting PC-LED spectral distributions as already detailed in our previous publication [97]. All phosphor combinations are simulated using the CCT achieved experimentally.

7.3.1 Simulation inputs

The same geometrical pattern representing LED type 1 (COB) is used as for YAG and LuAG (see Chapters 5 and 6). The silicone layer in this case is composed of a green and a red phosphor. The four phosphor combinations will be tested. Phosphors are homogeneously mixed within the silicone binder. Measured emission, reflection and excitation spectra of both phosphors are implemented. Concentration of each phosphor is adjusted to reach the appropriate CCT. PL properties play a very important role in the determination of the simulated spectra. Measurements have not been realized on single crystals as recommended by the software but for cost reasons, only on ground powder. Implemented PL data correspond to standard spectroscopic analyses realized on every production sample. The multiple reflection within the sample leads to erroneous measured PL data. Empirical re-scaling has been operated on the emission and absorption in order to optimize the simulations. Fig. 7.12 shows the emission spectra of all green and red phosphors used for simulations. Emission peaks have been extended to shorter wavelengths; hence the effect of the self re-absorption could be removed.

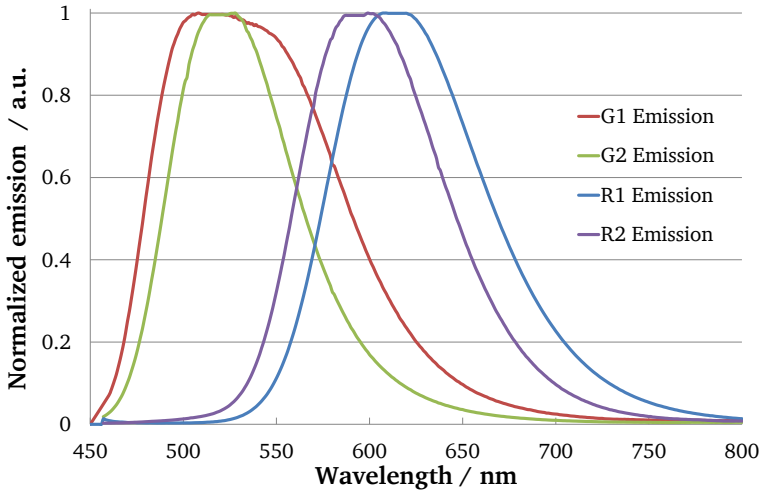

Figure 7.12.: Emission input parameters for G1, G2, R1 and R2

Absorption data (Fig. 7.13)have also been adjusted in order to counter the multiple reflections occurring during the measurements. Absorption is a very determinant parameter, particularly for the phosphor mixture, where phosphors interact strongly with each other. Indeed green phosphors influence by their strong absorption the PC-LEDs emission spectra in a single phosphor system. In more complex phosphor system green phosphors participate by their emissions in the excitation of red ones and will be then absorbed by the latter.

Excitation spectra are plotted in Fig. 7.14. They correspond to the exact measurement data.

7.3.2 Simulation results

Following the same method as in the practical part, optimized concentrations have been developed to fit the set of PC-LEDs measured. The spectral intensity distributions are presented in Fig. 7.15 and Fig. C.3, C.4 and C.5 in Appendix C for all phosphor combinations with G1,

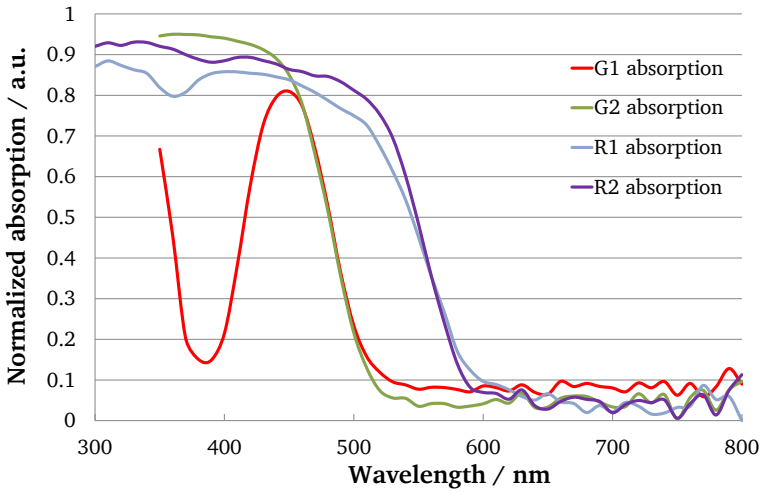

Figure 7.13.: Input parameters for absorption of G1, G2, R1 and R2

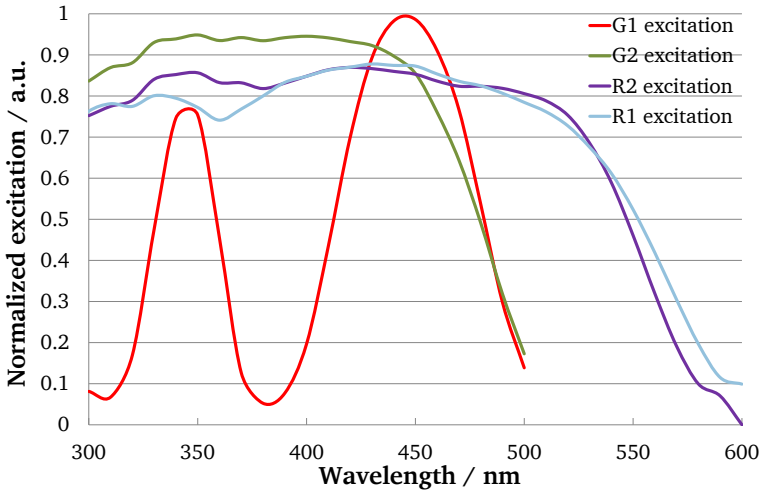

Figure 7.14.: Input of excitation parameters for G1, G2, R1 and R2

G2, R1 and R2. Simulated spectra are plotted with dashed lines in contrary to the measured ones with continuous lines. The difference depending on the wavelength is also represented with the corresponding color by dotted lines. Simulation and measurement of the same CCT are compared.

As shown in the experimental section, increasing green phosphor amount reduces the blue emission because blue rays are used to excite this phosphor. Increasing red phosphor amount results in a decrease of the blue and green emission intensities. The blue LED emission is partially absorbed by the red phosphor but also by the green phosphor which itself is also absorbed by the red phosphor. To increase the red emission keeping the same green emission, both red and green phosphor concentrations must be increased. This considerably decreases the blue light output. The PC-LED spectra behavior could be simulated successfully, as can be seen from the comparison of the measured and simulated spectral emission characteristics of Fig. C.3. For this, here again, appropriate phosphor input photoluminescent data had to be provided for the simulation software. A similar fit between the simulated and experimental spectral emission curves was obtained for the other phosphor mixtures (G1/R2, G2/R1,

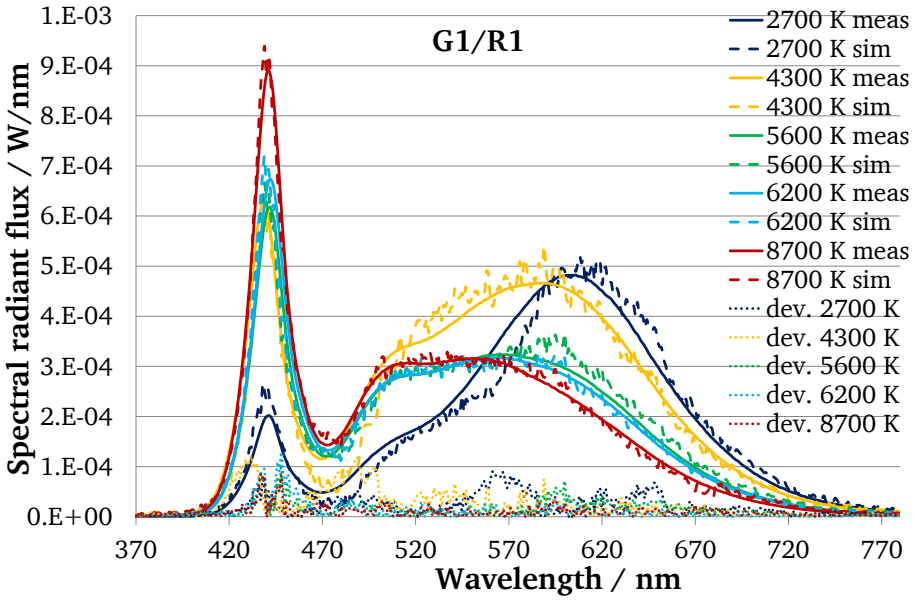

Figure 7.15.: Measured, simulated spectral distributions and their difference (full, dashed and dotted line) for G1/R1 system

G2/R2) as well. Proportions among the peak blue, peak green and peak red-orange spectral radiant flux values agreed well between the simulations and the measurements across the different CCTs.

To point out the effect of the differences between measurement and simulation on the human visual system (i.e. for the human user of the PC-LED light source), radiometric, photometric and colorimetric descriptor quantities were calculated for the above spectral emission curves. The differences of luminous flux, color rendering index (CRI) and CCT between the measured and simulated spectra were computed, see Tables 7.9 to 7.12. The distance between the chromaticity points of the measured and simulated PC-LEDs ($\Delta u'v'_{ms}$) and the distance between the measured (or simulated) chromaticity points of the PC-LED and its reference light source (the measure of visual white tone quality, $\Delta u'v'_{meas.}$ or $\Delta u'v'_{sim.}$) were also computed, see Tables 7.9 to 7.12. Relative and absolute radiant flux differences between simulation and measurement are shown in the last columns of these tables.

Table 7.9.: Photometric and radiometric variations between measured and simulated results for R1 G1 system at different CCT

CCT	$\Delta\Phi_v$ / lm	CRI $R_{a,meas.}$	ΔCRI $R_{a,ms}$	ΔCCT$_{ms}$ / K	$\Delta u'v'_{ms}$ /$\cdot 10^{-3}$	$\Delta u'v'_{meas.}$ /$\cdot 10^{-3}$	$\Delta u'v'_{sim.}$ /$\cdot 10^{-3}$	$\Delta\Phi_e$ / %	$\Delta\Phi_e$ / mW
2700	2	78	4	238	13.9	0.73	10.2	0.4	8.3
4300	1	82	7	182	10.9	0.41	8.90	3.6	9.4
5600	1	83	1	519	7.78	3.43	8.44	3.6	5.8
6200	0.1	84	1	260	4.30	4.72	3.13	0.5	4.4
8700	0.3	81	1	121	1.57	2.91	1.84	0.8	4.0

Table 7.10.: Photometric and radiometric variations between measured and simulated results for R2 G1 system at different CCT

CCT	$\Delta\Phi_v$ / lm	CRI $R_{a,meas.}$	ΔCRI $R_{a,ms}$	ΔCCT$_{ms}$ / K	$\Delta u'v'_{ms}$ /$\cdot 10^{-3}$	$\Delta u'v'_{meas.}$ /$\cdot 10^{-3}$	$\Delta u'v'_{sim.}$ /$\cdot 10^{-3}$	$\Delta\Phi_e$ / %	$\Delta\Phi_e$ / mW
2700	4	62	1	257	14.3	1.33	10.8	12.2	10.2
3000	2	67	0	208	8.03	1.46	4.51	6.4	5.8
4000	1	71	1	175	4.55	0.88	2.22	2.1	5.5
5000	1.9	73	3	198	6.55	3.85	0.0901	3.7	6.9
7900	0.9	76	1	536	4.49	2.34	3.48	3.1	5.2

Table 7.11.: Photometric and radiometric variations between measured and simulated results for R1 G2 system at different CCT

CCT	$\Delta\Phi_v$ / lm	CRI $R_{a,meas.}$	ΔCRI $R_{a,ms}$	ΔCCT$_{ms}$ / K	$\Delta u'v'_{ms}$ /$\cdot 10^{-3}$	$\Delta u'v'_{meas.}$ /$\cdot 10^{-3}$	$\Delta u'v'_{sim.}$ /$\cdot 10^{-3}$	$\Delta\Phi_e$ / %	$\Delta\Phi_e$ / mW
2700	0	82	2	50	2.18	1.72	2.29	2.5	5.2
3100	0	85	1	71	3.72	1.15	0.65	2.2	4.0
4300	1	85	2	23	2.92	0.58	3.66	1.9	6.3
4700	0	85	4	175	10.2	0.49	8.75	3.9	5.3
5200	0.4	85	3	7	2.26	4.98	7.28	2.8	5.0
6100	1.0	82	3	295	9.84	3.41	4.04	2.3	5.1
8000	0.2	81	1	329	3.63	2.89	1.35	2.5	5.3

Table 7.12.: Photometric and radiometric variations between measured and simulated results for R2 G2 system at different CCT

CCT	$\Delta\Phi_v$ / lm	CRI $R_{a,meas.}$	ΔCRI $R_{a,ms}$	ΔCCT$_{ms}$ / K	$\Delta u'v'_{ms}$ /$\cdot 10^{-3}$	$\Delta u'v'_{meas.}$ /$\cdot 10^{-3}$	$\Delta u'v'_{sim.}$ /$\cdot 10^{-3}$	$\Delta\Phi_e$ / %	$\Delta\Phi_e$ / mW
2700	0	63	1	91	6.64	0.98	5.18	3.6	7.7
3000	0	66	2	293	12.9	1.25	11.6	4.7	10.1
4000	0	72	4	67	6.01	1.14	5.26	3.4	6.1
4900	1.3	74	4	169	3.33	0.33	0.35	5.9	11.1
6800	0.3	76	7	35	6.21	3.82	2.23	2.5	9.7
7500	0	76	7	243	7.37	3.72	2.50	4.0	12.2

As can be seen from Tables 7.9 to 7.12, measured and simulated luminous flux and CRI values agree reasonably. The measured white tone characteristics ($\Delta u'v'_{meas.}$) remain less than $5{\cdot}10^{-3}$ (mean: $2.1{\cdot}10^{-3}$) which confirms that the sample PC-LEDs we built yielded reasonable white tones. Nevertheless, some white tone discrepancies between simulation and measurements exist. The measure of white tone quality of the simulated white PC-LED spectra ($\Delta u'v'_{sim.}$) reached values up to $1.23{\cdot}10^{-2}$ (mean: $5.2{\cdot}10^{-3}$). The maximum value ($\Delta u'v'_{sim.}$=$1.23{\cdot}10^{-2}$) corresponds to a visually not acceptable white tone. Simulated chromaticity points also deviate from measured ones (see the $\Delta u'v'_{ms}$ values). As a consequence, measured and simulated CCT values differ, as well and this difference is visually well noticeable. All these deviations result from the differences of the measured and simulated spectral power distributions. In Fig. C.4, it is possible to identify at which wavelengths the spectral power differences are the highest (for the example G1/R1). Absolute and relative radiant flux differences between the simulated and measured emission spectra ($\Delta\Phi_e$) vary from 1% to 12% (see Tables 7.9 to 7.12). These differences are ascribed to the simulated emission discrepancies occurring around the blue peak emission (420 nm - 440 nm), in the spectral transition range between the blue LED and the green phosphor emission (460 nm - 500 nm) and in the transition between the green and red-orange phosphor emissions (550 nm - 600 nm).

The reason of the spectral mismatch between simulation and measurement can be attributed to the discrepancies of phosphor absorption data (our input parameter for the simulation program). The deviation around the blue emission peak and at the transition range about 470 nm occurs due to similar reasons as discussed for YAG and LuAG in the previous sections 5.3.2 and 6.3.2. The PC-LED configuration considered in this section is represented by a complex system of two phosphors in which the red-orange phosphor's photoluminescent properties influence the emission spectra of the green phosphors. The absorption measurements on the phosphors used in this study to provide the input parameter for the simulation program influence the multiple phosphor interactions within these PC-LEDs made of the mixture of two phosphor components very strongly. In this case, down converting processes are influenced by the interaction of both phosphors resulting in the difficulty to simulate these emission spectra.

Important simulation input that have been optimized are the concentrations of green and red phosphors. These parameters are presented in Table 7.13. The ratios between simulated and measured number of phosphor particle is presented for each CCT and phosphor combination.

In the simulation and the measurement phosphor concentrations exhibit the same trend. High red phosphor amounts are required for warm white LEDs, which decreases the higher the CCT of white PC-LEDs. Logically green phosphor concentration increases in both cases when the WLED is getting colder. This behavior is validated by the simulation as well. A manual check consisting of varying the red phosphor concentration could confirm that the software takes into consideration the absorption of the green phosphor by the red one. The difference between experiment and simulation is situated in the proportion of green and red required in the WLEDs. The amount of red phosphor in the experiments is very low compared to the amount of the green one. The simulations do not show this behavior. The quantum efficiency (QE) might be the reason for this variation. QE required by the software are absolute QE. However the QE given as input in the software correspond to an internal quantum efficiency determined experimentally with an internal reference differing according to the color of the phosphor. Therefore the direct comparison of the concentrations is not relevant. The absolute number of particles differs in several orders of magnitude between

Table 7.13.: Ratios of simulated number of particles to measured ones for green and red phosphor involved in the PC-LED for G1, G2, R1 and R2

	G1			G2		
	CCT / K	ratio green / $\cdot 10^5$	ratio red / $\cdot 10^5$	CCT / K	ratio green / $\cdot 10^5$	ratio red / $\cdot 10^5$
R2	2700	4.1	1.1	2700	2.6	1.8
	3000	4.3	1.4	3000	2.9	1.8
	4000	4.5	1.1	4000	3.4	1.8
	5000	4.7	1.2	4900	4.0	1.9
	7900	5.8	1.3	6800	4.1	2.2
				7500	4.2	2.3
R1	2700	4.5	0.61	2700	2.8	0.85
	4300	4.7	0.8	3100	3.1	0.92
	5600	5.7	0.68	4300	3.3	0.89
	6200	5.6	0.61	4700	3.3	0.76
	8700	6.1	0.62	5200	4.1	1.1
				6100	3.7	0.98
				8000	3.8	0.83

simulation and measurements. However the comparison of the ratio between simulated and measured number of phosphor particles shows an almost constant factor for the same phosphor. For instance the ratio of green 1 is of about $4.5 \cdot 10^5$ in combination with R1 or R2. An absolute comparison is not possible, but a relative one.

The results obtained with Lighttools show that simulations could reproduce experimental data performed with a complex system of two phosphors for four different phosphor combinations. Standard spectroscopic measurements were implemented as parameters and enable the prediction of experimental spectral power distribution of PC-LEDs. PL properties must be scaled to take into account the possible multiple interactions occurring during the measurement. The deviations between simulation and measurements reach up to 4 % for the luminous flux and 1 % to 12 % for the radiant flux, which indicates encouraging results. The deviations between simulations and experiments concerning chromaticity points and thus CCT show discrepancies up to $\Delta u'v'_{ms}$=1.4·10^{-2} and ΔCCT_{ms}=536 K due to the spectral radiant distributions' mismatch though empirical adjustment of the phosphor PL parameters. The ratio of green and red phosphor has the same influence on the PC-LED emission spectra in the simulation as in the experiments. The concentrations necessary to reach the CCT are different, most likely because absolute QE are considered in the simulation and only relative ones could be measured. The differences in concentration reduce the chance to replace the experimental part completely by simulation. Still the proportion of green and red phosphor show a similar trend.

7.4 Conclusion on green and red phosphors LED systems

This chapter investigated two green phosphors, one LuAG and one orthosilcate. These green phosphors were separately mixed to two other red nitride phosphors. This provides a four phosphor system. The study describes firstly PL properties of the phosphors in a powder

state. All phosphors depict emission at different wavelength but are appropriate for the blue LED application because they are efficiently excitable in the blue wavelength range (440 nm-460 nm). This interesting system focuses on the impact of the green and red mixture ratio. The interaction of green and red phosphor together is of great importance because the green emission partly contributes to the red excitation.

The mixture ratio of these phosphors reveals several PC-LED characteristics differing in their light output but also in their colour quality. The combination of LuAG with oxyorthosilicate emitting at 600 nm exhibits the best radiometric properties but not the best light quality. Higher CRI values are reached for the system of orthosilicate and red-orange oxynitride emitting at 620 nm. Indeed the broader red-orange phosphor emission peaking at about 600 nm in the WLEDs enables the complete, continuous coverage of the visible spectrum and thereby enhancing the color quality of the LEDs. Simulations were carried out on the same phosphor system that was examined experimentally. Measured PL properties are implemented as input parameters in the software. By means of empirical adaptation of the absorption, emission spectra of PC-WLED were simulated revealing spectral distribution discrepancies resulting in radiometric, photometric and chromaticity deviations (see 7.3.2). PC-LEDs made of two phosphors imply a three-parameter system, so an increase in the variable number compared to single phosphor systems. CCT are experimentally even more difficult to reach. The ability to predict PC-LED emission spectra from PL phosphor properties still in the powder state represents a significant gain of time. Hence it represents a relevant advantage by reducing the number of experiments required. The simulation model developed with Lighttools is not only validated for a one phosphor system but the software is also able to predict laboratory results for a multiple phosphor system. It is possible to predict LED radiant flux distributions from PL properties. The software considers physical parameters of the system and reacts therefore to phosphor concentration changes in a very similar way as the experiments. However phosphor concentrations required for the simulation differ from the experiments which does not allow to exclude PC-LED measurements.

8 Conclusion and overview

In the actual context of exploring efficient technologies to produce white light, the solution combining a broad emitting phosphor excited by a blue LED represents a promising opportunity. This approach combines the strength of the LED efficiency with the benefits of phosphors. The numerous advantages of LEDs are proven: high light output, long lifetime and low maintenance costs. Dimmability, low power consumption saving energy and money belong to the many positive founding principles favoring LED technology versus conventional lighting using poisonous elements such as Mercury and other noxious and polluting gases. White LEDs featuring the use of phosphors stand out by their quality of light, adjustable from warm to cold without wasted energy from radiating in non-visible wavelengths, and are benefiting from renewed interest for this new method to generate white light.

This PhD dissertation concentrates on the influence of the phosphor on PC-LED properties. Physical characteristics such as phosphor particle size and chemical composition are investigated as well as their repercussions on PL properties. A first understanding of the luminescence processes occurring within PC LEDs was required. The YAG phosphor is a well-known system offering the possibility to illustrate the influence of phosphor particle size. Samples of narrow particle size distribution with diameter ranging closely from 5 μm to 40 μm were extracted from a single batch. Phosphor particles of increasing size show rising excitation, absorption and emission intensities. Small particles exhibit defects due to early growth stoppage during the synthesis resulting in light trapping effects. The phosphor concentration required to reach cool white LED depends linearly on the phosphor particle size. White PC-LEDs made of small phosphor particles contain a higher phosphor concentration. The expertise on the behavior between phosphor concentration and phosphor particle size reduces greatly the experimental time required to achieve LEDs of specific chromaticity. Phosphor particles of small size enable the reduction of the phosphor quantity necessary to achieve WLEDs, which correlates to financial benefits. Luminous efficiency also increases with phosphor particle size. Besides the PL properties, this phenomenon is attributed to the enhanced backscattering of phosphor particles of decreasing size which leads to the absorption of light by the LED chip. PC-LED light output can be optimized on the basis of phosphor particle size. Angular measurements reveal a yellow ring effect. Ray path to escape the LED chip directed to wide angles is longer than the way to the center of the LED. On the longer ray path more phosphor converting light events are possible. The length difference hence causes yellow tones off centered of the LED. Chromaticity distribution over the angles emphasized the importance of the physical parameters of the phosphor which is neglected in the simulations. Large particles settle on the top of the chip which contributes to an increase in the variation in chromaticity between the emission when observing the center of the LED and at wide angles. A CCT variation over the angles is found for particle sizes of 20 μm. Phosphor particle size influences the spatial chromaticity homogeneity of the light.

Previous experiments are reproduced on a LuAG phosphor system. In addition, LuAG phosphor experiments indicate how the chemical composition of the host lattice and the activator concentration tunes the phosphor emission. The replacement of Yttrium ions by Lutetium (larger ion) increases the crystal field splitting which provokes an emission shift towards longer wavelengths. This describes one possibility to tune the color of the PC-LED. Increasing the activator concentration also implies a shift to longer wavelengths. Results obtained

from measurements realized on different PC-LEDs made of a LuAG phosphor system validate the phenomenon observed on YAG. The activator concentration shows no change on the PC-LED properties previously noted.

Specific impact on PC-LEDs in their application as final product is related to the influence of phosphor, its chemical composition, activator concentration and particle size. The new discoveries gathered in this PhD dissertation concerning phosphor particle sizes indicate a compromise on the phosphor particle size applied in the PC-LEDs. A choice has to be made between high LED efficiency but high amount of phosphor and lower chromaticity homogeneity for large phosphor particles and lower LED output with smaller phosphor concentration.

LEDs combined with one phosphor suffer from poor color rendering. Two green and two red phosphors are mixed to analyze their impact on PC-LEDs. Green and red phosphor concentration in a two-phosphor-converted LED system highlights their interactions. The high green phosphor concentration required for the white PC-LEDs is ascribed to the PL properties of green and red phosphors. Red phosphor is excited and absorbs not only the blue radiations but also the green ones. Green phosphor concentration dominates clearly the green/red mixture when increasing the CCT of the WLED because the green emission participates to a significant part. The number of green phosphor particle must be higher than red phosphor particles which absorb the green emission. Results gained from this study enable one to determine phosphor characteristics to reach PC-LEDs of high light quality. The main differences between PC-LED radiant fluxes and color rendering are determined by the phosphor system and vary little for warm white or cold white LEDs. Red phosphors that exhibit emission spectra towards longer wavelengths induce PC-LEDs of higher CRI. Therefore their emission spectra match better with the reference illuminant on which the calculation is based to define CRI values. A better luminous efficacy is reached for a phosphor system emitting a spectrum close to the standard luminosity function at 555 nm so that luminous flux is high. This study enables one to make conclusions about the appropriate phosphor to use in PC-LEDs to reach high luminous efficiency, color quality and to predict the phosphor amount required depending on the target CCT.

Obtaining results experimentally is very time and material intensive. A predictive simulation method also received attention in this work. Experimental PL properties are implemented as parameters for the simulations and adjusted to compare simulations with experiments. “Lighttools” is a software based on Monte Carlo simulations and considers phosphor PL properties, their PSD as well as optical properties and refractive indices of the constituent materials. All these factors are relevant for the physical interpretation of the computation. Simulations are performed to estimate the capability of the software to predict the influence of phosphor particle sizes of YAG, LuAG and the mixture of green and red phosphors. Good prediction of power could be achieved but CCT could not be simulated in a satisfying way because simulated and measured spectral distributions did not match closely enough. Analyses on over-concentrated LEDs proved the effect of self-absorption that might occur during the PL measurements. Indeed PL parameters implemented do not originate from single crystal measurements which could be responsible for the discrepancies noticed between simulated and measured emissions. Simulations are adapted to give an idea of the PC-LED trend based on theoretical considerations. Practical experiments are not always realized on phosphors of spherical morphology, implying losses within the device and not perfectly controllable parameters. Fine tuning of the phosphor concentration required for the experiments cannot be reproduced with the simulation. In addition a major physical parameter, sedimentation, cannot be predicted by the simulation.

The study of the PL properties demonstrated the great influence of phosphors on the PC-LED properties from a light output and color quality point of view. We have seen that the arrangement of the phosphor plays an important role on the light escaping properties. Results reported in the literature carried out on remote phosphor packaging technology showed higher efficiencies. The association of remote phosphor and phosphor particle size holds efficiency improvement potential. This could extend the investigation on the phosphor particle size.

A new research field has started with the investigation of phosphor combined with laser technology. The use of lasers for highly powerful application is a conceivable opportunity [98]. This alternative method is based on the same mechanism as a PC-LED mixing blue exciting radiation and phosphor converted light. The difference resides in the working principle. PC-LEDs produce light by transmission through a phosphor layer whereas laser technology is suitable to reflect on the phosphor surface. Lasers have very focused beams which are desirable for some specific applications and would avoid the use of optics. The knowledge acquired on the PL properties by this PhD dissertation would considerably enrich and facilitate the research for this new topic. Large phosphor particles exhibit high emission intensities without the light inhomogeneity generated by the transmission process. The adjustment of the phosphor particle size enables the development of significant ameliorations.

These further domains of investigation are examples to broaden the field of research that would encourage the insertion and expansion of new efficient technologies for lighting applications based on the knowledge gained on this PhD dissertation.

Bibliography

[1] Energy Information Administration, U.S.A. *How much electricity is used for lighting in the United States*. 2014. URL: http://www.eia.gov/tools/faqs/faq.cfm?id=99&t=3.

[2] Hamins, A.; Bundy, M., and Dillon, S. *Characterization of candle flames*. In: "Journal of Fire Protection Engineering" 15.4 (2005), pages 265–285.

[3] Zukauskas, A.; Shur, M., and Gaska, R. *Introduction to solid state lighting*. John Wiley & Sons New York, 2002, pages 8–24.

[4] Munsell, A. *Color System*. 2012. URL: http://munsell.com/.

[5] Renoux, D. and Sabol, D. *Report on detailed data of investigated colour quality indices*. European Association of National Metrology Institutes, 2012.

[6] Smet, K.; Schanda, J.; Whitehead, L., and Luo, R. *CRI2012: A proposal for updating the CIE colour rendering index*. In: "Lighting Research and Technology" (2013).

[7] Davis, W. and Ohno, Y. *Color quality scale*. In: "Optical Engineering" 49.3 (2010), page 033602.

[8] Zukauskas, A.; Shur, M., and Gaska, R. *Introduction to solid state lighting*. John Wiley & Sons New York, 2002, pages 55–58.

[9] Narukawa, Y.; Ichikawa, M.; Sanga, D.; Sano, M., and Mukai, T. *White light emitting diodes with super-high luminous efficacy*. In: "Journal of Physics D: Applied Physics" 43 (2010), pages 354002–1–354002–6.

[10] Schubert, E. F.; Gessmann, T., and Kim, J. K. *Light Emitting Diodes*. 2nd edition, Cambridge University Press, 2003, pages 4–9.

[11] Kitai, A. *Luminescent Materials and Applications*. John Wiley & Sons VCH-Weinheim, 2008, pages 207–211.

[12] Setlur, A. *Phosphors for LED-based solid-state lighting*. In: "The Electrochemical Society Interface" 16.4 (2009), pages 32–36.

[13] Schubert, E. F.; Kim, J. K.; Luo, H., and Xi, J.-Q. *Solid-state lighting—a benevolent technology*. In: "Reports on Progress in Physics" 69.12 (2006), pages 3069–3099.

[14] Morkoç, H. *Handbook of Nitride Semiconductors and Devices, GaN-based Optical and Electronic Devices*. Volume 3. Wiley-VCH, Weinheim, 2009, pages 70–88.

[15] Liu, Z.; Liu, S.; Wang, K., and Luo, X. *Status and prospects for phosphor-based white LED packaging*. In: "Frontiers of Optoelectronics in China" 2.2 (2009), pages 119–140.

[16] Haque, S.; Steigerwald, D.; Rudaz, S.; Steward, B.; Bhat, J.; Collins, D.; Wall, F.; Subramanya, S.; Elpedes, C., and Elizondo, P. *Packaging challenges of high-power LEDs for solid state lighting*. In: "Society of Photo-Optical Instrumentation Engineers (SPIE)" (2003), pages 881–886.

[17] Esfandyarpour, M. *Solid State Lighting*. Stanford University, 2012. URL: http://large.stanford.edu/courses/2012/ph240/esfandyarpour-m2/.

[18] Chang, M.-H.; Das, D.; Varde, A., and Pecht, M. *Light emitting diodes reliability review*. In: "Microelectronics Reliability" 52.5 (2012), pages 762–782.

[19] Evolution, LED. *are LED less cost-effective*. 2013. URL: http://www.led-evolution.com/Technology/are-LEDs-cost-effective.html.

[20] Ye, S.; Xiao, F.; Pan, Q.; Ma, Z., and Zhang, Q. *Phosphors in phosphor-converted white light-emitting diodes: Recent advances in materials, techniques and properties*. In: "Materials Science and Engineering: R: Reports" 71.1 (2010), pages 1–34.

[21] Pan, Y.; Wu, M., and Su, Q. *Comparative investigation on synthesis and photoluminescence of YAG: Ce phosphor*. In: "Materials Science and Engineering: B" 106.3 (2004), pages 251–256.

[22] Potdevin, A.; Chadeyron, G.; Boyer, D., and Mahiou, R. *Sol-gel based YAG: Ce^{3+} powders for applications in LED devices*. In: "Physica Status Solidi (c)" 4.1 (2007), pages 65–69.

[23] Ekambaram, S.; Patil, K., and Maaza, M. *Synthesis of lamp phosphors: facile combustion approach*. In: "Journal of Alloys and Compounds" 393.1 (2005), pages 81–92.

[24] Yen, W. and Weber, M. *Inorganic phosphors: compositions, preparation and optical properties*. CRC Press, Boca Raton, 2004, pages 20–25.

[25] Lin, C. and Liu, R.-S. *Advances in phosphors for light-emitting diodes*. In: "The Journal of Physical Chemistry Letters" 2.11 (2011), pages 1268–1277.

[26] Shionoya, S.; Yen, W., and Hase, T. *Phosphor Handbook*. 2nd edition, CRC Press New York, 1999. Chapter 4, pages 341–349.

[27] Ropp, R. *Luminescence and the Solid State*. Elsevier Amsterdam, 1991, pages 447–500.

[28] Raukas, M.; Basun, S.; Schaik, W.; Yen, W., and Happek, U. *Luminescence efficiency of cerium doped insulators: The role of electron transfer processes*. In: "Applied Physics Letters" 69.22 (1996), pages 3300–3302.

[29] Dorenbos, P. *Relating the energy of the $[Xe]$ $5d^1$ configuration of Ce^{3+} in inorganic compounds with anion polarizability and cation electronegativity*. In: "Physical Review B" 65.23 (2002), pages 235110–235113.

[30] Haranath, D.; Chander, H.; Sharma, P., and Singh, S. *Enhanced luminescence of YAlO: Ce nanophosphor for white light-emitting diodes*. In: "Applied Physics Letters" 89 (2006), pages 173118–1–173118–4.

[31] Zhang, Y.; Li, L.; Zhang, X., and Xi, Q. *Temperature effects on photoluminescence of YAG: Ce^{3+} phosphor and performance in white light-emitting diodes*. In: "Journal of Rare Earths" 26.3 (2008), pages 446–449.

[32] Juestel, T. *Inorganic Luminescent Materials: Fundamentals and Applications*. University Münster, Lecture, 2011.

[33] Ronda, C. *Luminescence - From Theory to Applications*. Wiley-VCH, Weinheim, 2007, pages 3–24.

[34] Blasse, G. and Grabmaier, B. C. *Luminescent Materials*. Volume 44. Springer-Verlag Berlin, 1994, pages 10–31.

[35] Robertson, J. and Van Tol, M. *Cathodoluminescent garnet layers*. In: "Thin Solid Films" 114.1 (1984), pages 221–240.

[36] Wu, J.; Gundiah, G., and Cheetham, A. *Structure property correlations in Ce-doped garnet phosphors for use in solid state lighting*. In: "Chemical Physics Letters" 441.4 (2007), pages 250–254.

[37] Xie, R.-J. and Hirosaki, N. *Silicon-based oxynitride and nitride phosphors for white LEDs—A review*. In: "Science and Technology of Advanced Materials" 8.7 (2007), pages 588–600.

[38] Rohwer, S. and Srivastava, A. *Development of Phosphors for LEDS*. In: "Interface-Electrochemical Society" 12.2 (2003), pages 36–41.

[39] Congting, S. and Dongfeng, X. *Chemical bonding theory of single crystal growth and its application to YAG bulk crystal*. In: "CrystEngComm" 16.11 (2014), pages 2129–2135.

[40] Chabra, V.; Dorman, D.; Herko, S., and Taskar, N. *Light efficient packaging configurations for led lamps using high refractive index encapsulants*. WO Patent App. PCT/US2004/029,201. 2008. URL: http://www.google.com/patents/WO2005027576A3?cl=en.

[41] Lin, Y.-C.; Zhou, Y.; Tran, N., and Shi, F. *LED and optical device packaging and materials*. In: "Materials for Advanced Packaging". Springer, 2009, pages 629–680.

[42] Baillot, R.; Deshayes, Y.; Bechou, L.; Buffeteau, T.; Pianet, I.; Sorieul, S., and Ousten, Y. *Effects of silicone coating degradation on GaN MQW LEDs performances using physical and chemical analyses*. In: "Microelectronics Reliability" 50.9 (2010), pages 1568–1573.

[43] Yang, S.-C.; Lin, P.; Wang, C.-P.; Huang, S.; Chen, C.-L.; Chiang, P.-F.; Lee, A.-T., and Chu, M.-T. *Failure and degradation mechanisms of high-power white light emitting diodes*. In: "Microelectronics Reliability" 50.7 (2010), pages 959–964.

[44] Li, H.-T.; Hsu, C.-W., and Chen, K.-C. *Enhancement of light efficiency of LED using a novel high refractive encapsulant*. In: "Electronic Components and Technology Conference, 2008. ECTC 2008. 58th". IEEE. 2008, pages 1926–1930.

[45] Babiarz, A. *Silicone phosphor encapsulation for high power white LEDs*. Pan Pacific Symposium, 2008. URL: http://www.amtest.bg/press/asymtek/SiPhosphorEncapforHiPowerWhiteLEDs.pdf.

[46] Hou, S.-D. and Yan, G.-S. *Analysis and Simulation of Light Extraction of Light-Emitting Diodes: Simulation Efficiency*. In: "Journal of Electronic Science and Technology" 8.2 (2010), pages 126–130.

[47] Stefanov, E.; Shelton, B.; Venugopalan, H.; Zhang, T., and Eliashevich, I. *Optimizing the external light extraction of nitride LEDs*. In: "Solid State Lighting II, Ian Ferguson, Nadarajah Narendran, Steve DenBaars, Yoon-Soo Park, eds., Proc. SPIE". Volume 4776. 2002, pages 223–234.

[48] Bergh, A. and Saul, R. *Surface Roughening of Electroluminescent Diodes*. US Patent 3,739,217. 1973.

[49] Yamada, K.; Imai, Y., and Ishii, K. *Optical simulation of light source devices composed of blue LEDs and YAG phosphor*. In: "Journal of Light & Visual Environment" 27.2 (2003), pages 70–74.

[50] Liu, Z.; Liu, S.; Wang, K., and Luo, X. *Measurement and numerical studies of optical properties of YAG: Ce phosphor for white light-emitting diode packaging*. In: "Applied Optics" 49.2 (2010), pages 247–257.

[51] Tran, N. and Shi, F. *Studies of phosphor concentration and thickness for phosphor-based white light-emitting-diodes*. In: "Journal of Lightwave Technology" 26.21 (2008), pages 3556–3559.

[52] Sommer, C.; Reil, F.; Krenn, J.; Hartmann, P.; Pachler, P.; Tasch, S., and Wenzl, F. *The impact of inhomogeneities in the phosphor distribution on the device performance of phosphor-converted high-power white LED light sources*. In: "Journal of Lightwave Technology" 28.22 (2010), pages 3226–3232.

[53] You, J.; Tran, N.; He, Y., and Shi, F. *Packaging of phosphor based high power white LEDs: effects of phosphor concentration and packaging configuration*. In: "Journal of Electronic Packaging" 133 (2011), pages 011009–1–011009–5.

[54] Fujita, S.; Yoshihara, S.; Sakamoto, A.; Yamamoto, S., and Tanabe, S. *YAG glass-ceramic phosphor for white LED (II): luminescence characteristics*. In: "Fifth Int. Conf. on Solid-State Lighting, Proc. SPIE, San Diego". 2005, pages 59411–1–59411–2.

[55] Narendran, N.; Gu, Y.; Freyssinier-Nova, J.-P., and Zhu, Y. *Extracting phosphor-scattered photons to improve white LED efficiency*. In: "Physica Status Solidi (a)" 202.6 (2005), R60–R62.

[56] Zhu, Y.; Narendran, N., and Gu, Y. *Investigation of the optical properties of YAG: Ce phosphor*. In: "Journal of Light & Visual Environment" 32.2 (2008), pages 115–119.

[57] Abe, T. *Illuminating light source device using semiconductor laser element*. US Patent 5,535,230. 1996.

[58] Lowery, C. H. *Multiple encapsulation of phosphor-LED devices*. US Patent 5,959,316. 1999.

[59] Narendran, N. *Improved performance white LED*. In: "Optics & Photonics 2005". International Society for Optics and Photonics. 2005, pages 594108–594114.

[60] Zhu, Y. and Narendran, N. *Optimizing the performance of remote phosphor LEDs*. In: "Journal of Light & Visual Environment" 32.2 (2008), pages 115–119.

[61] Luo, H.; Kim, J. K.; Schubert, E. F.; Cho, J.; Sone, C., and Park, Y. *Analysis of high-power packages for phosphor-based white-light-emitting diodes*. In: "Applied Physics Letters" 86.24 (2005), pages 243505–1–243505–3.

[62] Kuo, H.-C.; Hung, C.-W.; Chen, H.-C.; Chen, K.-J.; Wang, C.-H.; Sher, C.-W.; Yeh, C.-C.; Lin, C.-C.; Chen, C.-H., and Cheng, Y.-J. *Patterned structure of remote phosphor for phosphor-converted white LEDs*. In: "Optics Express" 19.104 (2011), A930–A936.

[63] Huang, H.; Tsai, C.-C., and Huang, Y.-P. *Conformal phosphor coating using pulsed spray to reduce color deviation of white LEDs*. In: "Optics Express" 18.102 (2010), A201–A206.

[64] Liu, Z.-Y.; Liu, S.; Wang, K., and Luo, X.-B. *Studies on optical consistency of white LEDs affected by phosphor thickness and concentration using optical simulation*. In: "IEEE Transactions on Components and Packaging Technologies" 33.4 (2010), pages 680–687.

[65] Allen, S. and Steckl, A. *A nearly ideal phosphor-converted white light-emitting diode*. In: "Applied Physics Letters" 92 (2008), pages 143309–1–143309–3.

[66] Chen, L.; Chu, C., and Liu, R. *Improvement of emission efficiency and color rendering of high-power LED by controlling size of phosphor particles and utilization of different phosphors*. In: "Microelectronics Reliability" 52.5 (2012), pages 900–904.

[67] Huang, S.; Wu, J.; Hsu, W.; Chang, H.; Hung, H.; Lin, C.; Su H.and Bagkar, N.; Ke, W.; Kuo, H., et al. *Particle size effect on the packaging performance of YAG: Ce phosphors in white LEDs*. In: "International Journal of Applied Ceramic Technology" 6.4 (2009), pages 465–469.

[68] Masui, H.; Nakamura, S., and DenBaars, S. *Effects of phosphor application geometry on white light-emitting diodes*. In: "Japanese Journal of Applied Physics" 45 (2006), pages L910–L912.

[69] Hu, R.; Luo, X.; Feng, H., and Liu, S. *Effect of phosphor settling on the optical performance of phosphor-converted white light-emitting diode*. In: "Journal of Luminescence" 132.5 (2012), pages 1252–1256.

[70] Nazarov, M. *Luminescence mechanism of highly efficient YAG and TAG phosphors*. In: "Moldavian Journal of the Physical Sciences" 4.3 (2005), pages 247–356.

[71] Tran, N.; You, J., and Shi, F. *Effect of phosphor particle size on luminous efficacy of phosphor-converted white LED*. In: "Journal of Lightwave Technology" 27.22 (2009), pages 5145–5150.

[72] Shuai, Y.; Tran, N., and Shi, F. *Nonmonotonic phosphor size dependence of luminous efficacy for typical white LED emitters*. In: "Photonics Technology Letters, IEEE" 23.9 (2011), pages 552–554.

[73] Sommer, C.; Reil, F.; Krenn, J.; Hartmann, P.; Pachler, P.; Hoschopf, H., and Wenzl, F. *The impact of light scattering on the radiant flux of phosphor-converted high power white light-emitting diodes*. In: "Journal of Lightwave Technology" 29.15 (2011), pages 2285–2291.

[74] Jang, H. S.; Kang, J. H.; Won, Y.-H.; Chu, K.-M., and Jeon, D. Y. *Origin of the discrepancy between photoluminescence brightness of TAG: Ce and electroluminescence brightness of TAG: Ce-based white LED expected from phosphor brightness*. In: "Optics Letters" 33.18 (2008), pages 2140–2142.

[75] Sommer, C.; Hartmann, P.; Pachler, P.; Schweighart, M.; Tasch, S.; Leising, G., and Wenzl, F. *A detailed study on the requirements for angular homogeneity of phosphor converted high power white LED light sources*. In: "Optical Materials" 31.6 (2009), pages 837–848.

[76] Sommer, C.; Krenn, J.; Hartmann, P.; Pachler, P.; Schweighart, M.; Tasch, S., and Wenzl, F. *The effect of the phosphor particle sizes on the angular homogeneity of phosphor-converted high-power white LED light sources*. In: "IEEE Journal of Selected Topics in Quantum Electronics" 15.4 (2009), pages 1181–1188.

[77] Sommer, C.; Hartmann, P.; Pachler, P.; Hoschopf, H., and Wenzl, F. *The phosphor's optical properties—chromaticity coordinate relationship of phosphor converted white LEDs*. In: "Optical and Quantum Electronics" 44.3-5 (2012), pages 111–117.

[78] Liu, Z.; Li, C.; Yu, B.-H.; Wang, Y.-H.; Liu, S., and Niu, H.-B. *Effects of YAG: Ce phosphor particle size on optical performance of white LEDs*. In: "Electronic Packaging Technology and High Density Packaging (ICEPT-HDP), 2011 12th International Conference". IEEE. 2011, pages 1–6.

[79] Xie, R.-J.; Hirosaki, N.; Sakuma, K., and Kimura, N. *White light-emitting diodes (LEDs) using (oxy) nitride phosphors*. In: "Journal of Physics D: Applied Physics" 41.14 (2008), pages 144013–144017.

[80] Kimura, N.; Sakuma, K.; Hirafune, S.; Asano, K.; Hirosaki, N., and Xie, R.-J. *Extrahigh color rendering white light-emitting diode lamps using oxynitride and nitride phosphors excited by blue light-emitting diode*. In: "Applied Physics Letters" 90.5 (2007), pages 051109–1–051109–3.

[81] Fukui, T.; Sakuta, H.; Mishiro, K.; Miyachi, T.; Kamon, K.; Hayashi, H.; Nakamura, N.; Uchida, Y.; Kurai, S., and Taguchi, T. *Development of white light emitting diodes by multi-layered red, green, and blue phosphors excited by near-ultraviolet light emitting diodes*. In: "Journal of Light & Visual Environment" 32.1 (2008), pages 43–45.

[82] You, J. P.; Tran, N., and Shi, F. *Light extraction enhanced white light-emitting diodes with multi-layered phosphor configuration*. In: "Optics Express" 18.5 (2010), pages 5055–5060.

[83] Lee, S. J. *Analysis of light-emitting diodes by Monte Carlo photon simulation*. In: "Applied Optics" 40.9 (2001), pages 1427–1437.

[84] Sudiarta, W. and Chylek, P. *Mie scattering efficiency of a large spherical particle embedded in an absorbing medium*. In: "Journal of Quantitative Spectroscopy and Radiative Transfer" 70.4 (2001), pages 709–714.

[85] Hahn, D. *Light scattering theory*. report. Department of Mechanical and Aeorospace Engineering, University of Florida, 2009.

[86] Sun, C.-C.; Chen, C.-Y.; He, H.-Y.; Chen, C.-C.; Chien, W.-T.; Lee, T.-X., and Yang, T.-H. *Precise optical modeling for silicate-based white LEDs*. In: "Optics express" 16.24 (2008), pages 20060–20066.

[87] Kang, D.-Y.; Wu, E., and Wang, D.-M. *Modeling white light-emitting diodes with phosphor layers*. In: "Applied Physics Letters" 89.23 (2006), pages 231102–1–231102–3.

[88] Hung, C.-H.g and Tien, C.-H. *Phosphor-converted LED modeling by bidirectional photometric data*. In: "Optics Express" 18.103 (2010), A261–A271.

[89] Zollers, M.; Yang, H.; Melman, J.; David, S.; Wang, G., and Xu, X. *Process to measure particulate down-converting phosphors and create well-correlated software models of LED performance*. In: "SPIE OPTO". International Society for Optics and Photonics. 2011, pages 795414–1–795414–3.

[90] Borbely, A. and Johnson, S. *Performance of phosphor-coated light-emitting diode optics in ray-trace simulations*. In: "Optical Engineering" 44.11 (2005), pages 111308–111313.

[91] Tsao, C.; Freniere, E., and Smith, L. *Improved predictive modeling of white LEDs with accurate luminescence simulation and practical inputs with TracePro opto-mechanical design software*. In: "SPIE OPTO: Integrated Optoelectronic Devices". International Society for Optics and Photonics. 2009, pages 723111–723115.

[92] Allen, T. *Powder Sampling and Particle Size Determination*. Elsevier, Amsterdam, 2003, pages 56–90.

[93] Allen, T. *Particle Size Measurement: Volume 2: Surface Area and Pore Size Determination*. 5th edition, Springer, 1997, pages 68–96.

[94] Allen, T. *Powder Sampling and Particle Size Determination*. Elsevier, Amsterdam, 2003, pages 524–603.

[95] Bois, C.; Bodrogi, P.; Khanh, T.-Q., and Winkler, H. *White LED Light Characteristics as a Function of Phosphor Particle Size*. In: "ECS Journal of Solid State Science and Technology" 1.5 (2012), R131–R135.

[96] Setlur, A. and Srivastava, A. *On the relationship between emission color and Ce^{3+} concentration in garnet phosphors*. In: "Optical Materials" 29.12 (2007), pages 1647–1652.

[97] Bois, C.; Bodrogi, P.; Khanh, T.-Q., and Winkler, H. *Measuring, simulating and optimizing current LED phosphor systems to enhance the visual quality of lighting*. In: "Journal of Solid State Lighting" 1.1 (2014), pages 1–18.

[98] Denault, K.; Cantore, M.; Nakamura, S.; DenBaars, S., and Seshadri, R. *Efficient and stable laser-driven white lighting*. In: "AIP Advances" 3.7 (2013), pages 072107–072112.

A Appendix YAG investigations

Table A.1.: Average particle diameter d_{50}, particle size width $d_{10} - d_{90}$ and ratio d_{90}/d_{10} of YAG 2 and its sieved fractions

Sample	Treatment	d_{50}/ μm	d_{10}-d_{90}/ μm	d_{90}/d_{10}
YAG 2	bulk material not sieved	12	6-25	4
YAG 2 #0	sieved under 5 μm	9	6-12	1.9
YAG 2 #1	sieved between 11 and 5 μm	13	10-16	1.5
YAG 2 #2	sieved between 15 and 11 μm	17	12-19	1.5
YAG 2 #3	sieved between 20 and 15 μm	21	17-26	1.5
YAG 2 #4	sieved between 25 and 20 μm	28	21-33	1.5
YAG 2 #5	sieved between 28 and 25 μm	31	28-37	1.3
YAG 2 #6	sieved between 36 and 30 μm	36	30-42	1.7

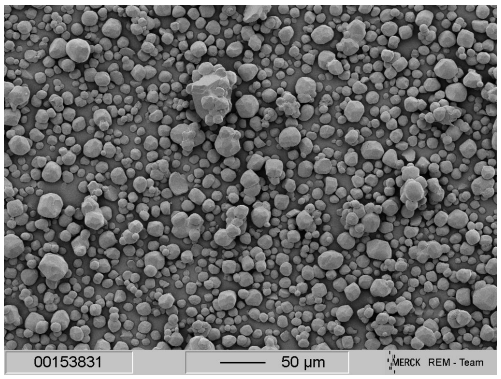

Figure A.1.: YAG 2 (d_{50}=12 μm)

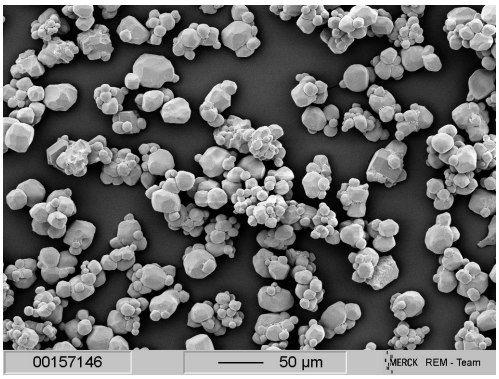

Figure A.2.: YAG2 #6 (d_{50}=36 μm)

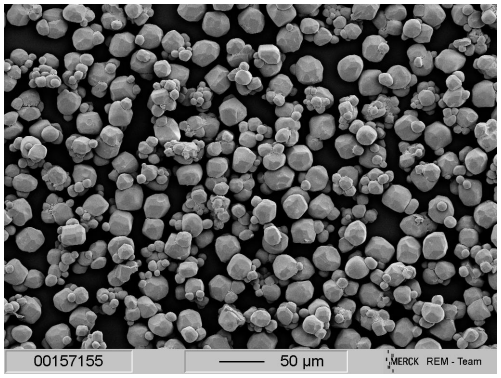

Figure A.3.: YAG2 #5 (d_{50}=31 μm)

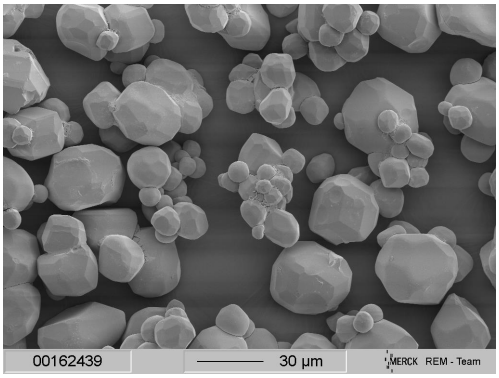

Figure A.4.: YAG2 #4 (d_{50}=28 μm)

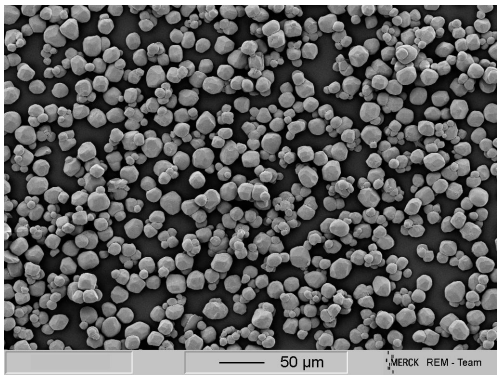

Figure A.5.: YAG2 #3 (d_{50}=21 μm)

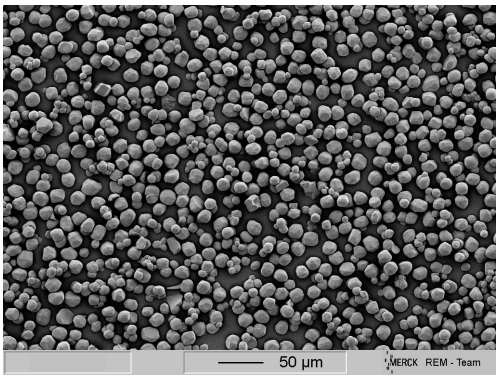

Figure A.6.: YAG2 #2 (d_{50}=17 μm)

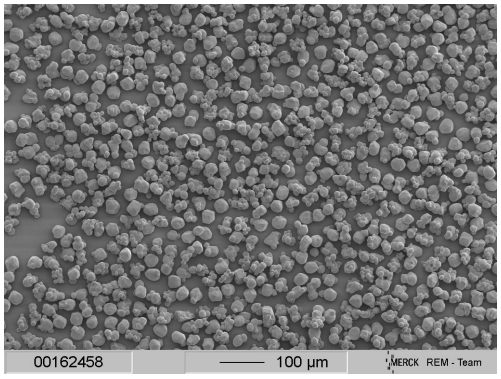

Figure A.7.: YAG2 #1 (d_{50}=13 μm)

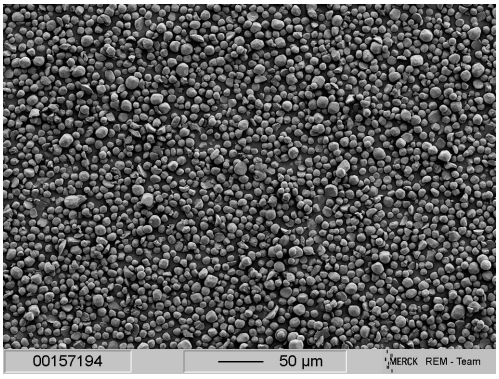

Figure A.8.: YAG2 #0 (d_{50}=9 μm)

Figure A.9.: SEM pictures from the sieved fraction of YAG 2

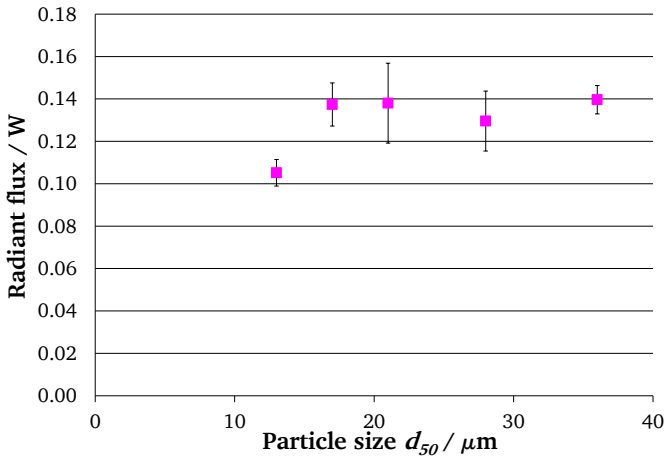

Figure A.10.: Radiant flux of WLEDs (YAG 2 # LED type 1 (COB))

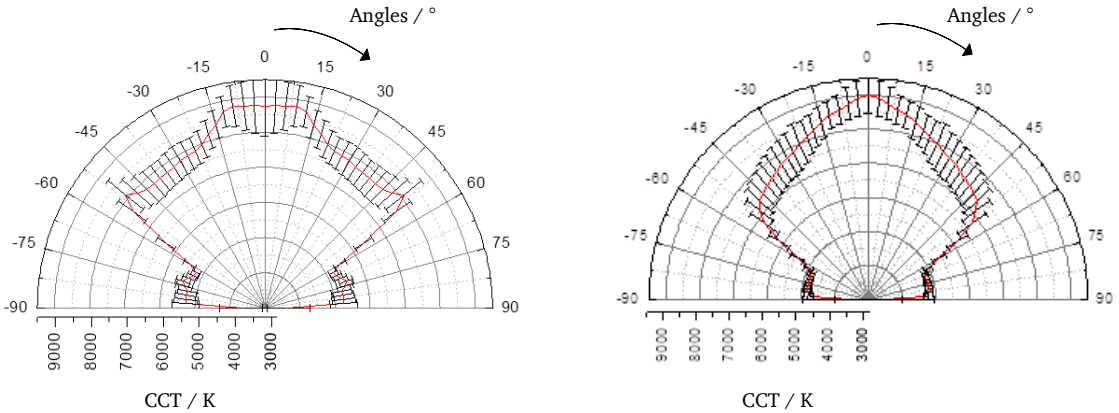

Figure A.11.: Chromaticity homogeneity over the angles of PC-LEDs type 4 (SMD) for YAG1 #5 (d_{50}=33 µm) on the left and YAG1 #1 (d_{50}=11 µm) on the right

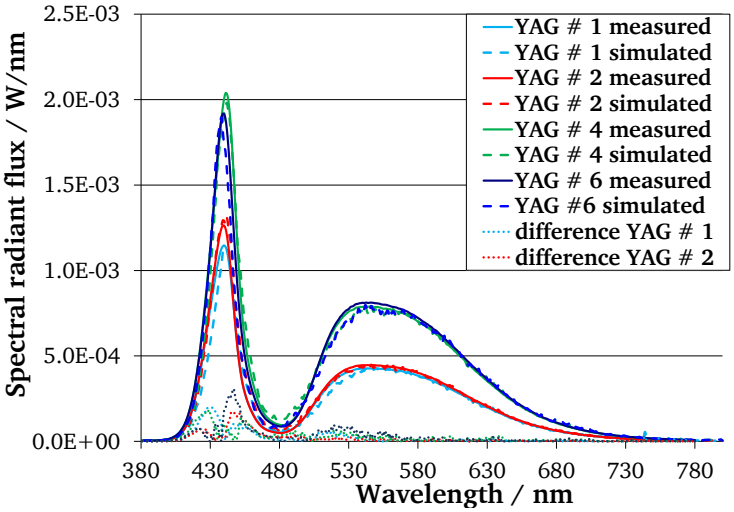

Figure A.12.: Comparison of simulation and measurements of the LED type 1 (COB LED) for YAG #1 (11 μm), YAG #2 (15 μm), YAG #4 (31 μm) and YAG #6 (37 μm)

Table A.2.: Simulated and measured characteristics of LEDs type 1 (COB LED)

	YAG #1		YAG #2		YAG #4		YAG #6	
	sim.	meas.	sim.	meas.	sim.	meas.	sim.	meas.
CCT / K	6797	7260	6601	6424	6569	6819	5608	6091
CRI R_a	76	75	76	74	77	74	71	72
R_9	24	26	16	11	17	13	-3	-1
luminous flux / lm	24.5	28.9	26.0	26.1	45.2	45.9	44.7	46.9
Δ $u'v'$	0.027	0.025	0.021	0.020	0.022	0.021	0.021	0.018
Q_9	77	75	80	79	81	78	80	79
Q_g	95	96	94	95	94	94	94	93
Q_a	62	63	65	64	65	63	63	63

Table A.3.: Simulated CCT and variation from detector at 0° and at 60° for the LED type 1

	CCT / K		
	0°	60°	Variation / K
YAG 1	6969	5744	1225
YAG 1 #7	6975	5775	1200
YAG 1 #6	6998	5851	1147
YAG 1 #4	6357	5526	831
YAG 1 #3	6486	5597	889
YAG 1 #2	6861	5386	1475
YAG 1 #1	6377	5473	904

B Appendix LuAG investigations

Table B.1.: Average particle diameter d_{50}, particle size width $d_{10} - d_{90}$ and ratio d_{90}/d_{10} of LuAG 1 and its sieved fractions

Sample	Treatment	d_{50}/μm	d_{10}-d_{90}/μm	d_{90}/d_{10}
LuAG 1	bulk material not sieved	46	4-120	30
LuAG 1 #1	sieved under 5 μm	6.5	5-9	1.8
LuAG 1 #2	sieved between 11 and 5 μm	10.5	6-15	2.5
LuAG 1 #3	sieved between 15 and 11 μm	18	10-20	2
LuAG 1 #4	sieved between 20 and 15 μm	21	16-24	1.5
LuAG 1 #5	sieved between 25 and 20 μm	28	22-31	1.4
LuAG 1 #6	sieved between 50 and 36 μm	46	38-59	1.5
LuAG 1 #7	sieved between 100 and 50 μm	74	57-101	1.7
LuAG 1 #8	sieved above 100 μm	114	92-145	1.5

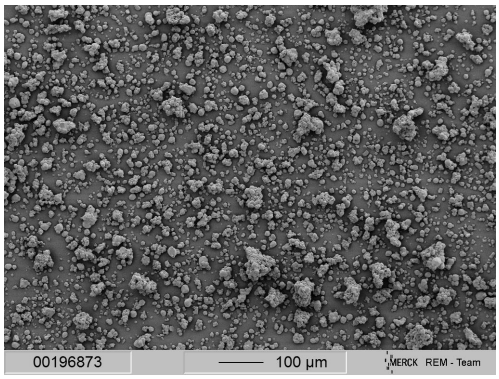

Figure B.1.: LuAG1 (d_{50}=46 μm)

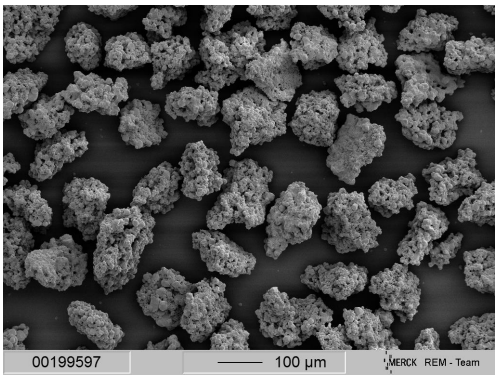

Figure B.2.: LuAG1 #8 (d_{50}=114 μm)

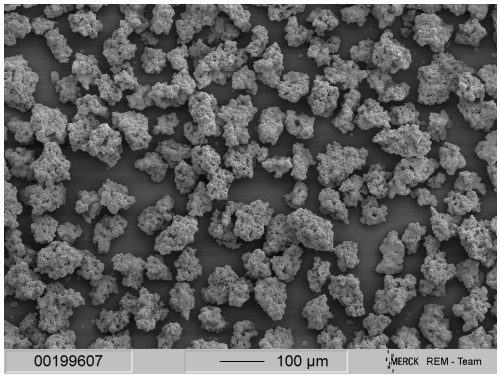

Figure B.3.: LuAG1 #7 (d_{50}=74 μm)

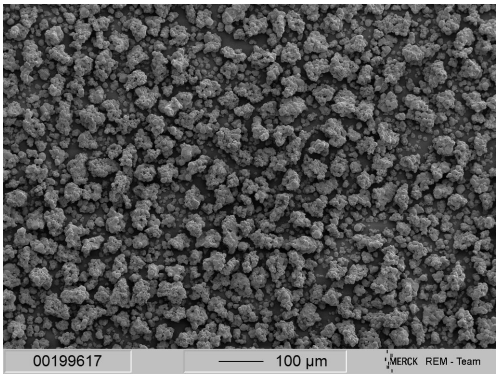

Figure B.4.: LuAG1 #6 (d_{50}=46 μm)

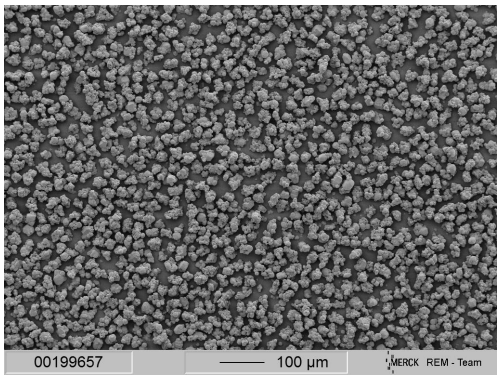

Figure B.5.: LuAG1 #5 (d_{50}=28 μm)

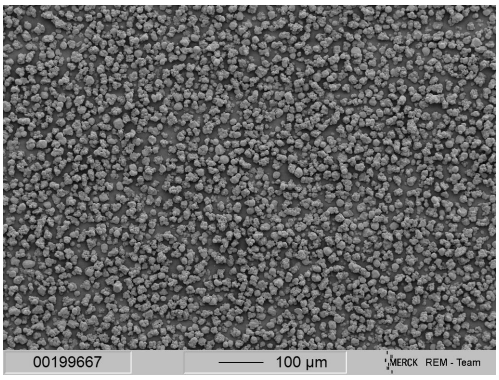

Figure B.6.: LuAG1 #4 (d_{50}=21 μm)

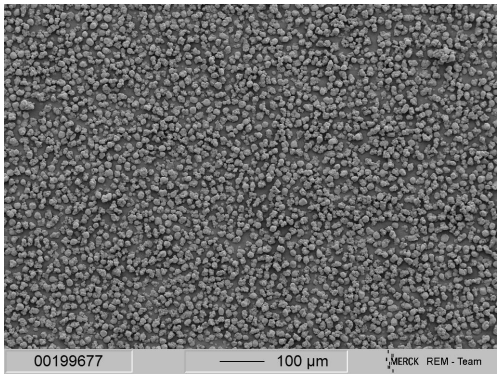

Figure B.7.: LuAG1 #3 (d_{50}=18 μm)

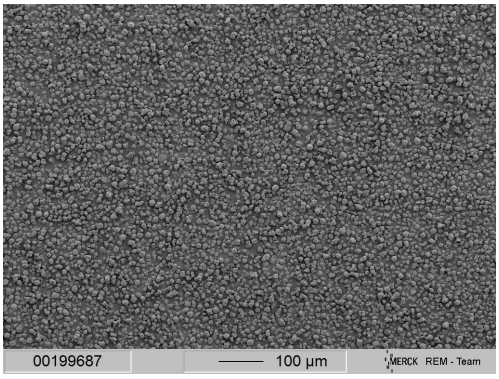

Figure B.8.: LuAG1 #2 (d_{50}=10 μm)

Figure B.9.: SEM pictures from the sieved fraction of LuAG 1

Table B.2.: PC-LEDs (LuAG 1) color characteristics (x,y) (u',v') and chromaticity deviations calculated from the color variation obtained for the repeated samples ($\Delta u'$, $\Delta v'$) and number of PC-LED fabricated for each sieved fraction

	x	y	u'	v'	$\Delta u'$	$\Delta v'$	number of LEDs
LuAG 1 #1	0.2623	0.2964	0.1739	0.4422	0.0002	0.0030	3
LuAG 1 #2	0.2597	0.2968	0.1720	0.4421	0.0005	0.0002	5
LuAG 1 #3	0.2594	0.2972	0.1716	0.4423	0.0005	0.0037	5
LuAG 1 #4	0.2596	0.2968	0.1718	0.4421	0.0003	0.0025	5
LuAG 1 #5	0.2604	0.2997	0.1715	0.4439	0.0004	0.0017	5
LuAG 1 #6	0.2622	0.3009	0.1723	0.4449	0.0004	0.0005	3
LuAG 1 #7	0.2615	0.2989	0.1725	0.4436	0.0003	0.0001	2

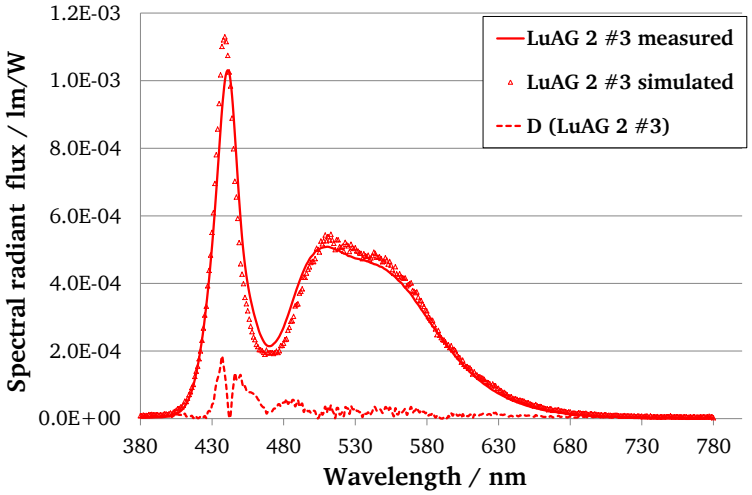

Figure B.10.: Simulation and measurement of PC-LEDs increasing particle sizes for LuAG 2#3 d_{50} =17 μm

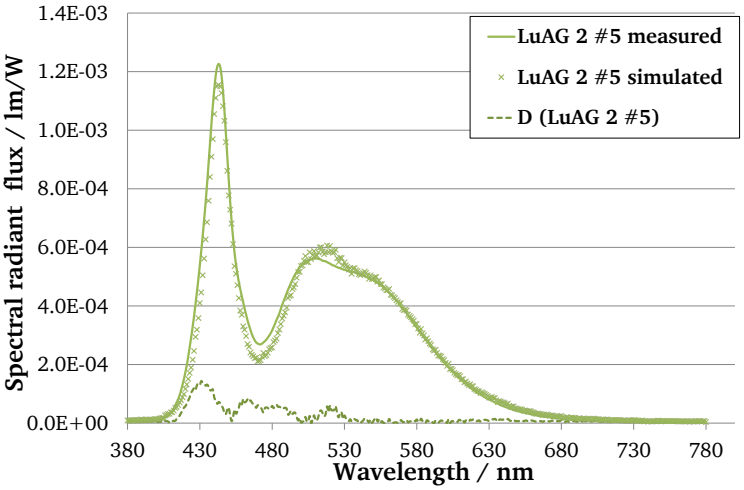

Figure B.11.: Simulation and measurement of PC-LEDs for LuAG 2#5 d_{50} =27 μm

C Appendix Green and Red phosphor LEDs

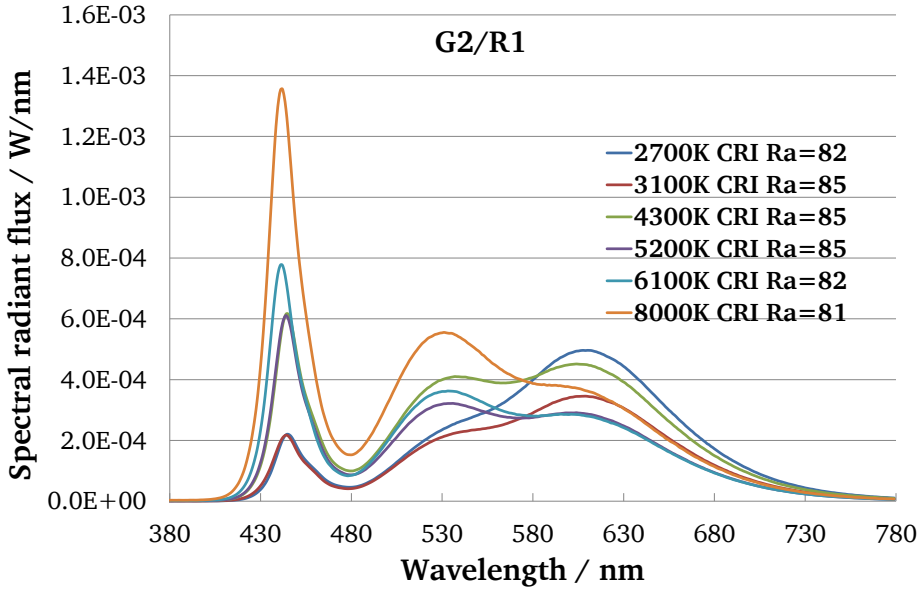

Figure C.1.: Spectral radiant fluxes of G2/R1 phosphor system for several CCT

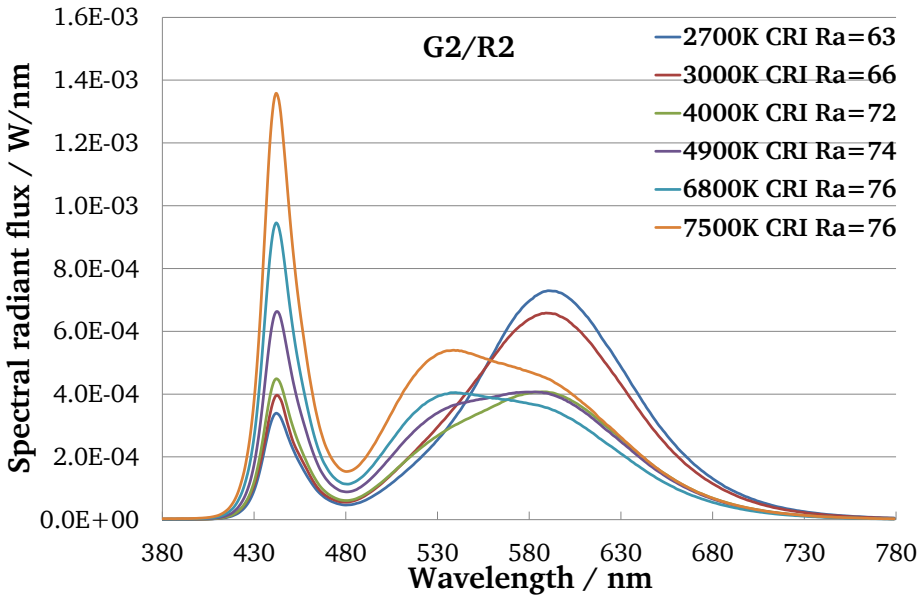

Figure C.2.: Spectral radiant fluxes of G2/R2 phosphor system for several CCT

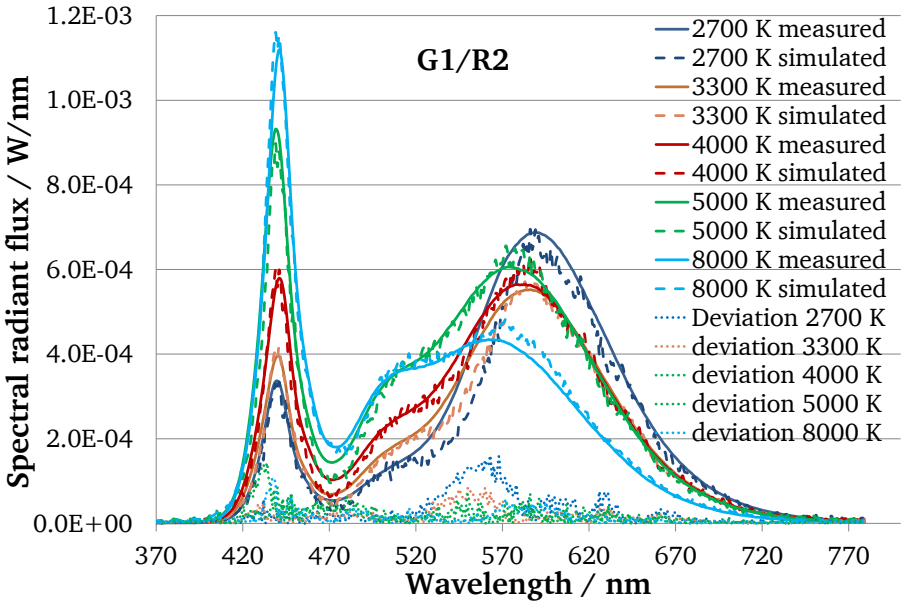

Figure C.3.: Measured, simulated spectral distributions and their difference (full, dashed and dotted line) for G1/R2 system

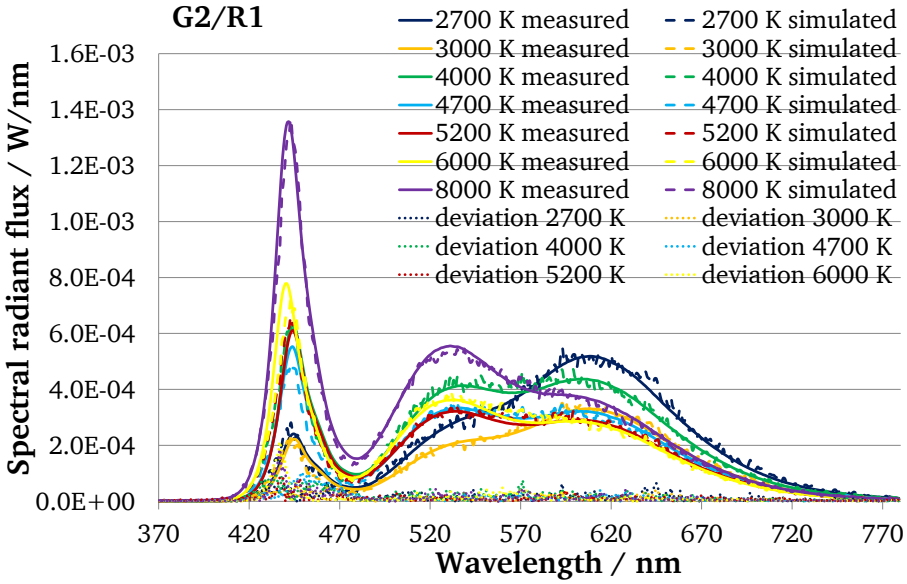

Figure C.4.: Measured, simulated spectral distributions and their difference (full, dashed and dotted line) for G2/R1 system

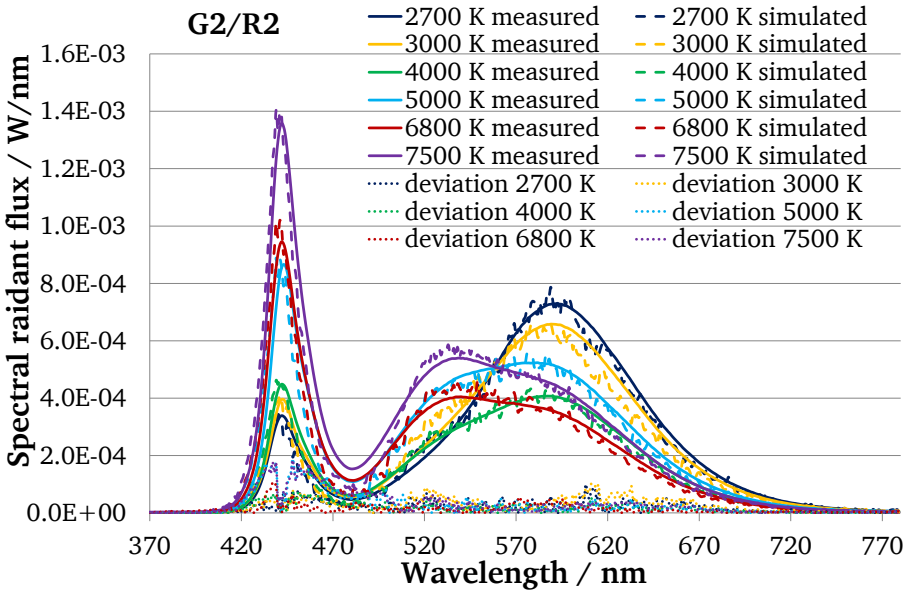

Figure C.5.: Measured, simulated spectral distributions and their difference (full, dashed and dotted line) for G2/R2 system

D Curriculum Vitae

Charlotte BOIS

Luisenstraße 18
64283 Darmstadt
Email: boischarlotte@yahoo.fr
Mobil: + 49 176/72571452

Geburtsdatum: 03.12.1986
Nationalität: Französisch
Familienstand: ledig

Ausbildung

01/2010 –05/ 2014 **Technische Universität Darmstadt, Institut für Elektromechanische Konstruktionen, Fachgebiet Lichttechnik**
Promotion in Industriekooperation mit Merck KGaA, Darmstadt:
Thema: "Alignment of Phosphor Properties for Improvement of Phosphor-Converted LED".

09/2008 – 03/2009 **Technische Universität Darmstadt, Fachbereich Materialwissenschaften**
Austauschstudium mit Kursen und Praktika zu nichtmetallischen anorganischen Werkstoffen, dispersen Feststoffen und Materialanalytik.

09/2006 – 09/2009 **Ecole Nationale Supérieure de Chimie et Physique de Bordeaux (Frankreich)**
Studium zum Diplomingenieur der Chemie und Physik (Diplôme d'Ingénieur).

09/2004 – 09/2006 **Ecole Préparatoire aux Ecoles d'Ingénieur Lille (Frankreich)**
Zweijähriges Intensivstudium der Mathematik, Physik und Chemie.

09/2001 – 06/2004 **Lycée Marguerite Filhol (Gymnasium), Fumel (Frankreich)**
Allgemeine Hochschulreife mit naturwissenschaftlichem Profil, erlangt mit Auszeichnung (Baccalauréat, mention bien).

Arbeitserfahrung

02/2014 –03/2014 **Technische Universität Darmstadt, Fachgebiet Lichttechnik**
Hilfswissenschaftler: Interkulturelle Charakterisierung der Helligkeitswahrnehmung und Farbpräferenz

01/2010 –12/2013 **Merck KGaA, Darmstadt, Solid State Lighting Department**
Doktorstipendiatin der Firma Merck, Thema: „Alignment of Phosphor Properties for Improvement of Phosphor-Converted LED".

11/2012 **University California Santa Barbara (USA), Department of Materials, Functional Inorganic Materials Group**
Gastforscher im Labor für Leuchtstoffsynthese:
Anwendung und Evaluierung alternativer Mikrowellen-Messtechnik zur Effizienzsteigerung des Leuchtstoffsynthese-Prozesses.

04/2009 - 9/2009 **Merck KGaA, Darmstadt**
Praktikantin im Bereich Performance Materials / Solid State Lighting:
Durchführung von Messungen, Analysen und Auswertungen an Leuchtstoffproben im UV und sichtbaren Bereich, und damit einen Beitrag geleistet zur Verbesserung der Effizienz von Forschungsmustern im Bereich der Lumineszenz-Eigenschaften.

07/2007 - 08/2007 **Symrise AG, Holzminden**
Praktikantin im Bereich Lebensmittel-Analyse:
Vorbereitung und Elementanalyse von Lebensmittelproben unter Anwendung von Gas-Chromatographie und Massenspektrometrie, sowie Klassifizierung von Zitrusfrüchten zur Marktevaluation.

07/2005 - 08/2005 **Institute National de la Recherche Agronomique, Bordeaux (France)**
Praktikant im Bereich Analytik: Aufbereitung und Analyse von Weinreben mittels UV-Spektralanalyse zur Identifizierung und Zerlegung in quantitative Bestandteile.

Wissenschaftliche Arbeiten

Veröffentlichungen

BOIS, Charlotte, et al. White LED Light Characteristics as a Function of Phosphor Particle Size. ECS Journal of Solid State Science and Technology, 2012, 1. Jg., Nr. 5, S. R131-R135.

BOIS, Charlotte, et al. Measuring, simulating and optimizing current LED phosphor systems to enhance visual illumination quality. Journal of Solid State Lighting, 2014, 1. Jg., Nr. 1, S. 1-18.

Vortrag – Poster
BOIS, Charlotte Messung, Simulation und Optimierung weißer YAG-LEDs in LICHT 2012, Berlin (Germany), p. 270-276.

Fähigkeiten

Sprachen

- Französisch (Muttersprache)
- Englisch (verhandlungssicher)
- Deutsch (verhandlungssicher)
- Spanisch (Grundkenntnisse)

Software Kenntnisse

- Microsoft Office (sehr gute Kenntnisse)
- LightTools (sehr gute Kenntnisse)
- Latex (Basiskenntnisse)

Technische Analysefähigkeiten

Elementanalyse:

- Massenspektrometrie
- Chromatography
- Röntgenbeugungsanalyse
- NMR (Kernspinresonanz)

Partikelanalyse:

- Laserbeugung
- Coulter-Counter Methodik

Optische Verfahren und Bildanalyse:

- Lichttechnische Analysen (Photo-Elektrolumineszenz, Goniometermessung)
- Mikroskopmessungen
- REM (Rasterelektronenmikroskop)

Engagements

Seit 5 Jahren	Arbeit als Französisch Nachhilfelehrerin und Sprachtandem
2004	Erste-Hilfe-Kurs
2009	Engagement als Tutorin der französischen Austauschstudenten in Darmstadt

Halter eines französischen (und in der EU gültigen) KFZ Führerscheins ohne jegliche Verstöße

Interessen

Sport	(Badminton Turniere, Tennisverein, Cheerleading Kontest, Fitnessstudio)
Tanzen und Klavierspielen	
Länder und Kulturen	(bspw. Juni-Aug 2008)

Darmstadt, September 2014